MACHINING CHARACTERISTICS

OF POLYMERS

NABIL NASR ZAKY GINDY, BSc, MSc

Thesis submitted for the degree of Doctor of Philosophy of the University of Aston in Birmingham

Department of Production Technology and Production Management

May, 1978

DECLARATION

No part of the work described in this thesis has been submitted in support of an application for another degree or other qualification for this or any other institution.

Dabil Ginda

SUMMARY

MACHINING CHARACTERISTICS OF POLYMERS

NABIL NASR ZAKY GINDY

Thesis submitted for the degree of Doctor of Philosophy

May 1978

This report deals with a research programme in which the cutting characteristics of certain polymers are investigated.

Tensile and compression tests are carried out to define the properties of various polymers and their mechanical state. The deformation during cutting is assumed to occur under plane strain conditions and a suitable yield equation is chosen to describe the behaviour of each polymer.

For the cutting process a single shear plane model is assumed and using the minimum energy criterion and the appropriate yield criterion, a shear angle relationship is developed. Orthogonal cutting tests are carried out, varying three main parameters, cutting speed, tool rake angle and depth of cut. Measured forces and shear angles are compared with the values predicted by the relevant theoretical analysis, and an excellent correlation obtained. It is concluded that the assumed mode of deformation during cutting is justified for the range of polymers studied.

Finally, the concept of critical rake angle which have been recommended by other workers as the correct tool geometry for cutting polymers, is discussed in the light of the results obtained in this program.

Polymers, Machining, Cutting

ACKNOWLEDGEMENTS

The Author would like to express his sincere gratitude to

Dr. T. J. Vickerstaff for his continuous encouragement, guidance and valuable advice he provided.

Professor R. H. Thornley for acting as an advisor.

The Machine Tool and Metrology Laboratories for their active, willing and cheerful support.

Ms. B. Drinkwater for typing the manuscript.

LIST OF CONTENTS

LIST OF FIGURES

7.32 (F) as a function of depth of cut for rolled Nylon

7.33 (N) as a function of depth of cut for as-received polycarbonate

7.34 (N) as a function of depth of cut for rolled polycarbonate

7.35 (N) as a function of depth of cut for as-received Nylon

7.36 (N) as a function of depth of cut for rolled Nylon

7.37 (F_s) as a function of depth of cut for as-received polycarbonate

7.38 (F_s) as a function of depth of cut for rolled polycarbonate

7.39 (F_s) as a function of depth of cut for as-received Nylon

7.40 (F_s) as a function of depth of cut for rolled Nylon

7.41 (F_n) as a function of depth of cut for as-received polycarbonate

7.42 (F_n) as a function of depth of cut for rolled polycarbonate

7.43 (F_n) as a function of depth of cut for as-received Nylon

7.44 (F_n) as a function of depth of cut for rolled Nylon

7.45 (F_c) as a function of cutting speed for as-received polycarbonate

7.46 (F_c) as a function of cutting speed for rolled polycarbonate

7.47 (F_c) as a function of cutting speed for as-received Nylon

7.48 (F_c) as a function of cutting speed for rolled Nylon

7.150 (μ) and (N) relationship for rolled Nylon,
V = 9.14 m/min

7.151 (μ) and (N) relationship for rolled Nylon,
V = 22.86 m/min

7.152 (μ) and (N) relationship for rolled Nylon,
V = 36.58 m/min

CHAPTER I

Introduction

Polymers are being used extensively in engineering applications because of their desirable mechanical properties and their versatility.

Machining polymers has become an important process in recent years. Although most of the parts made from plastics are usually moulded, moulding is an expensive process with high initial cost which makes it uneconomical for small scale production. Machining can also be used to produce complicated shapes with high dimensional accuracy, avoiding much of the residual stresses caused by moulding.

The machining characteristics of polymers appear to depend primarily on their mechanical, thermal and rheological properties. These properties do not only vary widely between different polymeric groups but just as widely between polymers from the same group. In studying the cutting characteristics of polymers an individual approach to suit the particular polymer under consideration should be adopted and a generalisation could be very much in error.

Most of the information about tooling and the choice of cutting parameters used in industry are based on practical experience, with little modification to the conventional metal or wood cutting machinery and tooling. This is due to the fact that the

analysis of the cutting process for polymers has not received the attention it deserves in the research literature. Very little information exists on the choice of cutting parameters and tooling, based on detailed analysis of the mechanical and thermal properties of polymers. The reported research is based on a single shear plane model similar to that experienced in metal cutting, and using the minimum energy criterion to arrive at a cutting solution. The approach, although sound in nature, lacks fundamental detailed information on the mechanical and thermal properties of polymers and also on the peculiarities of their deformation characteristics.

A gap in the research literature exists in relating the properties of polymeric solids to their cutting behaviour.

The approach used in this investigation is based on analyising the deformation in the cutting zone as a plane strain deformation process. The description of such deformation is carried out by choosing a suitable yield criterion for each polymer, able to represent its behaviour and account for fundamental properties of polymeric solids such as anisotropy and dependence on pressure. The material properties of each polymer and its mechanical state are evaluated by a series of tensile and compression tests. The material testing results are used, together with the yield criterion to develop a shear angle relationship to describe the individual polymer behaviour during cutting. Orthogonal cutting tests are conducted on Nylon 6 (crystalline polymer) and polycarbonate (amorphous polymer), to

provide experimental data on their cutting behaviour under different cutting conditions. The orthogonal cutting data is also used to evaluate the validity of the suggested shear angle relationships and the predicted cutting forces.

CHAPTER II

Material Cutting as a deformation process

Material cutting is an important area of material science; the cutting process is very widely used in industry because of its simplicity and versatility. In spite of many admirable steps forward taken by researchers in recent years to study the fundamental mechanics of the cutting process, the problem still needs attention before the characteristics and behaviour of different materials in a complicated deformation process are fully understood.

Research in material machining can prove very useful in the development of cutting tool design, choice of cutting conditions, the use of cutting fluids, and also to provide very much needed information on the cutting of new materials as they are developed.

In material cutting the deformation occurs under unusual conditions of a narrow deformation zone, high strains and strain rates, high temperature, ...etc. and a better understanding of the cutting problem would provide some basic information about the behaviour of different materials under conditions that are difficult to attain in conventional types of material tests.

2.1 The basic cutting mechanism

The chip removal action in the cutting process can be idealized to two types shown in figures (2.1) and (2.2), depending on the geometry of the cutting tool-workpiece engagement. Figure (2.2) shows the general case of oblique cutting and figure (2.1), orthogonal cutting. In orthogonal cutting the cutting edge is straight and perpendicular to the cutting direction. The angle between the tool face and the plane normal to the cutting direction is known as the rake angle (α). For simplicity, the following review of the fundamental mechanics of the cutting process is confined to considering the orthogonal cutting process.

In the idealized cutting picture shown in figure (2.3), the mechanics of the cutting process is based on using a wedge-shaped tool to remove a depth of cut from the material, converting it to a chip on the tool rake face. The deformation is assumed to occur by a shearing action on a shear plane (oA), generated inside the material, starting upwards from the cutting edge to the free surface. The angle between this shear plane and the direction of motion of the tool is known as the shear angle (ϕ). Considering the case of continuous chip flow on the rake face, it is possible to resolve the resultant cutting force (R) into three different force systems, shown in Figure (2.3).

The first system consists of the cutting force (F_c) acting in the direction of the cutting speed and the feed force (F_t) perpendicular to the cutting force (F_c). The second force system is the friction force (F) acting on the tool rake face and a

normal force (N) acting perpendicular to the rake face. The third force system is composed of the shearing force (F_s) acting in the shear plane direction and a normal force (F_n) acting perpendicular to the shear plane. In orthogonal cutting the deformation is assumed to occur under plane strain conditions and also that in general the shear plane is the direction of maximum shear stress.

2.1.1 Geometrical relationships

The ratio of t_1/t_2 is known as the cutting ratio r_c.

$$r_c = t_1/t_2 \qquad [2.1]$$

from Figure (2.3)

$$t_1 = oA.\ \sin \phi$$

$$t_2 = oA.\ \cos (\phi - \alpha)$$

$$r_c = t_1/t_2 = \frac{\sin \phi}{\cos (\phi - \alpha)} \qquad [2.2]$$

Solving for ϕ,

$$\tan \phi = \frac{r_c \cos \alpha}{1 - rc \sin \alpha} \qquad [2.3]$$

The shear plane area A_s is defined as,

$$A_s = \frac{t_1 .b}{\sin \phi} \qquad [2.4]$$

where b is the width of cut.

The shear angle ϕ obtained from equation [2.3] is a function of the rake angle α and the cutting ratio r_c. ϕ increases with increasing the cutting ratio. The effect of the rake angle on the value of the shear angle ϕ , varies according to the value of the cutting ratio. The smaller the cutting ratio r_c the more difficult it becomes to machine the material. The cutting ratio is also affected by the use of cutting fluids, for example carbon tetrachloride is very effective in increasing the cutting ratio. An increase in the cutting ratio is usually related to a reduction in the cutting force as will be shown later.

2.1.2 Velocity relations

The velocity relationships in the cutting process are based on three velocities.

1. The cutting velocity V - the velocity of the tool relative to the workpiece in a direction parallel to F_c.
2. The chip velocity V_c - the velocity of the chip relative to the tool in the direction of the tool rake face.
3. The shear velocity V_s - the velocity of the chip relative to the workpiece in the shear place direction.

The relationships between these three velocities can be determined from the geometrical relationships in figure [2.3] as shown in figure [2.4]

$$V_c = \frac{\sin \phi}{\cos (\phi - \alpha)} .V = r_c.V \qquad [2.5]$$

$$V_s = \frac{\cos \alpha}{\cos (\phi - \alpha)} .V \qquad [2.6]$$

2.1.3 Shear Strain (γs)

The shear strain (γ_s) can be defined as the ratio of the displacement of a layer of the material to the height of that layer (1)* as shown in Fig [2.5]

$$\gamma_s = \frac{\Delta s}{\Delta y} \qquad [2.7]$$

from figure (2.5)

$$\gamma_s = \tan (\phi - \alpha) + \cot \phi \qquad [2.8]$$

The shear strain rate ($\dot{\gamma} s$) can then be defined as,

$$\dot{\gamma}_s = \frac{\Delta s}{\Delta y . \Delta t} = \frac{V_s}{\Delta y} \qquad [2.9]$$

Where Δt is the time taken by the material to travel a distance Δs along the shear plane.

Δy is the spacing of successive shear planes.

* Numbers in parenthesis designate references listed in the reference section

As indicated by Kobayashi (2), the shear strain defined by equation [2.8] is a finite quantity and is a measure of large plastic deformation, which in general is expressed in the integral form according to the incremental strain theory. On the other hand, the finite strain theory defines the shear strain in terms of finite dimensions (2 -3).

$$\gamma_s = 2 \sinh E_1 \qquad [2.10]$$

where E_1 is a measure of the maximum elongation of a particular network of lines which remain orthogonal in the body before and after deformation.

2.1.4 Force and stress relationships

Treating the chip as a free body and considering the equilibrium of forces in the cutting process,

$$F_s = F_c \cos \phi - F_t \sin \phi \qquad [2.11]$$

$$F_n = F_t \cos \phi + F_c \sin \phi \qquad [2.12]$$

$$F_n = F_s \tan (\phi + \beta - \alpha) \qquad [2.13]$$

$$F = F_c \sin\alpha + F_t \cos\alpha \qquad [2.14]$$

$$N = F_c \cos\alpha - F_t \sin\alpha \qquad [2.15]$$

$$\tan (\beta - \alpha) = \frac{F_t}{F_c} \qquad [2.16]$$

$$\mu = \tan\beta = \frac{F}{N} \qquad [2.17]$$

$$\mu = \frac{F_c \sin\alpha + F_t \cos\alpha}{F_c \cos\alpha - F_t \sin\alpha} \qquad [2.18]$$

$$\mu = \frac{F_t + F_c \tan\alpha}{F_c - F_t \tan\alpha} \qquad [2.19]$$

2.1.5 Energy relationships.

In orthogonal cutting the total energy consumed in cutting per unit time is,

$$U = F_c . V \qquad [2.20]$$

The total energy per unit volume of the material removed is,

$$u = \frac{U}{V.b.t_1} = \frac{F_c}{b.t_1} \qquad [2.21]$$

The total energy per unit volume can be broken down into several components according to the way in which these components are consumed in the cutting process.

$$u = U_s + U_f + U_A + U_m \qquad [2.22]$$

where,

U_s = shear energy per unit volume.

U_f = friction energy per unit volume.

U_A = surface energy per unit volume.

U_m = momentum energy per unit volume.

The surface and momentum energies consumed in cutting represent a very small percentage of the total energy (4). The total energy per unit volume can be approximated to the sum of the friction energy and the shear energy.

$$u \simeq U_s + U_f \qquad [2.23]$$

The shear energy can be written as

$$U_s = \frac{F_s . V_s}{V . b . t_1} = \tau_s . \frac{V_s}{V . \sin \phi} = \tau_s . \gamma_s \qquad [2.24]$$

Similarly the friction energy takes the form,

$$U_f = \frac{F . V_c}{V . b . t_1} = \frac{F . r_c}{b . t_1} \qquad [2.25]$$

General discussion

Merchant (5-6) determined the value of the shear angle ϕ in relation to $(\beta-\alpha)$ by employing the minimum energy criterion, i.e. the shear angle ϕ will be such that the total energy consumed in cutting is a minimum. Merchant also assumed that the shear plane is the direction of maximum shear stress and that the friction conditions on the tool face are not affected by the variation in the shear angle. Two expressions for the shear angle relationship were suggested by Merchant.

$$2\phi + (\beta - \alpha) = 90^0 \qquad [2.26]$$

$$2\phi + (\beta - \alpha) = C \qquad [2.27]$$

In deriving equation [2.26] Merchant assumed that the shear stress τ_s is a material constant. On the other hand, in deriving equation [2.27] he assumed that (τ_s) would vary linearly with the normal compressive stress (σ_s) on the shear plane. The constant C was called the machining constant. Merchant's second solution, equation [2.27] proved more successful than the first in describing the experimental data. The average value of the machining constant C was approximately 75^0.

Lee and Shaffer (7, 8) assumed that the material under cutting conditions would behave as an ideal plastic solid and that the shear plane is in the direction of maximum shear stress. Assuming

a uniform stress field in the vicinity of the tool point and applying the slip line field theory, Lee and Shaffer arrived at a solution of the form

$$\phi + (\beta - \alpha) = 45^0 \qquad [2.28]$$

The same equation [2.28] was suggested earlier by Krystoff in 1939.

Equation [2.28] would yield a shear angle ϕ = zero for a friction angle $\beta = 45^0$ and a zero rake angle, and it is a poor description of experimental data. Stabler (9) in 1951 formulated another shear angle relationship based on the assumption that the maximum shear stress and shear strain are collinear on the shear plane.

$$\phi + \beta - \frac{\alpha}{2} = 45^0 \qquad [2.29]$$

Hucks (10) developed a shear angle relationship based on the assumption that there is a uniform distribution of stresses on the tool face and the shear plane, the shear plane is the direction of maximum shear stress, and that the normal stress on a plane perpendicular to the tool face is zero.

$$\phi = 45^0 - \frac{\tan^{-1} 2\mu}{2} + \alpha \qquad [2.30]$$

Shaw, Cook and Finnie (10) suggested a shear angle relationship of the form

$$\phi = 45^0 - \beta + \alpha + \gamma \qquad [2.31]$$

where η' represents the angle between the shear plane and the direction of the maximum shearing force, assuming that the shear plane does not coincide with the direction of maximum shear stress due to the interconnection between the shear and friction processes.

Kronenberg (1) proposed a shear angle relationship by establishing a direct relationship between the cutting ratio r_c and the coefficient of friction.

$$\tan \phi = \frac{\cos \alpha}{e^{\mu(\frac{\pi}{2} - \alpha)} - \sin \alpha} \qquad [2.32]$$

Colding (11) in 1958 presented a shear angle relationship introducing some measure of the anisotropic behaviour of the material into the cutting solution.

$$\phi + (\beta - \alpha) = \tan^{-1} \left[\frac{-2 \left(\frac{F}{H} + 2\right)}{\left(\frac{F}{H} + 1\right)} \cot 2\Omega \right] \qquad [2.33]$$

where F, H are parameters of anisotropy of the workpiece material

Ω = the angle between the shear plane and the direction of maximum principal stress

Mention should be made of the admirable work of Oxley and co-workers (12,13,14, 15,16) in which the Hencky equations were adapted to allow for the strain hardening effects on the material flow. Oxley was able to construct an orthogonal net of slip lines to which he applied the Hencky equations. The correlation between the theory and the experimental results was very much improved due to the introduction of empirical equations to describe the mechanical properties of the particular material under consideration based on a wide range of material tests.

Kobayashi and Thomsen (2) made a re-evaluation of the metal cutting analysis and introduced a new representation of the theories by using dimensional analysis and using the limit load theorems. They also introduced new parameters such as machinability and effectiveness factors.

Albercht (17)contributed to a better understanding of the mechanics of the cutting process by considering the ploughing force. This force occurs because of the finite sharpness of the cutting edge. He also suggested abandoning the assumption of collinearity of the resultant force on the tool face and the shear plane. Kececioglu (18-19) derived a relationship from which the average shear strain rate in the shear zone may be calculated and also a method for determining the average shear zone thickness. The average shear zone thickness was found to vary from 0.0007 to 0.007 in., and

the average shear strain rate varied from 2500 to 212,000 per sec. The shear flow stress was found to be from 2.3 to 3.25 times the static shear flow stress. These results were obtained when dry machining SAE 1015 steel.

Many attempts have been made to correlate the plastic deformation in the cutting process with the results of conventional static material tests. Lapsley (20) provided a reasonable correlation between the metal cutting data and the results of static tensile tests but the experimental range was rather limited.

Bastein and Weisz (21) also attempted an experimental correlation between the metal cutting data and pure torsion tests. Their results show a correlation in particular cases and also that this correlation is more satisfactory for materials with a low degree of work hardening.

Kobayashi et al (22) provided some new data to correlate the metal cutting tests with the experimental findings of compression tests. Their analysis was based on the effective stress-effective strain concept. They found a good correlation between the plastic-flow properties and the metal cutting data for ductile alloys.

2.3 General conclusion

The literature on the fundamental mechanics and physics of the cutting process is immense. The comments made in this discussion are just a brief mention of some references which cover some of the basic analysis. A test usually employed to compare the theoretical solutions with the experimental

findings is to plot the shear angle ϕ against $(\beta - \alpha)$. In most cases there is a marked disagreement between the experimental data and the theoretical solutions. The origin of these discrepancies may principally be due to the unwarranted idealization of some of the solutions and also to over-generalisation in trying to provide a cutting solution that would cover as wide a range as possible of the different materials being machined. Care should be taken to introduce the mechanical properties peculiar to the particular material being machined into the solution. As pointed out by Hill (23) the search for a unique steady state solution in the cutting problem is misplaced.

CHAPTER III

Machining of polymers

Orthogonal cutting is a special case of the general process of oblique cutting. Most machining operations such as turning, shaping planing, occur under semi-orthogonal conditions. Single point orthogonal cutting is relatively easy to conduct and analyse. It can also provide detailed information about the behaviour of the material being cut under controlled conditions of deformation. Orthogonal cutting is a useful first step analysis to the more complicated cutting processes such as milling, drilling and sawing, in which multiple cutting edges contribute to the cutting action.

The deformation in the cutting process is influenced by the choice of the cutting variables, speed, feed, depth of cut and by the cooling system. The cutting tool geometry and its material can also play an important part in controlling the deformation characteristics.

The workpiece material and its mechanical and thermal properties are the main factors that control the mode of deformation in cutting.

3.1 Mechanical properties

Polymers exhibit a very wide range of mechanical states at room temperature and also a wide mechanical response under the conditions of deformation.

As pointed out by Kazanskii (24), a fundamental feature of polymeric materials is the flexibility of the chains of the macromolecules which comprise them and the relaxation processes, of varying duration, connected with this flexibility. Since the molecules are not able to change shape sufficiently rapidly, the material becomes more rigid the more rapidly the deformation occurs.

Ductile thermoplastics, such as polyurethane, polyamide, polyethylene and polytetrafluoroethylene, show large elongations at fracture, while other thermoplastics e.g. polymethylemethacrylate and polystyrene have intermediate values of elongations at fracture. Because of these differences, the types of chips formed in cutting and the appearance of the machined surfaces of the different polymers will vary widely (25, 26)

Polymers are rate sensitive materials and at high strain rates their ductile fracture behaviour tends to be replaced by brittle fracture. There is a direct relation between the cutting rate and the deformation rate. The ductile-brittle transition was observed by Scrutton (27) when machining perspex.

While high strains and strain rates increase the strength of polymers, temperature rise has the reverse effect, increasing the ductility. Consequently, temperature can play an important part in deciding the type of chip formed during machining. Kobayashi (25 - 26) suggested that cutting behaviour of polymeric solids can be affected by strength differential properties, i.e. their different response under tensile and compressive loading. In most polymers the compressive strength is higher than the tensile strength.

Polymers experience some degree of elastic recovery during and

after cutting (28). The elastic recovery can interfere with the cutting action. Because of the expansion of the compressed material, the friction between the material and the tool clearance face increases. Elastic recovery after machining can cause distortion of the machined surface(25-26-28)

3.2 Thermal properties

Thermal properties such as specific heat, thermal conductivity, coefficient of thermal expansion and softening temperature can influence the cutting process (25-26)

The specific heat per unit weight for polymers is usually larger than that of metals. However, because the densities of polymers are much smaller than metals, the value of the volumetric or specific heat per unit volume for polymers is smaller than metals, i.e. the temperature rise in polymers will be larger when a given quantity of heat is applied to equal volumes of polymers and metals (24-25-26).

The thermal conductivity and thermal diffusivity of polymers is much smaller than that of metals. Therefore a very small amount of the heat generated during machining will be removed by the polymer. Only the surface of the polymer will experience a temperature rise while the bulk of the material is not affected (24) The low value of thermal conductivity can cause a problem when machining polymers, e.g. burning and gumming.

The coefficients of thermal expansion of polymers are much greater than for metals. It was suggested by Kobayashi (25-26) and Kazanskii (24) that the expansion of the heated polymer against the cutting tool increases the friction force and consequently

the amount of heat generated.

Polymers also have low softening points and their degradation temperatures are relatively low which can affect the accuracy of the machined surfaces (24)

3.3 Chip formation

It was suggested by Kobayashi (25-26-29-30-31), and Kazanskii (24) that the types of chips produced during the cutting of polymers can be classified into two main types. The first is continuous, which can be either a continuous flow type or a continuous shear type. The other main class of chip formation is discontinuous which in turn can be subdivided into three types, simple shear chip, complex crack chip and hetrogeneous crack chip.

3.3.1 Continuous flow chip

The continuous flow chip occurs with polymers which exhibit high elastic deformation when deformed at low strain rates. The thickness of the deformed chip is approximately equal to the depth of cut. This chip formation is different from the continuous chip produced when machining metals. Kobayashi suggested that it is a result of the high elastic deformation and not plastic flow (29).

The continuous flow chip was observed when cutting polytetrafluro-ethylene at low cutting speeds and produced a high quality machined surface.

3.3.2 Continuous shear chip

The continuous shear chip is produced by the generation of successive shear planes at small shear intervals in the direction of minimum work. The thickness of the deformed chip is greater than the depth of cut. It also produces good quality machined surfaces (25-26-29).

The chip is very similar to that produced when cutting ductile metals (25-26-30).

The continuous-shear chip was observed when cutting polystyrene with a tool having a rake angle of 10^0 cutting speed of 0.2 m/min and a depth of cut of 0.25 mm.

3.3.3 Discontinuous simple-shear chip

Formed by shearing action along a shear plane, but the shear intervals are rather large and discontinuous chips are formed (25-26-29-30-31-32).

The quality of the machined surface is poor. This type of chip formation was observed when cutting hard polymers like polymethylemthacrylate with a tool rake angle of 10^0, cutting speed of 0.8 m/min and a depth of cut of 0.5 mm.

3.3.4 Discontinuous complex-crack chip

Formed as a result of a combination of high stresses with elastic and brittle fractures. The multiple action of compressive, tensile and shear stresses produce this chip when large negative values of the tool rake angle are used (24-25-26).

The dimensional accuracy of the machined surface is poor and a sticky cutting action has been observed (25-26-31).
The complex-crack chip formation was obtained when cutting polystyrene with a tool having a negative rake angle of 30^0 at a cutting speed of 0.2 m/min and a depth of cut of 0.25 mm.

3.3.5 The hetrogeneous crack chip

This type of chip occurs as a result of a combination of elastic and brittle fractures. The hetrogeneous crack chip can be observed when cutting brittle polymers like polymethylmethacrylate, polystyrene and thermosetting materials(24-25-26-29-31).
Crack occurs at an oblique downward angle and a discontinuous chip is produced. The hetrogeneous chip is never observed when cutting metals. The quality of the machined surface is very poor (24-25-26).

3.4 Tool geometry and tool material

3.4.1 Rake angle

The value of the tool rake angle is one of the most important factors that have a direct influence on the deformation mode in the cutting process. The rake angles control the type of chip produced by machining. Generally, the force (F_t) changes direction from positive to negative as the rake angle varies from

negative to positive (31). When cutting with a tool having a negative rake angle the material experiences a compressive stress. However, when a positive rake angle is used the stresses change to tensile. Positive rake angles in most cases produce a continuous chip formation and as the rake angle decreases the tendency to produce discontinuous chips increases. Hetrogeneous crack chip formation was observed when using large positive rake angles while cutting brittle materials. The magnitudes of strain also vary with the rake angle (30).

There is always some value of the rake angle for every material which makes the feed force (F_t) equal to zero. This value of the rake angle was called the critical rake angle by Kobayashi et al (25-26-29-31).

The critical rake angle can be determined experimentally for each material for various cutting conditions (24).

In most cases, the critical rake angle is also the optimum rake angle for single-edge tools when cutting polymers to obtain the highest accuracy of the machined surfaces (25-26-29-33).

3.4.2 Clearance angle

The elastic recovery of polymers is high in the cutting process. The clearance angle is critical and should be as large as possible without affecting the strength of the cutting tool (24) A clearance angle of about 10^0 is usually sufficient for cutting most polymers.

3.4.3 Tool nose radius

The tool nose radius can influence the quality of the machined

surface and the type of chip produced. It was observed (26) that the cutting action does not occur if the depth of cut is smaller than the roundness of the tool edge, the material is compressed without producing a chip. When the depth of cut was increased to a larger value than the tool roundness, a chip begins to form.

3.4.4 Tool material

Musuki et al (33) observed that the flank wear is larger when using high speed steel tools than when using carbide tools in the cutting of hard polymers.

Depending on the properties of the polymer being machined, it was observed that some classes of carbide tools are more suitable than others. Kazaniskii (24) proposed the use of alloyed tool steel when cutting unfilled thermoplastics, and the use of only hard alloys or diamond tools when cutting high resistance polymers.

The properties of the cutting tool material can also be affected by the rise in temperature and the low heat removal rate from the cutting edge.

3.5 Cutting variables

3.5.1 Cutting speed

Cutting speed is an important factor in the cutting of polymers because of their rheological properties. The cutting speed has a direct effect on the type of chip formed and on the size and shape of the deformation zone. The cutting force (F_c) shows a

dependence on the cutting speed, first a rise in (F_c) at low speeds and then a decrease in its magnitude with increasing cutting speed (29).

The cutting speed also influences the cutting zone temperature and the friction conditions on the rake face. The decrease in the value of the cutting force can be attributed to the decrease in the material resistance with temperature rise when increasing the cutting speed.

3.5.2 Feed rate

The value of the feed rate influences the quality of the machined surface. The smaller the feed rate the better the quality of the machined surface. If very small feed rates are used, the rate of heat removal from the cutting zone becomes very small due to the low thermal conductivity of polymers. This can cause burning of thermosets; melting and gumming when machining thermoplastics.

5.3.3 Depth of cut

The quality of the machined surface generally improves with increasing the depth of cut. With small values of depth of cut the machining process tends to become a rubbing action which causes excessive temperature rise and deterioration of the machined surface quality.

3.5.4 Cooling System

Special care should be taken to maintain a high rate of heat removal from the cutting zone. The use of cutting fluids for this purpose is recommended only when it does not affect the properties

of the machined material. Liquid cooling is only used when cutting a limited number of thermoplastics. Cooling with compressed air is recommended because it does not affect the properties of the polymer being machined (24). If the cooling system is effective, continuous chips are formed and burning, gumming and other overheating effects are absent from the machined surface (25-26).

3.6 Shear angle relationship for polymers

Kobayashi (25-26-29-31-32) suggested that the deformation in orthogonal cutting of polymers occurs under a sensibly fixed volume, with the deformed chip thickness t_2 equal to the depth of cut t_1 for continuous flow type of chip. The elastic deformation predominates. As a first approximation Kobayashi used the single shear plane model and the minimum energy criterion suggested earlier by Merchant (5) shown in Figure[3.1] to describe the shear angle relationship.

$$t_1 \doteq t_2 \qquad [3.1]$$

$$r_c = 1 \qquad [3.2]$$

and $$2\phi + (\beta + \alpha) = \frac{\pi}{2} \qquad [3.3]$$

where $\beta = \tan^{-1} \mu$

μ = coefficient of friction

The friction angle β was calculated to be nearly zero and equation [3.3] becomes

$$2\phi - \alpha = \frac{\pi}{2} \qquad [3.4]$$

For $\beta = 0$ the resultant cutting force R coincides with the normal to the rake face and the magnitude of the shear plane angle (ϕ) can be calculated from the equation suggested by Merchant (5), i.e.,

$$\tan \phi = \frac{r_c \cos \alpha}{1 - r_c \sin \alpha} \qquad [3.5]$$

for $r_c = 1$

$$\tan \phi = \frac{\cos \alpha}{1 - \sin \alpha} \qquad [3.6]$$

$$\phi = \frac{\pi}{4} + \frac{\alpha}{2} \qquad [3.7]$$

For the case of continuous shear chip formation Kobayashi suggested the use of the shear angle relationship proposed by Lee and Shaffer (8) i.e.,

$$\phi + \beta - \alpha = \frac{\pi}{4} \qquad [3.8]$$

For the discontinuous shear type of chip, the shearing action is acting upwards from the tool edge at larger shear intervals to those of the continuous chip type. Positive values of ($\beta - \alpha$) will produce this discontinuous shear type of chip (29).

The hetrogeneous crack chip is produced by brittle fracture that occurs in the classical range of stored elastic energy. The crack initiates in tension by the wedge action of the tool before the inelastically deformed zone can expand.

Kobayashi et al (31) also suggested the critical rake angle concept. The critical rake angle is the tool rake angle which makes the force (F_t) equal to zero. The critical rake angle α_c varies with the kind of polymer being machined and also with the depth of cut and cutting speed.

$$\alpha_c = \beta = \tan^{-1} \frac{F}{N} \qquad [3.9]$$

Therefore, the value of the critical rake angle is influenced by the frictional behaviour of the chips on the cutting tool rake face.

Rao et al (35) also assumed a single shear plane model, a constant dynamic shear stress τ_s and that the temperature rise during cutting has a compensating effect on the plastic-flow conditions.

Rao and co-workers used the minimum energy criterion in their analysis. Again it was observed that the deformed chip t_2 is equal to the depth of cut t_1 , with a friction angle β nearly equal to zero.

$$r_c = 1$$

and $$\tan \phi = \frac{r_c \cos \alpha}{1 - r_c \sin \alpha}$$

$$\phi = \frac{\pi}{4} + \frac{\alpha}{2} \qquad [3.10]$$

Equation [3.10] is identical to equation [3.7] suggested by Kobayashi et al (29).

The tool forces can be calculated as follows,

$$F_c = R \cos \alpha \qquad [3.11]$$

$$F_t = R \sin \alpha$$

The shear stress (τ_s) can be evaluated from static tests or from cutting tests as the slope of the suggested linear relationship between the shear force (F_s) and the shear plane area (A_s).

Rubenstein et al (36) applied a theory formulated for the cutting of metals to the cutting of polymers. The theory assumes a lower boundary of the shear zone that can be represented by two intersecting planes as shown in Figure [3.2] One plane OA extends from the tool tip into the workpiece for a length (L) in the direction of cut and the other, AB is inclined to OA at an angle θ and meets the free surface of the workpiece at 45^0. OB is the Merchant shear plane which meets the plane OA at an angle ϕ, the Merchant shear angle so that,

$$L = t_1 (\cot\phi - 1) \qquad [3.13]$$

by assuming,

i) a uniformly distributed shear stress (S) acting along OA

ii) a uniformly distributed shear stress (S) acting along AB

iii) a uniformly distributed normal stress P = S on AB

iv) a mean normal stress P_1 acting on OA

Rubenstein deduced the following relations for the cutting force (F_c) and the feed force (F_t)

$$F_c = F_c^1 + b.\ S\ (2t_1 + L) \qquad [3.14]$$

$$F_t = F_t^1 + P_1\ b\ L \qquad [3.15]$$

Where F_c^1, F_t^1 are force components attributable to the finite radius of curvature of the cutting edge and b is the width of cut.

As shown by Rubenstein, this results in the angle θ being the external angle of the triangle OAB. It follows that the Merchant shear angle (ϕ) can not exceed 45^0, a result that is observed in the cutting of metals. However, in the cutting of polymers the shear angle (ϕ) often exceeds 45^0 as observed by Kobayashi (25-26-29), Rao (35) and as will be shown later in discussion, the cutting tests conducted in this thesis.

Discussion

The approach used by Kobayashi et al and Rao et al based on a single shear plane model and assuming that the energy consumed in cutting is minimum is sound in nature. The previous analysis lacks the fundamental detailed information about the mechanical and thermal properties of polymers that needs to be incorporated

in the shear angle relationship if a successful presentation of the experimental data is to be found. The suggested solutions are also too general, without enough care being taken to include the individual polymer properties and their peculiarities under the conditions of a complex deformation process.

CHAPTER IV

On the deformation of polymers

A polymer is a substance consisting of molecules characterized by repetition (neglecting end, branch junctions and other minor irregularities) of one or more types of monomeric units (37).

Polymers can be classified, according to their processing characteristics, into two main categories, thermosets and thermoplastics.

Thermosets

These materials experience an irreversible chemical transformation during moulding, after which thermosets are rigid, hard, insoluable and relatively unaffected by temperature.

Thermoplastics

A plastic that can be repeatedly softened by heating and hardened by cooling, through a temperature range characteristic of the plastic.

On a microscopic level, most polymers can exhibit either crystalline or amorphous morphology. In some cases, polymer structure can be a combination of the crystalline and amorphous morphologies.

Examples of crystalline polymers include nylons and polyethylene, while polystrene, polycarbonate and polymethylmethacrylate exhibit amorphous morphology.

4.1 Deformation of amorphous polymers

Robertson, (38, 39, 40) based his explanation of amorphous polymers yielding on a molecular flow theory, suggesting that, under an applied stress system, the polymer will exhibit a viscous like state which leads to yielding.

Litt et al (41,42) used the free volume theory to explain amorphous polymers yielding i.e., the polymer will deform when the applied stress supplies enough free volume for the plastic deformation to take place. As indicated by Li et al (43), the free volume concept is not very useful in understanding yielding, due to its inconsistancies in explaining yielding in compression. There is more than one process controlling the deformation.

4.2 Deformation of crystalline polymers

The deformation of crystalline polymers is a complicated process in which some regions of the structure may deform before other regions, this is due to the existence of amorphous regions between the crystals which can allow some relative motion. The plastic deformation is expected to take place without destroying the crystalline order, except in the case of very large deformations when the crystals may be broken down and new crystals form. The new crystals may have no specific crystallographic relationship with the original structure.

Polymer crystals can deform plastically by slip, by twinning and by martensitic transformation, but the first one is the more important, since it is capable of producing larger plastic strains that the other two (44).

A slip plane is the crystallographic plane parallel to which slip takes place, and in polymer crystals is restricted to a plane which contains the chain direction because the covalent bonds in the chain backbone remain unbroken during deformation. The slip direction is the direction in the slip plane in which slip takes place, (44).

The concepts of crystalline polymer deformation have been discussed in detail by Geil (45), Peterlin (46) and Powden (44).

4.3 Effects of hydrostatic pressure on the deformation of polymers

Many accurate observations concerning the effects of pressure on the deformation of polymers have been reported recently.

Bridgman (47) showed that polymers can exhibit a ductile behaviour induced by increasing the hydrostatic pressure. Ainbinder (48) carried out tests on ductile polymers in which the compressive yield stress showed a marked increase when increasing the hydrostatic pressure.

Holiday et al (49), reported a large increase in the tensile yield stress of polymers like polystyrene under an increasing hydrostatic pressure.

Sardar et al (50), reported measurements of the true stress and true strain during uniaxial tensile tests which allowed a more detailed examination of the validity of the microscopic flow and fracture laws of polymers. Ainbinder et al (48) related the pressure effect on polymer to the following three factors.

1. A change in the interatomic distance, since the forces of interaction between the atoms are non-linear functions of the distance between them.
2. A decrease in specific volume; in this case, conformational movements are made more difficult and consequently the high elastic deformations are reduced.
3. The finite nature of the deformation. At the yield point the deformation amounts to 10 -15% for thermoplastics and

2-3% for thermosets and under these conditions, the equations of the theory of elasticity, based on the assumption that the deformations are small, are invalid.

Polymers show a non-linear preyield region of the stress-strain curve. For this reason, it is particularly difficult to define the elastic moduli for polymers in the usual way from the curve slope.

The reported research showed a marked increase in the elastic moduli with pressure for both amorphous and semicrystalline polymers. The variation of the modulus with pressure appears to be approximately linear for many polymers. The principal reason why the moduli change more drastically with pressure for polymers than for metals is simply that the ratio of the imposed pressure to the initial tensile, shear or bulk moduli is much greater (51).

Pressure also has a large effect on the yield behaviour of many ductile polymers such as polyethylene, polypropylene and polytetrafluoroethylene. In some cases, the relationship between the yield stress and pressure is not linear. The strength differential or the difference between the tensile and compressive yield stresses in polymers can be explained as a direct consequence of the pressure effect on polymer yielding (52). The pressure dependence of the yield behaviour of amorphous polymers is much greater than that of metals. The difference is probably due to the fact that amorphous polymers yield at much higher stresses, relative to their bulk moduli than do metals (53).

Studying the hydrostatic pressure effects on polymer deformation is of potential importance in the cold-forming processing of polymers, due to the suppressing effects it has on the brittle-fracture characteristics of many amorphous polymers.

4.4 Volume Change

Whitney and Andrews (53) have made direct dilatometric measurements on polystyrene, polymethylmethacrylate, polycarbonate and polyvinyleformal, in axial compression. They observed both a volume contraction proportional to stress and a volume expansion, which depends on the extent and history of plastic yielding. As outlined by Pampillo and Davis (54) according to the principles of thermodynamics, an increase in volume of a system under an applied pressure requires work. During plastic deformation, this work is done by the applied stress. Hence, a pressure dependence of the flow stress can be expected if the change in volume is of sufficient magnitude. Li et at (43), identified several volume effects during the deformation of polymers. An instantaneous volume change can be measured during deformation. This instantaneous volume change can be separated into two parts, the elastic volume change and a plastic volume change. The plastic volume change was found positive for polymethylmethacrylate and negative for polycarbonate, both in the case of compression. Another volume change identified was the residual volume change which can be defined when the stress reaches zero. The residual volume change is found positive in polyethylene and negative in

polymethylmethacrylate and polycarbonate. As a result of these tests, it was found that while studying the effect of pressure on the flow stress for polycarbonate all these volume effects are negative. However, none of these changes can explain the pressure effect on the flow stress. Another quantity defined by Li et al (43) was the activation volume. The activation volume can be interpreted as the volume difference between the activated and the normal states of the mobile entity of the material. The activation volume is not macroscopically measurable except through the effect of pressure on the strain rate. The conclusion reached by Li (43) was that the plastic deformation of polymers under ordinary conditions is not a near-equilibrium process and that the activation volume is the only correct quantity for correlation with the pressure effects on deformation.

4.5 Plasic anisotropy

If the properties of a material are different in different directions, the material is called anisotropic. It is convenient to define two types of anisotropy; planar anisotropy which describes the variations of the mechanical properties in the plane of the sheet and normal anisotropy which describes the properties of the material through the thickness of the sheet relative to its strength in the plane of the sheet (55).

Polymers exhibit mechanical anisotropy in varying degrees according to their processing and heat treatment history. Due to the complex morphylogical structure of both crystalline and

amorphous polymers the effects of anisotropy are more pronounced. The degree of anisotropy should be related to the usually low yield stresses of polymers. Any degree of anistropy however small, should be taken into account in the analysis of polymer yielding characteristics.

4.6 Yield criteria studies of polymers

The yielding behaviour of polymers is a difficult physical property to characterise and understand. In conventional plasticity theory, yielding is defined as the onset of completely plastic deformation that follows a perfectly reversible elastic deformation. The deformation of polymers is almost always reversible in some sense. Prior to yielding polymers exhibit a non-linear stress-strain relationship. Polymer, elastic, viscoelastic and plastic behaviour show dependency on hydrostatic pressure, temperature, strain rate and deformation history.

In this section the general considerations of the classical plasticity theory as outlined by (55-56) are considered as are some of the special forms of the yield criteria suggested to describe the yielding behaviour of polymers. A more detailed consideration of the yield criteria to be used later as a base for the polymer cutting solution development, is provided in Chapter 5. The yield criteria to be used in the cutting analysis are some of the yield equations that have been used successfully to describe the yielding behaviour of polymers.

4.6.1 General considerations

A yield criterion is a hypothesis concerning the limit of elasticity under any possible combination of stresses (55). The yield criterion in a general form is a function of the six independent stress components.

$$F(\sigma_x, \sigma_y, \sigma_z, \tau_{xy}, \tau_{yz}, \tau_{zx}) = \text{Constant} \qquad [4.1]$$

The yield function F is independent of the choice of axes, for isotropic solids. The yield function F can also be represented in terms of non-varying quantities of the stress (stress-invariants), I_1, I_2 and I_3, where

$$I_1 = \sigma_x + \sigma_y + \sigma_z$$

$$I_2 = -(\sigma_x \sigma_y + \sigma_y \sigma_z + \sigma_z \sigma_x) + \tau^2_{xy} + \tau^2_{yz} + \tau^2_{zx}$$

$$I_3 = \sigma_x \sigma_y \sigma_z + 2\tau_{xy}\tau_{yz}\tau_{zx} - \sigma_x \tau^2_{yz} - \sigma_y \tau^2_{zx} - \sigma_z \tau^2_{xy}$$

The stress invariants can be written in terms of the principal stresses.

$$I_1 = \sigma_1 + \sigma_2 + \sigma_3 \qquad [4.2]$$

$$I_2 = -(\sigma_1\sigma_2 + \sigma_2\sigma_3 + \sigma_3\sigma_1) \qquad [4.3]$$

$$I_3 = \sigma_1\sigma_2\sigma_3 \qquad [4.4]$$

The mean of the normal stresses, i.e. $I_{1/3}$ is called the hydrostatic stress.

If the yield function [4.1] is independent of the hydrostatic component of the stress, it is possible to express F in a reduced form, obtained by taking away ($I_1/3$) from the original stress system.

The stress invariants can then be written as,

J_1, J_2, and J_3

$$J_1 = 0 \qquad [4.5]$$

$$J_2 = \frac{1}{3} [I_1^2 + 3I_2] \qquad [4.6]$$

$$J_3 = \frac{1}{27} [2 I_1^3 + 9 I_1 I_2 + 27 I_3] \qquad [4.7]$$

where J_1, J_2 and J_3 are described as the first, second and third invariants of the reduced stresses. The yield function F can be written as,

$$F (J_2, J_3) = \text{constant} \qquad [4.8]$$

If the absolute magnitudes of the tensile and compressive yield stresses are equal the yield function F, is only a function of the second invariant of the reduced stress, J_2 only

$$F (J_2) = \text{constant} \qquad [4.9]$$

Equation [4.9] represents the familiar form of Von-Mises yield criterion. In terms of the six components of the stress tensor,

equation [4.9] could be written as,

$$(\sigma_x - \sigma_y)^2 + (\sigma_y - \sigma_z)^2 + (\sigma_z - \sigma_x)^2 + 6(\tau^2_{xy} + \tau^2_{yz} + \tau^2_{yz}) = 2Y^2 \quad [4.10]$$

where Y = yield stress in tension and compression.

A simpler yield criterion has been proposed by Tresca (1864), based on the assumption that yielding would occur when the maximum shear stress reaches a critical value.

$$|\sigma_1 - \sigma_3| = \text{constant} \quad [4.11]$$

$$\sigma_1 > \sigma_2 > \sigma_3$$

In his review of the yield behaviour of polymers, Ward (57) concluded that the use of the Von-Mises and Tresca yield equations to describe the yielding behaviour of polymers has not been successful for three main reasons:-

1. Lack of isotropy
2. Dependence on pressure
3. A Bauschinger effect

A number of modifications have been introduced to both the Von-Mises and Tresca yield equations to include the anisotropic, pressure and Baschinger effects.

4.6.2 Isotropic polymers

Sternstein (58) and Bauwens (59) proposed yield equations for polymers based on the octahedral shear stress concept. As proposed by Nadai (3), the octahedral shear stress is a function of the mean normal stress.

Bauwens (59) expressed the proposed yield equation as,

$$\tau_o + A\,p = f(\dot{e}, T) \qquad [4.12]$$

where

A = constant

p = hydrostatic stress

T = temperature

$\dot{e}$ = strain rate

τ_o = octahedral shear stress

Equation [4.12] reduces to the Von-Mises yield criterion when the hydrostatic stress vanishes.

The yield criterion expressed in equation [4.12] provided a good fit to the experimental data obtained by direct compression and tension-torsion tests for polyvinyl-chloride (59).

Equation [4.12] also predicts that the tensile yield stress σ_t must differ from the compressive yield stress σ_c and that,

$$\frac{\sigma_t}{\sigma_c} = \frac{2 - A}{2 + A} \qquad [4.13]$$

Sternstein (58) expressed his yield equation as,

$$\tau_{oct} = \tau_o - \mu \sigma_m \qquad [4.14]$$

where τ_{oct} = octahedral shear stress

$\sigma_m = \frac{\sigma_1 + \sigma_2 + \sigma_3}{3}$ = mean normal stress

$\tau_{o,\mu}$ = rate and temperature-dependent material constants

Equation [4.14] also reduces to the Von-Mises yield equation by setting $\mu = 0$.

The dependence of the yield criterion [4.14] on σ_m implies that the isotropic component of the stress tensor alters the shear stress at which yielding would occur. The magnitudes of the uniaxial tension and uniaxial compression yield stresses are not equal.

$$\frac{C}{T} = \frac{2 + \mu}{2 - \mu} \qquad [4.15]$$

where C = compressive yield stress

T = tensile yield stress

Eqaution [4.14] provided a good fit to the experimental results for polymethylmethacrylate.

The yield equations [4.12] and [4.14] are based on the same principle although they use different constants in the yield equations.

Whitney (53) suggested a yield criterion based on a modification to the Tresca yield equation. The yield equation takes the form,

$$\tau_{max} = \frac{\sigma_1 - \sigma_3}{2} = \frac{Y}{2} + \sigma_m \tan \phi \qquad [4.16]$$

σ_1 and σ_3 = maximum and minimum principal stresses respectively

τ_{max} = maximum shear stress

σ_m = mean normal stress

Y = tensile yield stress

Equation [4.16] expresses the direction of yielding (θ) or the direction of maximum shear stress as,

$$\theta = \frac{\pi}{4} + \frac{\phi}{2} \qquad [4.17]$$

i.e. the direction of yielding, θ, is inclined at more than 45° to the direction of the more positive principal stress.

Bowden (60) proposed some modifications to both the Von-Mises and Tresca yield equations by different ways of defining the shear flow stress of the material.

The Von-Mises yield equation can be written as,

$$(\sigma_1 - \sigma_2)^2 + (\sigma_2 - \sigma_3)^2 + (\sigma_3 - \sigma_1)^2 = 6\,K^2 \qquad [4.18]$$

The Tresca yield equation takes the form,

$$\frac{\sigma_1 - \sigma_3}{2} = K \qquad [4.19]$$

Where K = Shear flow stress in pure shear

The value of the shear flow stress can be determined from two assumptions:

1. Assuming a linear relationship between K and the normal pressure P_n

$$K = Ko + \mu\, P_n \qquad [4.20]$$

μ and Ko = constants

P_n = normal pressure

2. Assuming that the value of K depends on the hydrostatic component of the stress system,

$$K = K_o + \mu p \qquad [4.21]$$

where

$$p = -\frac{1}{3}(\sigma_1 + \sigma_2 + \sigma_3) \qquad [4.22]$$

Using equation [4.18] and equation [4.21] a modified Von-Mises yield eqation is obtained,

$$[(\sigma_1 - \sigma_2)^2 + (\sigma_2 - \sigma_3)^2 + (\sigma_3 - \sigma_1)^2]^{\frac{1}{2}} = 6[K_o + \mu_1 p] \qquad [4.23]$$

Using equation [4.19] and equation [4.20] the Mohr-Coulomb criterion becomes,

$$\frac{\sigma_1 - \sigma_3}{2} = K_o + \mu_2 \frac{(\sigma_1 + \sigma_3)}{2} \qquad [4.24]$$

Using equation [4.19] and equation [4.21] a modified Tresca criterion is obtained,

$$\frac{\sigma_1 - \sigma_3}{2} = Ko + \mu_3 p \qquad [4.25]$$

Equation [4.23] has a similar form to the yield equations proposed by Sternstein (58), Bauwens (59) and Nadai (3). Equation [4.24] is called the Mohr-Coulomb equation and it has been used successfully in the field of soil mechanics.

Equation [4.25] has also been used in the field of soil mechanics.

Raghava et al (61-62) have proposed a general form of a yield criterion taking into account the effects of pressure, anisotropy and the difference between the tensile and compressive yield stresses.

The isotropic pressure dependent form of the proposed yield equation is:

$$(\sigma_x - \sigma_y)^2 + (\sigma_y - \sigma_z)^2 + (\sigma_z - \sigma_x)^2 + 6(\tau^2_{xy} + \tau^2_{yz} + \tau^2_{zx}) + 2(C - T)(\sigma_x + \sigma_y + \sigma_z) = 2CT \qquad [4.26]$$

C, T = the absolute values of compressive and tensile yield stresses measured at atmospheric pressure

Equation [4.26] reduces to the Von-Mises yield equation for pressure independent materials. This yield criterion have been used successfully to describe the behaviour to isotropic-pressure dependent polymers (63-64-65-66).

4.6.3 Anisotropic polymers

Hill (56) proposed a modification to the well known Von-Mises yield equation to account for the anisotropic effects on the yielding characteristics. Hill's yield criterion take the form,

$$H(\sigma_x - \sigma_y)^2 + F(\sigma_y - \sigma_z)^2 + G(\sigma_z - \sigma_x)^2 + 2L\tau^2_{yz} + 2M\tau^2_{zx} + 2N\tau^2_{xy} = 1 \qquad [4.27]$$

where,

F, G, H, L, M and N are parameters characteristic of the current state of anisotropy.

Equation [4.27] has been very successful in describing the yielding of anisotropic metals. It has also provided an excellent fit to the deformation band direction of polyethylene terephthalate (57).

Rider and Hargreaves (67) modified the Hill-Von Mises equation [4.27] to introduce a Bauschinger effect into the yield criterion. Their modification is based on reducing the component of the applied stress in the direction of molecular alignment by a constant amount a_x,

The yield criterion becomes,

$$H(\sigma_x - a_x - \sigma_y)^2 + F(\sigma_y - \sigma_z)^2 + G(\sigma_z - \sigma_x + a_x)^2$$

$$+ 2N\ \tau_{xy}^2 + 2L\ \tau_{yz}^2 + 2M\tau_{zx}^2 = 1 \qquad [4.28]$$

For each draw ratio there were the values of four constants F, H, N and ax to be determined. This was done in the following way. A set of values of a_x increasing from zero in steps of 0.5 Kg/mm^2 were taken, and for each value of a_x the values of F, H and N were computed from the measured yield stresses at angles 0, 45^0 and 90^0 to the draw direction. Then for each draw ratio the set of constants F, H, N and a_x were chosen that provide the

best fit to the experimental data. By using this method a good fit was obtained to the experimental data for oriented polyvinylchloride.

The general form of the yield criterion proposed by Raghava (61-62) is suitable for anisotropic pressure-dependent solids. This yield criterion is a modification to the Hill - Von-Mises yield equation for anisotropic solids.

The yield equation takes the form,

$$H(\sigma_x - \sigma_y)^2 + F(\sigma_y - \sigma_z)^2 + G(\sigma_z - \sigma_x)^2 + 2N\,\tau^2_{xy} + 2L\,\tau^2_{yz}$$

$$+ 2M\,\tau^2_{zx} + K_x\sigma_x + K_y\sigma_y + K_z\sigma_z = 1 \qquad [4.29]$$

where the various parameters in equation [4.29] depend on the absolute values of the tensile and compressive yield stresses in the three reference directions.

The yield criterion, equation [4.29] has been used successfully to describe the yielding behaviour of both amorphous and cyrstalline polymers such as polycarbonate, polyvinylchloride and polyethylene.

4.7 Yield criteria for the cutting process

A number of attempts have been made to describe the yielding of polymers at macroscopic level. The cutting process is a general and complex deformation process. The yield criterion that may be expected to successfully describe the deformation in cutting

should be general enough to include the special properties of polymers under a complex stress system, and it should be able to describe the yield behaviour of a wide range of polymers with different mechanical states that are usually machined.

The yield criteria used later in the cutting analysis are equation [4.26] for isotropic pressure-dependent polymers, equation [4.29] for anisotropic pressure-dependent polymers and equation [4.27] for anisotropic pressure-independent polymers.

CHAPTER V

Theoretical background and solution development

5.1 Problem formulation and solution requirements

Material cutting is basically a deformation process, which occurs under unusual conditions when compared with other metal forming processes. A successful attempt to reach a solution for the cutting problem of polymers should be based on an individual approach to the particular polymer under consideration, trying to include its special properties into the solution.

A reasonable solution to polymer cutting should at least take into account the major part of the following considerations,

- The effect of the mechanical state of the polymer on its cutting characteristics (isotropy and anisotropy).
- The effect of the hydrostatic or normal stress on the yielding of the polymer.
- The rheological factors of polymer behaviour and their relation to the cutting process (time and temperature)
- The effects of the high strains and strain rates that occur in the cutting process on the polymer properties
- The elastic strains experienced by the material during cutting and also the effects of the elastic recovery on the geometry of the cutting zone.

The above mentioned considerations are general by nature and their importance varies in relation to the cutting process. The material properties and its mechanical state can be expected to play an important part in deciding its behaviour

during cutting. The time effect in cutting can be safely ignored due to the very short time in which the deformation occurs. The polymer properties are affected by the high strains and strain rates in the cutting process but the rise in temperature may well compensate for their effects.

The elastic strains experienced by the material and the geometrical effects of the elastic recovery in the cutting zone can play a part in the solution development. However, the complexity of the cutting zone geometry and the theoretical difficulties of trying to separate the elastic strains from the total strain using the recognised incremental theory of plasticity makes the task extremely difficult without using complicated numerical solutions which in itself can affect the accuracy of the whole solution.

The objective of any analysis is to try to define and represent the problem in a simple manner, and to find a solution that represents the real situation in an acceptable way.

5.2 Basic approach

The development of the solution to the cutting of polymers in this thesis can be summarised by the following steps.

1. A single shear plane model is assumed, i.e. a single shear plane is generated inside the material upwards from the cutting tool tip to the free surface, with a shear angle (ϕ) to the cutting direction

2. The shear plane is assumed to contain the maximum shear stress τ_s

3. The material will yield at the point of maximum shear stress. The value of the maximum shear stress (τ_s) depends on the material properties and its mechanical state.

4. In the middle portion of the chip, plane strain conditions are present. The familiar equations for axes rotation in plane strain are used to represent the stresses in the cutting zone.

$$\sigma_x = -\sigma_s + \tau_s \sin 2\phi$$

$$\sigma_y = -\sigma_s - \tau_s \sin 2\phi \qquad [5.1]$$

$$\tau_{xy} = -\tau_s \cos 2\phi$$

see Johnson (55)

5. Depending on the material properties and its mechanical state evaluated by material testing, a suitable yield criterion is used to describe the yielding characteristics of the material under consideration.

6. Assuming that the yield criterion also represents the plastic potential F (σ_{ij}). The flow rules or the incremental strains are thus derived by partially differentiating F (σ_{ij}) with respect to (σ_{ij}).

$$d\,\epsilon_{ij} = \frac{\partial F(\sigma_{ij})}{\partial \sigma_{ij}} \, d\,\lambda \qquad [5.2]$$

7. Applying equation [5.2] to the yield criterion to obtain the flow rules and also applying the plane strain conditions on the yield criterion, a special form of the yield criterion for the plane strain situation is obtained.

Plane strain conditions are,

$$d\,\epsilon_z = 0 \quad , \quad \tau_{yz} = \tau_{zx} = 0 \qquad [5.3]$$

8. Substituting equations [5.1] in the plane strain yield equation developed in 7 and using the geometrical relationship between (τ_s) and (σ_s) i.e.,

$$\sigma_s = \tau_s \tan(\phi + \beta - \alpha) \qquad [5.4]$$

a quadratic equation in τ^2_s is obtained.

9. Solving the quadratic equation in τ^2_s an equation in τ_s in terms of the material constant, (ϕ) and $(\beta - \alpha)$ is derived.

10. Using the geometry of the cutting zone and the force equilibrium

$$\tau_s = \frac{F_c \sin\phi \cos(\phi + \beta - \alpha)}{A_o \cos(\beta - \alpha)} \qquad [5.5]$$

11. Substituting the right hand side of equation [5.5] for (τ_s) and separating for $\frac{F_c}{A_o}$

an equation which represents the energy consumed in the cutting process is obtained.

12. Using the minimum energy criterion, i.e. assuming that the shear angle will be such that the energy consumed in cutting is minimum

$$\frac{\partial F_c}{\partial \phi} = 0 \qquad [5.6]$$

the shear angle relationship is derived (a relationship between (ϕ) and $(\beta - \alpha)$ that represents the cutting situation).

5.3 Solution development

Depending upon the properties and mechanical state of the polymer under consideration, a suitable yield equation is required to represent its yielding characteristics. The yield criterion must have sufficient generality to account for the wide difference in properties between polymers. In this chapter a solution is derived for the cutting of polymers based on some of the yield equations suggested for polymeric solids. The yield equations chosen have been applied successfully to describe the yielding behaviour of polymers.

The applicability of a certain yield equation to the cutting situation will be judged by comparison between the derived solution and the experimental data from cutting tests.

5.3.1 General consideration of yield criteria

Starting with the most general form of a yield criterion suggested by Raghava et al (61 - 62), for the case of anisotropic and pressured dependent polymers. This general form of the yield criterion also serves as a classification to the special cases to be investigated later in the analysis.

The yield criterion takes the general form of,

$$H(\sigma_x - \sigma_y)^2 + F(\sigma_y - \sigma_z)^2 + G(\sigma_z - \sigma_x)^2 + 2N\,\tau^2_{xy} + 2L\,\tau^2_{yz}$$

$$+ 2M\,\tau^2_{zx} + K_x\sigma_x + K_y\,\sigma_y + K_z\,\sigma_z = 1 \qquad [5.7]$$

The parameters F, G, H, L, M and N characterize the mechanical state of anisotropy in the material. K_x, K_y and K_z depend on the absolute values of the tensile and compressive yield strengths in the three reference directions.

The relations between the parameters in equation [5.7] are,

$$H + G = \frac{1}{C_x T_x}$$

$$F + H = \frac{1}{C_y T_y} \qquad [5.8]$$

$$G + F = \frac{1}{C_z T_z}$$

$$K_x = \frac{C_x - T_x}{C_x T_x}$$

$$K_y = \frac{C_y - T_y}{C_y T_y} \qquad [5.9]$$

$$K_z = \frac{C_z - T_z}{C_z T_z}$$

$$2H = \frac{1}{C_x T_x} + \frac{1}{C_y T_y} - \frac{1}{C_z T_z}$$

$$2G = \frac{1}{C_z T_z} + \frac{1}{C_x T_x} - \frac{1}{C_y T_y} \qquad [5.10]$$

$$2F = \frac{1}{C_y T_y} + \frac{1}{C_z T_z} - \frac{1}{C_x T_x}$$

$$2N = \frac{1}{\tau^2_{xy}} \qquad [5.11]$$

From the nature of equation [5.7] and its relations with equations [5.8], [5.9], and [5.10] some special cases may be noted.

1. IF $C_x = C_y = C_z = T_x = T_y = T_z$

equation [5.7] would reduce to,

$$(\sigma_x - \sigma_y)^2 + (\sigma_y - \sigma_z)^2 + (\sigma_z - \sigma_x)^2 + 6(\tau^2_{xy} + \tau^2_{yz} + \tau^2_{zx}) = 2Y^2 \qquad [5.12]$$

2. IF $C_x = T_x$, $C_y = T_y$, $C_z = T_z$ but $T_x \neq T_y \neq T_z$

equation [5.7] takes the form,

$$H(\sigma_x - \sigma_y)^2 + F(\sigma_y - \sigma_z)^2 + G(\sigma_z - \sigma_x)^2 + 2N\,\tau^2_{xy} + 2L\,\tau^2_{yz} + 2M\,\tau^2_{zx} = 1 \qquad [5.13]$$

equation [5.13] is the yield criterion proposed by Hill (56) and is a modification of Von-Mises yield equation to account for the anisotropy of the material.

3. IF $C_x = C_y = C_z$ and $T_x = T_y = T_z$ but $C_x \neq T_x$ equation [5.7] reduces to,

$$(\sigma_x - \sigma_y)^2 + (\sigma_y - \sigma_z)^2 + (\sigma_z - \sigma_x)^2 + 6(\tau^2_{xy} + \tau^2_{yz} + \tau^2_{zx}) + 2(C - T)(\sigma_x + \sigma_y + \sigma_z) = 2CT \qquad [5.14]$$

Equation [5.14] is a special form of the general equation [5.7] used when the material is isotropic but pressure sensitive. The pressure influence is accounted for by the quantity $(\sigma_x + \sigma_y + \sigma_z)$. IF $C = T$ equation [5.14] reduces to equation [5.12]

The general equation [5.7] and the special cases derived from it represent the yielding of a material under a triaxial stress system. The parameters F, G, H, N, L, M, K_x, K_y and K_z depend on the absolute values of the yield strength of the material in the three reference directions.

The parameters in equation [5.7] can be evaluated from the results of tensile and compression tests performed at different directions to a reference axis in the material.

5.3.2 Material testing considerations

The material tests required to evaluate the parameters of the yield equations are tensile and compression tests performed at various orientations with respect to a reference axis in the material. The purpose of these tests is to decide whether the mechanical state of the material is isotropic or anistropic, and also to decide experimentally if a Bauschinger effect exists.

Consider a sheet of polymer, from which the compressive and tensile properties are to be investigated at various orientations to a reference axis (x) (orientation direction for anisotropic material).

Tensile and Compression specimens are cut at various angles θ to the x direction.

These specimens would be subjected to a stress σ, at which yielding would occur.

For tensile specimens,

$$\sigma_z = \tau_{yz} = \tau_{zx} = 0 \qquad [5.15]$$

At the onset of yielding in a direction (θ) to the reference axis (x)

$$\begin{aligned} \sigma_x &= \sigma \cos^2 \theta \\ \sigma_y &= \sigma \sin^2 \theta \\ \tau_{xy} &= -\sigma \sin\theta \cos\theta \end{aligned} \qquad [5.16]$$

(Note) A parallel description applies to compression tests

5.3.2.1 Anisotropic pressure -dependent solids

Substituting equations [5.15] and [5.16] in the general equation [5.7]

$$\sigma^2[(G + H)\cos^4\theta + (H + F)\sin^4\theta + 2(N - H)\sin^2\theta\cos^2\theta] + \sigma[K_x\cos^2\theta + K_y\sin^2\theta] = 1 \qquad [5.17]$$

Equation [5.17] is a quadratic equation which predicts two roots of opposite sign and unequal magnitude for each value of (θ). In this way, theoretical curves for tensile and compressive yield stresses as a function of (θ) can be obtained, and these curves can be compared with the experimental material testing data.

The parameters of equation [5.17] can be evaluated as follows. Since equation [5.17] predicts different values of 2(N - H) for variations in (θ), if the tensile and compressive yield stresses are not equal, it may be concluded that only one condition will provide the unique value of 2(N - H). This condition is satisfied when,

$$\sigma[K_x\cos^2\theta + K_y\sin^2\theta] = 0$$

$$\tan^2\theta^* = -\frac{K_x}{K_y} \qquad [5.18]$$

(θ^*) is the value of (θ) at which the absolute values of the tensile and compressive yield stresses are equal 62). Hence to get this unique value of (N), equation [5.17] would take

the form,

$$\sigma^{*2}\ [(G + H)\ \sin^4\theta^* + (H + F)\ \sin^4\theta^* + 2(N - H)$$

$$\sin^2\theta^*\ \cos^2\theta^*\ ] + \sigma^*\ [K_x\cos^2\theta^* + K_y\sin^2\theta^*] = 1 \quad [5.19]$$

The parameters F, G, H, K_x and K_y can be evaluated from the relations [5.8],[5.9], and[5.10]

where θ^* = the value of the angle θ at which the value of tensile and compressive yield stresses are equal

σ^* = the value of the yield stress at orientation θ^*

5.3.2.2 Anisotropic solids

Substituting equations [5.15] and[5.16] in Hill's Yield Criterion equation [5.13] i.e.,

$$\sigma^2[(G + H)\ \cos^4\theta + (H + F)\ \sin^4\theta + 2(N - H)\sin^2\theta\cos^2\theta] = 1$$

[5.20]

The values of F, G, H and N can be deduced from the observed dependence of the yield stress on orientation. It may be shown that the maxima and minima of (σ) occur along the anisotropic axes, and also in directions $\bar{\theta}$ such that

$$\tan^2\bar{\theta} = \frac{N - G - 2H}{N - F - 2H} \quad [5.21]$$

Hence the value of N can be determined at orientation $\bar{\theta}$ using the value of yield stress $\sigma_{\bar{\theta}}$ at that orientation.

IF $N > F + 2H$ and $G + 2H$ the yield stress has maximum (unequal) values in the x and y directions, and minimum (equal) values in the $\bar{\theta}$ directions, Hill (56).

Hence equation [5.20] takes the form,

$$\sigma_{\bar{\theta}}^2 \left[(G + H)\cos^4\bar{\theta} + (H + F)\sin^4\bar{\theta} + 2(N - H)\sin^2\bar{\theta}\cos^2\bar{\theta}\right] = 1 \qquad [5.22]$$

For anisotropic pressure independent solids

$$C_x = T_x, \quad C_y = T_y, \quad C_z = T_z, \quad T_x \neq T_y$$

and the equations [5.8], [5.9] and [5.10] reduce to the form,

$$G + H = \frac{1}{T_x^2}$$

$$F + H = \frac{1}{T_y^2} \qquad [5.23]$$

$$G + F = \frac{1}{T_z^2}$$

$$2H = \frac{1}{T_x^2} + \frac{1}{T_y^2} - \frac{1}{T_z^2}$$

$$2G = \frac{1}{T_z^2} + \frac{1}{T_x^2} - \frac{1}{T_y^2} \qquad [5.24]$$

$$2F = \frac{1}{T_y^2} + \frac{1}{T_z^2} - \frac{1}{T_x^2}$$

5.3.2.3 Isotropic pressure dependent solids

$C_x = C_y = C_z \qquad T_x = T_y = T_z$ but $C_x \neq T_x$

Substituting equations [5.15] and [5.16] in equation [5.14]

$$\sigma^2 + (C - T)\sigma - C\,T = 0 \qquad [5.25]$$

The parameters in equation [5.25] can be evaluated from the values of the tensile and compressive yield stresses measured at atmospheric pressure.

5.3.3 The shear angle relationship

The shear angle relationship is a plot between the shear plane angle (ϕ) and the friction angle (β) - the tool rake angle (α). Such a relationship is a test usually employed to evaluate the success of the theoretical solutions in describing the experimental findings. A theoretical evaluation of the shear angle relationship can contribute important information about the cutting process by predicting the interaction between the significant geometrical quantities in material machining. The shear angle (ϕ) can be measured experimentally and from a theoretical solution the friction angle (β) can be derived for each rake angle without having to use complicated force measuring arrangements.

5.3.3.1 The shear angle relationship for pressure dependent anisotropic solids

The state of the material can be characterized as,

$$C_x \neq T_x \quad C_y \neq T_y, \quad C_z \neq T_z \quad \text{and } C_x \neq T_y \neq T_z$$

Using equation [5.7] to represent the yielding behaviour of the material,

$$H(\sigma_x - \sigma_y)^2 + F(\sigma_y - \sigma_z)^2 + G(\sigma_z - \sigma_x)^2 + 2N\tau^2_{xy}$$

$$+ 2L\tau^2_{yz} + 2M\tau^2_{zx} + K_x\sigma_x + K_y\sigma_y + K_z\sigma_z = 1 \qquad [5.7]$$

Applying the basic approach from Section (5.2) to equation [5.7] the shear angle relationship takes the form,

$$\sqrt{B^2 + CE}\ \left[CA - (B + \sqrt{B^2 + CE})\ (D + C(\cot \phi - \tan(\phi + \beta - \alpha))\right]$$

$$+ \quad ABC \quad + \quad \frac{1}{2}\ CED \quad = \quad 0 \qquad [5.26]$$

where

$$\begin{aligned} A &= K_3 \sec^2(\phi + \beta - \alpha) + 2\ K_4 \cos 2\phi \\ B &= K_3 \tan(\phi + \beta - \alpha) + K_4 \sin 2\phi \\ C &= (K_1 - K_2) \sin^2 2\phi + K_2 \\ D &= 4\ (K_1 - K_2)\ \sin 2\phi \cos 2\phi \\ E &= 4\ K_5 \end{aligned} \qquad [5.27]$$

and

$$\begin{aligned} K_1 &= \left[\ 4\ \frac{(FG + FH + GH)}{(F + G)}\ \right] \\ K_2 &= 2N \\ K_3 &= [\ K_x + K_y + K_z\ ] \\ K_4 &= \left[\ K_y + K_z\ (\frac{F - G}{F + G}) - K_x\right] \\ K_5 &= \left[\ \frac{K_z^{\,2}}{4\ (F + G)} + 1\ \right] \end{aligned} \qquad [5.28]$$

The full development leading to equation [5.26] is outlined in Appendix (A).

5.3.3.2 The shear angle relationship for anisotropic solids

The mechanical state of the material is,

$$C_x = T_x \,, \quad C_y = T_y \,, \quad C_z = T_z \quad \text{but } T_x \neq T_y \neq T_z$$

Using equation 5.13

$$H(\sigma_x - \sigma_y)^2 + F(\sigma_y - \sigma_z)^2 + G(\sigma_z - \sigma_x)^2 + 2N\,\tau^2_{xy} + 2\,\tau^2_{yz} + 2M\,\tau^2_{zx} = 1 \qquad [5.13]$$

Using the procedure outlined in section (5.2) to equation [5.13] the shear angle relationship takes the form

$$\tan\phi = \frac{[(K_1 - K_2)\,\sin^2 2\phi + K_2]}{\tan(\phi + \beta - \alpha)\,[(K_1 - K_2)\sin^2 2\phi + K_2] - 2(K_1 - K_2)\sin 2\phi \cos 2\phi} \qquad [5.29]$$

where

$$K_1 = 4\,\frac{(FG + FH + GH)}{(F + G)} \qquad [5.30]$$

$$K_2 = 2N$$

The full development leading to equation [5.29] is explained in Appendix (B).

5.3.3.3 The shear angle relationship for isotropic pressure-dependent solids

The mechanical state of the material is,

$$C_x = C_y = C_z \quad \text{and} \quad T_x = T_y = T_z \quad \text{but} \quad C_x \neq T_x$$

Using equation [5.14] to represent the yielding behaviour of the material, i.e.

$$(\sigma_x - \sigma_y)^2 + (\sigma_y - \sigma_z)^2 + (\sigma_z - \sigma_x)^2 + 6(\tau^2_{xy} + \tau^2_{yz} + \tau^2_{zx})$$

$$+ 2(C - T)(\sigma_x + \sigma_y + \sigma_z) = 2CT \qquad [5.14]$$

and applying the basic approach in section (5.2) to equation [5.14] the shear angle relationship takes the form,

$$\tan\phi = \frac{\cos^2(\phi + \beta - \alpha)}{\cos(\phi + \beta - \alpha)\sin(\phi + \beta - \alpha) + \sqrt{\tan^2(\phi + \beta - \alpha) + \frac{1}{3}(\gamma/\rho)^2}} \qquad [5.31]$$

where
$$\gamma = C + T$$
$$\rho = C - T \qquad [5.32]$$

The full development leading to equation [5.31] is shown in Appendix (C).

Chapter VI

Experimental Investigation

The purpose of the experimental investigation was to study the behaviour and cutting characteristics of crystalline and armorphous polymers in both the isotropic and anisotropic states.

In addition, the possibility of finding a solution to the cutting process of polymers based on the deformation analysis in the cutting zone was evaluated and the use in the solution of the mechanical properties peculiar to each polymer was investigated.

6.1 Materials

Two commercially available polymers were chosen for the present investigation.

1. Nylon 6 to represent crystalline polymers
2. Polycarbonate (Lexan) to represent amorphous polymers

In the as-received state both Nylon 6 and polycarbonate were in the form of a sheet of 6 mm thickness. Nylon 6 showed a degree of anisotropy even in the as-received state. Polycarbonate was essentially isotropic in the as-received state.

To be able to study the polymer mechanical properties and cutting characteristics in the anisotropic state, both Nylon 6 and polycarbonate were oriented by hot rolling to induce a state of mechanical anisotropy.

Nylon 6 did exhibit another state of mechanical anisotropy different to its as-received state. Polycarbonate showed

anisotropic behaviour after hot rolling.

6.2 Experimental procedure

The experimental investigation can be divided into three steps.

1. Hot rolling to orient the material and induce either a different degree of anisotropy to the as-received state in the case of Nylon 6, or to induce anisotropic behaviour to an essentially isotropic as-received state in the case of polycarbonate.

2. Material testing to define the mechanical properties of the polymer and its mechanical state. The material testing results obtained for each polymer are used later in developing a theoretical cutting shear angle relationship based on the analysis of the deformation in the cutting process.

3. Conducting orthogonal cutting tests, varying three cutting variables, the cutting speed, depth of cut and the rake angle. The results of the orthogonal cutting tests conducted on polymers with different properties and mechanical states formulated the base for studying the cutting characteristics of polymers under varying cutting conditions. The orthogonal cutting tests also provided the necessary data for a comparison between the suggested theoretical shear angle relationship and the experimental findings.

6.3 Material orientation

From the as-received material, sections of approximately (500 x

150 x 6) mm, were cut to be hot rolled. The size of these sections after rolling was enough to produce a set of tensile or compressive specimens cut at various angles to the orientation direction (direction of rolling).

The material sections were placed in an electric induction oven with an air circulating fan, for four hours at a steady temperature of 160^{0}C. The longitudinal side of each section was marked as the x axis, and the material was rolled with its x axis as the rolling direction.

The rolls were preheated to avoid a temperature drop on the specimen surface and to minimize specimen distortion. The thickness of the specimens was reduced from the original 6 mm to 3.5 mm in two steps.

The specimens were placed in the oven after the first rolling pass for 1 hour at 160^{0}C to relieve some of the residual stresses induced by rolling.

The second rolling pass was performed from the same point of entry of the specimens to the rolls to avoid reverse rolling. The specimens were then placed back in the oven and allowed to cool to room temperature in the oven, keeping the air circulating fan on to allow a uniform air circulation during cooling.

6.4 Material tests

The material tests conducted on Nylon 6 and polycarbonate in this investigation consisted of tensile and compression tests using specimens cut at various angles to a reference axis. The results of these tests were used to evaluate the material properties in

the plane of the sheet and gave the following information.

1. The mechanical state of the material, i.e. whether isotropic or anisotropic

2. The yield stress of the material in tension and compression

3. The dependence of the material yield stress on the angle of inclination to the reference direction in the case of anisotropic materials.

The results of the tensile and compressive tests supplied enough information to characterize the material properties and its mechanical state according to which suitable cutting solution could be chosen and the material constants in that solution evaluated.

Each material state was tested in tension and compression at seven directions to the reference axis in steps of 15^0. The values of the angles of inclination to the reference axis were (0, 15, 30, 45, 60, 75, 90) degrees.

The material sections were marked at these angles to the reference axis and then machined using a special fixture on a numerically controlled milling machine, Cincinnati 3VT-1000, to produce parallel-sided tensile specimens over their full gauge length as in figure [6.1]

Two tensile specimens were cut simultaneously. One was used in

a tensile test and the other was used to produce the compression test specimens from the gauge length.

The tensile test specimens were dumb-bell shaped with a gauge length of 54 mm and a square cross-section of 6 x 6 mm in the case of the as-received sheet and 6 x 3.5 mm cross-section in the case of the rolled sections. The compression test specimens were of the same cross-section. Three compression specimens of varying lengths were produced from the gauge length of a tensile test specimen. The lengths of the compression specimens were in the range 4 - 19 mm.

The tensile and compression specimens were tested using the same machine, a Hayes ES 100D, shown in figures [6.2] and [6.3] A load-extension curve was produced directly on the machine recorder. The machine also had the facility of an extra output socket which could drive an x-y recorder. A recorder, Hewlett Packard, Moseley 7004A was connected to the machine output socket to produce a magnified load-extension curve which allowed a higher accuracy in defining the yield point from the curve. The tensile and compression tests were conducted at a cross-head speed of 5 mm/min.

The compression specimens were compressed between hardened and ground platens on the machine and were lubricated to minimize frictional effects between the specimens and the machine platens.

6.5 Determination of yield stress

The yield load was taken as the first maximum on the load-extension curve both in tension and compression. The yield stress was determined by dividing the yield load by the current cross-sectional area at yield, which was determined by stopping the machine and measuring the area by a micrometer.

When the load-extension did not show a load drop, only a change in the slope, the yield load was taken as the point of intersection of two tangents drawn in the regions before and after the slope change.

The compression yield stress was determined for specimens with different heights and was extrapolated to infinite length to correct for end constraints (56-68).

6.6 Orthogonal cutting tests

The cutting specimens were cut from the as-received and rolled sections of both Nylon 6 and polycarbonate, and clamped on the machine such that their reference direction x coincided with the cutting direction, i.e. the axes of anisotropy in the anisotropic material coincided with the reference directions x, y and z in the cutting zone.

The orthogonal cutting tests were conducted on a Swift Summerskill planing machine shown in figure [6.4] with the specimens clamped on the machine table. The machine was equiped with a Kistler three-component dynamometer. The dynamometer produced an output charge signal proportional to the applied load in the three reference directions x, y and z. The charge signal from each channel was then fed to a Kistler 5001e charge amplifier which produced a proportional output voltage to the applied load. The amplifier output was recorded on a Medelec recording oscilloscope capable of producing a visual screen display of the force signal and also a continuous recording of the force signal on a Kodak Linagraph direct print paper. The continuous force print out was used to evaluate the forces during orthogonal cutting. By adjusting the sensitivities of the charge amplifier and the recorder the accuracy of evaluating the force signal could be increased even at very low level of forces.

The cutting tools used in this investigation were high speed steel (MoMax Cobalt ground tool bits). The tools were ground to the required values of the rake and clearance angles on a

Universal tool and cutter grinding machine, Precimax UPJ. The experimental set up is shown in figure [6.4]

The grinding wheel used was a cup-shaped Universal grinding wheel. After grinding, the tools were lapped using a diamond hand lapping tool to produce a keen cutting edge and a finish on the rake and clearance faces of better than 3 microns C.L.A.

The cutting variables investigated were, the cutting speeds, depth of cut and the rake angle. Five levels of cutting speed and depth of cut were used and six values of rake angle.

The levels used for the cutting variables investigated are shown in tables [1],[2],[3] and [4]. All the cutting tests were conducted without coolant and the cutting tools had a constant clearance angle of 10^0. The cutting conditions used were arbitrarily chosen but were intended to be as representative as possible of the orthogonal cutting process under various cutting conditions.

The cutting ratio r_c was calculated from the undeformed chip thickness t_1 (depth of cut), divided by the final chip thickness t_2, which was measured using a linear displacement transducer with a digital readout accurate to 0.001 mm shown in Figure [6.5] Under most of the cutting conditions used, the chips produced were smooth and uniform in thickness, which justified using a direct measuring method of the chip to evaluate the cutting ratio r_c. Ten measurements of each chip were performed and the average value was considered to be the deformed chip thickness t_2. The standard deviation of the ten measurements was also calculated and in most cases was less than 0.002 mm.

CHAPTER VII

Results and Discussion

7.1 Material testing results

The results described in this section were obtained by conducting direct tensile and compression tests on specimens cut at different angles to a reference direction (x), on polycarbonate and Nylon in both the as-received and rolled states. The results of the tests were used to define the material properties and its mechanical state which decided the type of shear angle relationship to be used and its evaluation.

7.1.1 As-received polycarbonate

Figure [7.1] shows the load-extension curve for the as-received polycarbonate. The test was conducted on a tensile specimen cut in the reference direction x. The load extension showed a maximum load after which yielding occurs. The tensile yield stress was determined by dividing the maximum load by the current cross-sectional area (68).

Figure [7.2] is the result of compression tests conducted on specimens of different height cut in the x direction. The compressive yield stress was determined by extrapolating to infinite length the compressive yield stresses of the different specimens in order to correct for end constraints (55).

Figure [7.3] is the result of tensile and compression tests on specimens cut at different angles to the reference direction (x).

The material showed a different response in tension to compression, the compressive yield stress being higher than the tensile yield stress. However, there was no dependence on the angle at which the specimens were cut.

From the material testing results on the as-received polycarbonate it can be concluded that the material is an isotropic pressure-dependent solid.

From the material testing considerations, discussed in section (5.3.2.3) , the yielding of the as-received polycarbonate can be described by equation [5.25] i.e.,

$$\sigma^2 + (C - T)\sigma - C\,T = 0 \qquad [7.1]$$

where

$$C = 81.1 \quad N/mm^2 \qquad [7.2]$$

$$T = 73.438 \quad N/mm^2$$

$$\sigma^2 + 7.662\,\sigma - 5955.822 = 0 \qquad [7.3]$$

Equation[7.3] provides a theoretical prediction of the tensile and compressive yield stresses for polycarbonate. The positive root represents the tensile yield stress, while the negative root represents the compressive yield stress. Equation [7.3] is shown in Figure [7.3] as the solid lines. It provides an excellent fit with the experimental results.

7.1.2 Rolled polycarbonate

Figure [7.4] is a load-extension curve for rolled polycarbonate for a tensile specimen cut in the rolling direction x.

Figure [7.5] represents the results of compression tests on specimens of different heights cut in the rolling direction.

Figure [7.6] shows the results of tensile and compression tests conducted on specimens cut at different angles to the rolling direction x.

From Figure [7.6] it can be seen that the material showed a different response in tension to compression and also that the value of the tensile and compressive yield stresses depend on the orientation angle θ to the rolling direction x. The material is an anisotropic and pressure dependent solid.

From the material testing considerations discussed in section (5.3.2.1), the yielding behaviour of rolled polycarbonate can be described by equation [5.17] i.e.,

$$\sigma^2[(G + H)\cos^4\theta + (H + F)\sin^4\theta + 2(N - H)\sin^2\theta\cos^2\theta]$$

$$+ \sigma[K_x \cos^2\theta + K_y \sin^2\theta] = 1 \qquad [7.4]$$

The values of the parameters G, H, F and K_x and K_y can be determined from the values of tensile and compressive yield stresses in the x and y direction, while the unique value of N can be determined from equation [5.19] i.e.,

$$\sigma^{*2}[(G + H)\cos^4\theta^* + (H + F)\sin^4\theta^* + 2(N - H)\sin^2\theta^*\cos^2\theta^*]$$

$$+ \sigma^*[K_x\cos^2\theta^* + K_y\sin^2\theta^*] = 1 \qquad [7.5]$$

As shown in Figure [7.6]

C_x	=	6.4	Kg/mm^2
T_x	=	8.857	Kg/mm^2
C_y	=	7.3	Kg/mm^2
T_y	=	6.758	Kg/mm^2
σ^*	=	7.1	Kg/mm^2
θ^*	=	60^0	

[7.6]

Assuming transverse isotropy i.e.

$$C_y = C_z, \quad T_y = T_z \qquad [7.7]$$

The parameters F, G, H, K_x, K_y in equation [7.4] can be determined from equations[5.8],[8.9] and [5.10] i.e.

$$G + H = \frac{1}{C_x T_x} = + 0.017641 \quad mm^4/Kg^2$$

$$F + H = \frac{1}{C_y T_y} = + 0.020270 \quad mm^4/Kg^2$$

$$G + F = \frac{1}{C_z T_z} = \frac{1}{C_y T_y} = 0.020270 \quad mm^4/Kg^2$$

$$K_x = \frac{C_x - T_x}{C_x T_x} = - 0.043345$$

$$K_y = \frac{C_y - T_y}{C_y T_y} = + 0.010986 \qquad [7.8]$$

$$K_z = \frac{C_z - T_z}{C_z T_z} = \frac{C_y - T_y}{C_y T_y} = + 0.010986$$

$$2H = \frac{1}{C_x T_x} + \frac{1}{C_y T_y} - \frac{1}{C_z T_z} = + 0.017641$$

$$2G = \frac{1}{C_z T_z} + \frac{1}{C_x T_x} - \frac{1}{C_y T_y} = + 0.017641 \quad mm^4/Kg^2$$

$$2F = \frac{1}{C_y T_y} + \frac{1}{C_z T_z} - \frac{1}{C_x T_x} = + 0.022899 \quad mm^4/Kg^2$$

Solving equation [7.5] for N using the relations [7.8]

$$N = 0.029351 \quad mm^4/Kg^2 \qquad [7.9]$$

Using the value of N from [7.9] and the relations [7.8] equation [7.4] becomes,

$$\sigma^2(0.017641\cos^4\theta + 0.02027\sin^4\theta + 0.041061\sin^2\theta\cos^2\theta)$$

$$+ \sigma(-0.043345\cos^2\theta + 0.010986\sin^2\theta) = 1 \qquad [7.10]$$

Equation [7.10] represents a theoretical prediction of the tensile and compressive yield stresses. The positive root is the tensile yield stress, while the negative root represents the compressive yield stress. The solid lines in Figure [7.6] represent the solution equation [7.10] The equation provides a good fit to the experimental results.

7.1.3 As-received Nylon

Figure [7.7] is the load-extension curve for the as-received Nylon for a tensile specimen cut in the direction of the reference axis. The load-extension curve showed no load drop, only a gradual increase in load with extension. The curve showed a change in the slope and in this case the yield load was determined as the point of intersection of the two tangents drawn in the regions before and after the change in the slope (68).

Figure [7.8] shows the results of compression tests conducted on specimens cut in the x direction. The compressive yield stress was determined by extrapolating the yield stress of specimens of different heights to infinite length (55).

Figure [7.9] shows the results of tensile and compression tests on specimens cut at different angles to the orientation direction x. The material yield stress showed a dependence on the orientation angle, but the tensile and compressive yield stresses are nearly equal. The material was treated as an anisotropic pressure independent solid.

From section (5.3.2.2) the yielding of the as-received Nylon can be described according to Hill's yield equation [5.20] ie.

$$\sigma^2 [(G + H) \cos^4\theta + (F + H) \sin^4\theta + 2(N - H) \sin^2\theta\cos^2\theta] = 1 \qquad [7.11]$$

The values of the parameters F, G and H can be evaluated from the values of the yield stress in the x and y direction. The value of N can be determined using equation [5.22] i.e.

$$\sigma_{\bar{\theta}}^2 [(G + H)\cos^4\bar{\theta} + (F + H)\sin^4\bar{\theta} + 2(N - H)\sin^2\bar{\theta}\cos^2\bar{\theta}] = 1 \qquad [7.12]$$

As shown in Figure [7.9]

$$\begin{aligned} C_x = T_x &= 2.8 \quad \text{Kg/mm}^2 \\ C_y = T_y &= 3.0 \quad \text{Kg/mm}^2 \\ \bar{\theta} &= 45^0 \\ \sigma_{\bar{\theta}} &= 2.65 \quad \text{Kg/mm}^2 \end{aligned} \qquad [7.13]$$

F, G and H can be determined from the relations [5.23] and [5.24]

Assuming transverse isotropy i.e.

$$T_y = T_z$$

$$G + H = \frac{1}{T_x^2} = 0.127551 \quad mm^4/Kg^2$$

$$F + H = \frac{1}{T_y^2} = 0.111111 \quad "$$

$$G + F = \frac{1}{T_y^2} = 0.111111 \quad "$$

$$2F = \frac{1}{T_y^2} + \frac{1}{T_y^2} - \frac{1}{T_x^2} = 0.094671 \ mm^4/Kg^2 \qquad [7.14]$$

$$2G = \frac{1}{T_z^2} + \frac{1}{T_x^2} - \frac{1}{T_y^2} = 0.127551 \quad "$$

$$2H = \frac{1}{T_x^2} + \frac{1}{T_y^2} - \frac{1}{T_z^2} = 0.127551 \quad "$$

Solving equation [7.12] for N using the relations [7.14]

$$N = 0.229244 \quad mm^4/Kg^2 \qquad [7.15]$$

Using the value of N from [7.15] and the relations [7.14] equation [7.11] becomes,

$$\sigma^2[0.127551 \cos^4\theta + 0.111111 \sin^4\theta + 0.330937 \sin^2\theta\cos^2\theta] = 1 \qquad [7.16]$$

Equation [7.16] represents a theoretical prediction of the dependence of the yield stress on the oreintation angle. The solid line in Figure [7.9] represents the solution of [7.16] and it can be seen that it closely follows the experimental results.

7.1.4 Rolled Nylon

The load-extension curve of the rolled Nylon is shown in Figure [7.10] for a specimen cut in the direction of rolling. As can be seen from the curve, no load drop was observed. The yield load was determined as the point of intersection of two tangents in the regions before and after the slope change.

Figure [7.11] shows the results of compression tests performed on specimens cut from the rolling direction. The compressive yield stress was determined by extrapolating the yield stress of specimens of different heights to infinite length.

The relation between the tensile and compressive yield stresses with the orientation angle (θ) is shown in Figure [7.12] The material yield stress showed a dependence on the orientation angle. The tensile and compressive yield stresses are nearly the same. The rolled Nylon was treated as anisotropic pressure-independent solid.

The yield equation for the rolled Nylon was determined using equation [7.11] and [7.12]

From Figure [7.12]

$$C_x = T_x = 3.6 \quad Kg/mm^2$$

$$C_y = T_y = 3.8 \quad Kg/mm^2 \qquad [7.17]$$

$$\bar{\theta} = 45^0$$

$$\sigma_{\bar{\theta}} = 3.35 \quad Kg/mm^2$$

The values of the parameters F, G and H are determinable from the relations [5.23] and [5.24]

$$\begin{aligned} G + H &= 0.077160 \quad mm^4/Kg^2 \\ F + H &= 0.069252 \quad " \\ G + F &= 0.069252 \quad " \\ 2F &= 0.061344 \quad " \\ 2G &= 0.077160 \quad " \\ 2H &= 0.077160 \quad " \end{aligned} \qquad [7.18]$$

Solving equation [7.12] for N using the relations [7.18]

$$N = 0.143587 \quad mm^4/Kg^2 \qquad [7.19]$$

Using the values of N from [7.19], equation [7.11] becomes

$$\sigma^2 [\, 0.07716 \cos^4\theta + 0.069252 \sin^4\theta + 0.210014 \sin^2\theta\cos^2\theta \,] = 1 \qquad [7.20]$$

Equation [7.20] predicts the dependence of the yield stress on the orientation angle for rolled Nylon. The solution of equation [7.20] is shown as the solid line in Figure [7.12] and it can be seen that it closely represents the experimental results.

7.2 Orthogonal cutting results

The results described in this section were obtained by conducting orthogonal cutting tests on polycarbonate and Nylon in the as-received and rolled states. The cutting conditions used for the tests are shown in tables 1, 2, 3 and 4. The orthogonal cutting data was used to study the behaviour of polymeric solids of different mechanical properties under various cutting conditions and also in evaluating the shear angle relationship suggested for each material.

7.2.1 Influence of rake angle

The effects of the rake angle on the cutting forces (F_c) and (F_t) are shown in figures [7.116] and [7.117] for as-received polycarbonate, figures [7.121] and [7.122] for rolled polycarbonate, figures [7.126] and [7.127] for as-received Nylon

and Figures [7.131] and [7.132] for rolled Nylon. The solid lines in these figures represent the predicted values of (F_c) and (F_t), discussed later in section (7.3).

The rake angle has a significant influence on (F_c) and (F_t). A sharp decrease occurs in both forces with increasing rake angle from negative to positive values for each depth of cut. The rate of decrease is higher for large values of depth of cut. (F_t) also shows a change in direction i.e., (F_t) changes from positive to negative values at a certain value of rake angle and for every depth of cut. The rake angle at which (F_t) becomes zero is known as the critical rake angle (25-26).

The influence of rake angle on the other cutting zone forces is shown in Figures [7.13] through to [7.28] for all materials used.

The rake angle has a large influence on the friction and normal forces on the rake face both (F) and (N) decreasing as the rake angle was increased from negative to positive values. The rate of decrease of (N) is larger than that of (F).

The rake angle also showed a marked influence on both the shear and normal forces on the shear plane (F_s) and (F_n). Both (F_s) and (F_n) decrease with increasing rake angle from negative to positive values for all materials used.

7.2.2 Influence of depth of cut

The influence of depth of cut on the cutting forces (F_c) and (F_t) are shown in Figures [7.114] and [7.115] for as-received polycarbonate, figures [7.119] and [7.120] for rolled polycarbonate, figures [7.124] and [7.25] for as-received Nylon, and in figures [7.129] and [7.130] for rolled Nylon. The solid lines in these figures represent the predicted values of (F_c) and (F_t) to be discussed later in section (7.3).

(F_c) and (F_t) showed a linear dependence on depth of cut, with (F_c) and (F_t) increasing with increasing depth of cut for every rake angle used.

The influence of depth of cut on the rest of the cutting zone forces is shown in Figures [7.29] through to [7.44] The depth of cut showed a similar effect on F, N, F_s and F_n to its observed effect on (F_c) and (F_t). Some departure from linearity was observed in depth of cut and friction force relationship and also in the case of depth of cut and normal force relationship.

7.2.3 Influence of cutting speed

Over the range considered cutting speed showed an influence on the cutting zone forces. Figures [7.45] through to [7.68] inclusive, show the effects of cutting speed on the cutting zone forces, for as-received polycarbonate, rolled polycarbonate, as-received Nylon and rolled Nylon.

For the as-received polycarbonate, the cutting force (F_c) showed a decrease with increasing cutting speed for each rake angle used. The effect was more pronounced when negative rake angles were used.

The cutting speed - (F_c) relationship for rolled polycarbonate showed an increase in (F_c) with increasing cutting speed, reaching a peak value of (F_c) at a cutting speed of 15 m/min, for each rake angle used. After that peak the cutting force level dropped to a practically constant value with increasing cutting speed.

In cutting as-received and rolled Nylon, the cutting force (F_c) and cutting speed were substantially independent of each other for all rake angles used.

The force perpendicular to cutting direction (F_t) showed a marked dependence on cutting speed for as-received and rolled polycarbonate. (F_t) decreased with an increase in cutting speed for each rake angle. The rate of decrease in (F_t) was smaller when positive rake angles were used. The influence of cutting speed on (F_t) for as-received and rolled Nylon was not so marked, but the same trend of a decrease in (F_t) with increasing cutting speed was observed.

The influence of cutting speed on the friction force (F) under all the cutting conditions investigated was very pronounced. The friction force (F) decrease quite sharply with cutting speed for each rake angle used with a slightly lower rate of decrease with increasing rake angle from negative to positive values.

In cutting as-received and rolled polycarbonate, the normal force on the rake face (N) decreased with increasing cutting speed, only when (-5^0, 0^0, 10^0) rake angles were used. (N) was substantially independent of cutting speed for large positive values of rake angle.

The cutting speed showed little influence on (N) when cutting as-received and rolled Nylon.

The cutting speed had little effect on the shear force (F_s) for all materials used. The shear force (F_s) stayed substantially constant with increasing cutting speed, although more fluctuation in (F_s) was observed when cutting as-received and rolled polycarbonate than when cutting as-received and rolled Nylon.

The normal force on the shear plane (F_n) showed a dependence on cutting speed. (F_n) decrease with increasing cutting speed for all rake angles used, except when cutting rolled Nylon, where (F_n) showed no marked dependence on cutting speed.

Cutting speed did not significantly affect the cutting ratio (r_c). A slight increase in (r_c) with increasing cutting speed was observed when cutting as-received polycarbonate. However, (r_c) was essentially constant for each value of rake angle when cutting rolled polycarbonate.

7.2.4 Shear and normal stresses

The influence of cutting variables, rake angle, depth of cut and cutting speed on the shear and normal stresses (τ_s) and (σ_s) are shown in Figures [7.73] through to [7.96] for all materials used.

The shear stress (τ_s) slightly decreased with increasing rake angle from negative to positive values for the as-received and rolled polycarbonate. However (τ_s) stayed essentially constant for the as-received and rolled Nylon. The shear stress (τ_s) showed a dependence on the value of depth of cut used. A small decrease in (τ_s) was observed with increasing depth of cut for all materials used.

The cutting speed showed no influence on (τ_s) for as-received and rolled polycarbonate. However (τ_s) showed a slight increase with increasing cutting speed for as-received and rolled Nylon.

The rake angle had a large effect on the normal stress on the shear plane (σ_s) for all materials used. A sharp decrease in (σ_s) was observed with increasing rake angle when cutting as-received and rolled polycarbonate. However, a more gradual decrease in (σ_s) was noticed when cutting as-received and rolled Nylon for each depth of cut and rake angle.

The depth of cut and (σ_s) relationship showed a small decrease in (σ_s) with increasing depth of cut for each rake angle used. The cutting speed had a marked influence on normal stress (σ_s) for as-received and rolled polycarbonate. (σ_s) decrease with increasing cutting speed for each value of rake angle. The

normal stress (σ_s) was essentially constant with increasing cutting speed when cutting as-received and rolled Nylon.

7.2.4.1 Effects of normal stress on shear stress

The effects of normal stress on shear stress when cutting all the materials used can be established from figures [7.97] through to [7.100]
A consistant increase in (τ_s) with increasing (σ_s) can be observed for all materials used.
Merchant (5) suggested that there is a definite increase in (τ_s) with increasing (σ_s). Shaw (10) believes that (σ_s) has a secondary significance on (τ_s). The results of this investigation on polymer cutting show that (τ_s) increases with increasing (σ_s).

7.2.4.2 Effects of shear strain on shear stress

Figures [7.101] through to [7.104] show the influence of shear strain (γ_s) on the shear stress for each material used. From these figures it can be seen that (τ_s) increases with increasing shear strain (γ_s). The experimental data showed some scatter, but the values of the shear strain were substantially constant for each value of rake angle used. The values of shear strain in polymer cutting are moderate compared with those experienced during metal cutting. However, the increase in shear stress with increasing shear strain is more consistant than in metal cutting.

7.2.4.3 Shear stress determination from cutting tests

The shear stress (τ_s) observed in machining is generally considered a material constant. An experimental correlation of the plastic deformation in conventional material tests and the plastic deformation in the cutting process for polymeric solids may not be fruitful. The theoretical difficulties of introducing the hydrostatic and anisotropic effects in the plastic deformation are complex.

The value of the shear stress for polymers may be calculated from cutting data. The shear angle (ϕ) can be determined from chip measurements as in equation [2.3] The shear plane area (A_s) can then be determined from equation[2.4] The shear force (F_s) is determined from the measured values of cutting forces (F_c) and (F_t), using the experimentally determined value of (ϕ). The shear stress can then be determined as $\tau_s = F_s/A_s$. The experimental relationships between (F_s) and (A_s) are shown in Figures[7.105] through to [7.108] for all the materials used. In this type of data a large scatter is inevitable. A linear least square regression analysis was performed on the F_s-A_s data for each cutting speed. The relationship was found to be linear with high coefficient of correlation for all materials used and at all cutting speeds investigated. The regression analysis showed that (τ_s) is dependent on cutting speed. To avoid the cutting speed effects on (τ_s) the values of (τ_s) used later in predicting the cutting forces were determined from a linear relationship between (F_s) and (A_s) for each cutting speed used.

The comments made by Rao et al (35) about shear stress determination for polymers are very much to the point. The value of the shear angle (ϕ) for each test, calculated from chip measurements, neglects the elastic deformation which is recovered after the chip passes out of the cutting zone. Consequently, the shear plane area (A_s) must actually be smaller than calculated because of the relatively large elastic deformation in polymers relative to metals. It follows that the true shear stress must be larger by an unknown amount than the calculated values, and must be regarded as approximate.

7.3 Shear angle relationship and force prediction

The validity of the shear angle relationships developed to describe the behaviour of polymers can be evaluated by their application to orthogonal cutting data. Depending on the material properties and its mechanical state, evaluated from material tests, a suitable shear angle relationship was chosen to describe the material behaviour under different cutting conditions. The validity of the suggested shear angle relationship was then compared with cutting tests results, and also with the shear angle relationships suggested by Merchant (5) and Lee-Shaffer (7).

The validity of the shear angle relationships were further checked by their ability to predict the cutting forces (F_c) and (F_t) under different cutting conditions. To arrive at an estimate of the cutting forces it is sufficient to know

the shear angle relationship, provided that the material shear stress (τ_s) is known. An estimated value of (τ_s) was calculated from orthogonal cutting results as described in section [7.2.4.3]

7.3.1 As-received polycarbonate

The results of tensile and compression tests conducted on the as-received polycarbonate showed that, the material is isotropic with different values of tensile and compressive yield stresses, i.e. the material is an isotropic pressure dependent solid.

The shear angle relationship developed for isotropic pressure dependent solids is given by equation [5.31] i.e.

$$\tan\phi = \frac{\cos^2(\phi + \beta - \alpha)}{\cos(\phi + \beta - \alpha)\sin(\phi + \beta - \alpha) + \dfrac{1}{\sqrt{\tan^2(\phi + \beta - \alpha) + \frac{1}{3}(\gamma/\rho)^2}}} \qquad [7.21]$$

where $\gamma = (C + T)$

$\rho = (C - T)$

from [7.1.1] $C = 81.1 \quad N/mm^2$

$T = 73.438 \quad N/mm^2$ [7.22]

using the values of C and T from [7.22], equation [7.21] becomes

$$\tan\phi = \frac{\cos^2(\phi + \beta - \alpha)}{\cos(\phi + \beta - \alpha)\sin(\phi + \beta - \alpha) + \dfrac{1}{\sqrt{\tan^2(\phi + \beta - \alpha) + 135.601}}} \qquad [7.23]$$

Equation [7.23] represents the shear angle relationship for the as-received polycarbonate. The results of the cutting tests conducted on this material under the cutting conditions in table (1) are shown in figure [7.109] . The solution of equation [7.23] which predicts these results is also shown. It can be seen from the figure, that equation [7.23] predicts the experimental results very closely which warrants its use to represent the shear angle relationship, for the as-received polycarbonate. The dashed lines in figure [7.109] represent the shear angle relationships suggested by Merchant (5) and Lee-Shaffer (7). Lee-Shaffer solution shows a poor prediction to the cutting data while Merchant's is relatively a better prediction. The shear angle relationship, equation [7.23] provided closer fit than either the Merchant or Lee-Shaffer solutions.

The cutting forces were also estimated using equation [7.23] The shear force (F_s) was calculated from a linear least square regression equation at a cutting speed of 15.24 m/min. (F_s) divided by the shear plane area (A_s), provided the value of the shear stress (τ_s) at different cutting conditions. Equation [7.23] and the estimated values of (τ_s) were used to estimate the cutting forces (F_c) and (F_t).

The experimental values of the cutting forces (F_c) and (F_t) together with their estimated values are shown in figures [7.110] through to [7.113] as a function of the rake angle and depth of cut.

The predicted values of the cutting forces agree reasonably

closely with the experimental data, and are sufficiently accurate to justify their use for most practical purposes.

7.3.2 Rolled polycarbonate

The results of the material tests conducted on the rolled polycarbonate show that the material exhibits a different response in tension to that of compression and also that both the values of the tensile and compressive yield stresses depended on the angle of oreintation to the reference axis. The material is an anisotropic pressure dependent solid. The shear angle relationship suggested for anisotropic pressure dependent solids is equation[5.26] i.e.

$$\sqrt{B^2 + CE}\ \left[CA - (B + \sqrt{B^2 + CE}\ )\ \{ D + C\ (\cot\phi - \tan\ (\phi + \beta - \alpha))\}\right]$$

$$+ ABC + \frac{1}{2}\ CED = 0 \qquad [7.24]$$

where

$$\begin{aligned} A &= K_3 \sec^2(\phi + \beta - \alpha) + 2\ K_4 \cos 2\phi \\ B &= K_3 \tan\ (\phi + \beta - \alpha) + K_4 \sin 2\phi \\ C &= (K_1 - K_2) \sin^2 2\phi + K_2 \\ D &= 4\ (K_1 - K_2) \sin 2\phi \cos 2\phi \\ E &= 4\ K_5 \end{aligned} \qquad [7.25]$$

and

$$K_1 = 4 \frac{(FG + FH + GH)}{(F + G)}$$

$$K_2 = 2N$$

$$K_3 = (K_x + K_y + K_z) \qquad [7.26]$$

$$K_4 = [K_y + K_z \frac{F - G}{F + G} - K_x]$$

$$K_5 = [\frac{K_z^2}{4 (F + G)} + 1]$$

From the material tests the values of the parameters in the relations [7.25] and [7.26] can be evaluated,

$$K_1 = 0.055214$$
$$K_2 = 0.058701$$
$$K_3 = 0.065317 \qquad [7.27]$$
$$K_4 = -0.030934$$
$$K_5 = 1.001488$$

Substituting [7.27] in [7.25] and solving equation [7.24] the shear angle relationship can be obtained.

The orthogonal cutting results conducted on the rolled polycarbonate are shown in figure [7.114] and also the predicted shear angle relationship equation [7.24]. From the figure it

can be seen that equation [7.24] is reasonably close to the experimental data. Although there is a difference between the experimental results and the solution of equation [7.24], the equation accurately predicts the slope of the experimental data. The dashed lines in figure [7.114] represent the shear angle relationships suggested by Merchant (5) and Lee-Shaffer (7). It can be seen that these solutions are a poor prediction of the experimental data. Equation [7.24] is a better prediction than both the suggested relationships by Merchant and Lee - Shaffer.

In a similar manner to that outlined in[7.3.1]for the as-received polycarbonate, the cutting forces (F_c) and (F_t) were calculated. The experimental and predicted force values are shown in figures [7.115] through to [7.118] The predicted values of the cutting forces agree reasonably with the experimental values.

7.3.3 As-received Nylon

The results of the material tests conducted on the as-received Nylon show that material yield stress showed a dependence on the oreintation angle, but the tensile and compressive yield stresses are nearly equal, i.e. the material is anisotropic but pressure independent solid.

The shear angle relationship suggested for anisotropic solids is equation [5.29] ie.

$$\tan \phi = \frac{[(K_1 - K_2) \sin^2 2\phi + K_2]}{\tan (\phi + \beta - \alpha) [(K_1 - K_2) \sin^2 2\phi + K_2] - 2 (K_1 - K_2) \sin 2\phi \cos 2\phi} \qquad [7.28]$$

where

$$K_1 = 4 \frac{(FG + FH + GH)}{(F+G)}$$

$$K_2 = 2 N$$

from the results of the material tests,

$$K_1 = 0.363781$$
$$K_2 = 0.458488 \qquad [7.29]$$

Substituting the values of K_1 and K_2 from [7.29] in equation [7.28] and solving, the shear angle relationship can be obtained.

The solution of equation [7.28] is shown as the solid line in figure [7.119] and also orthogonal cutting results obtained for the as-received Nylon under different cutting conditions shown in Table (3).

Equation [7.28] is a reasonable prediction to the experimental cutting results. The dashed lines in figure [7.119] represent Merchant and Lee-Shaffer solutions. The suggested shear angle relationship equation [7.28] is a better representation to the experimental results than Merchant and Lee-Shaffer solutions.

The estimated values of (τ_s), together with equation [7.28] were used to predict the cutting forces. The experimental and predicted values of the cutting forces are shown in figures [7.120] through to [7.123] as a function of depth of cut and rake angle. The predicted values of (F_c) and (F_t) are close to the experimental results, and are sufficiently accurate to warrant their use for most practical purposes.

7.3.4 Rolled Nylon

Material tests conducted on the rolled Nylon show that the material yield stress depends on the orientation angle, but the tensile and compressive yield stresses are nearly equal, i.e. the material is anisotropic pressure independent solid. The shear angle relationship suggested for anisotropic solids is equation [5.29] i.e.

$$\tan\phi = \frac{[(K_1 - K_2)\sin^2 2 + K_2]}{\tan(\phi + \beta - \alpha)\ [(K_1 - K_2)\sin^2 2\phi + K_2] - 2(K_1 - K_2)\cos 2\phi \sin 2\phi} \quad [7.30]$$

where

$$K_1 = 4\ \frac{(FG + FH + GH)}{(F + G)}$$

$$K_2 = 2N$$

from material tests

$K_1 = 0.222669$

$K_2 = 0.287175$ [7.31]

Substituting the values of K_1 and K_2 from [7.31] in equation [7.30] and solving, the shear angle relationship for the rolled Nylon can be obtained.
The solution of equation [7.30] is shown as the solid line in figure [7.124].
The results of orthogonal cutting tests conducted on rolled Nylon are also shown.

As shown from figure [7.124] the suggested shear angle relationship is a reasonable representation to the experimental results. The dashed lines in figure [7.124] represent Merchant and Lee-Shaffer solutions. Equation [7.30] agree more closely with the experimental results than Merchant and Lee-Shaffer solutions. Equation [7.30] were used together with the estimated values of (τ_s) to predict the cutting forces. The experimental and predicted values of the cutting forces are shown in figures [7.125] through to [7.128] as a function of depth of cut and rake angle. The predicted values of cutting forces agree closely with experimental results.

7.4 Critical rake angle determination

The purpose of any machining process is to achieve a high material removal rate and to produce a product with the required dimensional accuracy and surface finish, without introducing severe deformation by the cutting action.

Close to the cutting edge the material is subject to tensile or compressive stresses under the action of the feed force (F_t). The direction of (F_t), which affects the character of the stresses, is to a considerable extent determined by the rake angle (24). Due to the high elasticity of polymers, the recovery of the outside layers of the surface may reduce the dimensional accuracy of the machined surface and also increase the friction on the tool clearance face.

In polymer cutting, it was observed by Kobayashi (25-26-29) Rao (35) and Kazanskii (24) that the feed force (F_t) direction varies with variation in the rake angle. At a rake angle characteristic of the material being machined and the cutting conditions being used the feed force (F_t) becomes zero. Kobayashi (25) defined the value of rake angle at which (F_t) becomes zero as the critical rake angle (α_c). At rake angles which are more negative than the critical value the feed force is directed into the body of the material being cut. If, however, the rake angle is more positive than the critical value, the feed force (F_t) is directed away from the material. Forces into the material are termed positive, and forces out of the material are termed negative.

The critical rake angle (α_c) is considered to be the optimum rake angle for cutting polymers. It produces the highest accuracy of the machined surface and minimum tool wear (24-25-26). This is because the direction of the resultant cutting force coincides with the direction of cutting, which minimizes the deformation of the machined surface (24).

The zero value of (F_t) and the consequent direction change was observed when cutting polycarbonate and Nylon in both their as-received and rolled states, at all the values of cutting speed and depth of cut used in this investigation. The critical rake angle (α_c) as a function of depth of cut and cutting speed are shown in figures [7.129] through to [7.132] It can be seen from the figures that cutting speed and depth of cut have a marked effect on (α_c). The critical rake angle decreased with increasing cutting speed and also decreased with increasing depth of cut. Kobayashi (25) and Kazanshkii (24) concluded that the critical rake angle should be determined experimentally for each polymer used and at different cutting conditions. However, the results obtained in this investigation indicate that providing the feed force (F_t) can be estimated, the critical rake angle can be predicted. In section [7.3] feed forces are predicted for all materials used. The solid lines in figures [7.113],[7.118],[7.123] and [7.128] represent the predicted values of (F_t). From the figures the direction change of (F_t) can be observed.

7.5 On Polymer friction in orthogonal cutting

The nature of frictional conditions in the cutting process is very confusing, with the experimental results being unexplained satisfactorily using the available friction theories.
According to Shaw and Finnie (69) the friction picture, is viewed as being composed of three factors,

1. A mechanical interlocking of surface asperities
2. A ploughing of the surface asperities of the harder of the two metals through the softer
3. A welding of the surface asperities of the one metal to the other, resulting in metallic junctions

For relatively smooth surfaces, such as in metal cutting the frictional resistance is primarily due to the shearing of asperities (69). It was shown by Wallace (70) and Boothroyd (71) that during metal cutting when a continuous chip is formed with the absence of built-up edge, the normal pressure between the chip and the tool is sufficiently large to cause the real area of contact (A_r) to become equal to the apparent area of contact (A_a), over a region of the tool rake face. In this region, termed as the sticking region, the frictional stress is constant and equal to the shear stress of the chip material in the region. In the section from the end of the sticking region to the point where the chip loses contact with the tool, the ratio A_r/A_a is less than unity and the coefficient of friction is constant.

This is termed the sliding region (70).

The friction mechanism in these two regions is fundamentally different. In the sliding region, where the frictional contact is between the surface asperities of the chip and tool, the frictional force arises from the shearing of the juctions of the asperities. In the sticking region, bulk deformation of the lower layers of the chip takes place (71)

The theories suggested for polymer friction are very contradictory, without definitive conclusion being drawn. Bahadur and Ludema (72) provided an indirect proof of the adhesion theory of friction. According to the adhesion theory of friction, the sliding force or friction resistance to motion is due to the making and breaking of adhesive bonds between sliding bodies. Thus the sliding force (F) is proportional to the shear strength (S) of the adhesive bonds and the area of contact (A) between contacting bodies. The results reported by Bahadur et al (72) for polyethylene, polypropylene and copolymers suggested a strong connection between (A), (S) and (F) which lends support to the adhesion theory of friction (72).

Bikerman (73-74) suggested that the adhesion theory of friction is incorrect and that the deformation theory of polymer friction is the most probable.

Bikerman's (73) explanation was that the volume significantly deformed by a moving slider may be expressed as a product wdL;

w is the width of the disturbed material, d is its depth, and L is the length of the trajectory. Consequently, the work of deformation may be approximated as the product KWdL, K being a constant which depends on the mechanical properties of the two solids. Frictional force (F) is the ratio of frictional work and the path length. Hence,

$$F = K W d \qquad [7.32]$$

where both W and d are functions of the normal load N, and in many systems may be represented as,

$$W = K_1 N^m$$

$$d = K_2 N^n$$

n, m, K_1, K_2 are constants

$$F = K \; N^{m+n} \qquad [7.33]$$

The coefficient of friction (μ) can be written as,

$$\mu = \frac{F}{N} = K \; N^{m+n-1} \qquad [7.34]$$

where $1 > m + n$

From equation [7.34] it can be concluded that (μ) decreases on an increase in the normal load N.

The results of the variation of the coefficient of friction (μ) in orthogonal cutting are shown in figures [7.133] through to [7.152] for as-received and rolled polycarbonate, as-received and rolled Nylon, for different cutting speeds. From the experimental results, it can be seen that the coefficient of friction (μ) consistantly decreases with increasing the normal force (N). The solid line in these figures represents a power curve fit of the same type as equation [7.34], obtained from regression analysis. It should be noticed that in all the fitted regression equations, the exponents were less than unity which confirms Bikerman's ('73-74) results for polymer friction.

CHAPTER VIII

Conclusions and Future Work

Conclusions

1. The yield equations used in describing the material yield behaviour agree closely with the material testing data. These equations, successfully describe the anisotropic and pressure dependent behaviour of the materials used.

2. The cutting speed has a pronounced effect on the cutting characteristics of the polymers used.

3. The value of the shear stress along the shear plane (τ_s) decrease with increasing rake angle, and also decrease with increasing depth of cut. The shear stress shows a dependence on the normal stress on the shear plane (σ_s). The shear stress consistently increases with increasing (σ_s) for all polymers used. The value of the shear stress also increases with increasing shear strain.

4. The normal stress (σ_s) decreases sharply with increasing rake angle. (σ_s) shows a dependence on cutting speed when cutting polycarbonate. However, it is essentially independent of cutting speed when cutting Nylon.

5. It has been shown that a single shear plane model and the minimum energy criterion can be applied to describing the cutting behaviour of polymers. The suggested shear angle relationships show an excellent correlation with the experimental cutting data. The success of this type of equation is due to incorporating fundamental material properties into the solution.

6. The predicted values of cutting forces (F_c) and (F_t) are sufficiently accurate to warrant their use for practical applications.

7. The critical rake angle (α_c) shows a marked dependence on the material being machined and also on cutting speed and depth of cut.

8. The dependence of the coefficient of friction (μ) on the normal force (N) can be described as a power curve

$$\mu = K_1 \; N^{K_2}$$

This is in agreement with observations made by Bikerman on polymer friction.

Suggestions for future work

1. Due to the high elasticity of polymeric solids, the values of the shear angle (ϕ), based on chip measurements are affected by the amount of elastic recovery experienced by the chip after passing through the cutting zone. Consequently, the calculated values of shear stress must be considered as approximate. An evaluation of the effect of elastic recovery and elastic strain should be made.

2. The material constants used in the shear angle relationships were obtained from material tests conducted at low strain rates and room temperature. Further study should be made measuring the material properties at strain rates and temperatures closer to those experienced in the cutting process. Further studies should also be made to relate the deformation behaviour of polymers in conventional material testing to the cutting zone deformation, similar to the type of analysis done for metals using the equivalent stress-equivalent strain concept.

3. Polymers are very sensitive to temperature rise and measurements of the cutting zone temperature could be useful in avoiding the overheating effects in polymer cutting.

4. To ensure the universality of the suggested shear angle relationships, other polymers of different mechanical properties should be subjected to the same analysis using a wider experimental range.

5. There is sufficient theoretical and experimental data on the behaviour of thermosetting and filled polymers to justify a fruitful study of their cutting characteristics. This could be very useful because of their increasing use as engineering materials.

References

1. H. Kronenberg, Machining Science and applications, Pergaman Press (1966)

2. S. Kobayashi and E. G. Thomsen, ASME series B, Feb (1962), P63

3. A. Nadai, Theory of flow and fracture of solids Mc Graw - Hill (1950)

4. C. Shaw, Metal Cutting Principles, MIT Cambridge Mass. (1954)

5. M. E. Merchant, J. Applied Physics, June (1945) p267

6. M. E. Merchant, J. Applied Physics, June (1945) p318

7. E. H. Lee and B. W. Shaffer, Office of Naval Research Tech. Report No. 43 September 1949

8. E. H. Lee and B. W. Shaffer, ASME, J. of Appl.Mech. Dec. (1951) p405

9. G. V. Stabler, Proc. Instn. Mech.Engrs. London (1951) p165

10. M. C. Shaw, N. H. Cook and I. Finnie, ASME Feb(1953) p273

11. B. Colding, CIRP meeting Sept. (1958) England

12. P. L. B. Oxley, Int.J.Mech.Sci. V3, p68 (1961)

13. W. B. Palmer and P.L.B.Oxley, Proc.Instn.Mech.Engrs. V173, n24, (1959) p623

14. W. F. Hastings, P.L.B.Oxley and M. G. Stevenson, 12th Int. MTDR Conf.Manchester September (1971)

15. R. G. Fenton and P.L.B.Oxley, Proc.Inst.Mech.Engrs. Vol 183, no 22, p417 (1969) Vol 184 n49, p927 (1970)

16. P.L.B.Oxley, ASME series B, Nov. (1963) p335

17. P. Albercht, ASME series B, Nov. (1960) p348 Nov. (1961) p557

18. D. Kececioglu, ASME, Jan. (1958) p149-168

19. D. Kececioglu, ASME, series B, Feb. (1960) p79

20. J. T. Lapsley, R. C. Grassi and E. G. Thomsen ASME, October (1950) p979

21. P. Bastien and M. Weisz, Int.Instn. for Production Research, Microtecnic Vol XI, n4, p122

22. S. Kobayashi, R. P. Herzog, B. H. Eggleston and E.G.Thomsen ASME, series B, Nov. (1960) p333

23. R. Hill, J.Mech.Phys. Solids, V8, p47 (1954)

24. Yu W. Kazanskii, Sov. Plastics, n5, (1971) p78

25. A. Kobayashi, Mod Plastics, V40, July (1963) p110-186, V41, Sept. p144-152, Oct. p229-370, Nov. p121-205, Dec. p127-134, Jan. (1964) p163-222

26. A. Kobayashi, Machining of Plastics, McGraw-Hill (1967)

27. R. F. Scrutton, Int.J. of Prod.Research, V4, n1, p3 (1965)

28. J.J. Dwyer, American Machinist, Feb. 27 (1967) p131

29. A.Kobayashi and K. Saito, Interscience, John-Wiley (1964) p489

30. A. Kobayashi, Bull.Electrotechnical Lab. Tokyo, (1963) p291

31. A. Kobayashi and K. Saito, Bull. Electrotechnical lab. Tokyo, (1961) p433

32. A. Kobayashi and K. Saito, C.I.R.P.-Annalen, 11:2 Oct. (1963) p82

33. A. Kobayashi, Bull.Electrotechnical lab. Tokyo, (1963) p 837

34. M. Masuko, J. Kumabe and S. Ammi, Bull.Japan Sco. Mech. Engr. V7, n25, Feb. (1964) p209

35. U.M.Rao, J.D. Cumming and E. G. Thomsen, ASME series B May (1964) p78

36. C. Rubenstein and R. M. Storie, Int.J.M.T.Des Res., V9 (1969) p117

37. ASTM Designation D883-759

38. R. E. Robertson, J.of appl.Polymer science, 7 (1963) p443

39. R. E. Robertson, J.Chem.Phys., 44, (1966) p3950

40. R. E. Robertson, Appl.Polymer Symp., 7, (1967) p201

41. M. H. Litt, A. V. Tobolsky, J.Macromol.Sci(Phys), 1 (1967) p433

42. M. H. Litt, P. J. Koch and A. V. Tobolsky, abid.1. (1967) p587

43. J. C. H. Li, C. A. Pampillo and L. A. Davis, Battlelle Inst.Mat.Science, Colloquila, Germany 1972, Pelenum Press (1973) p239

44. P. B. Bowden and R. J. Young, J. of Mat.Science 9, (1974) p2032

45. P. H. Geil, Polymer Single Crystals, Interscience (1973)

46. A. Peterlin, J. of Polymer Science, C9 (1965) p61

47. P. W. Bridgman, J.Appl.Phys. 24, (1953) p560

48. P. W. Ainbinder, M. G. Laka and I.Y. Maiors, DOKL, AKas, Nauk. SSR 159 (1964) p1244

49. L. Holliday, J. Mann, G. A. Pogany, H.L.I.Pugh and D. A. Gun, Nature 202, 381 (1964)

50. D. Sardar, S. V. Radcliffie and E. Baer, Polymer Eng. Sci. 8 (1968) p290

51. J. A. Sauer, Polymer Eng. and Science, V17,n3 (1977)p150

52. S. V. Radcliffe, Battelle Inst.Mat.Science Colloquia, Germany (1972) Pelenum Press (1973)

53. W. Whitney and R. D. Andrews, J. of Polymer Science, C16, (1967) p2981

54. C. A. Pampillo and L. A. Davis, J. of Appl.Phys. V42, n12, (1971)

55. W. Johnson and P. B. Mellor, Engineering Plasticity, Van-Nostrand (1972)

56. R. Hill, The mathematical theory of plasticity Oxford Press, (1950)

57. I. M. Ward, J. of Material Science, 6 (1971) p1397

58. S. S. Sternstein and F. A. Myers, US-Japan seminar on the polymer solid state (1972) Marcel Dekker (1974) p539

59. J. C. Bauwens, J. of Polymer Science, A-2, V8 (1970)p893

60. P.W. Bowden and J. A. Jukes, J. of Material Science, 7 (1972) p52

61. R. S. Raghava and R. M. Caddell, int. J. of Mat.Science, V16 (1974) p789

62. R. M. Caddell, R. S. Raghava and A. G. Atkins, J. of Material science, V8, (1973) p1641

63. R. S. Raghava and R. M. Caddell, J. of Material Science 8, (1973) p225

64. R. S. Raghava and R. M. Caddell, int.J.Mech.Sci., V15 (1973) p967

65. R. M. Caddell, R. S. Raghava and A. G. Atkins, Mat.Sci. Engineering, 13, (1974) p113

66. R. S. Raghava, PhD thesis, University of Michigan (1972)

67. J. G. Rider and E. Hargreaves, J. of Polymer Sci., A-2, V7 (1969) p829

68. F. F. Rawson and J. G. Rider, J. Polymer Sci., No 33 (1971) p87

69. I. Finnie and M. C. Shaw, Trans. ASME, Nov. (1956)

70. P. W. Wallace and G. Boothroyd, J.Mech.Eng.Sci. (1964) p74

71. G. Boothroyd, J. J. Eagle and A. W. I. Chisholm, 8th MTDR Conf. Sept. (1967) p667

72. S. Bahadur and K. C. Ludema, Wear, 18, (1971) p109

73. J. J. Bikerman, American Chem.Soc.Int. Symposium Los Angeles (1974) V1, p149

74. J. J. Bikerman, J.Macromol.Sci-Rev.Macromol.Chem (1974)

Appendix (A)

Shear angle relationship for anisotropic pressure dependent solids.

The suggested yield criterion is,

$$H(\sigma_x - \sigma_y)^2 + F(\sigma_y - \sigma_z)^2 + G(\sigma_z - \sigma_x)^2 + 2N\tau^2_{xy}$$

$$+ 2L\tau^2_{yz} + 2M\tau^2_{zx} + K_x\sigma_x + K_y\sigma_y + K_z\sigma_z = 1 \qquad [A.1]$$

Assuming that equation [A.1] also represent the plastic potential.

The flow rules could be obtained by partially differentiating $F(\sigma_{ij})$ with respect to (σ_{ij}). The plastic potential is a scalar function of the stresses, from which the ratios of the components of the plastic strain increments $d\epsilon_{ij}$ are derived by partially differentiating $F(\sigma_{ij})$ with respect to σ_{ij} (55).

Thus

$$d\epsilon_{ij} = \frac{\partial F(\sigma_{ij})}{\partial \sigma_{ij}} d\lambda \qquad [A.2]$$

applying [A.2] to the yield equation [A.1]

$$d\epsilon_x = 2\, d\lambda \left[H(\sigma_x - \sigma_y) + G(\sigma_x - \sigma_z) + \frac{1}{2} K_x \right] \qquad [A.3]$$

$$d\epsilon_y = 2\, d\lambda \left[F(\sigma_y - \sigma_z) + H(\sigma_y - \sigma_x) + \frac{1}{2} K_y \right] \qquad [A.4]$$

$$d\epsilon_z = 2\, d\lambda \left[G(\sigma_z - \sigma_x) + F(\sigma_z - \sigma_y) + \frac{1}{2} K_z \right] \qquad [A.5]$$

applying the plane strain conditions on equation [A.5]
i.e.

$$d\epsilon_z = 0 \qquad \tau_{yz} = \tau_{xz} = 0 \qquad [A.6]$$

$$\sigma_z = \left[\frac{G\sigma_x + F\sigma_y - \frac{1}{2} K_z}{F + G} \right] \qquad [A.7]$$

Substituting equation [A.6] and[A.7] to the yield equation [A.1] and arranging.

$$\left[\frac{FG + FH + GH}{F + G} \right] (\sigma_x - \sigma_y)^2 + 2N \tau^2_{xy} + K_x\sigma_x + K_y\sigma_y$$

$$+ K_z \left[\frac{G\sigma_x + F\sigma_y}{F + G} \right] - \left[\frac{K_z^2}{4(F + G)} + 1 \right] = 0 \qquad [A.8]$$

Substituting the plane strain stress equation [5.1] in [A.8]

$$\sigma_x = -\sigma_s + \tau_s \sin 2\phi$$

$$\sigma_y = -\sigma_s - \tau_s \sin 2\phi \qquad [A.9]$$

$$\tau_{xy} = -\tau_s \cos 2\phi$$

$$\left[\frac{FG + FH + GH}{(F + G)}\right] 4\tau_s^2 \sin^2 2\phi + 2N\tau_s^2 \cos^2 2\phi - \sigma_s(K_x + K_y + K_z)$$

$$- \tau_s \sin 2\phi \left[K_y + K_z\left(\frac{F - G}{F + G}\right) - K_x\right] - \left[\frac{K_z^2}{4(F + G)} + 1\right] = 0$$

.....[A.10]

Substituting equation [5.4] for the relationship between (τ_s) and σ_s in equation [A.10]

$$\sigma_s = \tau_s \tan(\phi + \beta - \alpha) \qquad [A.11]$$

$$\left[\frac{FG + FH + GH}{F + G}\right] 4\tau_s^2 \sin 2\phi + 2N\tau_s^2 \cos 2\phi - \tau_s \tan(\phi + \beta - \alpha)$$

$$\left[K_x + K_y + K_z\right] - \tau_s \sin 2\phi \left[K_y + K_z \frac{F - G}{F + G} - K_x\right]$$

$$-\left[\frac{K_z^2}{4(F + G)} + 1\right] = 0 \qquad [A.12]$$

Putting

$$K_1 = 4\,\frac{(FG + FH + GH)}{(F + G)}$$

$$K_2 = 2\,N$$

$$K_3 = [\,K_x + K_y + K_z\,] \qquad [A.13]$$

$$K_4 = [\,K_y + K_z\,\frac{F - G}{F + G} - K_x\,]$$

$$K_5 = [\,\frac{K_z^{\,2}}{4\,(F + G)} + 1\,]$$

Substituting the relations [A.13] in [A.12] and arranging,

$$\tau_s^{\,2}[(K_1 - K_2)\,\sin^2 2\phi + K_2\,] - \tau_s\,[K_3\tan(\phi + \beta - \alpha) + K_4\sin 2\phi] - K_5 = 0 \qquad [A.14]$$

Solving the quadratic equation A.14 for τ_s

$$\tau_s = \frac{K_3\tan(\phi + \beta - \alpha) + K_4\sin 2\phi \pm \sqrt{(K_3\tan(\phi + \beta - \alpha) + K_4\sin 2\phi)^2 + 4K_5\,[(K_1 - K_2)\sin^2 2\phi + K_2]}}{2\,[(K_1 - K_2)\,\sin^2 2\phi + K_2\,]}$$

[A.15]

Using equation [5.5] to substitute for (τ_s)

$$\tau_s = \frac{F_c \sin\phi \cos(\phi + \beta - \alpha)}{A_o \cos(\beta - \alpha)} \qquad [A.16]$$

$$\frac{F_c \sin\phi\cos(\phi + \beta - \alpha)}{A_o\cos(\beta - \alpha)} = \frac{[K_3\tan(\phi + \beta - \alpha) + K_4\sin2\phi] \pm \sqrt{(K_3\tan(\phi + \beta - \alpha) + K_4\sin2\phi)^2 + 4K_5[(K_1 - K_2)\sin^2 2\phi + K_2]}}{2[(K_1 - K_2)\sin^2 2\phi + K_2]}$$

[A.17]

arranging [A.17] for $\frac{F_c}{A_o}$ which represent the energy per unit volume consumed in cutting

$$K_6 \frac{F_c}{A_o} = \frac{[K_3\tan(\phi + \beta - \alpha) + K_4\sin2\phi] \pm \sqrt{(K_3\tan(\phi + \beta - \alpha) + K_4\sin2\phi)^2 + 4K_5[(K_1 - K_2)\sin^2 2\phi + K_2]}}{\sin\phi\cos(\phi + \beta - \alpha)[(K_1 - K_2)\sin^2 2\phi + K_2]} \qquad [A.18]$$

K_6 = constant

applying the minimum energy criterion on equation [A.19]

$$\frac{\partial F_c}{\partial \phi} = 0$$

$$\frac{\partial F_c}{\partial \phi} = \frac{vdu - udv}{v^2} = 0 \qquad \therefore \quad vdu = udv$$

$$v = \sin\phi \cos(\phi + \beta - \alpha) \quad [(K_1 - K_2)\sin^2 2\phi + K_2]$$

$$dv = [4(K_1 - K_2)\sin\phi\cos(\phi + \beta - \alpha)\sin 2\phi\cos 2\phi]$$

$$+ [(K_1 - K_2)\sin^2 2\phi + K_2][\cos(\phi + \beta - \alpha)\cos\phi$$

$$- \sin(\phi + \beta - \alpha)\sin\phi]$$

$$u = K_3 \tan(\phi + \beta - \alpha) + K_4 \sin 2\phi$$

$$\pm \sqrt{(K_3\tan(\phi + \beta - \alpha) + K_4\sin 2\phi)^2 + 4K_5[(K_1 - K_2)\sin^2 2\phi + K_2]}$$

$$du = [K_3\sec^2(\phi + \beta - \alpha) + 2K_4\cos 2\phi]$$

$$\pm \frac{[K_3\tan(\phi + \beta - \alpha) + K_4\sin 2\phi][K_3\sec^2(\phi + \beta - \alpha) + 2K_4\cos 2\phi] + 8K_5(K_1 - K_2)\sin 2\phi\cos 2\phi}{\sqrt{(K_3\tan(\phi + \beta - \alpha) + K_4\sin 2\phi)^2 + 4K_5[(K_1 - K_2)\sin^2 2\phi + K_2]}}$$

$$vdu = udv \qquad [A.20]$$

Put

$$A = K_3\sec^2(\phi + \beta - \alpha) + 2K_4\cos 2\phi$$

$$B = K_3\tan(\phi + \beta - \alpha) + K_4\sin 2\phi$$

$$C = [(K_1 - K_2)\sin^2 2\phi + K_2] \qquad [A.21]$$

$$D = 4(K_1 - K_2)\sin 2\phi\cos 2\phi$$

$$E = 4K_5$$

Substituting equation [A.21] in [A.20] and arranging

$$\sqrt{B^2 + CE}\left[CA - \left(B + \sqrt{B^2 + CE}\right)\left(D + C(\cot\phi - \tan(\phi + \beta - \alpha))\right)\right]$$

$$+ ABC + \frac{1}{2} CED = 0 \qquad [A.22]$$

Equation [A.22] together with the relations [A.21] represent the shear angle relationship for anisotropic pressure dependent solids.

Appendix (B)

Shear angle relationships for anisotropic solids

The proposed yield criterion is Hill's yield equation for anisotropic materials.

$$H(\sigma_x - \sigma_y)^2 + F(\sigma_y - \sigma_z)^2 + G(\sigma_z - \sigma_x)^2 + 2L\tau^2_{yz}$$

$$+ 2M\,\tau^2_{zx} + 2N\,\tau^2_{xy} = 1 \qquad [B.1]$$

The hypothesis is made that the yield criterion and the plastic potential are the same. Thus,

$$d\epsilon_{ij} = \frac{\partial F(\sigma_{ij})}{\partial\,\sigma_{ij}}\, d\,\lambda \qquad [B.2]$$

applying [B.2] to [B.1] the flow rules are obtained,

$$d\epsilon_x = d\,\lambda\,[H(\sigma_x - \sigma_y) + G(\sigma_x - \sigma_z)] \qquad [B.3]$$

$$d\epsilon_y = d\,\lambda\,[F(\sigma_y - \sigma_z) + H(\sigma_y - \sigma_x)] \qquad [B.4]$$

$$d\epsilon_z = d\,\lambda\,[G(\sigma_z - \sigma_x) + F(\sigma_z - \sigma_y)] \qquad [B.5]$$

applying the plane strain conditions on equations [B.1] and [B.5]

$$d\epsilon_z = 0 \qquad \tau_{yz} = \tau_{xz} = 0 \qquad [B.6]$$

$$\sigma_z = \frac{G\,\sigma_x + F\,\sigma_y}{F + G} \qquad [B.7]$$

Substituting the equations [B.6] and [B.7] in [B.1] and arranging,

$$\left[\frac{FG + FH + GH}{F + G}\right] (\sigma_x - \sigma_y)^2 + 2N\,\tau^2_{xy} = 1 \qquad [B.8]$$

Equation [B.8] represents a plane strain yield equation for anisotropic solids (23).

Substituting the plane strain stress equations [5.1] in equation [B.8]

$$\begin{aligned} \sigma_x &= -\sigma_s + \tau_s \sin 2\phi \\ \sigma_y &= -\sigma_s + \tau_s \sin 2\phi \\ \tau_{xy} &= -\tau_s \cos 2\phi \end{aligned} \qquad [B.9]$$

$$\left[4\,\frac{FG + FH + GH}{F + G}\right] \tau_s^2 \sin^2 2\phi + 2N\,\tau_s^2 \cos^2 2\phi = 1 \qquad [B.10]$$

Put
$$\begin{aligned} K_1 &= 4\,\frac{FG + FH + GH}{F + G} \\ K_2 &= 2N \end{aligned} \qquad [B.11]$$

$$\tau_s^2 \left[K_1 \sin^2 2\phi + K_2 \cos^2 2\phi \right] - 1 = 0 \qquad [B.12]$$

Solving the quadratic [B.12] for (τ_s)

$$\tau_s = \pm \sqrt{\frac{1}{K_1 \sin^2 2\phi + K_2 \cos^2 2\phi}} \qquad [B.13]$$

Using equation [5.5] to substitute for (τ_s)

$$\tau_s = \frac{F_c \sin\phi \cos(\phi + \beta - \alpha)}{A_o \cos(\beta - \alpha)} \qquad [B.14]$$

$$K \frac{F_c}{A_o} = \frac{1}{\sin\phi \cos(\phi + \beta - \alpha) \sqrt{(K_1 - K_2) \sin^2 2\phi + K_2}} \qquad [B.15]$$

K = constant

Applying the minimum energy criterion on equation [B.15]

$$\frac{\partial F_c}{\partial \phi} = 0$$

$$\frac{\partial F_c}{\partial \phi} = \frac{u}{v} = \frac{vdu - udv}{v^2} = 0 \qquad u = 1 \quad du = 0$$

$$V = \sin\phi\cos(\phi + \beta - \alpha)\ \sqrt{(K_1 - K_2)\sin^2 2\phi + K_2}$$

$$dv = \sin\phi\cos(\phi + \beta - \alpha)\ \frac{2(K_1 - K_2)\sin 2\phi\cos 2\phi}{\sqrt{(K_1 - K_2)\sin^2 2\phi + K_2}}$$

$$+ \sqrt{(K_1 - K_2)\sin^2 2\phi + K_2}\ [\cos\phi\cos(\phi + \beta - \alpha)$$

$$- \sin\phi\sin(\phi + \beta - \alpha)]$$

$$\frac{\partial F_c}{\partial \phi} = - dv$$

$$[(K_1 - K_2)\sin^2 2\phi + K_2][\cot\phi - \tan(\phi + \beta - \alpha)] =$$

$$- 2\ (K_1 - K_2)\sin 2\phi\cos 2\phi$$

$$\cot\phi = \tan(\phi + \beta - \alpha) - \frac{2\ (K_1 - K_2)\sin 2\phi\cos 2\phi}{(K_1 - K_2)\sin^2 2\phi + K_2}$$

$$\tan\phi = \frac{[(K_1 - K_2)\sin^2 2\phi + K_2]}{\tan(\phi + \beta - \alpha)\ [(K_1 - K_2)\sin^2 2\phi + K_2] - 2\ (K_1 - K_2)\sin 2\phi\cos 2\phi} \qquad [B.16]$$

Equation [B.16] represents the shear angle relationship for anisotropic solids.

Appendix (C)

The shear angle relationship for isotropic pressure dependent solids

The proposed yield criterion is,

$$(\sigma_x - \sigma_y)^2 + (\sigma_y - \sigma_z)^2 + (\sigma_z - \sigma_x)^2 + 6(\tau^2_{xy} + \tau^2_{yz} + \tau^2_{zx})$$

$$+ 2(C - T)\ (\sigma_x + \sigma_y + \sigma_z) = 2CT \qquad [C.1]$$

Put $(C - T) = \rho$ and $C + T = \gamma$

assuming that equation [C.1] also represent the plastic potential

$$d\epsilon_{ij} = \frac{\partial F(\sigma_{ij})}{\partial \sigma_{ij}}\ d\lambda \qquad [C.2]$$

applying [C.2] to equation [C.1] to obtain the flow rules

$$d\epsilon_x = 2\, d\lambda\, [(\sigma_x - \sigma_y) + (\sigma_x - \sigma_z) + \rho] \qquad [C.3]$$

$$d\epsilon_y = 2\, d\lambda\, [(\sigma_y - \sigma_y) + (\sigma_y - \sigma_x) + \rho] \qquad [C.4]$$

$$d\epsilon_z = 2\, d\lambda\, [(\sigma_z - \sigma_x) + (\sigma_z - \sigma_y) + \rho] \qquad [C.5]$$

applying the plane strain conditions to equations [C.1] and [C.5]

$$d\epsilon_z = 0 \qquad \tau_{xz} = \tau_{yz} = 0 \qquad [C.6]$$

$$\sigma_z = \frac{\sigma_x + \sigma_y}{2} - \frac{\beta}{2} \qquad [C.7]$$

Substituting [C.6] and [C.7] in the yield equation [C.1] and arranging

$$(\sigma_x - \sigma_y)^2 + 2\beta(\sigma_x + \sigma_y) + 4\tau^2_{xy} - \frac{1}{3}\eta^2 = 0 \qquad [C.8]$$

Equation [C.8] represents the plane strain yield equation for isotropic pressure dependent solid (66).

Substituting the plane strain stress equation to equation [C.8]

$$\sigma_x = -\sigma_s + \tau_s \sin 2\phi$$

$$\sigma_y = -\sigma_s - \tau_s \sin 2\phi \qquad [C.9]$$

$$\tau_{xy} = -\tau_s \cos 2\phi$$

$$4\,\tau_s^2 \sin^2 2\phi - 4\rho\sigma_s + 4\,\tau_s^2 \cos^2 2\phi - \frac{1}{3}\,\eta^2 = 0 \qquad [C.10]$$

Substituting equation [5.4] for the relation between (τ_s) and (σ_s) in equation [C.10]

$$\sigma_s = \tau_s \tan(\phi + \beta - \alpha) \qquad [C.11]$$

$$\tau_s^2 - \rho \tan(\phi + \beta - \alpha)\,\tau_s - \frac{1}{12}\,\eta^2 = 0 \qquad [C.12]$$

Solving the quadratic [C.12] for (τ_s)

$$\tau_s = \frac{\rho}{2}\left[\tan(\phi + \beta - \alpha) \pm \sqrt{\tan^2(\phi + \beta - \alpha) + \frac{1}{3}\,(\eta/\rho)^2}\,\right] \qquad [C.13]$$

using the equation [5.5] to substitute for (τ_s)

$$\tau_s = \frac{F_c \sin\phi \cos(\phi + \beta - \alpha)}{A_o \cos(\beta - \alpha)} \qquad [C.14]$$

arranging [C.14] for $\frac{F_c}{A_o}$ which represent the energy per unit volume consumed in cutting

$$K\,\frac{F_c}{A_o} = \frac{\tan(\phi + \beta - \alpha) + \sqrt{\tan^2(\phi + \beta - \alpha) + \frac{1}{3}\,(\eta/\rho)^2}}{\sin\phi \cos(\phi + \beta - \alpha)} \qquad [C.15]$$

K = constant

applying the minimum energy criterion on equation [C.15]

$$\frac{\partial F_c}{\partial \phi} = 0 \qquad [C.16]$$

$$\frac{\partial F_c}{\partial \phi} = \frac{u}{v} = \frac{vdu - udv}{v^2} = 0 \qquad vdu = udv$$

$$v = \sin\phi\cos(\phi + \beta - \alpha)$$

$$dv = (\cos\phi\cos(\phi + \beta - \alpha) - \sin\phi\sin(\phi + \beta - \alpha))$$

$$u = \tan(\phi + \beta - \alpha) + \sqrt{\tan^2(\phi + \beta - \alpha) + \frac{1}{3}(\gamma/\rho)^2}$$

$$du = \sec^2(\phi + \beta - \alpha) + \frac{\tan(\phi + \beta - \alpha)\sec^2(\phi + \beta - \alpha)}{\sqrt{\tan^2(\phi + \beta - \alpha) + \frac{1}{3}(\gamma/\rho)^2}}$$

$$\therefore \sin\phi\cos(\phi + \beta - \alpha)\left[\sec^2(\phi + \beta - \alpha) + \frac{\tan(\phi + \beta - \alpha)\sec^2(\phi + \beta - \alpha)}{\sqrt{\tan^2(\phi + \beta - \alpha) + \frac{1}{3}(\gamma/\rho)^2}}\right]$$

$$= [\tan(\phi + \beta - \alpha) + \sqrt{\tan^2(\phi + \beta - \alpha) + \frac{1}{3}(\gamma/\rho)^2}]$$

$$[\cos\phi\cos(\phi + \beta - \alpha) - \sin\phi\sin(\phi + \beta - \alpha)]$$

arranging for $\tan \phi$

$$\tan \phi = \frac{\cos^2 (\phi + \beta - \alpha)}{\cos (\phi + \beta - \alpha) \sin (\phi + \beta - \alpha) + \dfrac{1}{\sqrt{\tan^2 (\phi + \beta - \alpha) + \frac{1}{3}}}} \qquad (\gamma/\rho)^2$$

[C.17]

equation [C.17] represents the shear angle relationship for isotropic pressure dependent solids.

Appendix (D)

Orthogonal cutting data

Table 1

Work material	:	As-received polycarbonate
Tool material	:	High speed steel
Cutting fluid	:	Dry cutting
Width of cut	:	6 mm

Table 2

Work material	:	Rolled polycarbonate
Tool material	:	High speed steel
Cutting fluid	:	Dry cutting
Width of cut	:	3.593 mm

Table 3

Work material	:	As-received Nylon
Tool material	:	High speed steel
Cutting fluid	:	Dry cutting
Width of cut	:	6 mm

Table 4

Work material	:	Rolled Nylon
Tool material	:	High speed steel
Cutting fluid	:	Dry cutting
Width of cut	:	4.05 mm

Table (1)

PH RUN NO.	V (m/min)	α (Deg)	t_1 (mm)	t_2 (mm)	F_c (N)	F_t (N)	ϕ (Deg)
1	15.24	-5	0.127	0.240	215.0	80.0	26.744
2	"	0	"	0.210	182.0	70.0	31.164
3	"	10	"	0.194	144.0	35.4	36.031
4	"	20	"	0.181	121.5	11.0	40.943
5	"	30	"	0.174	109.0	-5.0	44.866
6	"	40	"	0.163	86.0	-14.2	50.093
7	"	-5	0.2032	0.380	290.0	112.0	26.973
8	"	0	"	0.293	260.0	87.2	34.742
9	"	10	"	0.292	221.5	44.0	37.937
10	"	20	"	0.278	180.0	9.0	42.483
11	"	30	"	0.268	152.0	-13.7	46.602
12	"	40	"	0.250	126.5	-30.2	52.513
13	"	-5	0.254	0.400	346.0	136.0	30.939
14	"	0	"	0.360	312.0	97.4	35.205
15	"	10	"	0.351	250.0	46.0	39.183
16	"	20	"	0.342	210.0	7.1	43.093
17	"	30	"	0.328	171.5	-18.0	47.580
18	"	40	"	0.312	142.0	-40.0	52.606
19	"	-5	0.3048	0.435	390.0	148.0	33.339
20	"	0	"	0.425	363.0	107.4	35.647
21	"	10	"	0.420	300.0	46.4	39.274
22	"	20	"	0.410	240.0	4.2	43.130
23	"	30	"	0.395	202.0	-25.4	47.415
24	"	40	"	0.380	166.0	-50.6	51.749
25	"	-5	0.381	0.560	480.0	172.0	32.612
26	"	0	"	0.54	430.0	120.0	35.205
27	"	10	"	0.518	349.0	48.0	39.707
28	"	20	"	0.510	290.0	-4.0	43.318
29	"	30	"	0.495	236.0	-26.4	47.298
30	"	40	"	0.455	190.0	-60.0	54.252

PH RUN NO.	V (m/min)	α (Deg)	t_1 (mm)	t_2 (mm)	F_c (N)	F_t (N)	ϕ (Deg)
31	30.48	-5	0.127	0.220	202.0	75.0	28.702
32	"	0	"	0.208	180.0	52.0	31.407
33	"	10	"	0.190	143.5	23.0	36.675
34	"	20	"	0.180	120.0	2.0	41.150
35	"	30	"	0.164	100.0	-8.0	47.580
36	"	40	"	0.160	80.0	-18.0	51.148
37	"	-5	0.2032	0.300	270.0	87.6	32.503
38	"	0	"	0.290	241.0	60.0	35.019
39	"	10	"	0.282	200.0	20.0	39.046
40	"	20	"	0.270	162.0	-5.6	43.602
41	"	30	"	0.260	142.0	-25.8	48.009
42	"	40	"	0.246	120.0	-38.0	53.452
43	"	-5	0.254	0.350	312.0	95.2	34.214
44	"	0	"	0.345	297.0	67.8	36.362
45	"	10	"	0.340	230.0	19.0	40.210
46	"	20	"	0.338	198.5	-12.0	43.545
47	"	30	"	0.318	160.0	-32.2	49.032
48	"	40	"	0.290	133.0	-46.0	56.923
49	"	-5	0.3048	0.423	360.0	108.0	34.036
50	"	0	"	0.420	338.0	72.8	35.969
51	"	10	"	0.392	262.5	18.8	41.517
52	"	20	"	0.380	225.0	-18.0	46.087
53	"	30	"	0.365	180.0	-40.0	51.152
54	"	40	"	0.352	154.0	-60.0	56.239
55	"	-5	0.381	0.52	426.0	124.0	34.454
56	"	0	"	0.498	400.0	82.0	37.418
57	"	10	"	0.492	320.5	16.0	41.384
58	"	20	"	0.478	261.5	-24.4	45.839
59	"	30	"	0.469	220.0	-54.0	49.834
60	"	40	"	0.442	180.0	-76.0	55.968

PH RUN NO.	V (m/min)	α (Deg)	t_1 (mm)	t_2 (mm)	F_c (N)	F_t (N)	ϕ (Deg)
61	9.14	-5	0.127	0.200	257.5	87.8	30.939
62	"	0	"	0.190	165.0	67.0	33.760
63	"	10	"	0.187	145.4	39.2	37.171
64	"	20	"	0.180	114.0	13.05	41.150
65	"	30	"	0.161	88.8	0.0	48.444
66	"	40	"	0.148	80.0	-12.45	55.70
67	"	-5	0.2032	0.350	375.0	129.6	28.833
68	"	0	"	0.295	276.0	109.6	34.560
69	"	10	"	0.291	263.0	45.3	38.045
70	"	20	"	0.283	175.6	15.15	41.808
71	"	30	"	0.278	142.0	-7.5	44.931
72	"	40	"	0.260	127.0	-27.4	50.266
73	"	-5	0.254	0.372	435.0	152.0	32.70
74	"	0	"	0.370	327.0	127.0	34.469
75	"	10	"	0.367	313.0	55.0	37.764
76	"	20	"	0.361	206.5	16.5	41.046
77	"	30	"	0.345	176.5	-11.8	45.258
78	"	40	"	0.310	146.0	-33.2	52.980
79	"	-5	0.3048	0.454	428.0	200.0	32.286
80	"	0	"	0.450	378.0	144.0	34.111
81	"	10	"	0.435	301.5	70.2	38.154
82	"	20	"	0.420	239.5	17.0	42.211
83	"	30	"	0.418	201.5	-16.0	44.823
84	"	40	"	0.372	168.0	-40.8	52.980
85	"	-5	0.381	0.563	520.0	236.5	32.481
86	"	0	"	0.555	449.0	166.0	34.469
87	"	10	"	0.548	395.0	75.4	37.908
88	"	20	"	0.528	296.0	17.6	41.995
89	"	30	"	0.484	242.0	-22.8	48.346
90	"	40	"	0.471	212.5	-56.0	52.236

PH RUN NO.	V (m/min)	α (Deg)	t_1 (mm)	t_2 (mm)	F_c (N)	F_t (N)	ϕ (Deg)
91	22.86	-5	0.127	0.215	195.0	78.0	29.233
92	"	0	"	0.190	172.6	57.0	33.760
93	"	10	"	0.183	144.6	27.0	37.851
94	"	20	"	0.177	120.0	6.3	41.781
95	"	30	"	0.169	104.0	-8.0	46.192
96	"	40	"	0.135	76.0	-14.0	61.254
97	"	-5	0.2032	0.340	280.0	100.0	29.505
98	"	0	"	0.282	245.0	70.6	35.775
99	"	10	"	0.290	205.0	28.4	38.154
100	"	20	"	0.274	180.0	0.0	43.037
101	"	30	"	0.261	140.0	-20.0	47.830
102	"	40	"	0.257	120.0	-38.8	50.926
103	"	-5	0.254	0.354	322.5	108.0	33.929
104	"	0	"		290.0	76.6	
105	"	10	"	0.348	237.0	28.6	39.459
106	"	20	"	0.339	200.0	-5.0	43.431
107	"	30	"	0.323	167.5	-29.0	48.298
108	"	40	"	0.302	135.5	-46.0	54.511
109	"	-5	0.3048	0.428	374.0	123.2	33.742
110	"	0	"	0.419	341.5	84.0	36.034
111	"	10	"	0.408	280.5	27.3	40.210
112	"	20	"	0.400	229.0	-10.0	44.081
113	"	30	"	0.390	191.5	-38.6	48.009
114	"	40	"	0.364	153.0	-56.0	54.252
115	"	-5	0.381	0.511	446.0	139.0	34.893
116	"	0	"	0.503	405.0	96.0	37.142
117	"	10	"	0.497	330.0	25.5	41.052
118	"	20	"	0.483	274.0	-19.2	45.430
119	"	30	"	0.473	227.0	-52.0	49.431
120	"	40	"	0.462	185.0	-73.0	53.357

PH RUN NO.	V (m/min)	α (Deg)	t_1 (mm)	t_2 (mm)	F_c (N)	F_t (N)	ϕ (Deg)
121	36.58	-5	0.127	0.197	169.20	58.0	31.302
122	"	0	"	0.193	170.0	42.6	33.346
123	"	10	"	0.188	133.0	16.5	37.005
124	"	20	"	0.170	106.0	-3.5	43.318
125	"	30	"	0.161	94.4	-9.6	48.444
126	"	40	"	0.152	78.4	-18.4	54.123
127	"	-5	0.2032	0.270	250.0	74.2	35.129
128	"	0	"	0.265	225.0	48.7	37.481
129	"	10	"	0.262	182.0	12.6	41.434
130	"	20	"	0.258	159.0	-13.4	45.369
131	"	30	"	0.253	137.5	-28.2	49.293
132	"	40	"	0.249	113.0	-40.0	52.746
133	"	-5	0.254	0.339	302.0	87.4	35.017
134	"	0	"	0.368	272.5	55.4	34.614
135	"	10	"	0.330	217.0	10.4	41.184
136	"	20	"	0.324	183.0	-20.0	45.187
137	"	30	"	0.294	150.0	-33.0	52.794
138	"	40	"	0.290	131.5	-51.6	56.923
139	"	-5	0.3048	0.502	335.5	92.0	29.876
140	"	0	"	0.453	310.5	57.9	33.935
141	"	10	"	0.395	255.0	9.2	41.267
142	"	20	"	0.384	204.0	-25.0	45.675
143	"	30	"	0.373	180.0	-46.0	50.114
144	"	40	"	0.353	148.5	-61.4	56.070
145	"	-5	0.381	0.508	405.0	104.6	35.042
146	"	0	"	0.50	369.0	66.0	37.307
147	"	10	"	0.495	312.0	6.2	41.184
148	"	20	"	0.483	247.5	-34.8	45.430
149	"	30	"	0.470	210.0	-60.0	49.733
150	"	40	"	0.440	174.5	-76.8	56.239

Table (2)

PRH RUN NO.	V (m/min)	α (Deg)	t_1 (mm)	t_2 (mm)	F_c (N)	F_t (N)	ϕ (Deg)
1	15.24	-5	0.127	0.243	110.5	63.8	26.472
2	"	0	"	0.225	100.0	43.0	29.442
3	"	10	"	0.210	68.0	22.0	33.642
4	"	20	"	0.193	63.0	7.0	38.587
5	"	30	"	0.192	60.0	-2.75	40.561
6	"	40	"	0.165	47.2	-7.5	49.407
7	"	-5	0.2032	0.380	172.5	88.0	26.975
8	"	0	"	0.350	150.0	60.6	30.138
9	"	10	"	0.340	125.0	29.0	33.294
10	"	20	"	0.333	104.0	7.2	35.929
11	"	30	"	0.300	86.8	-7.0	41.572
12	"	40	"	0.272	68.4	-15.9	47.751
13	"	-5	0.254	0.452	205.0	103.6	28.088
14	"	0	"	0.443	180.5	72.4	29.828
15	"	10	"	0.428	149.4	33.3	33.088
16	"	20	"	0.411	120.0	7.3	36.367
17	"	30	"	0.358	100.0	-9.5	43.599
18	"	40	"	0.345	84.6	-21.0	46.955
19	"	-5	0.3048	0.528	230.0	113.4	28.702
20	"	0	"	0.520	206.5	89.6	30.377
21	"	10	"	0.498	171.0	37.8	33.997
22	"	20	"	0.467	145.0	7.0	38.294
23	"	30	"	0.425	118.6	-12.3	44.078
24	"	40	"	0.408	97.2	-26.3	47.751
25	"	-5	0.381	0.620	285.0	134.2	30.159
26	"	0	"	0.600	255.0	100.0	32.416
27	"	10	"	0.558	210.5	43.9	37.339
28	"	20	"	0.565	167.0	7.2	39.476
29	"	30	"	0.543	140.4	-17.1	43.108
30	"	40	"	0.513	113.0	-32.4	47.430

PRH RUN NO.	V (m/min)	α (Deg)	t_1 (mm)	t_2 (mm)	F_c (N)	F_t (N)	ϕ (Deg)
31	30.48	-5	0.127	0.255	111.1	52.0	25.431
32	"	0	"	0.246	75.0	29.0	27.306
33	"	10	"	0.228	70.0	17.8	31.270
34	"	20	"	0.195	62.6	4.0	38.217
35	"	30	"	0.183	55.4	-3.8	42.626
36	"	40	"	0.172	48.4	-10.2	47.112
37	"	-5	0.2032	0.448	172.5	68.0	23.493
38	"	0	"	0.412	152.5	48.0	26.253
39	"	10	"	0.375	115.0	17.6	30.501
40	"	20	"	0.310	99.0	0.0	38.448
41	"	30	"	0.303	85.6	-13.7	41.146
42	"	40	"	0.270	68.0	21.4	48.157
43	"	-5	0.254		181.0	73.2	
44	"	0	"	0.510	167.5	52.0	26.475
45	"	10	"	0.446	131.0	20.0	31.898
46	"	20	"	0.385	114.4	-2.3	38.681
47	"	30	"	0.365	94.4	-16.6	42.746
48	"	40	"	0.342	80.0	-28.0	47.430
49	"	-5	0.3048		214.0	82.0	
50	"	0	"	0.543	199.0	58.0	29.307
51	"	10	"	0.472	160.0	19.6	35.613
52	"	20	"	0.452	132.2	-5.7	39.476
53	"	30	"	0.425	110.4	-21.5	44.078
54	"	40	"	0.408	88.0	-32.1	47.751
55	"	-5	0.381		251.5	92.6	
56	"	0	"		229.0	62.4	
57	"	10	"	0.590	180.0	21.6	35.613
58	"	20	"	0.580	159.0	-8.0	38.525
59	"	30	"	0.522	127.0	-28.6	44.866
60	"	40	"	0.500	104.2	-42.6	48.846

PRH RUN NO.	V (m/min)	α (Deg)	t_1 (mm)	t_2 (mm)	F_c (N)	F_t (N)	ϕ (Deg)
61	9.14	-5	0.127	0.292	110.8	62.6	22.658
62	"	0	"		100.4	46.6	•
63	"	10	"		77.6	23.3	
64	"	20	"	0.207	66.6	7.8	36.116
65	"	30	"	0.195	54.4	-1.96	39.909
66	"	40	"	0.166	43.8	-6.8	49.069
67	"	-5	0.2032	0.384	169.2	91.7	26.744
68	"	0	"		148.0	66.1	
69	"	10	"	0.361	124.0	34.0	31.566
70	"	20	"	0.340	100.0	8.68	35.218
71	"	30	"	0.301	78.6	-5.68	41.429
72	"	40	"	0.284	67.0	-15.0	45.422
73	"	-5	0.254	0.464	197.0	108.0	27.497
74	"	0	"	0.459	179.0	80.0	28.959
75	"	10	"	0.449	145.5	38.7	31.708
76	"	20	"	0.431	120.0	9.54	34.745
77	"	30	"	0.385	96.0	-8.40	40.451
78	"	40	"	0.355	77.6	-18.5	45.422
79	"	-5	0.3048	0.593	227.5	124.6	26.109
80	"	0	"	0.570	206.5	92.4	28.135
81	"	10	"	0.508	162.5	42.8	33.409
82	"	20	"	0.488	133.6	10.16	36.736
83	"	30	"	0.446	109.6	-10.3	41.957
84	"	40	"	0.425	89.2	-22.2	45.546
85	"	-5	0.381	0.619	272.5	148.6	30.197
86	"	0	"	0.596	249.0	108.6	32.589
87	"	10	"	0.590	205.0	52.3	35.613
88	"	20	"	0.580	157.2	11.02	38.525
89	"	30	"	0.562	133.5	-14.0	41.611
90	"	40	"	0.494	107.4	-28.4	49.52

PRH RUN NO.	V (m/min)	α (Deg)	t_1 (mm)	t_2 (mm)	F_c (N)	F_t (N)	ϕ (Deg)
91	22.86	-5	0.127	0.256	84.0	43.5	25.348
92	"	0	"		98.0	37.8	
93	"	10	"	0.220	71.0	16.3	32.286
94	"	20	"	0.190	58.9	5.06	39.155
95	"	30	"	0.185	57.2	-3.56	42.152
96	"	40	"	0.158	42.6	-8.0	51.87
97	"	-5	0.2032	0.425	149.0	64.0	24.572
98	"	0	"	0.412	142.0	50.0	26.253
99	"	10	"	0.340	106.6	20.85	33.294
100	"	20	"	0.330	88.0	3.0	36.241
101	"	30	"	0.288	78.0	-9.0	43.352
102	"	40	"	0.267	62.6	-17.5	48.776
103	"	-5	0.254	0.473	173.5	72.2	27.069
104	"	0	"	0.461	161.5	56.0	28.854
105	"	10	"	0.411	131.0	23.05	34.285
106	"	20	"	0.394	111.0	0.92	37.852
107	"	30	"	0.374	92.2	-13.35	41.687
108	"	40	"	0.334	75.2	-23.8	48.734
109	"	-5	0.3048	0.568	202.5	84.2	27.053
110	"	0	"	0.503	190.0	64.0	31.214
111	"	10	"	0.498	153.6	25.1	33.997
112	"	20	"	0.439	126.0	-0.82	40.551
113	"	30	"	0.395	104.5	-17.2	47.415
114	"	40	"	0.389	85.6	-29.0	50.412
115	"	-5	0.381	0.602	240.0	99.6	30.859
116	"	0	"		225.0	72.0	
117	"	10	"	0.576	178.5	26.7	36.351
118	"	20	"	0.558	148.6	-3.3	39.933
119	"	30	"	0.545	127.0	-24.1	42.946
120	"	40	"	0.500	101.6	-37.4	48.845

PRH RUN NO.	V (m/min)	α (Deg)	t_1 (mm)	t_2 (mm)	F_c (N)	F_t (N)	ϕ (Deg)
121	36.58	-5	0.127	0.221	89.0	38.5	28.598
122	"	0	"		72.0	28.0	
123	"	10	"	0.211	78.4	12.2	33.502
124	"	20	"	0.198	67.6	1.28	37.672
125	"	30	"	0.184	58.6	-6.4	42.388
126	"	40	"	0.177	47.3	-12.0	45.571
127	"	-5	0.2032	0.448	157.8	55.8	23.493
128	"	0	"		133.2	36.4	
129	"	10	"	0.334	107.2	12.2	33.819
130	"	20	"	0.327	90.6	-3.6	36.558
131		30	"	0.294	79.6	-14.65	42.447
132		40	"	0.260	65.0	-21.7	50.266
133		-5	0.254	0.538	183.5	65.2	24.310
134		0	"		155.0	40.0	
135		10	"	0.419	126.0	12.4	33.713
136		20	"	0.405	109.6	-7.0	36.88
137		30	"	0.388	90.4	-19.5	40.124
138		40	"	0.350	76.0	-28.4	46.178
139		-5	0.3048	0.530	209.0	71.8	28.615
140		0	"		177.5	45.8	
141		10	"	0.468	145.2	12.05	35.873
142		20	"	0.463	125.0	-10.0	38.603
143		30	"	0.450	107.0	-26.0	41.572
144		40	"	0.398	87.8	-35.9	49.125
145		-5	0.381		251.0	84.6	
146		0	"		204.0	48.4	
147		10	"	0.601	172.0	11.5	35.051
148		20	"	0.580	146.5	-14.5	38.525
149		30	"	0.556	126.0	-32.4	42.074
150		40	"	0.491	100.8	-43.6	49.863

Table (3)

NH RUN NO.	V (m/min)	α (Deg)	t_1 (mm)	t_2 (mm)	F_c (N)	F_t (N)	ϕ (Deg)
1	15.24	-5	0.127	0.209	172.0	70.0	29.946
2	"	0	"	0.171	159.0	47.3	36.649
3	"	10	"	0.154	130.0	20.8	43.562
4	"	20	"	0.140	117.5	0.0	50.971
5	"	30	"	0.132	92.0	-8.0	58.233
6	"	40	"	0.129	71.0	-20.8	64.196
7	"	-5	0.2032	0.294	250.0	93.5	32.997
8	"	0	"	0.246	230.0	61.0	39.523
9	"	10	"	0.240	200.0	23.8	44.322
10	"	20	"	0.238	175.0	-7.7	48.536
11	"	30	"	0.235	150.0	-23.6	52.910
12	"	40	"	0.228	112.0	-40.0	58.089
13	"	-5	0.254	0.344	319.0	110.0	34.635
14	"	0	"	0.304	281.0	70.4	39.862
15	"	10	"	0.293	237.5	24.6	45.147
16	"	20	"	0.283	192.5	-10.6	50.566
17	"	30	"	0.280	170.0	-30.8	55.226
18	"	40	"	0.271	131.0	-48.4	61.010
19	"	-5	0.3048	0.423	367.0	122.0	34.050
20	"	0	"	0.391	323.0	78.6	37.954
21	"	10	"	0.364	273.0	25.0	44.004
22	"	20	"	0.353	233.0	-15.0	48.911
23	"	30	"	0.345	200.0	-40.0	53.857
24	"	40	"	0.334	150.0	-58.0	59.496
25	"	-5	0.381	0.529	435.0	138.5	34.061
26	"	0	"	0.501	375.0	88.0	37.271
27	"	10	"	0.447	330.0	26.0	44.560
28	"	20	"	0.438	270.0	-21.0	49.376
29	"	30	"	0.429	237.0	-52.0	54.518
30	"	40	"	0.414	184.0	-74.6	59.960

NH RUN NO.	V (m/min)	α (Deg)	t_1 (mm)	t_2 (mm)	F_c (N)	F_t (N)	ϕ (Deg)
31	30.48	-5	0.127	0.206	185.0	80.0	30.254
32	"	0	"	0.195	177.5	44.2	33.064
33	"	10	"	0.174	152.0	20.0	39.464
34	"	20	"	0.159	119.0	-2.1	45.835
35	"	30	"	0.149	100.0	-16.2	52.063
36	"	40	"	0.142	80.0	-24.0	58.224
37	"	-5	0.2032	0.295	260.0	79.6	32.959
38	"	0	"	0.276	225.5	51.8	36.353
39	"	10	"	0.247	206.0	18.8	43.44
40	"	20	"	0.237	170.5	-11.5	48.771
41	"	30	"	0.233	138.5	-29.3	53.246
42	"	40	"	0.225	120.0	-46.0	58.829
43	"	-5	0.254	0.356	302.5	90.2	33.807
44	"	0	"	0.343	288.0	60.0	36.501
45	"	10	"	0.300	249.0	17.6	44.322
46	"	20	"	0.292	198.0	-16.2	49.33
47	"	30	"	0.282	167.0	-40.0	54.682
48	"	40	"	0.276	131.5	-52.2	59.894
49	"	-5	0.3048	0.430	353.0	102.0	33.632
50	"	0	"	0.408	326.0	65.6	36.760
51	"	10	"	0.367	276.0	16.8	43.723
52	"	20	"	0.355	234.0	-24.0	48.818
53	"	30	"	0.344	190.0	-48.0	54.023
54	"	40	"	0.335	155.0	-64.2	59.296
55	"	-5	0.381	0.518	430.0	118.4	34.533
56	"	0	"	0.498	392.5	75.4	37.416
57	"	10	"	0.450	346.0	14.2	44.362
58	"	20	"	0.438	275.0	-38.0	49.284
59	"	30	"	0.429	227.5	-60.0	54.189
60	"	40	"	0.413	177.0	-74.0	60.026

NH RUN NO.	V (m/min)	α (Deg)	t_1 (mm)	t_2 (mm)	F_c (N)	F_t (N)	ϕ (Deg)
61	9.14	-5	0.127	0.196	180.0	77.6	31.424
62	"	0	"	0.167	171.6	60.0	37.252
63	"	10	"	0.155	134.8	23.6	43.252
64	"	20	"	0.146	114.6	5.0	49.324
65	"	30	"	0.142	106.0	-10.0	54.483
66	"	40	"	0.138	85.6	-18.7	59.913
67	"	-5	0.2032	0.287	261.0	104.0	33.597
68	"	0	"	0.272	246.5	76.0	36.762
69	"	10	"	0.247	193.5	26.5	43.386
70	"	20	"	0.241	172.5	-1.0	48.071
71	"	30	"	0.236	147.5	-21.2	52.630
72	"	40	"	0.231	126.4	-36.8	57.182
73	"	-5	0.254	0.358	310.0	119.6	33.649
74	"	0	"	0.339	293.5	86.8	36.843
75	"	10	"	0.308	246.5	31.2	43.468
76	"	20	"	0.292	204.0	-4.25	49.324
77	"	30	"	0.279	171.0	-26.0	55.355
78	"	40	"	0.271	140.0	-43.0	61.028
79	"	-5	0.3048	0.454	365.0	136.2	32.286
80	"	0	"	0.416	340.0	96.8	36.230
81	"	10	"	0.366	284.0	33.9	43.795
82	"	20	"	0.351	236.5	-7.05	49.255
83	"	30	"	0.346	200.0	-35.2	53.742
84	"	40	"	0.336	166.5	-56.0	59.039
85	"	-5	0.381	0.547	436.5	157.0	33.191
86	"	0	"	0.495	406.5	110.6	37.585
87	"	10	"	0.455	338.5	35.5	43.978
88	"	20	"	0.438	285.0	-12.0	49.324
89	"	30	"	0.433	243.5	-48.0	53.686
90	"	40	"	0.423	196.5	-70.0	58.608

NH RUN NO.	V (m/min)	α (Deg)	t_1 (mm)	t_2 (mm)	F_c (N)	F_t (N)	ϕ (Deg)
91	22.86	-5	0.127	0.188	172.4	64.7	32.438
92	"	0	"	0.176	165.4	45.0	35.814
93	"	10	"	0.147	130.0	15.4	45.028
94	"	20	"	0.139	110.0	-1.65	51.314
95	"	30	"	0.134	101.4	-15.5	57.340
96	"	40	"	0.131	84.0	-23.1	63.096
97	"	-5	0.2032	0.296	262.5	86.8	32.833
98	"	0	"	0.269	230.0	55.6	37.067
99	"	10	"	0.245	201.5	16.0	43.658
100	"	20	"	0.238	172.5	-11.2	48.573
101	"	30	"	0.234	150.5	-31.8	53.043
102	"	40	"	0.228	118.0	-42.8	57.969
103	"	-5	0.254	0.356	313.0	100.0	33.789
104	"	0	"	0.336	282.5	63.2	37.088
105	"	10	"	0.296	236.0	16.0	44.80
106	"	20	"	0.286	202.5	-15.8	50.163
107	"	30	"	0.282	173.0	-40.0	54.830
108	"	40	"	0.278	141.0	-54.0	59.474
109	"	-5	0.3048	0.440	367.5	112.0	33.056
110	"	0	"	0.400	330.0	71.2	37.307
111	"	10	"	0.355	280.0	16.5	44.819
112	"	20	"	0.345	237.5	-20.8	49.951
113	"	30	"	0.335	193.5	-46.0	55.326
114	"	40	"	0.328	162.0	-65.4	60.504
115	"	-5	0.381	0.519	437.5	129.2	34.502
116	"	0	"	0.503	400.0	81.6	37.142
117	"	10	"	0.437	332.0	16.0	45.336
118	"	20	"	0.426	284.0	-29.4	50.447
119	"	30	"	0.421	240.0	-61.6	55.063
120	"	40	"	0.418	191.5	-81.2	59.329

NH RUN NO.	V (m/min)	α (Deg)	t_1 (mm)	t_2 (mm)	F_c (N)	F_t (N)	ϕ (Deg)
121	36.58	-5	0.127	0.179	166.4	58.0	33.649
122	"	0	"	0.166	160.0	44.6	37.418
123	"	10	"	0.146	133.6	15.6	45.259
124	"	20	"	0.137	123.0	-3.3	51.904
125	"	30	"	0.134	95.8	-16.0	57.340
126	"	40	"	0.129	76.6	-24.0	64.040
127	"	-5	0.2032	0.297	265.0	77.6	32.750
128	"	0	"	0.268	237.5	55.8	37.170
129	"	10	"	0.240	200.0	15.8	44.349
130	"	20	"	0.231	173.5	-12.3	49.775
131	"	30	"	0.227	140.0	-32.0	54.526
132	"	40	"		116.5	-45.4	
133	"	-5	0.254	0.334	300.0	85.4	35.394
134	"	0	"	0.305	284.0	61.4	39.787
135	"	10	"	0.299	241.0	12.8	44.461
136	"	20	"	0.292	205.0	-19.8	49.324
137	"	30	"	0.281	163.5	-40.4	55.004
138	"	40	"	0.268	132.0	-54.6	61.708
139	"	-5	0.3048	0.402	345.0	96.0	35.318
140	"	0	"	0.357	330.0	66.0	40.490
141	"	10	"	0.335	274.5	12.0	46.780
142	"	20	"	0.325	223.0	-21.4	52.377
143	"	30	"	0.321	189.5	-48.8	57.433
144	"	40	"	0.318	152.0	-64.0	62.398
145	"	-5	0.381	0.495	420.0	110.8	35.70
146	"	0	"	0.434	397.5	74.0	41.279
147	"	10	"		321.5	12.0	
148	"	20	"	0.426	280.0	-32.6	50.447
149	"	30	"	0.415	229.0	-64.0	55.769
150	"	40	"	0.391	176.0	-78.4	63.409

Table (4)

NRH RUN NO.	V (m/min)	α (Deg)	t_1 (mm)	t_2 (mm)	F_c (N)	F_t (N)	ϕ (Deg)
1	15.24	-5	0.127	0.204	132.0	50.0	30.469
2	"	0	"	0.183	118.0	35.6	34.760
3	"	10	"	0.165	93.5	13.2	41.184
4	"	20	"	0.153	90.0	-1.0	47.446
5	"	30	"	0.148	74.0	-12.0	52.465
6	"	40	"	0.132	56.0	-16.0	62.629
7	"	-5	0.2032	0.279	170.0	60.0	34.303
8	"	0	"	0.269	164.0	44.2	37.067
9	"	10	"	0.245	145.0	14.4	43.723
10	"	20	"	0.238	125.0	-6.8	48.573
11	"	30	"	0.226	104.0	-20.0	54.743
12	"	40	"	0.221	86.5	-33.4	59.858
13	"	-5	0.254	0.365	216.5	74.0	33.169
14	"	0	"	0.346	201.5	50.0	36.283
15	"	10	"	0.296	171.5	14.4	44.80
16	"	20	"	0.286	145.0	-9.4	50.163
17	"	30	"	0.283	126.0	-28.0	54.656
18	"	40	"	0.275	100.0	-40.0	60.134
19	"	-5	0.3048	0.434	250.0	82.0	33.396
20	"	0	"	0.405	231.0	54.6	36.965
21	"	10	"	0.370	200.0	14.4	43.431
22	"	20	"	0.351	170.0	-13.0	49.255
23	"	30	"	0.343	144.0	-33.4	54.168
24	"	40	"	0.329	115.0	-48.0	60.319
25	"	-5	0.381	0.535	300.0	95.4	33.742
26	"	0	"	0.497	280.0	64.0	37.474
27	"	10	"	0.445	240.0	14.0	44.724
28	"	20	"	0.433	202.5	-17.8	49.787
29	"	30	"	0.426	171.5	-43.6	54.483
30	"	40	"	0.417	140.0	-61.4	59.474

NRH RUN NO.	V (m/min)	α (Deg)	t_1 (mm)	t_2 (mm)	F_c (N)	F_t (N)	ϕ (Deg)
31	30.48	-5	0.127	0.202	134.0	47.6	30.701
32	"	0	"	0.194	130.0	34.0	33.210
33	"	10	"	0.161	100.5	9.4	41.991
34	"	20	"	0.153	92.0	-2.0	47.446
35	"	30	"	0.142	72.0	-9.4	54.483
36	"	40	"	0.134	60.0	-18.6	61.708
37	"	-5	0.2032	0.293	182.0	57.4	33.084
38	"	0	"	0.279	173.5	40.0	36.066
39	"	10	"	0.247	146.5	8.8	43.386
40	"	20	"	0.239	107.0	-6.2	48.405
41	"	30	"	0.235	110.0	-26.4	52.836
42	"	40	"	0.229	87.5	-36.0	57.705
43	"	-5	0.254	0.354	213.0	68.0	33.929
44	"	0	"	0.326	196.0	44.0	37.924
45	"	10	"	0.300	170.5	8.0	44.349
46	"	20	"	0.288	156.5	-15.0	49.881
47	"	30	"	0.277	126.0	-31.2	55.710
48	"	40	"	0.273	100.0	-44.0	60.579
49	"	-5	0.3048	0.423	251.0	72.0	34.035
50	"	0	"	0.387	230.0	48.4	38.224
51	"	10	"	0.348	199.0	9.4	45.491
52	"	20	"	0.340	170.0	-17.6	50.542
53	"	30	"	0.336	149.0	-40.0	55.180
54	"	40	"	0.326	118.5	-55.6	60.878
55	"	-5	0.381	0.525	255.0	84.0	34.214
56	"	0	"	0.507	286.0	54.8	36.924
57	"	10	"	0.456	250.0	6.0	43.905
58	"	20	"	0.437	212.5	-25.4	49.416
59	"	30	"	0.427	177.5	-49.6	54.368
60	"	40	"	0.422	140.0	-70.0	58.751

NRH RUN NO.	V (m/min)	α (Deg)	t_1 (mm)	t_2 (mm)	F_c (N)	F_t (N)	ϕ (Deg)
61	9.14	-5	0.127	0.204	126.0	58.0	30.467
62	"	0	"	0.193	114.6	40.5	33.346
63	"	10	"	0.156	101.0	20.9	43.037
64	"	20	"	0.148	84.2	5.6	48.776
65	"	30	"	0.141	72.4	-5.2	54.830
66	"	40	"	0.134	58.6	-12.65	61.708
67	"	-5	0.2032	0.309	177.5	74.6	31.782
68	"	0	"	0.299	166.0	51.6	34.20
69	"	10	"	0.248	144.6	23.0	43.20
70	"	20	"	0.240	129.6	0.0	48.237
71	"	30	"	0.235	108.0	-16.0	52.836
72	"	40	"	0.228	85.8	-26.9	57.969
73	"	-5	0.254	0.399	226.5	90.0	30.999
74	"	0	"	0.379	200.0	60.0	33.829
75	"	10	"	0.318	177.0	24.1	42.405
76	"	20	"	0.303	150.0	-2.75	47.839
77	"	30	"	0.286	122.5	-21.0	54.140
78	"	40	"	0.278	101.0	-35.0	59.474
79	"	-5	0.3048	0.459	260.5	101.6	32.019
80	"	0	"	0.440	232.5	67.4	34.711
81	"	10	"	0.362	201.0	26.0	44.163
82	"	20	"	0.348	174.0	-5.15	49.601
83	"	30	"	0.341	146.5	-27.7	54.455
84	"	40	"	0.335	117.0	-43.8	59.220
85	"	-5	0.381	0.570	310.0	114.8	32.179
86	"	0	"	0.535	273.0	76.0	35.457
87	"	10	"	0.446	239.5	26.2	44.649
88	"	20	"	0.435	210.0	-10.0	49.601
89	"	30	"	0.429	171.0	-37.2	54.140
90	"	40	"	0.422	142.0	-56.0	58.751

NRH RUN NO.	V (m/min)	α (Deg)	t_1 (mm)	t_2 (mm)	F_c (N)	F_t (N)	ϕ (Deg)
91	22.86	-5	0.127	0.185	120.8	45.7	32.833
92	"	0	"	0.178	124.8	33.0	35.507
93	"	10	"	0.156	99.6	11.0	43.037
94	"	20	"	0.146	79.0	-1.8	49.324
95	"	30	"	0.135	66.4	-12.8	56.973
96	"	40	"	0.129	46.4	-15.6	64.040
97	"	-5	0.2032	0.276	186.6	62.0	34.575
98	"	0	"	0.258	162.0	39.3	38.224
99	"	10	"	0.233	144.0	10.55	45.345
100	"	20	"	0.226	122.0	-8.10	50.661
101	"	30	"	0.218	102.6	-24.7	56.517
102	"	40	"	0.214	84.0	-36.0	61.823
103	"	-5	0.254	0.336	216.5	70.0	35.242
104	"	0	"	0.326	224.0	41.4	37.924
105	"	10	"	0.290	170.0	10.4	45.491
106	"	20	"	0.282	147.5	-13.2	50.733
107	"	30	"	0.277	123.5	-32.0	55.710
108	"	40	"	0.266	95.5	-44.0	62.167
109	"	-5	0.3048	0.417	251.0	77.8	34.393
110	"	0	"	0.390	232.5	51.2	38.009
111	"	10	"	0.348	197.0	10.0	45.491
112	"	20	"	0.335	173.5	-17.5	51.143
113	"	30	"	0.328	140.0	-38.0	56.367
114	"	40	"	0.322	118.0	-52.0	61.632
115	"	-5	0.381	0.519	303.5	90.2	34.502
116	"	0	"	0.490	276.5	58.3	37.867
117	"	10	"	0.447	240.5	9.6	44.573
118	"	20	"	0.427	206.0	-23.1	50.352
119	"	30	"	0.416	167.5	-46.6	55.65
120	"	40	"	0.404	136.5	-67.0	61.405

NRH RUN NO.	V (m/min)	α (Deg)	t_1 (mm)	t_2 (mm)	F_c (N)	F_t (N)	ϕ (Deg)
121	36.58	-5	0.127	0.174	130.2	44.9	34.357
122	"	0	"	0.171	117.4	28.6	36.601
123	"	10	"	0.147	100.0	11.95	45.028
124	"	20	"	0.142	80.0	-4.5	50.447
125	"	30	"	0.137	70.8	-14.5	56.246
126	"	40	"	0.131	50.6	-16.5	63.096
127	"	-5	0.2032	0.278	180.0	56.0	34.393
128	"	0	"	0.265	166.6	34.8	37.481
129	"	10	"	0.238	150.6	10.5	44.630
130	"	20	"	0.231	121.6	-11.4	49.775
131	"	30	"	0.219	104.4	-27.3	56.291
132	"	40	"	0.212	79.2	-35.4	62.398
133	"	-5	0.254	0.336	213.5	63.0	35.242
134	"	0	"	0.326	199.5	39.3	37.924
135	"	10	"	0.287	170.0	10.15	45.842
136	"	20	"	0.276	146.5	-16.5	51.607
137	"	30	"	0.268	121.0	-33.8	57.340
138	"	40	"	0.262	94.0	-45.6	63.096
139	"	-5	0.3048	0.410	250.0	70.0	34.819
140	"	0	"	0.386	233.0	43.8	38.296
141	"	10	"	0.356	210.0	8.6	44.724
142	"	20	"	0.333	169.0	-21.9	51.387
143	"	30	"	0.325	141.5	-42.0	56.820
144	"	40	"	0.318	107.0	-54.0	62.398
145	"	-5	0.381	0.504	303.0	81.6	35.242
146	"	0	"	0.486	276.0	50.0	38.095
147	"	10	"	0.422	241.0	7.10	46.518
148	"	20	"	0.418	205.0	-27.90	51.216
149	"	30	"	0.412	171.0	-52.2	56.126
150	"	40	"	0.405	123.0	-64.6	61.254

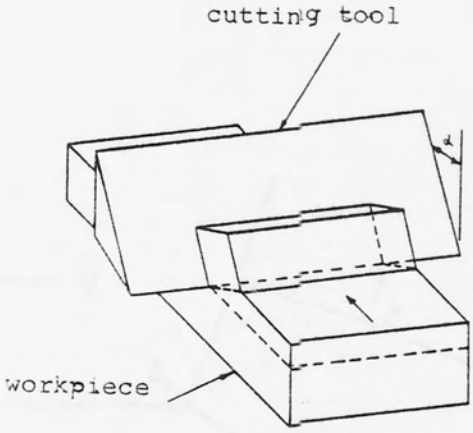

Fig. (2.1) Orthogonal cutting

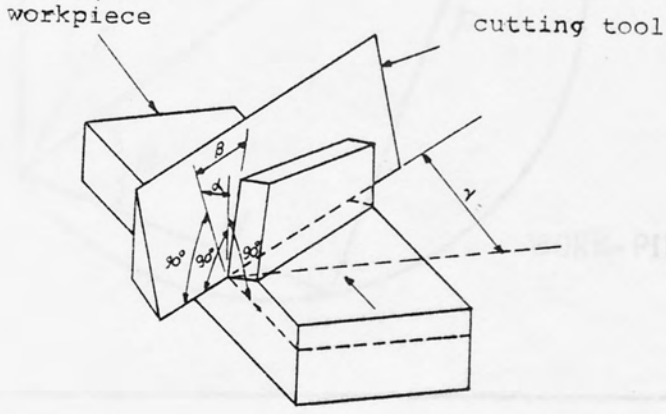

Fig. (2.2) Oblique cutting

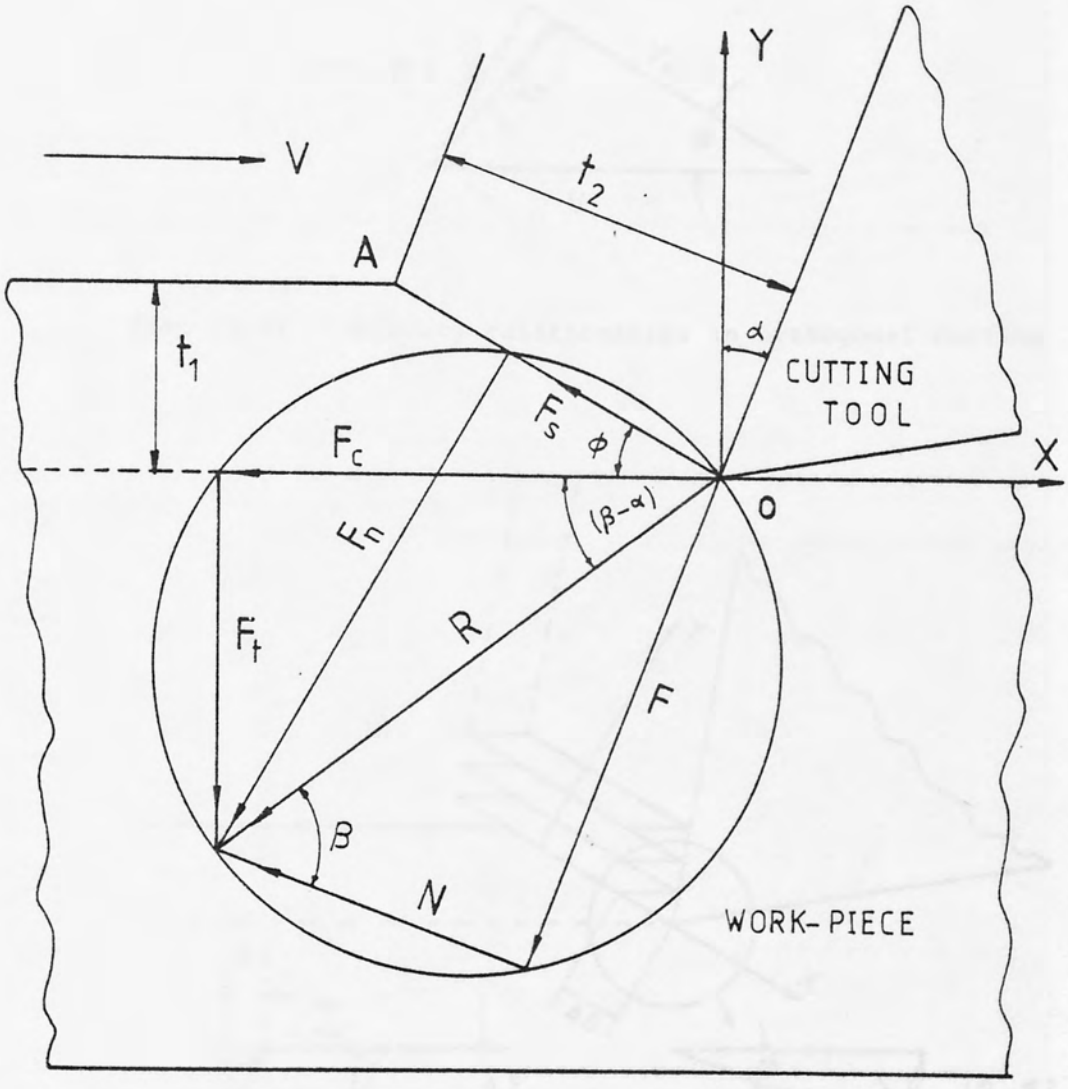

Fig. (2.3) Orthogonal cutting force equilibrium diagram

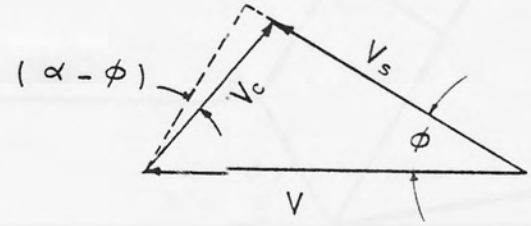

Fig. (2.4) Velocity relationships in orthogonal cutting

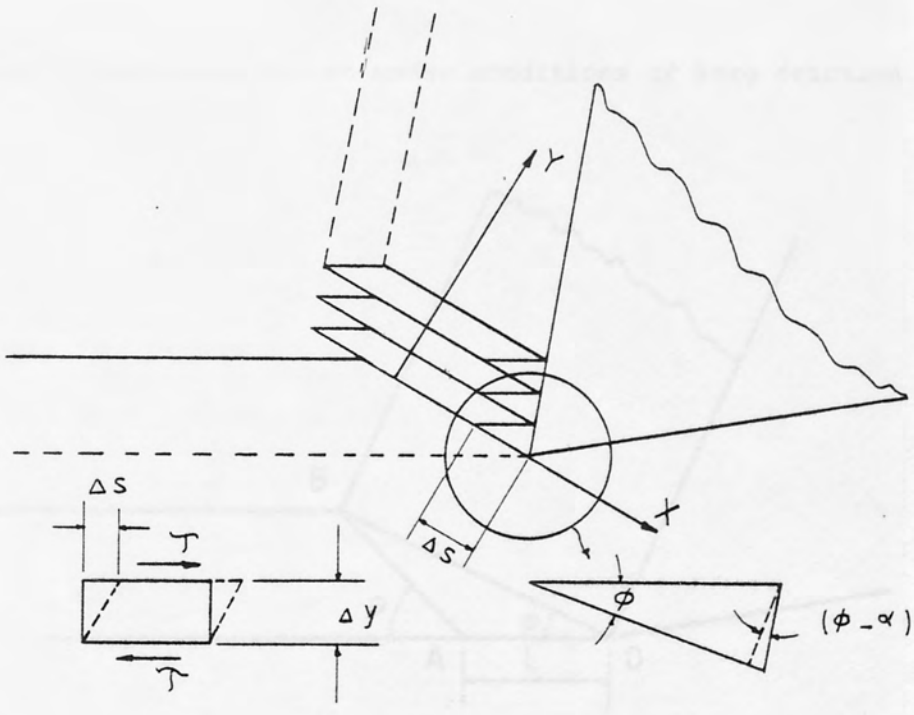

Fig. (2.5) Shear strain in orthogonal cutting

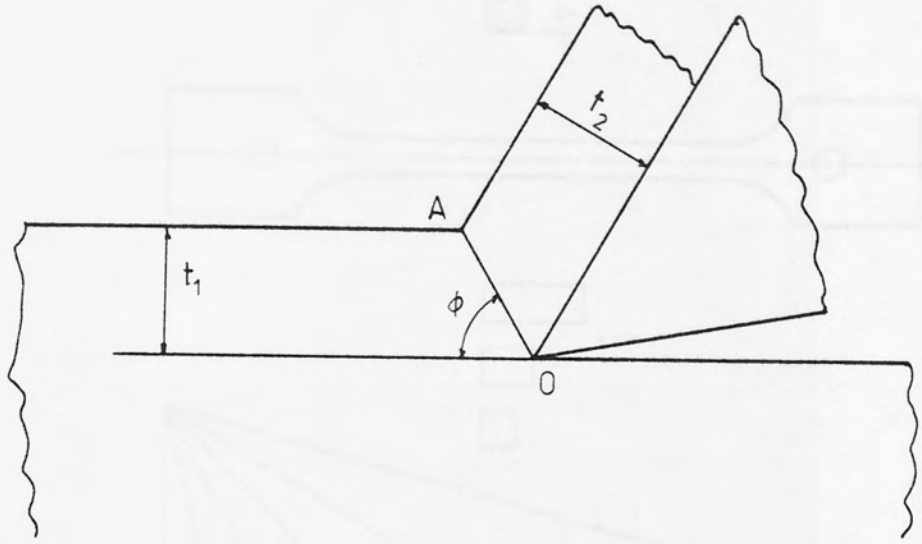

Fig. (3.1) Ideal chip formed under conditions of zero friction

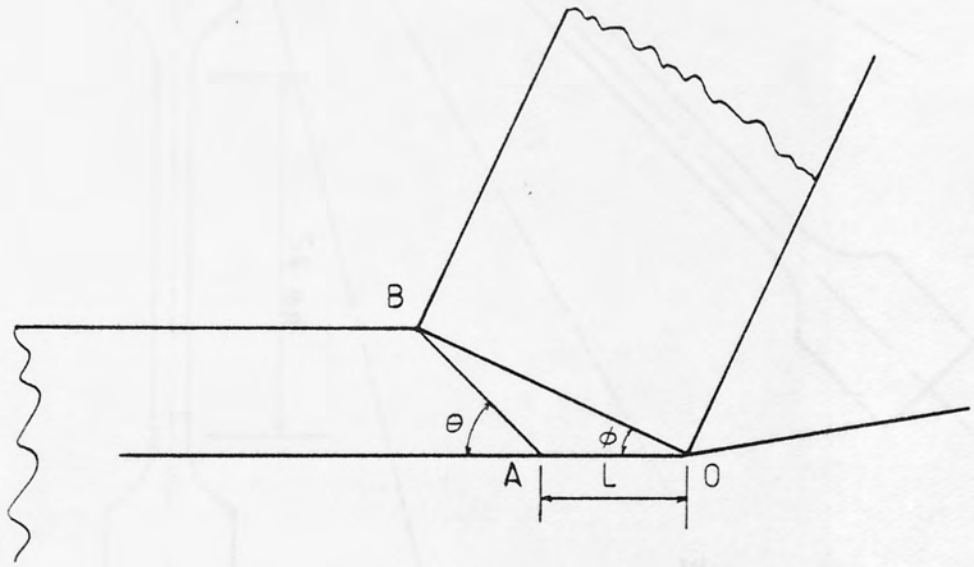

Fig. (3.2) Lower boundary of primary deformation zone

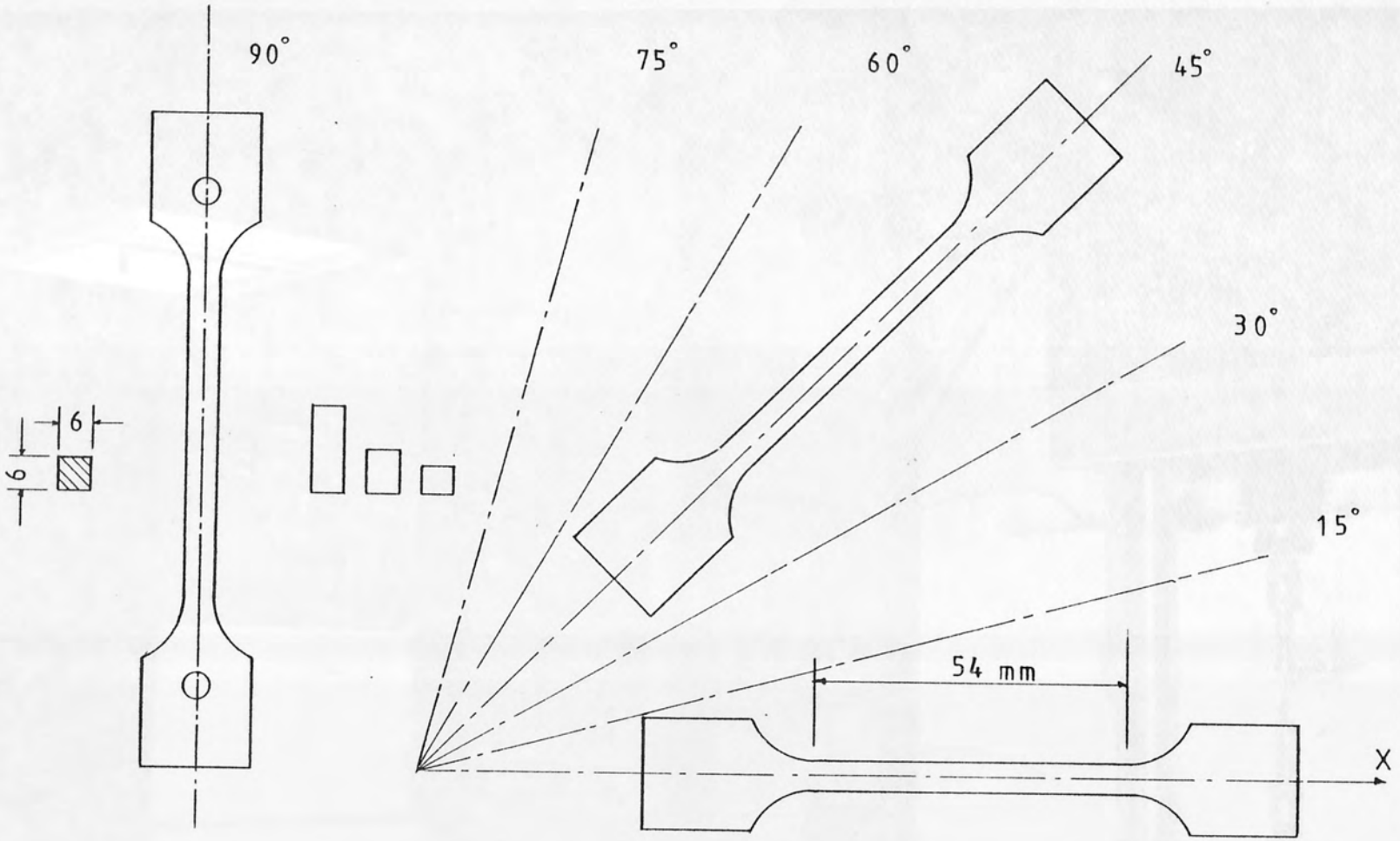

Fig. (6.1)

Fig. (6.1) Tensile and compression specimens

Fig 6·2

FIG 6·3

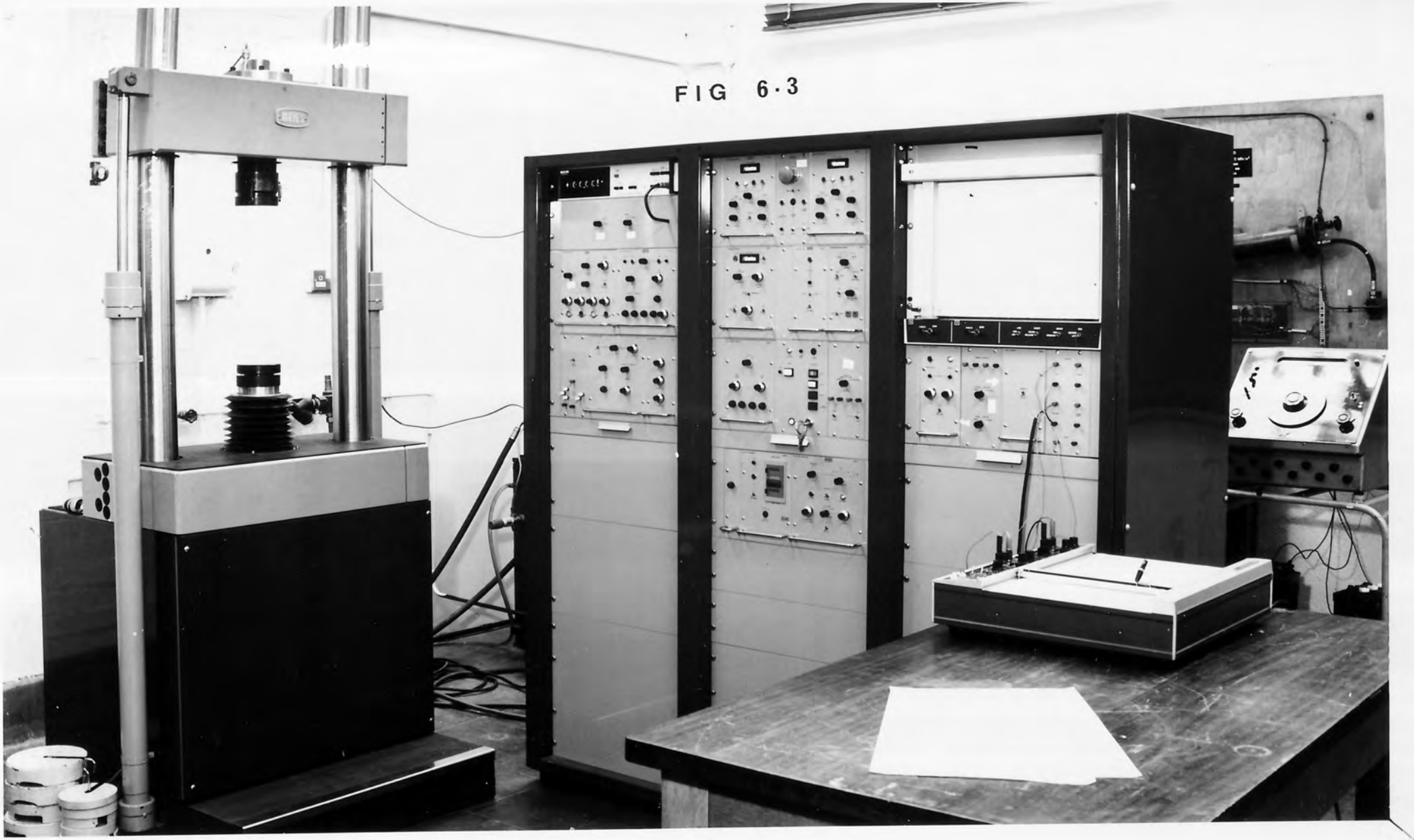

6·3

Fig 6·4

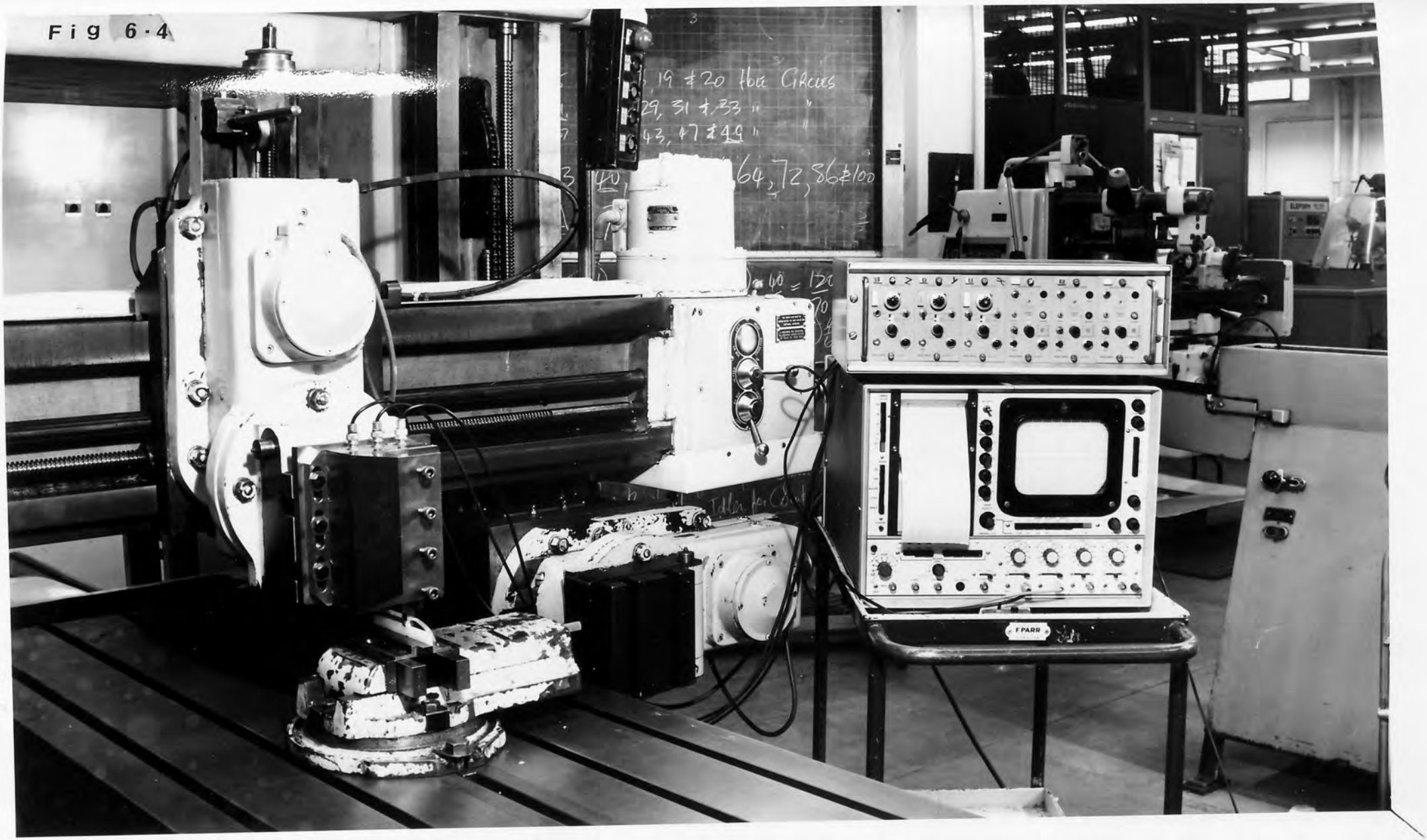

6·4

Fig 6.5

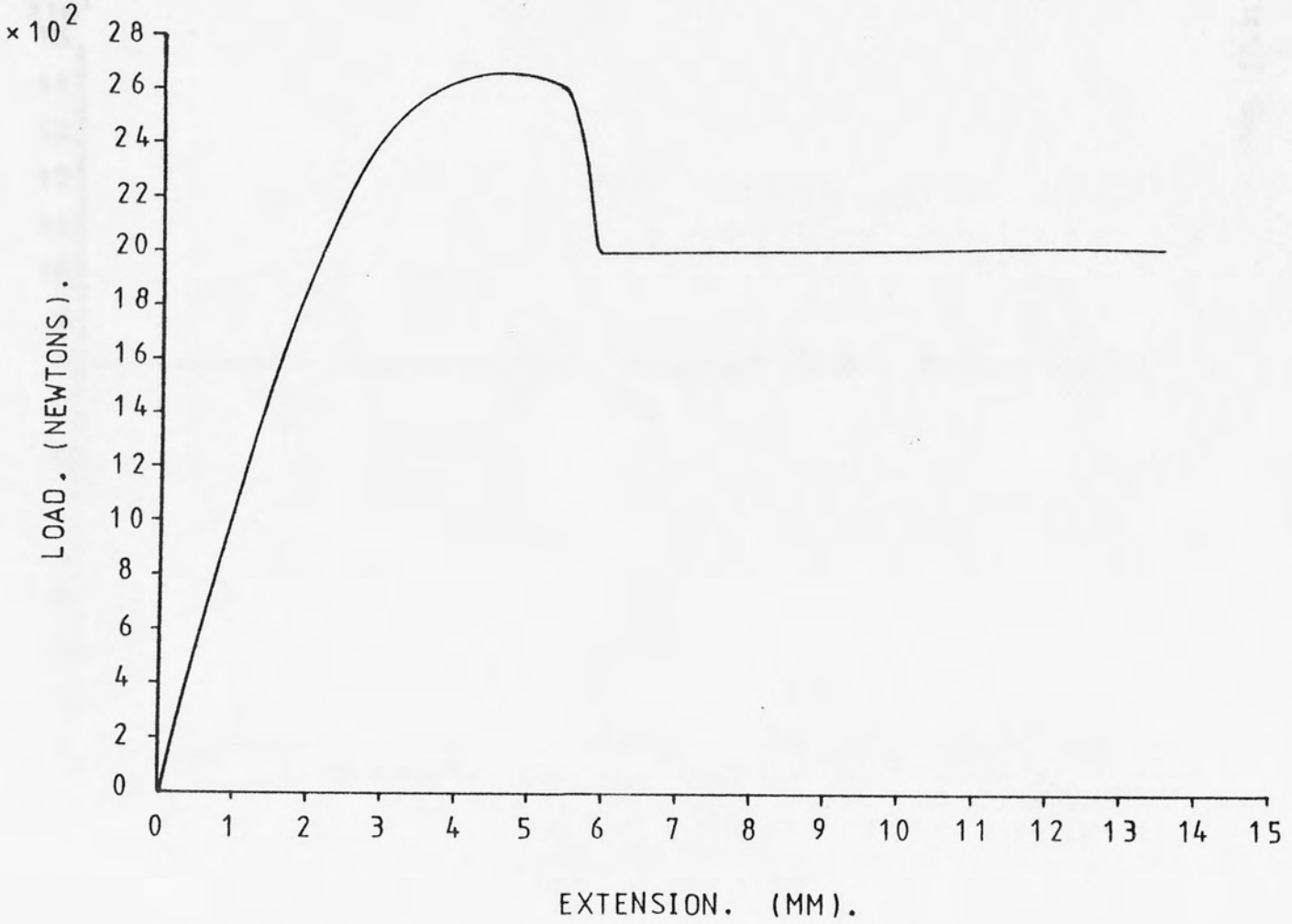

Fig. (7.1)

Fig. (7.1) Load extension curve for the as-received polycarbonate (Tensile)

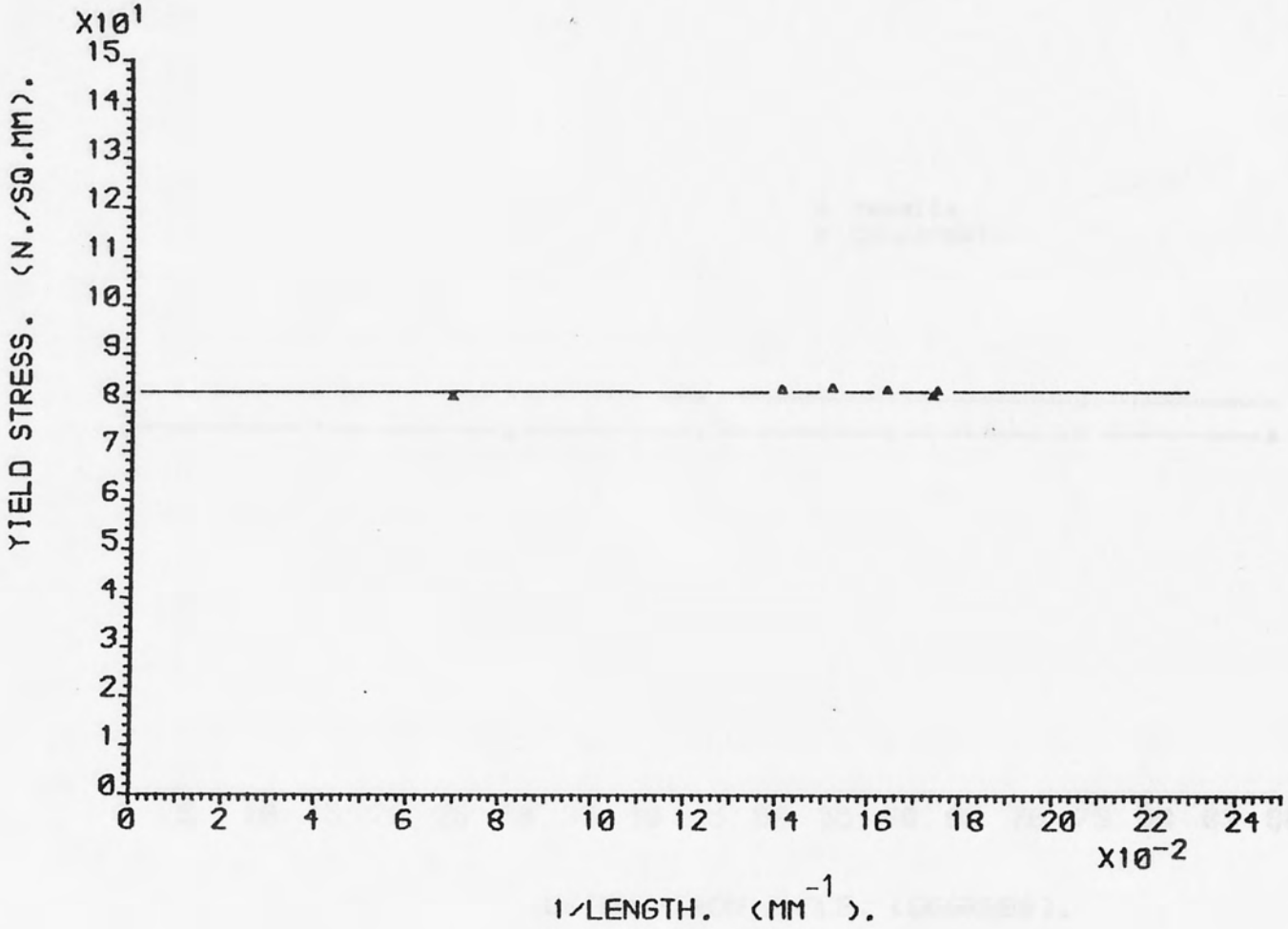

Fig. (7.2)

Fig. (7.2). Plot of the compressive yield stress against reciprocal of specimens length for the as-received polycarbonate

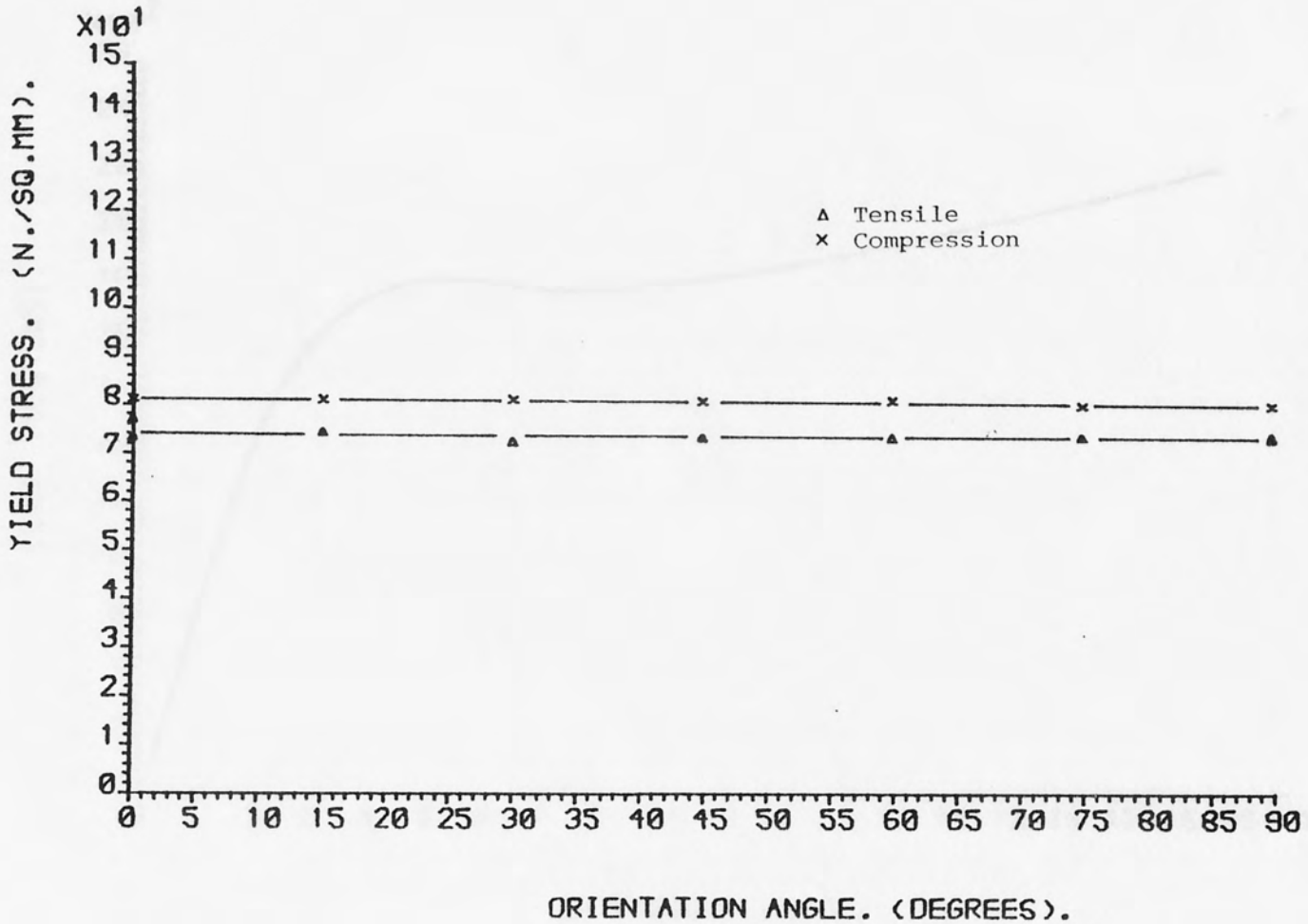

Fig. (7.3)

Fig. (7.3) Variation of tensile and compressive yield stress with the orientation angle for the as-received polycarbonate

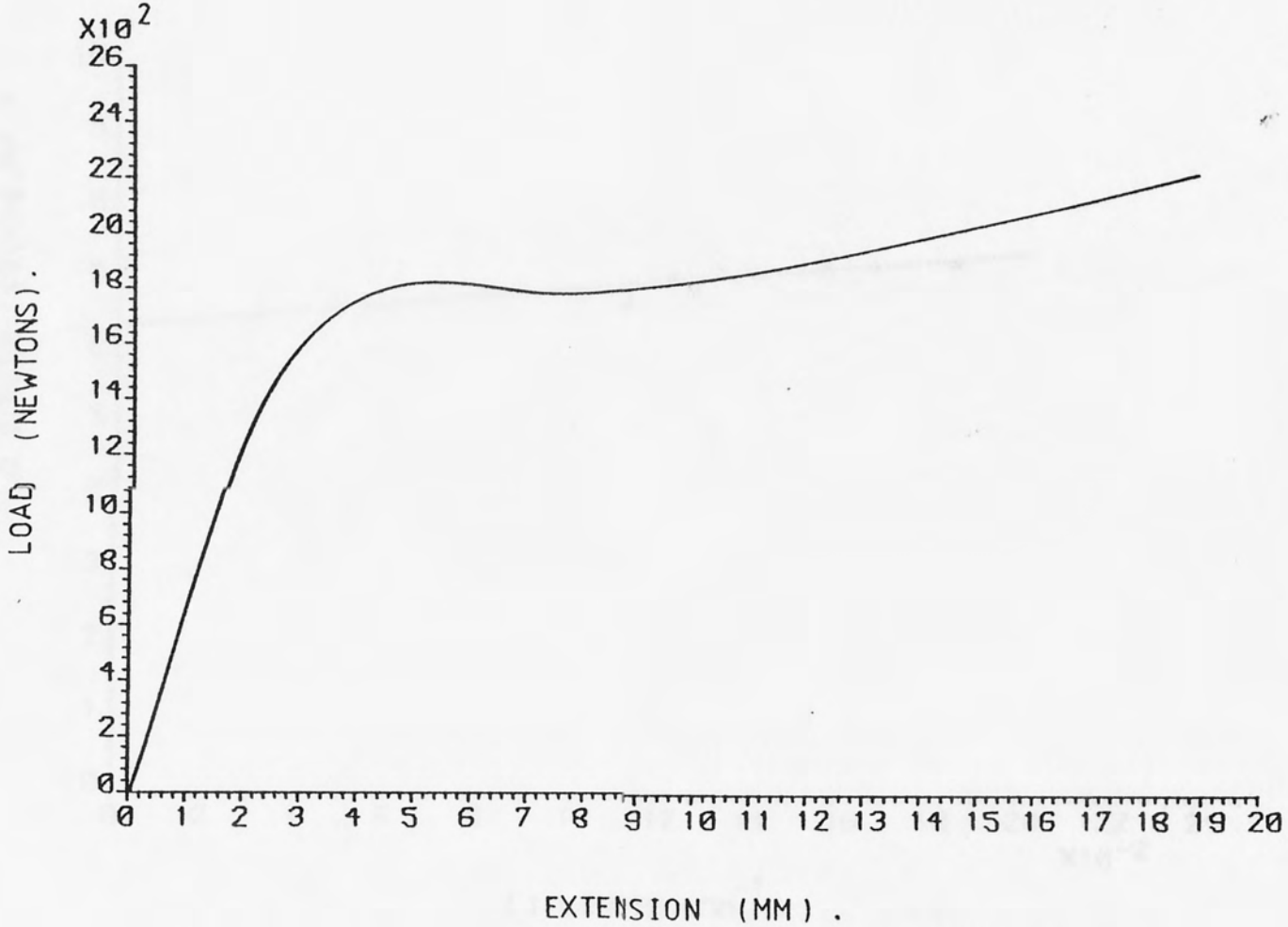

Fig. (7.4)

Fig. (7.4) Load-extension curve for rolled polycarbonate (Tensile)

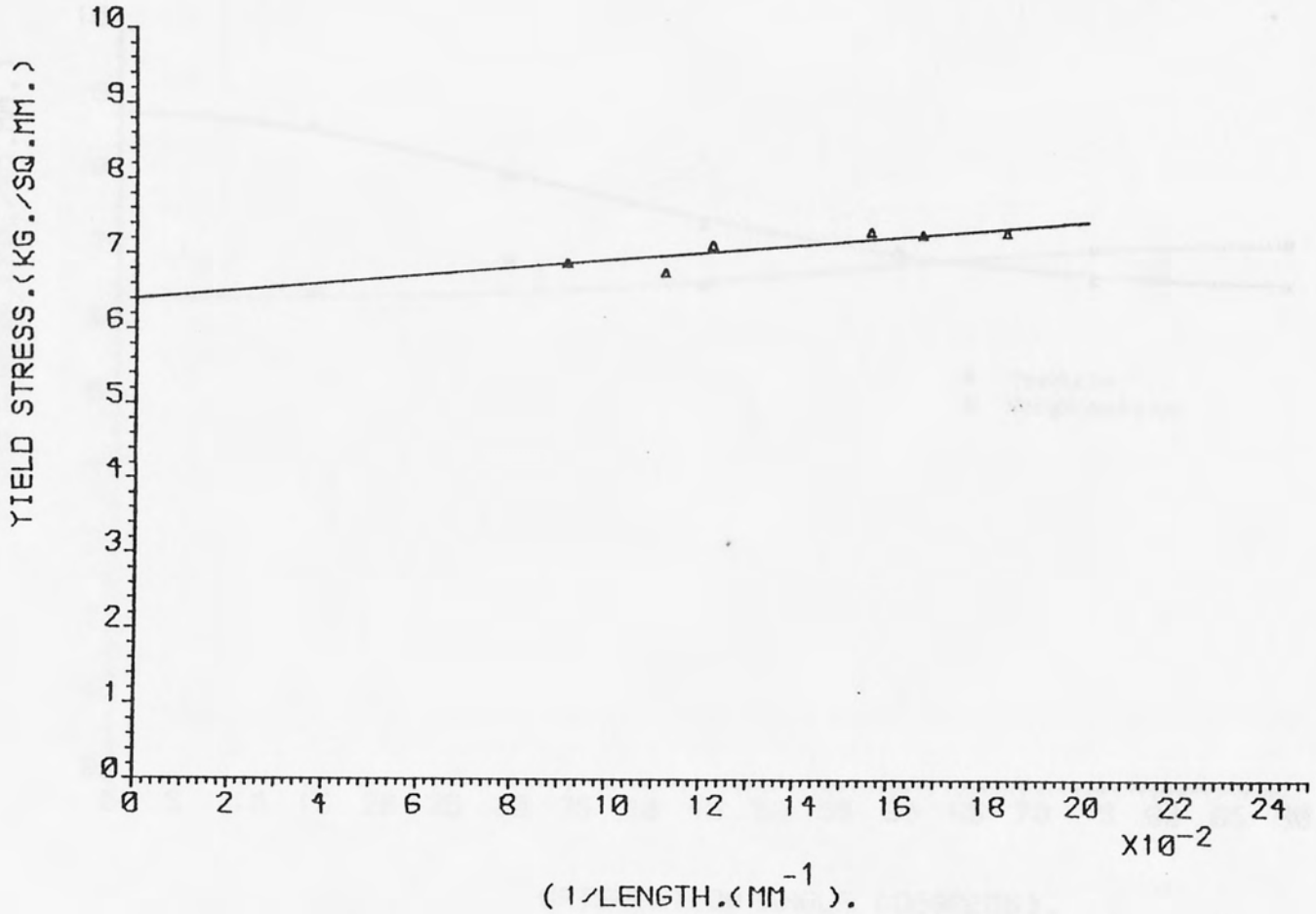

Fig. (7.5)

Fig. (7.5) Plot of the compressive yield stress against reciprocal of specimen length for rolled polycarbonate

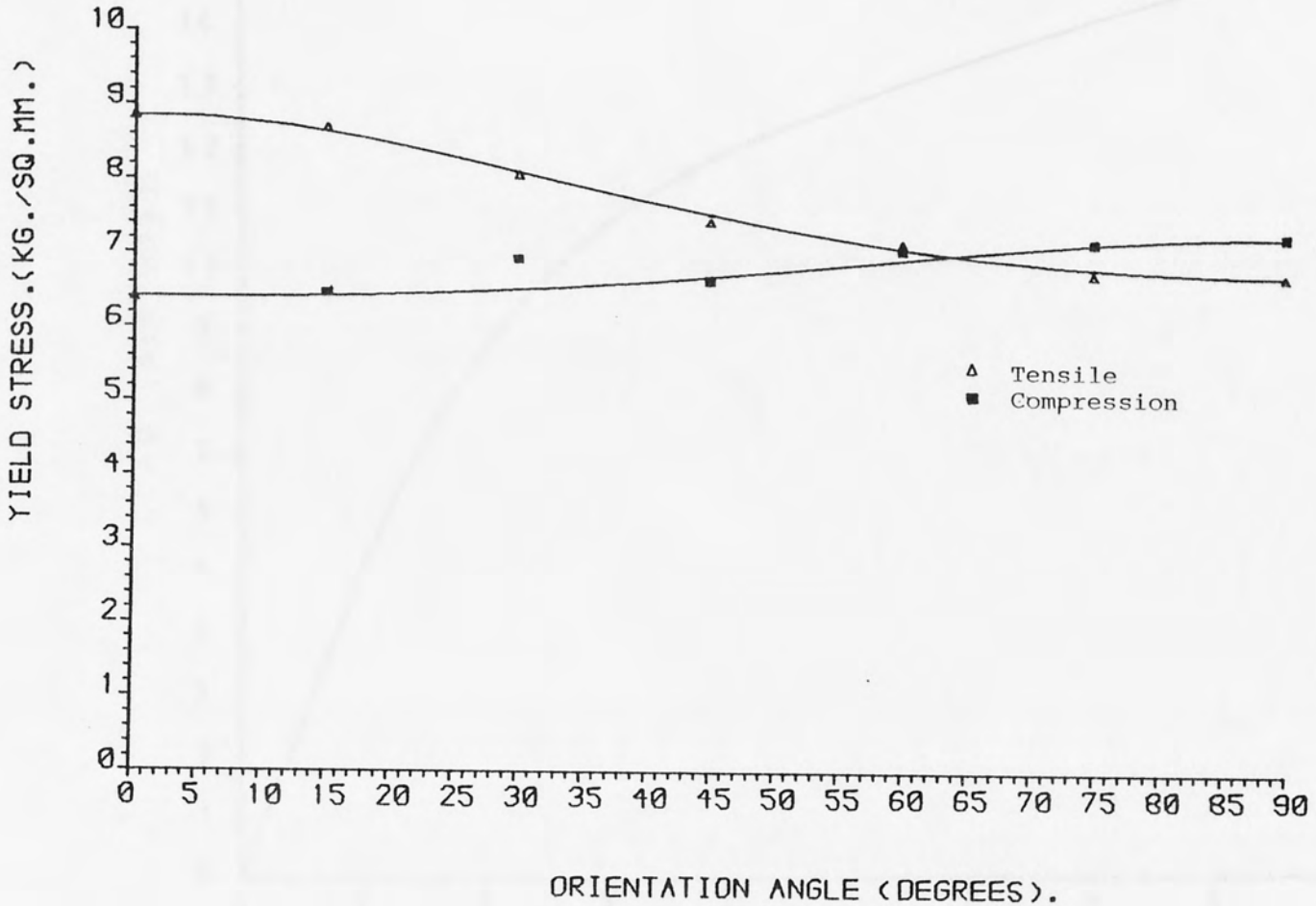

Fig. (7.6)

Fig. (7.6) Variation of tensile and compressive yield stresses with the orientation angle for rolled polycarbonate

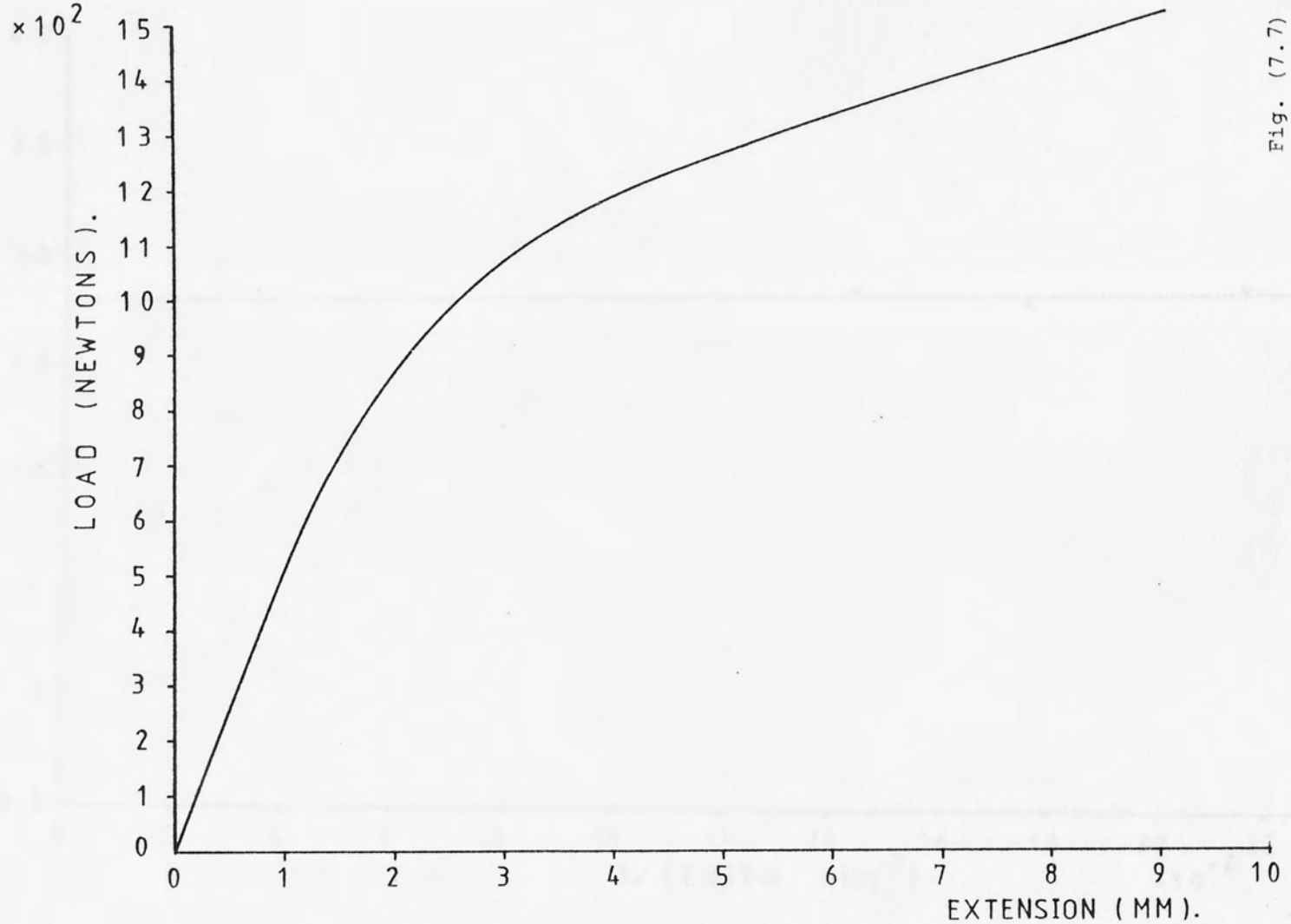

Fig. (7.7)

Fig. (7.7) Load-extension curve for as-received Nylon (Tensile)

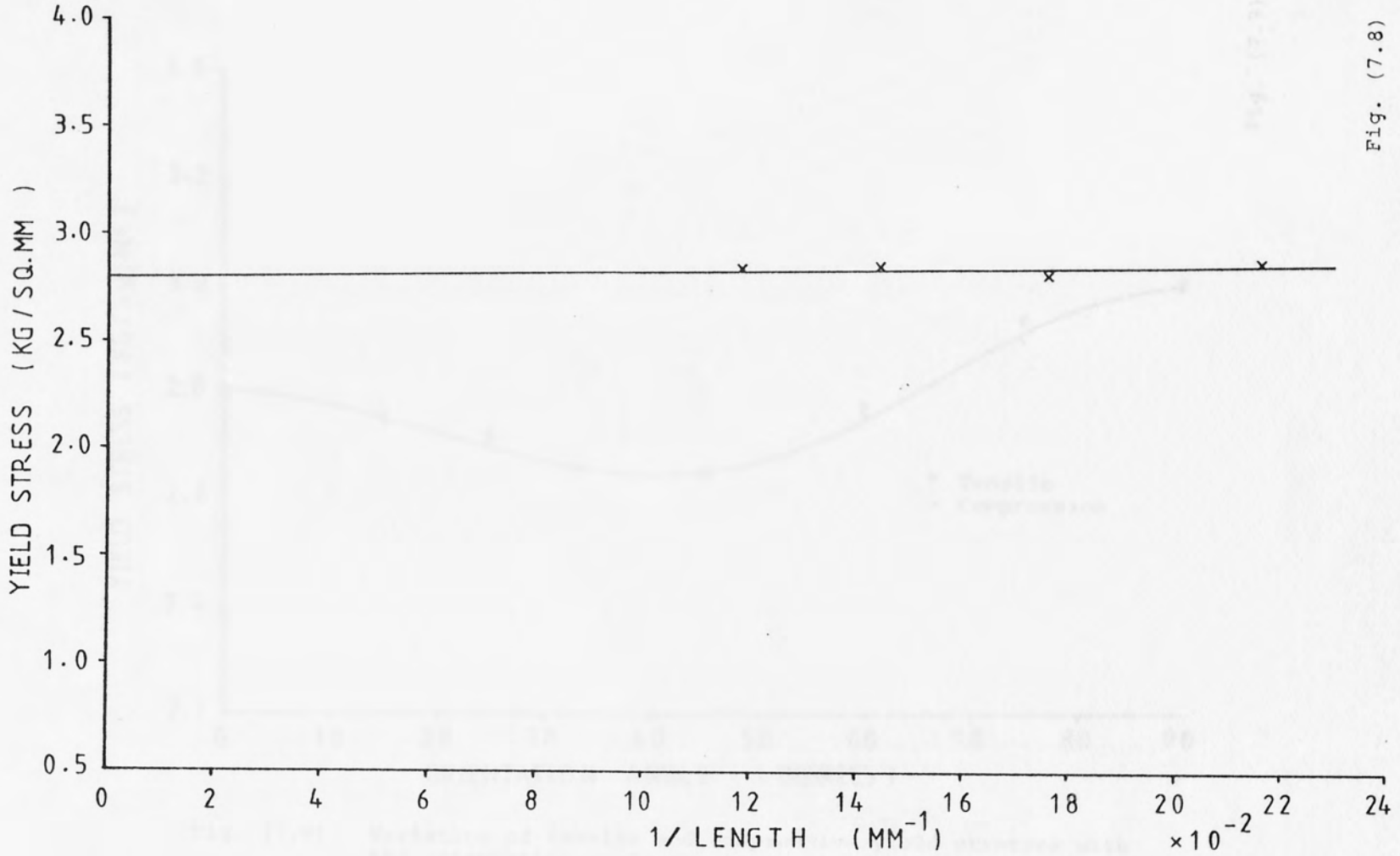

Fig. (7.8)

Fig. (7.8) Plot of the compressive yield stress against reciprocal of specimen length for as-received Nylon

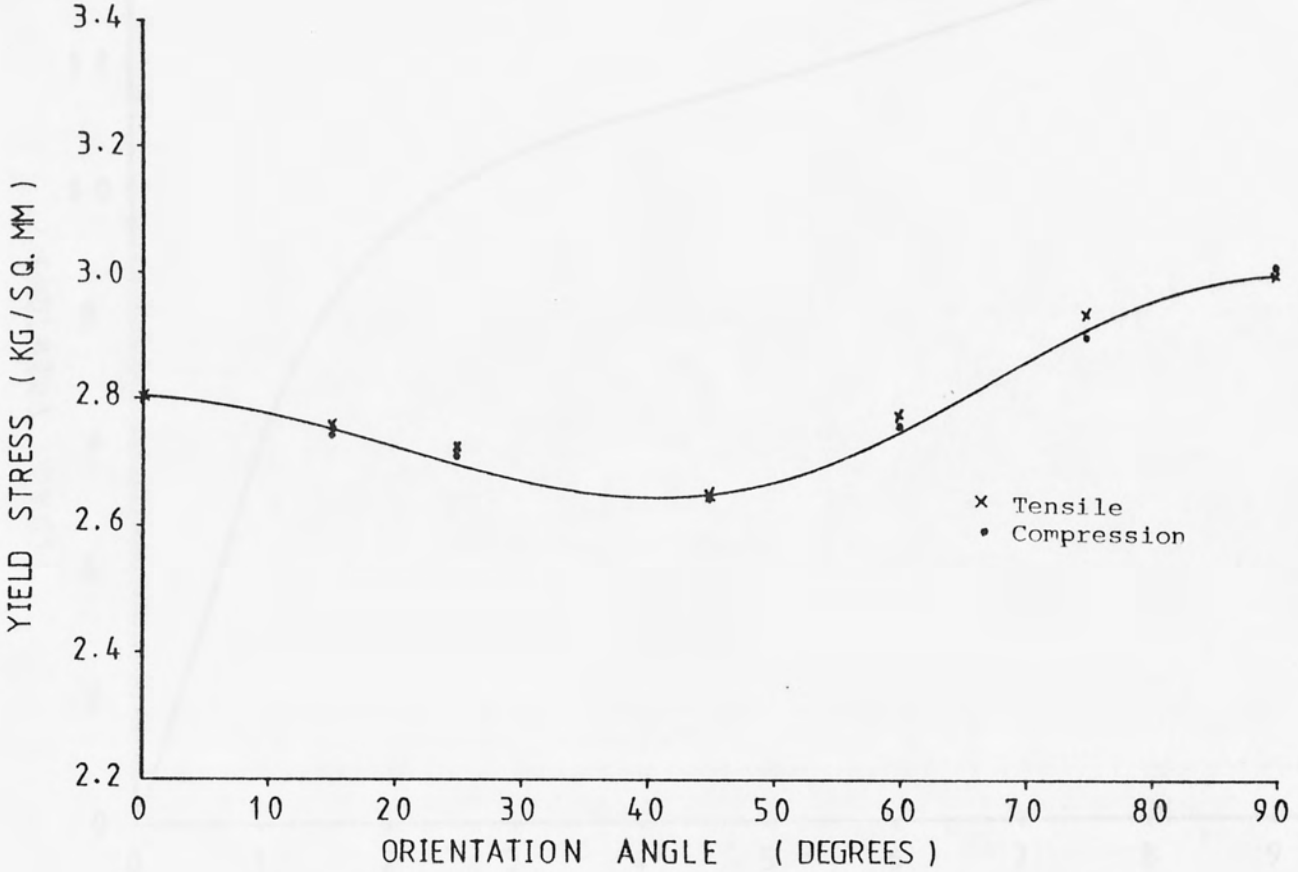

Fig. (7.9)

Fig. (7.9) Variation of tensile and compressive yield stresses with the orientation angle for as-received Nylon

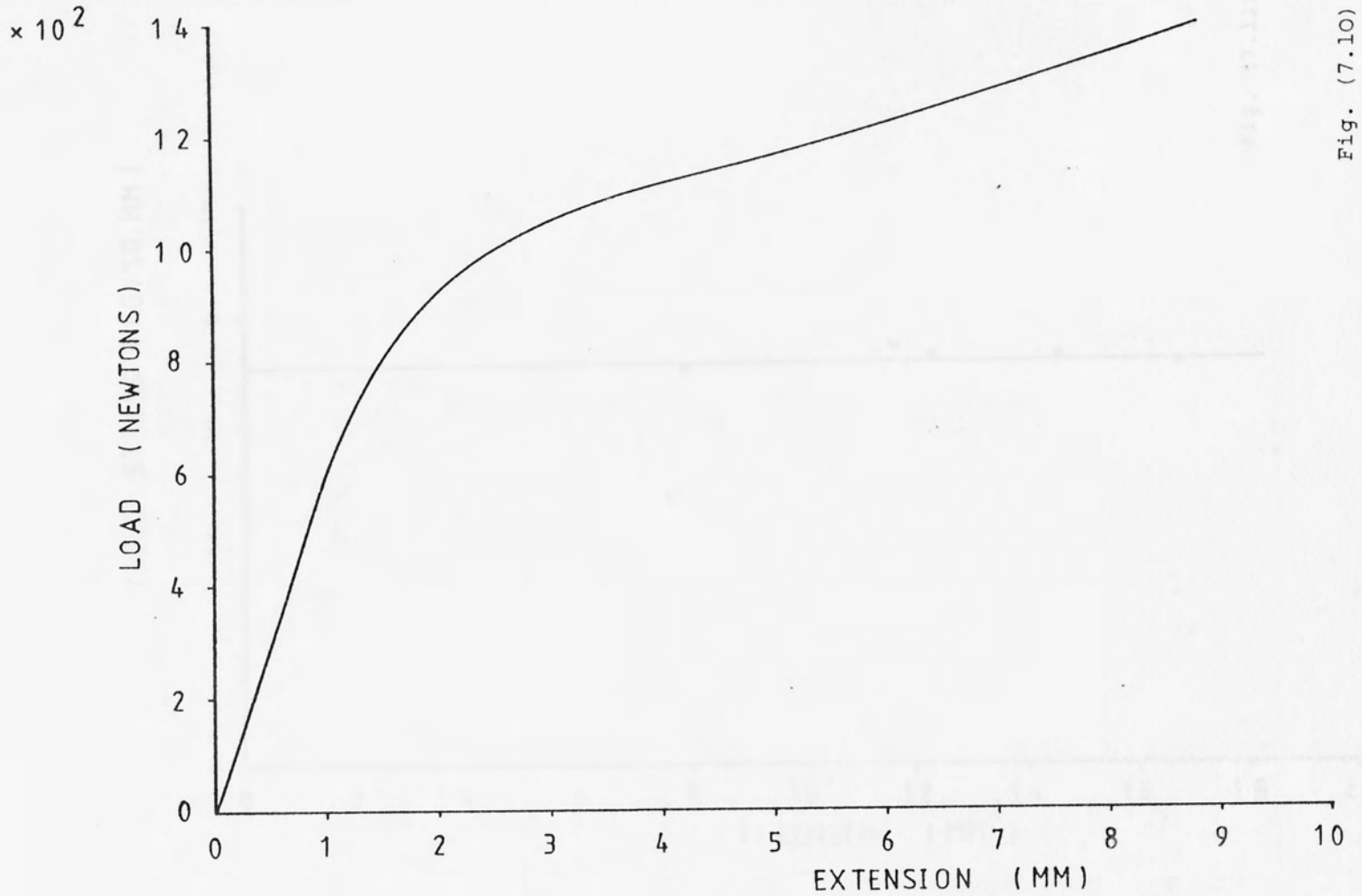

Fig. (7.10)

Fig.(7.10) Load-extension curve for rolled Nylon (Tensile)

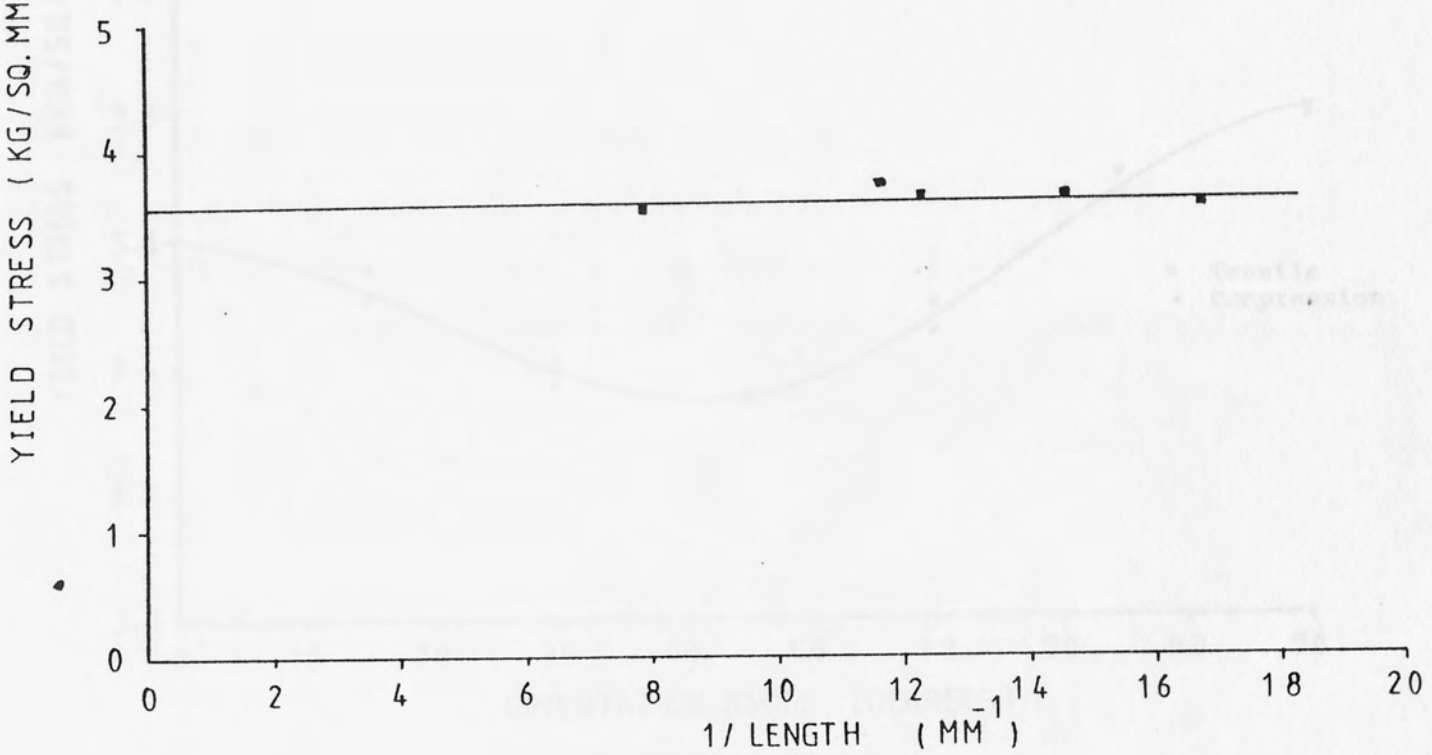

Fig. (7.11) Plot of the compressive yield stress against reciprocal of specimen length for rolled Nylon

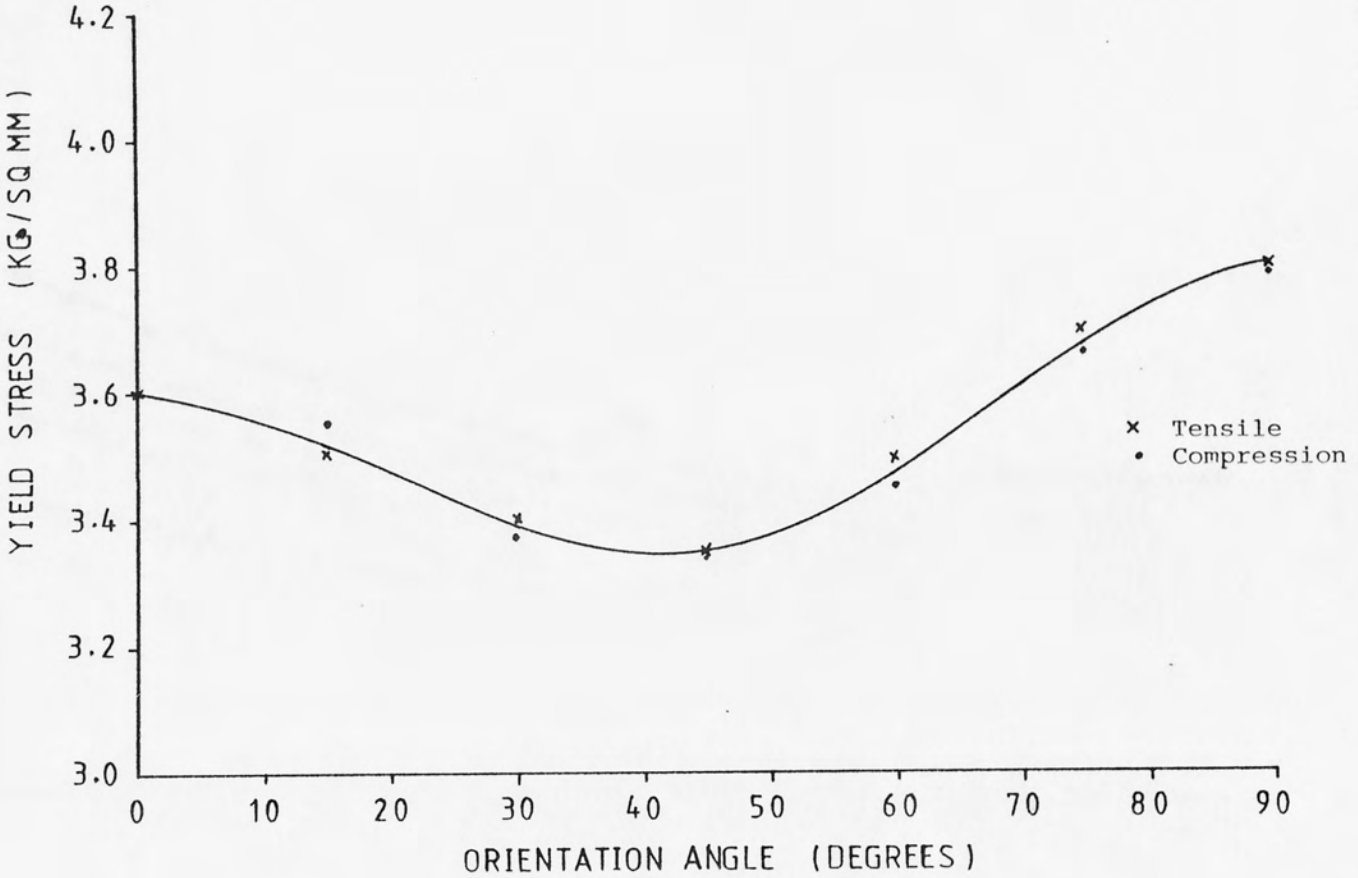

Fig. (7.12)

Fig. (7.12) Variation of tensile and compressive yield stresses with the orientation angle for rolled Nylon

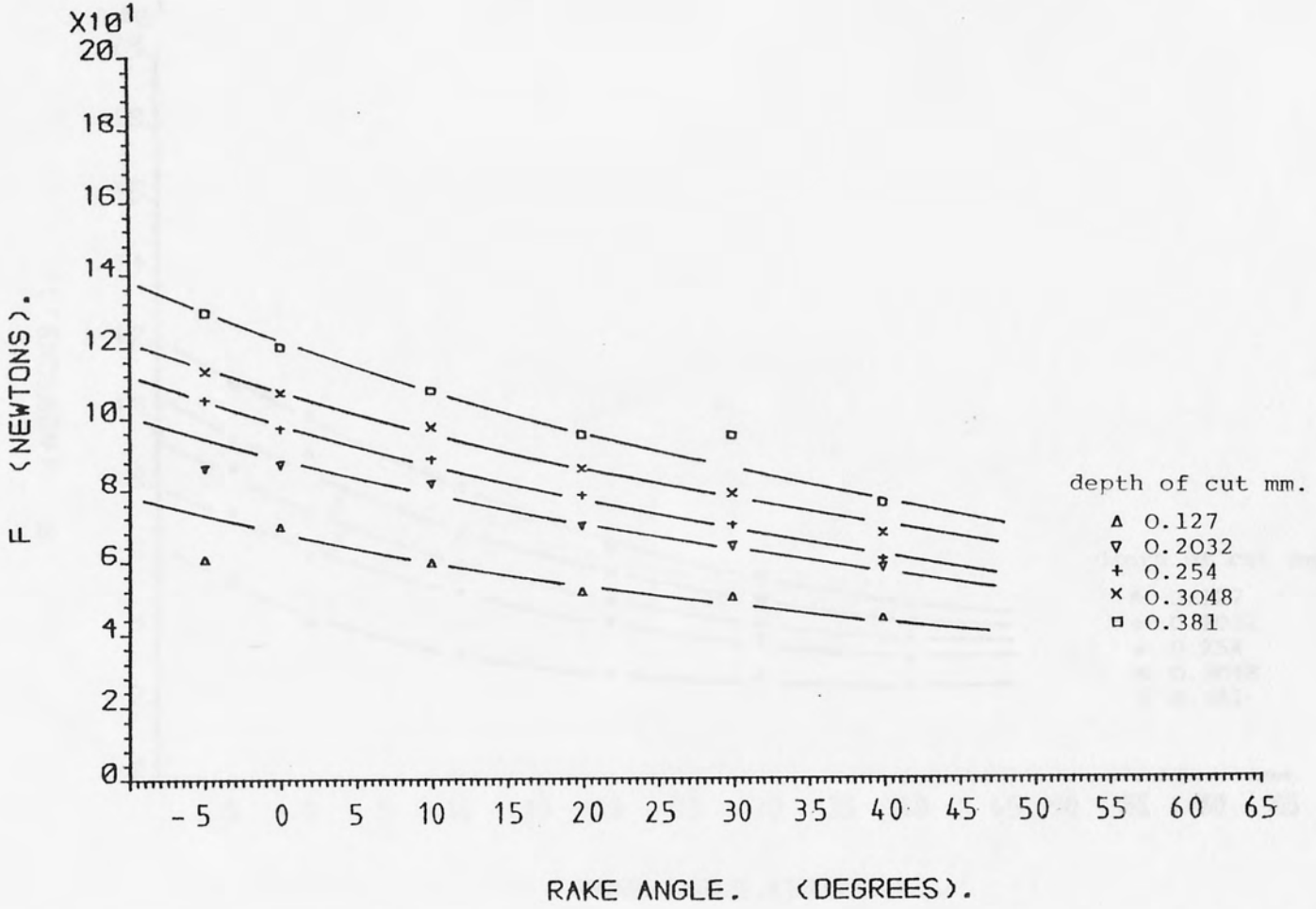

Fig. (7.13)

FIG. (7.13). F as a function of rake angle for as-received polycarbonate, cutting speed 15.24 m/min.

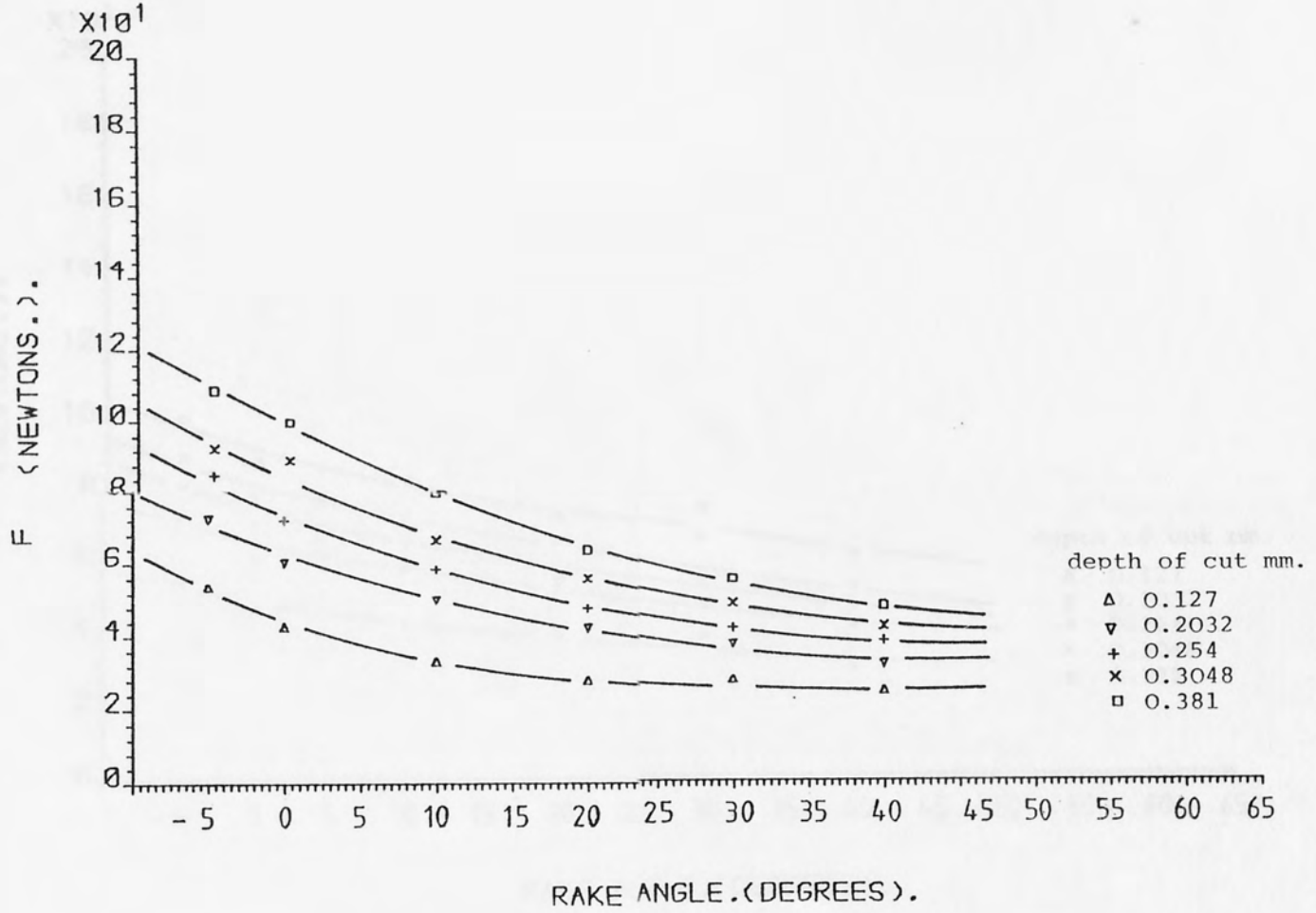

Fig. (7.14)

FIG. (7.14) F as a function of rake angle for rolled polycarbonate, cutting speed 15.24 m/min.

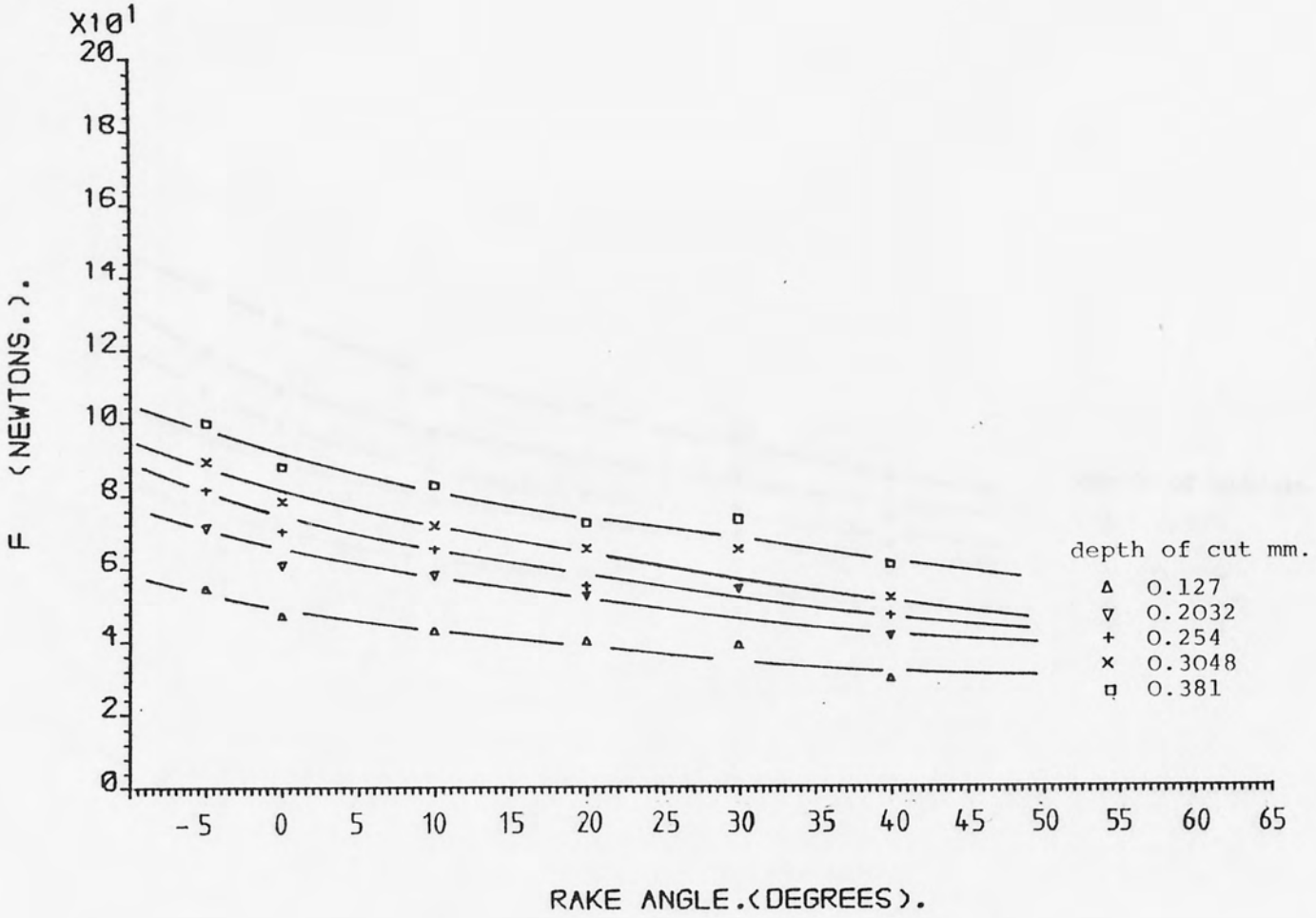

Fig. (7.15)

FIG. (7.15). F as a function of rake angle for as-received Nylon, cutting speed 15.24 m/min.

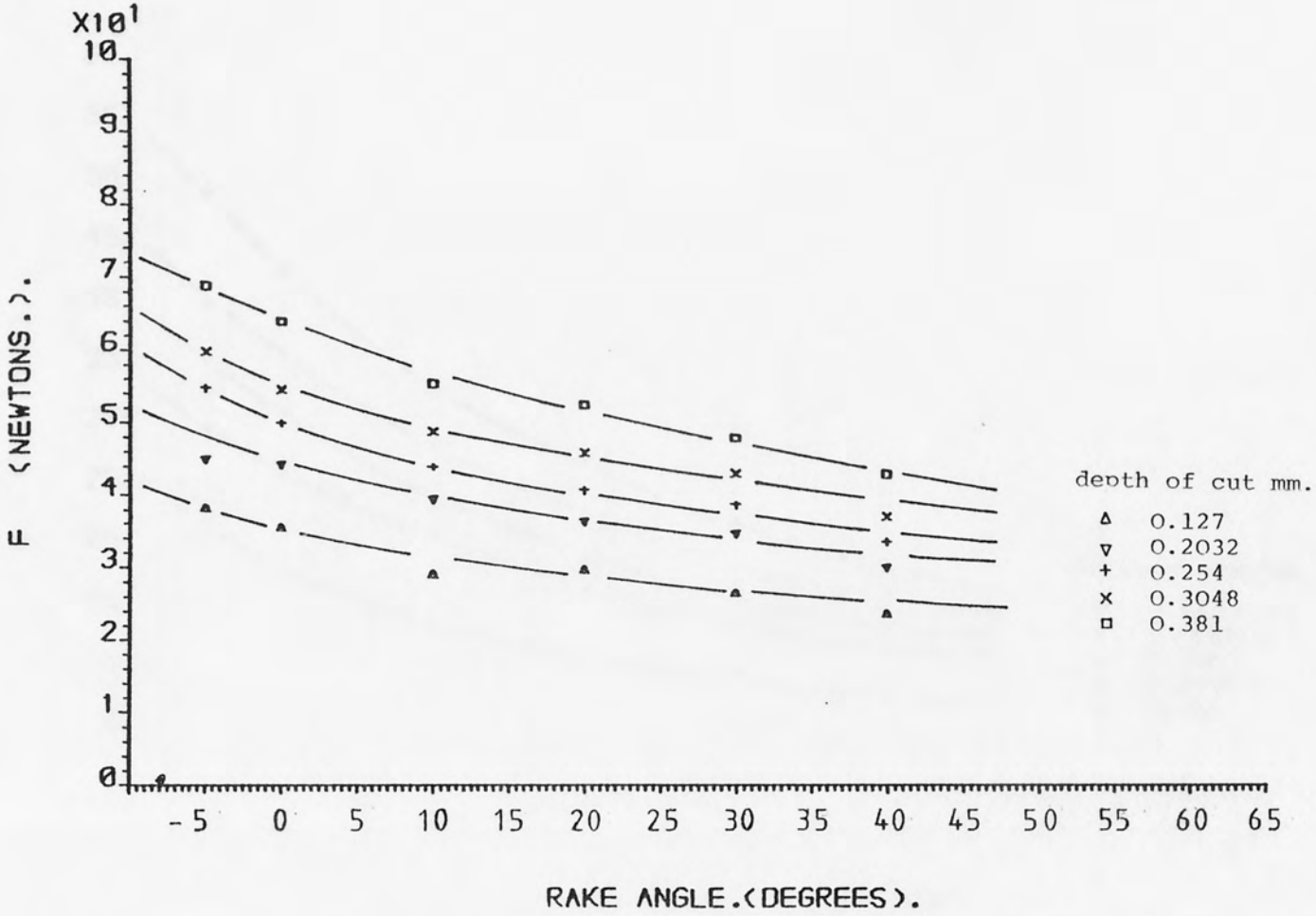

Fig. (7.16)

FIG. (7.16). F as a function of the rake angle for rolled Nylon, cutting speed 15.24 m/min.

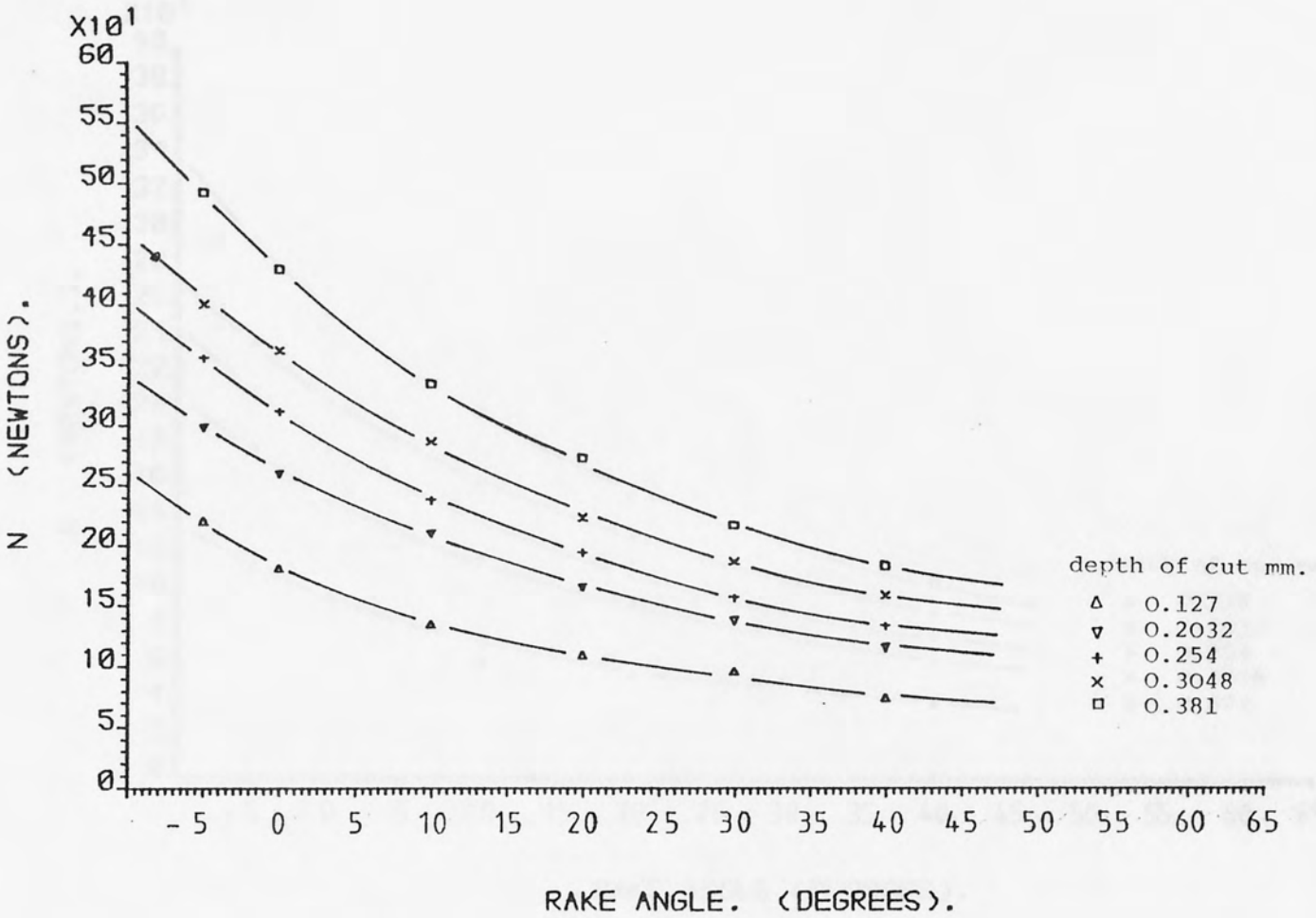

Fig. (7.17)

FIG. (7.17) N as a function of rake angle for as-received polycarbonate, cutting speed 15.24 m/min.

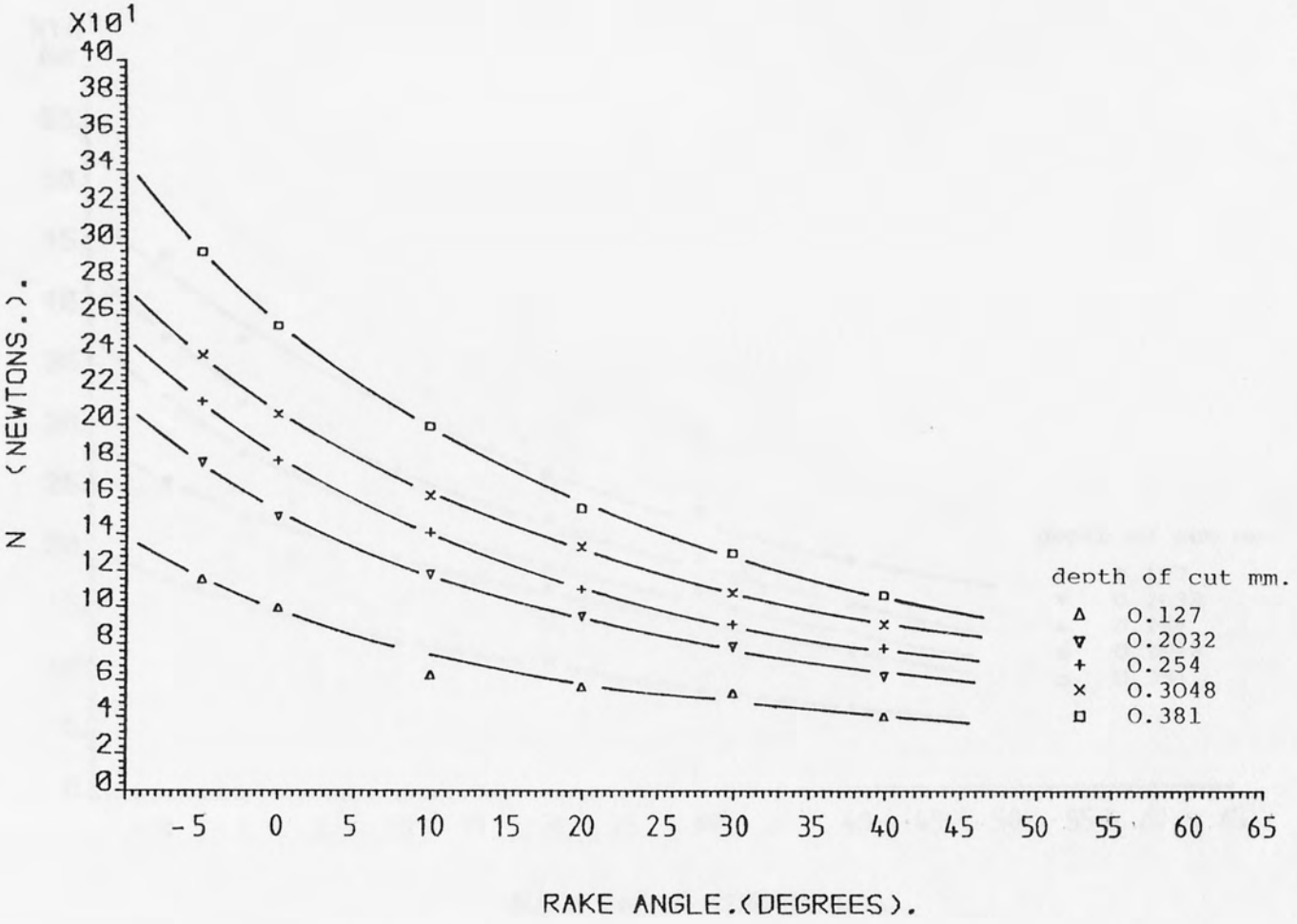

Fig. (7.18)

FIG. (7.18). N as a function of rake angle for rolled polycarbonate, cutting speed 15.24 m/min.

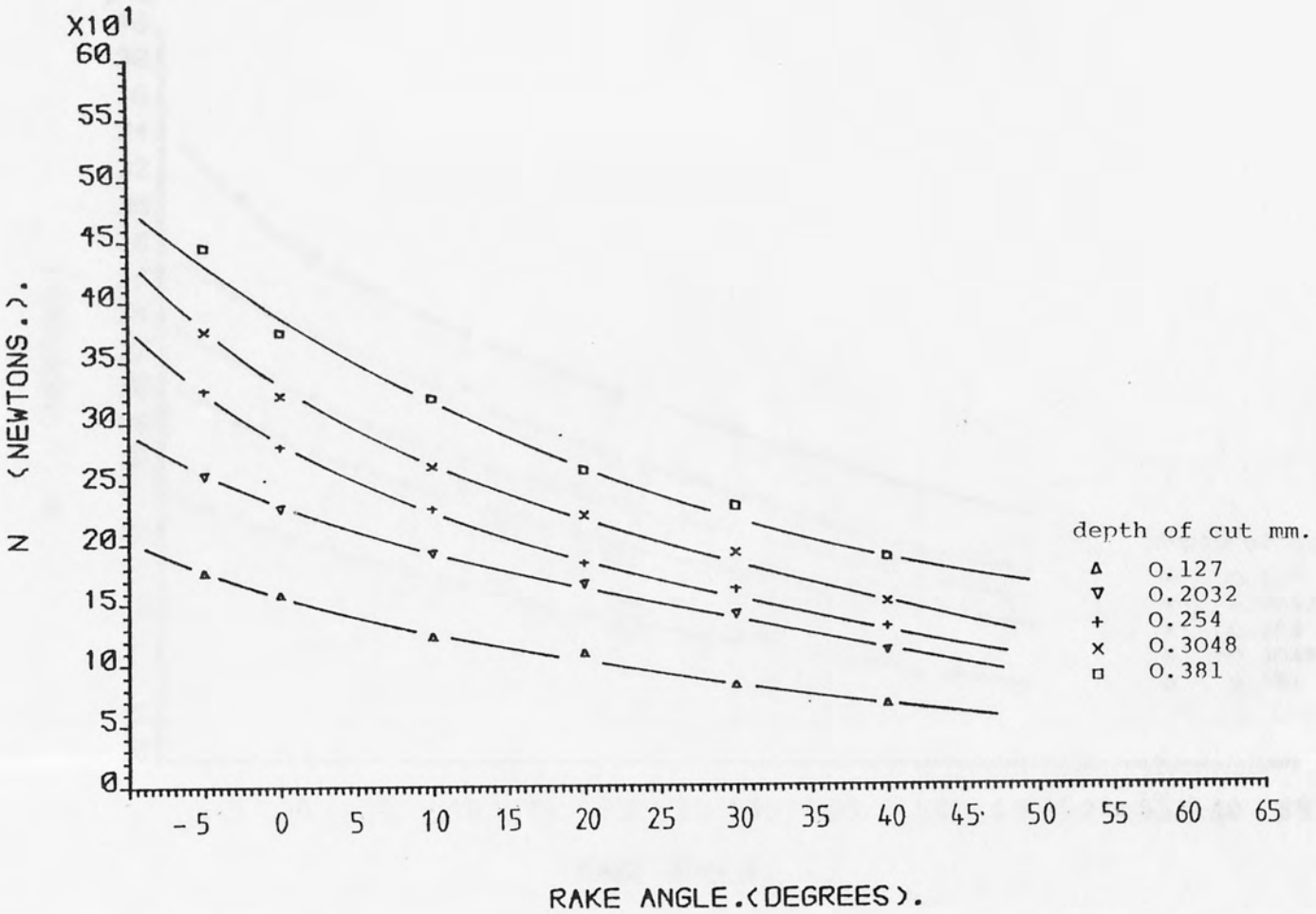

Fig. (7.19)

FIG. (7.19). N as a function of rake angle for as-received Nylon, cutting speed 15.24 m/min.

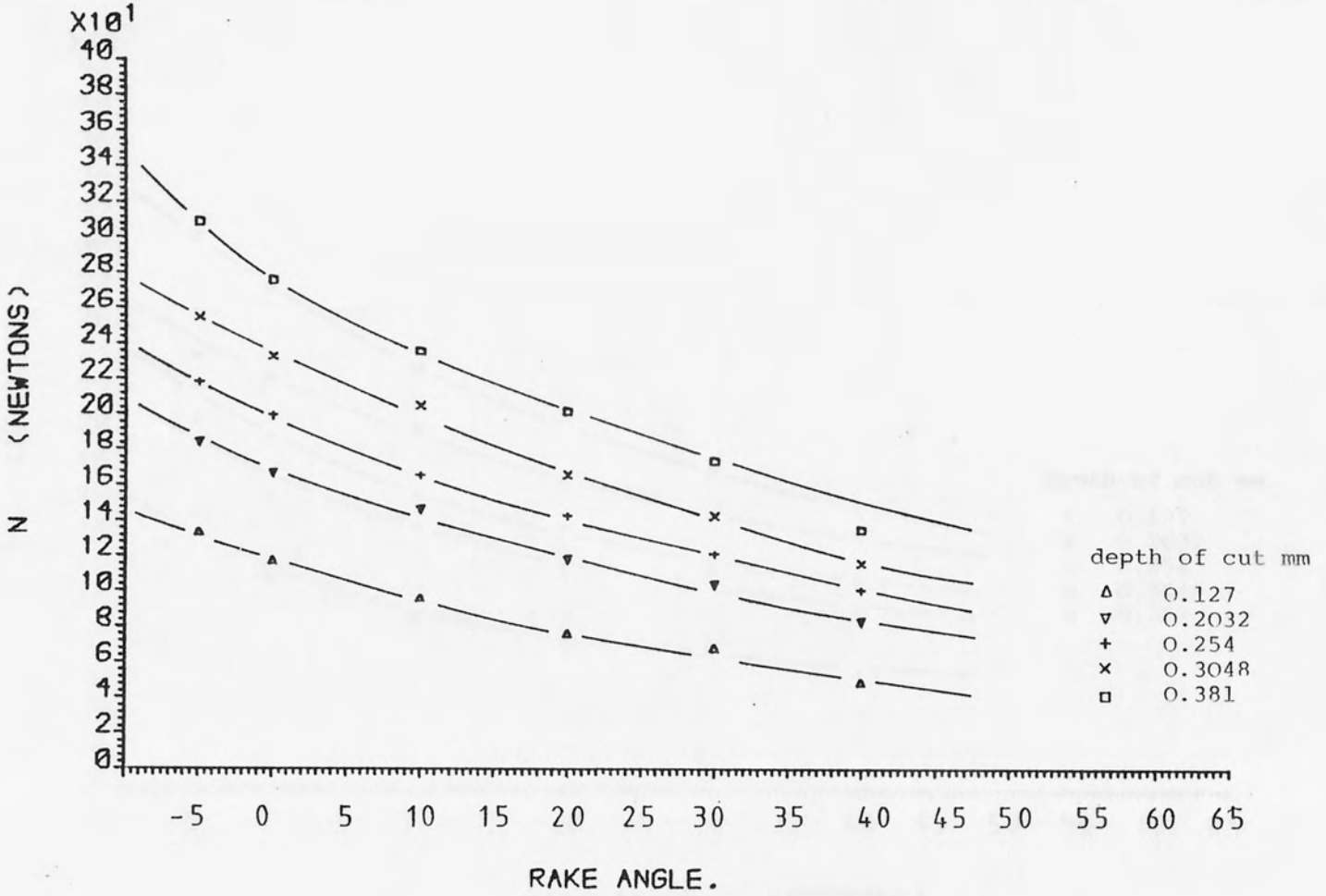

Fig. (7.20)

Fig. (7.20). N as a function of rake angle for rolled Nylon, cutting speed 15.24 m/min.

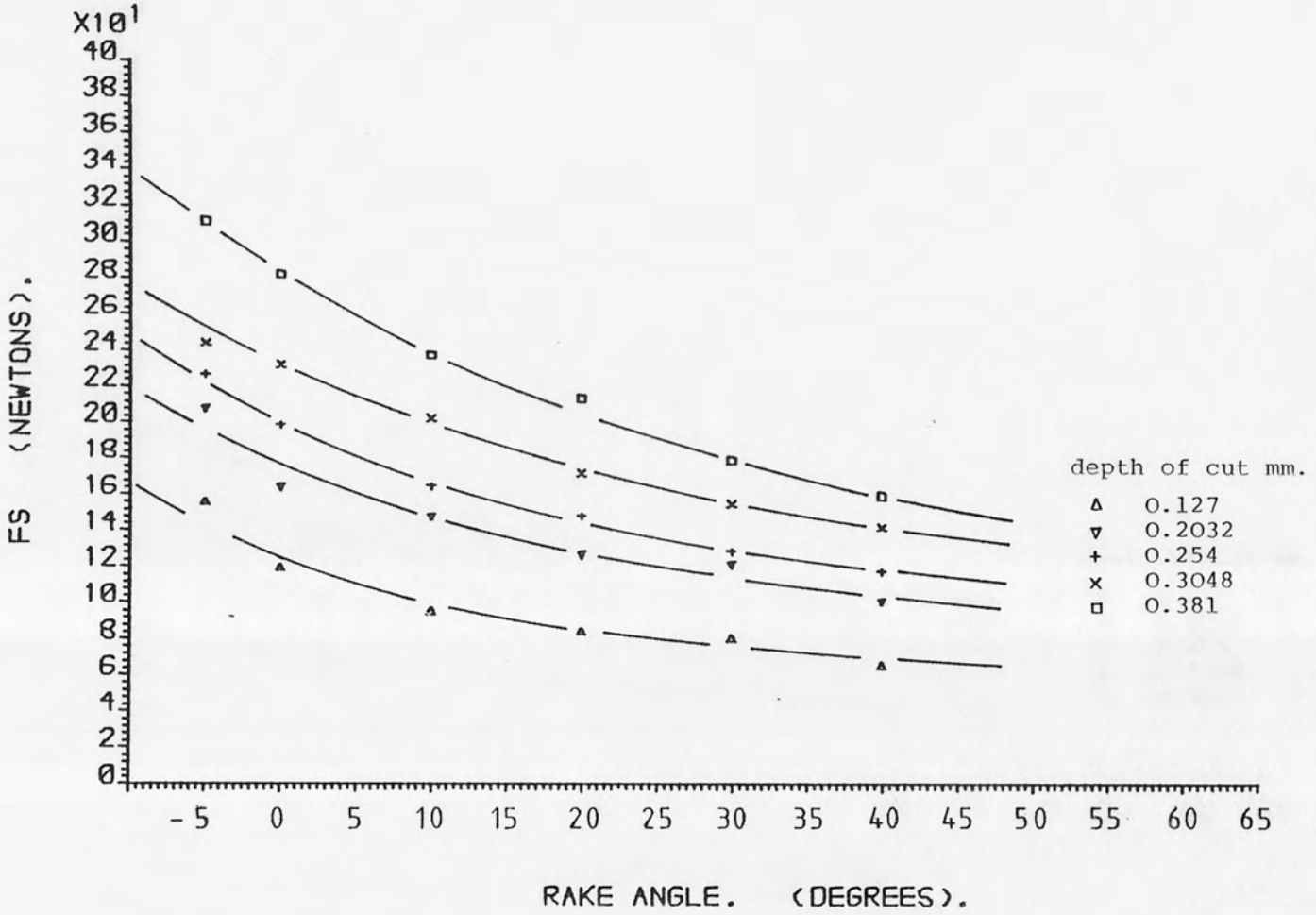

Fig. (7.21)

FIG. (7.21). F_s as a function of rake angle for as-received polycarbonate, cutting speed 15.24 m/min.

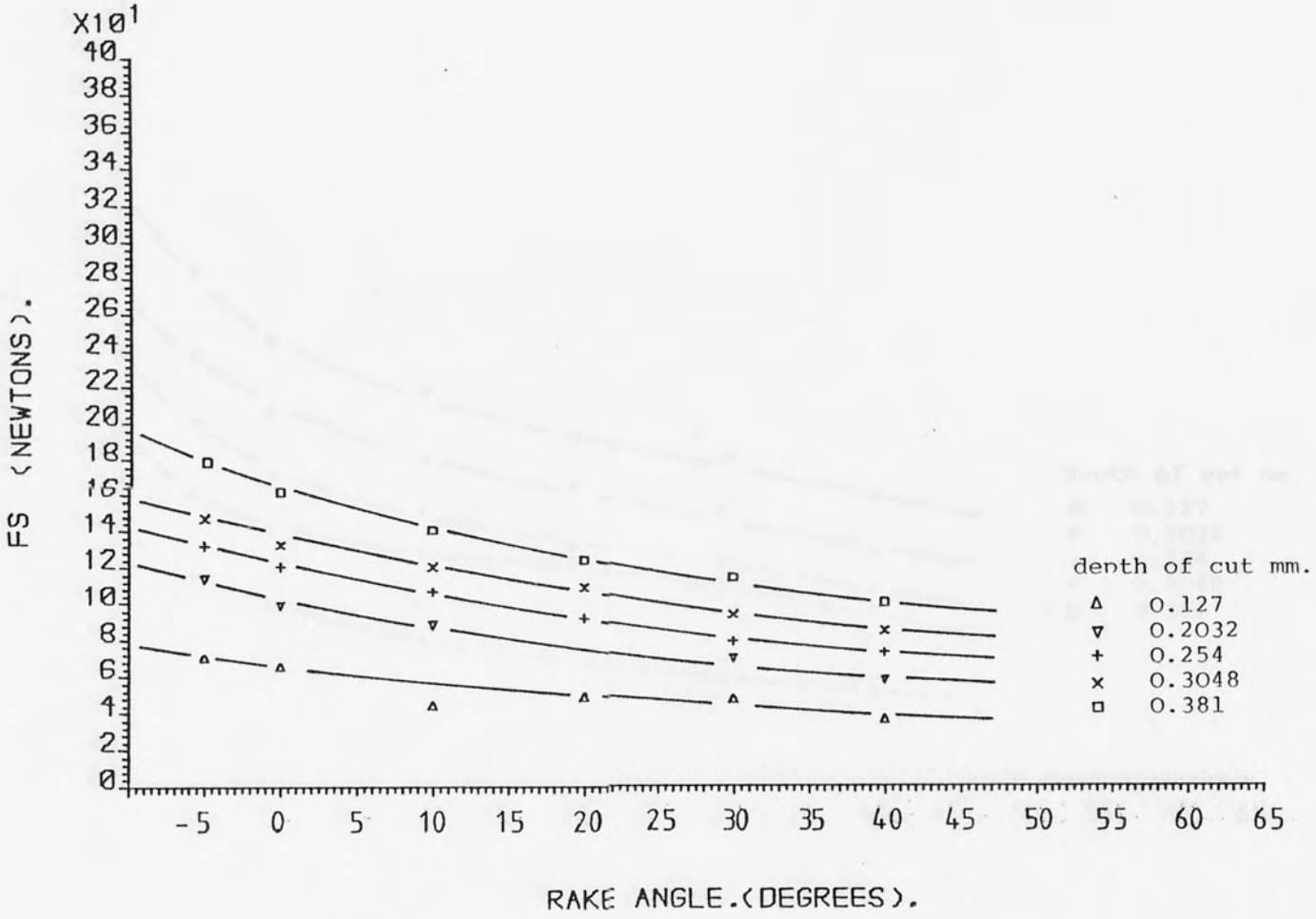

FIG. (7.22) F_s as a function of rake angle for rolled polycarbonate, cutting speed 15.24 m/min.

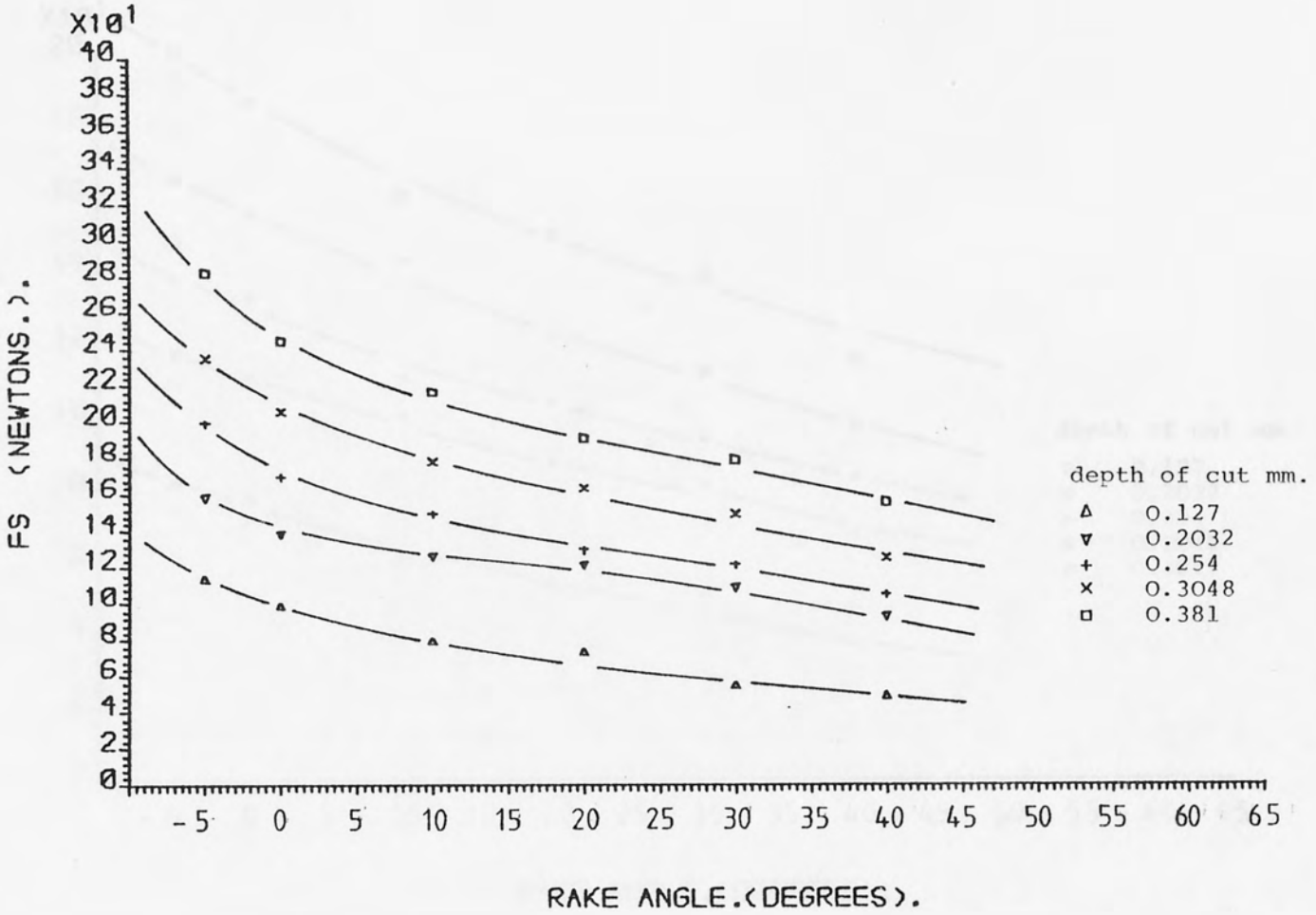

Fig. (7.23)

FIG. (7.23). F_s as a function of rake angle for as-received Nylon, cutting speed 15.24 m/min.

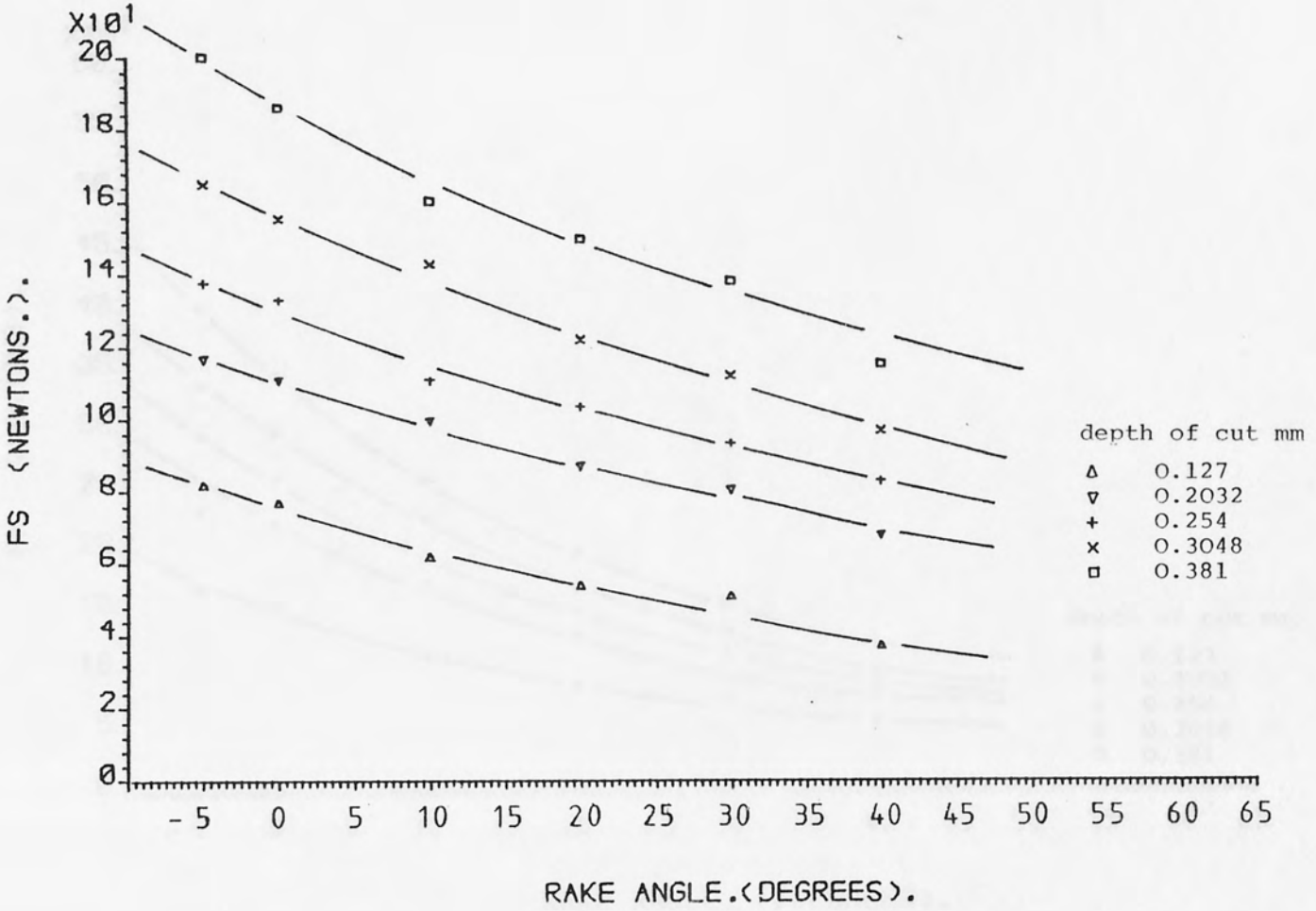

Fig. (7.24)

FIG. (7.24). F_s as a function of rake angle for rolled Nylon, cutting speed 15.24 m/min.

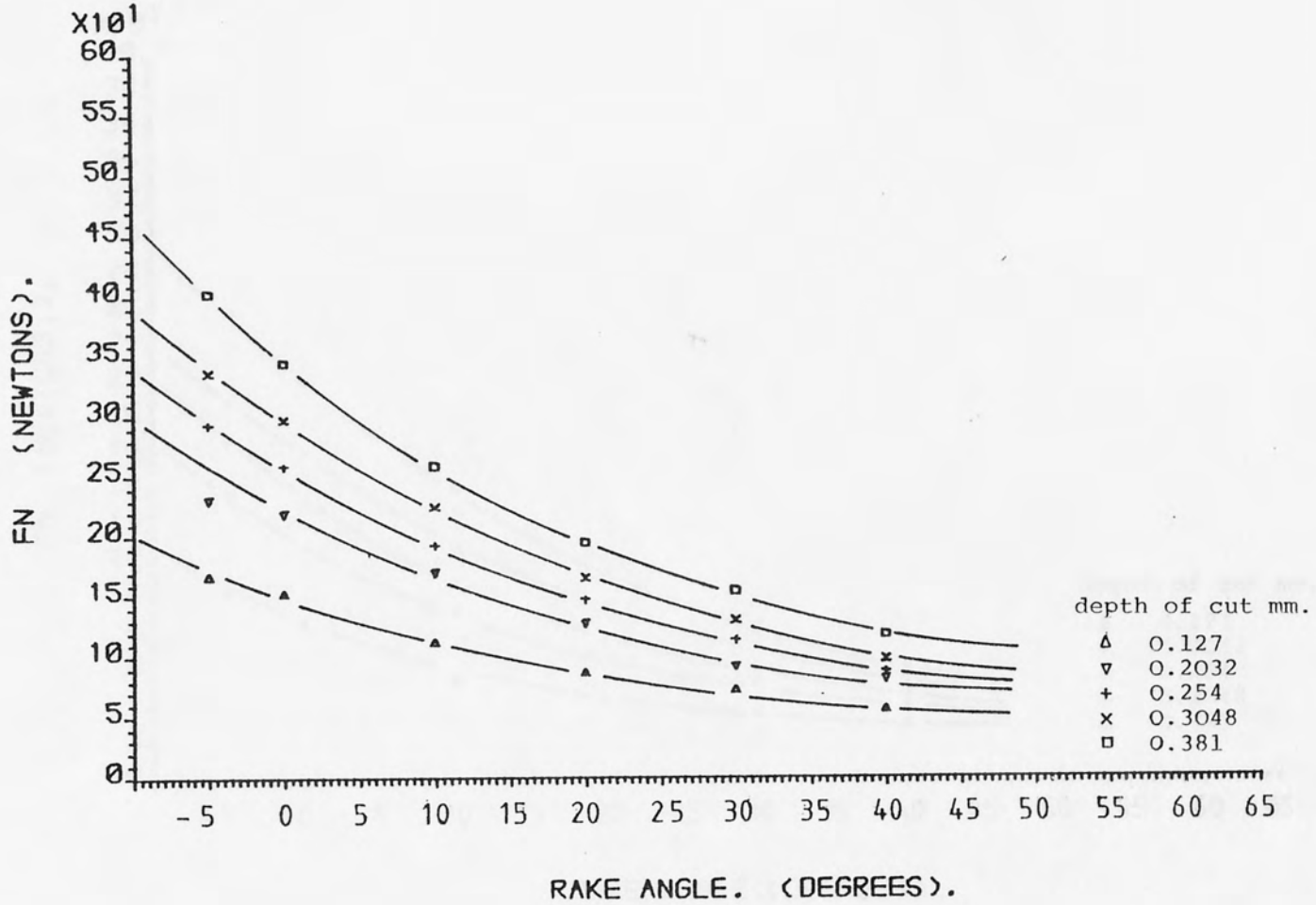

Fig. (7.25)

FIG. (7.25). F_n as a function of rake angle for as-received polycarbonate, cutting speed 15.24 m/min.

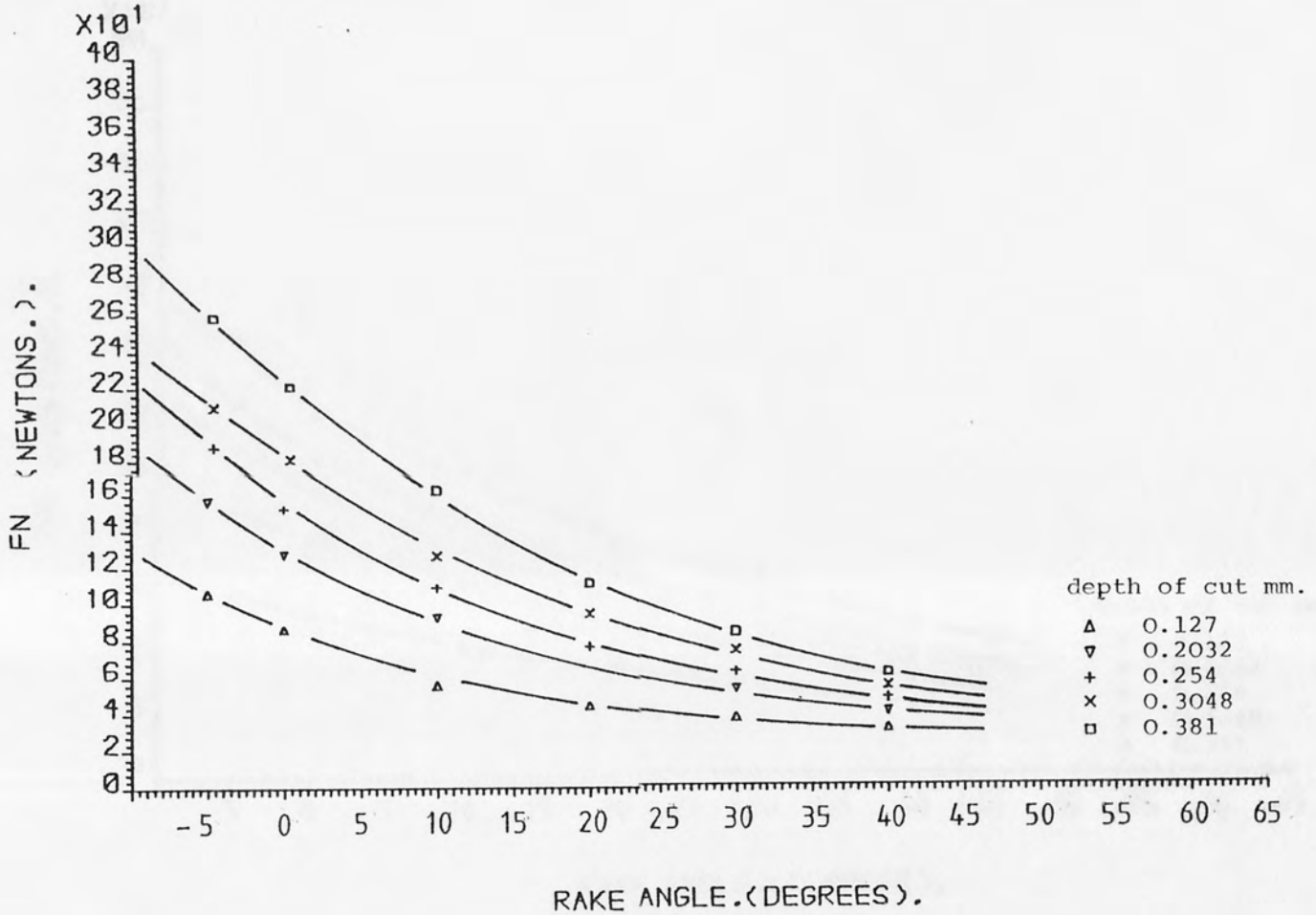

Fig. (7.26)

FIG. (7.26). F_n as a function of rake angle for rolled polycarbonate, cutting speed 15.24 m/min.

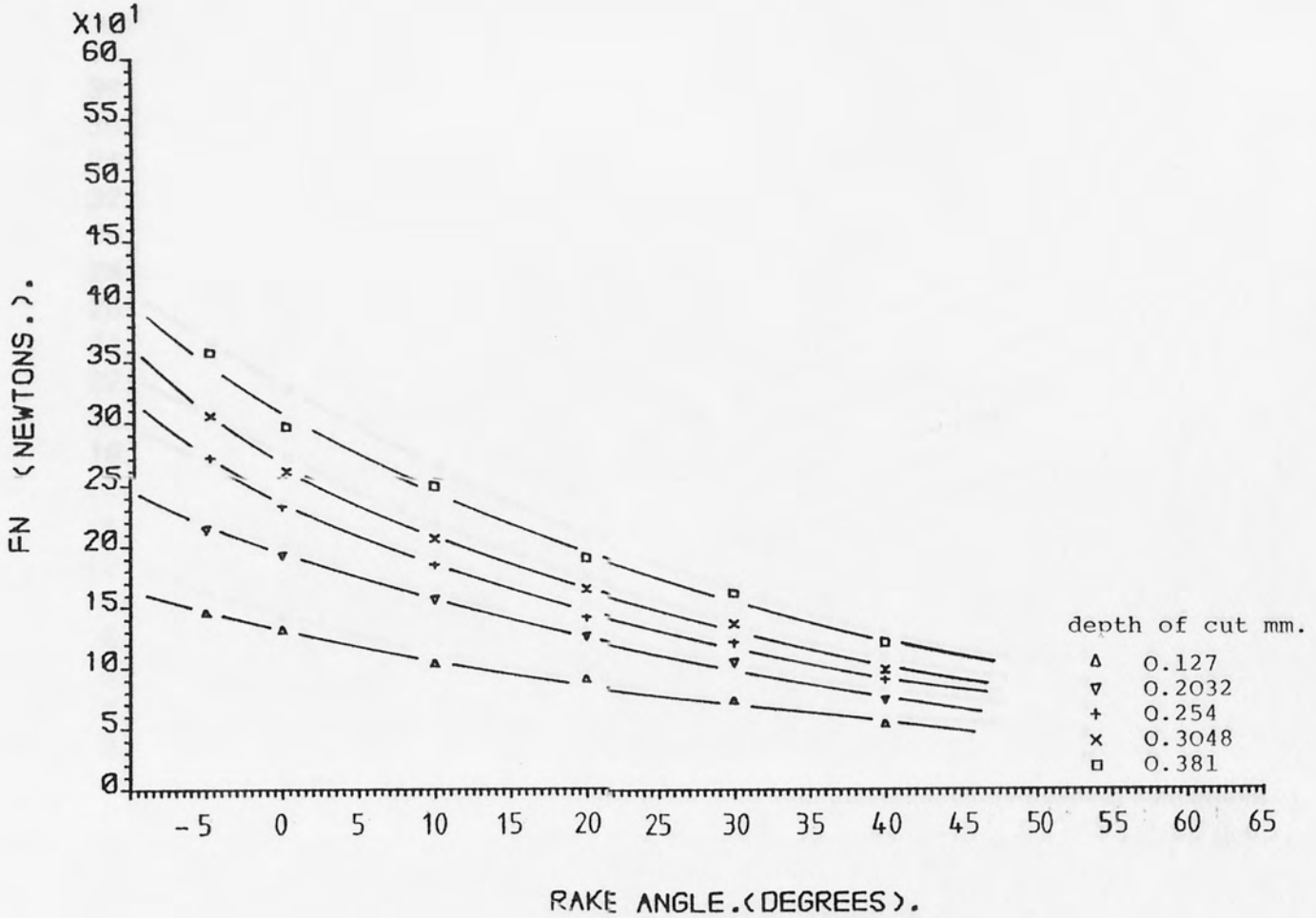

Fig. (7.27)

FIG. (7.27). F_n as a function of rake angle for as-received Nylon, cutting speed 15.24 m/min.

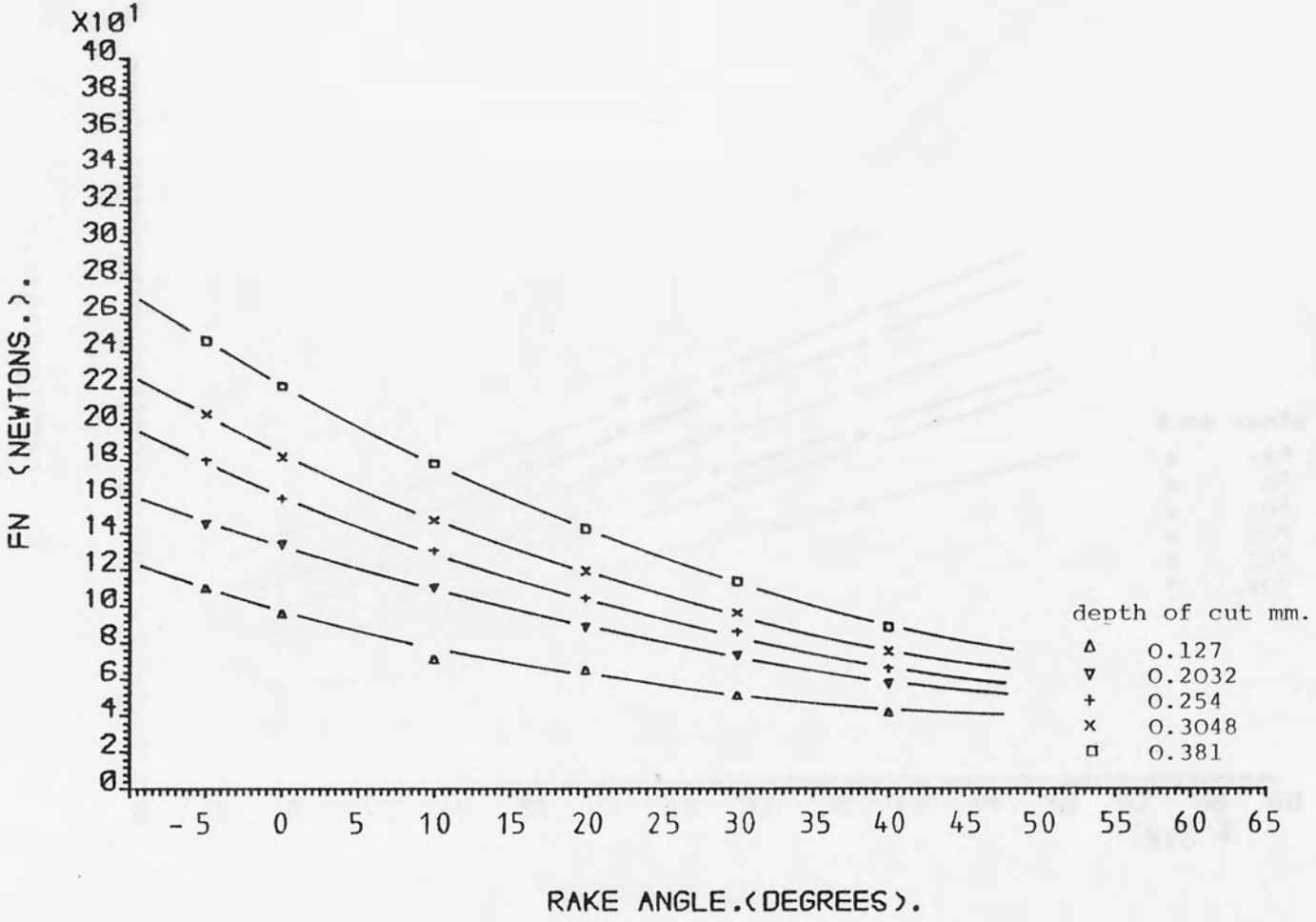

Fig. (7.28)

FIG. (7.28). F_n as a function of rake angle for rolled Nylon, cutting speed 15.24 m/min.

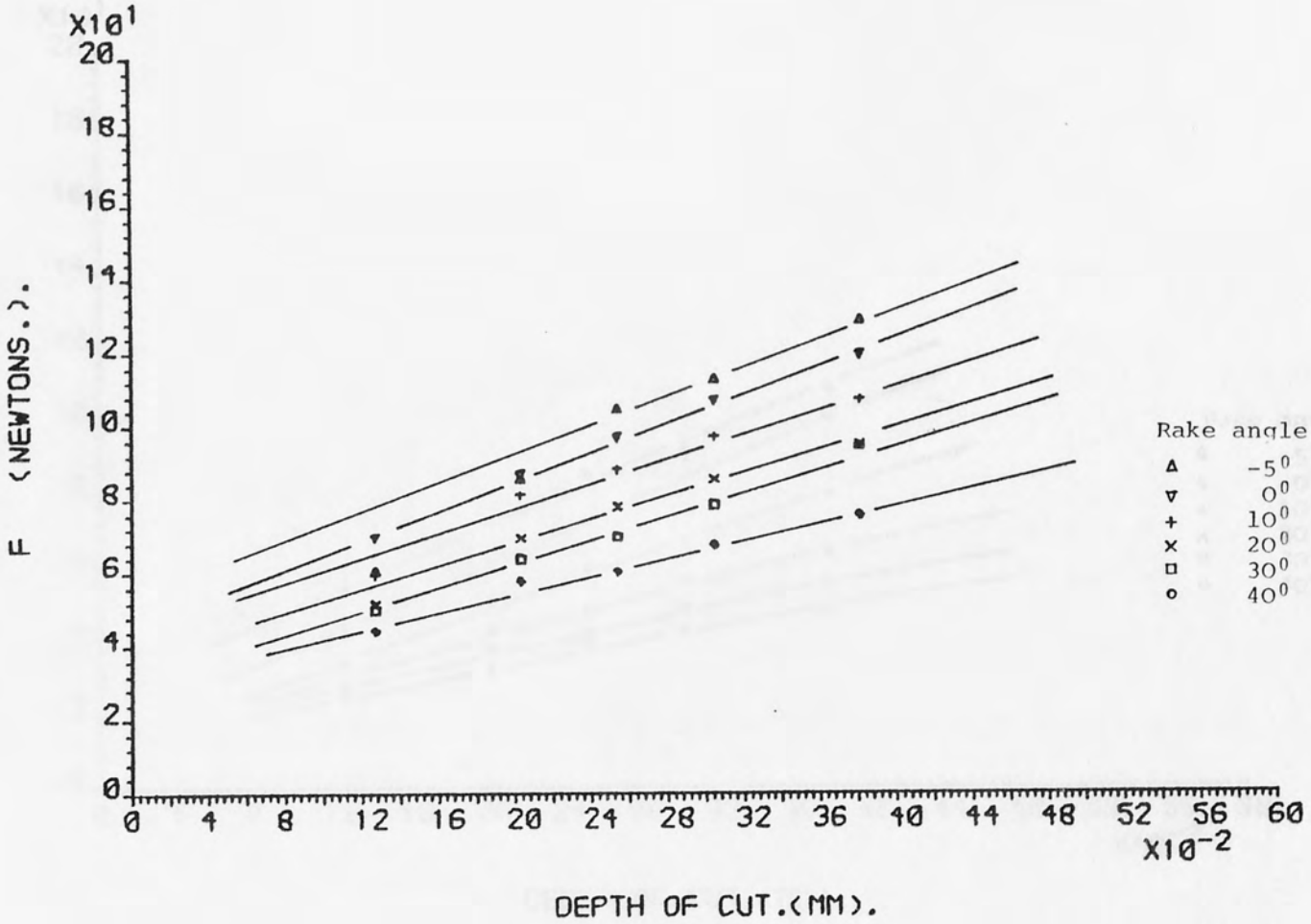

Fig. (7.29)

FIG. (7.29). F as a function of depth of cut for as-received polycarbonate, cutting speed 15.24 m/min.

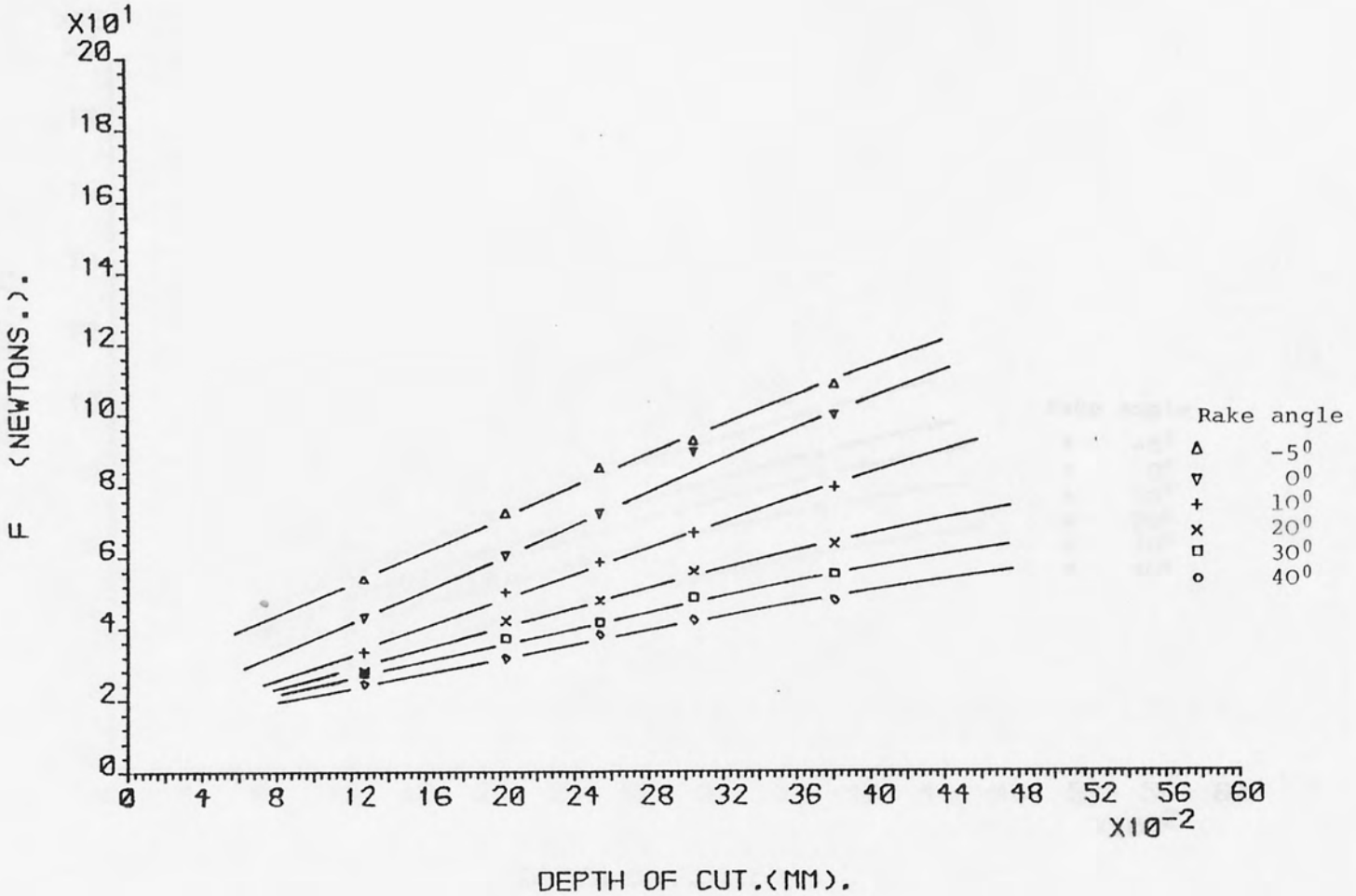

Fig. (7.30)

FIG. (7.30). F as a function of depth of cut for rolled polycarbonate, cutting speed 15.24 m/min.

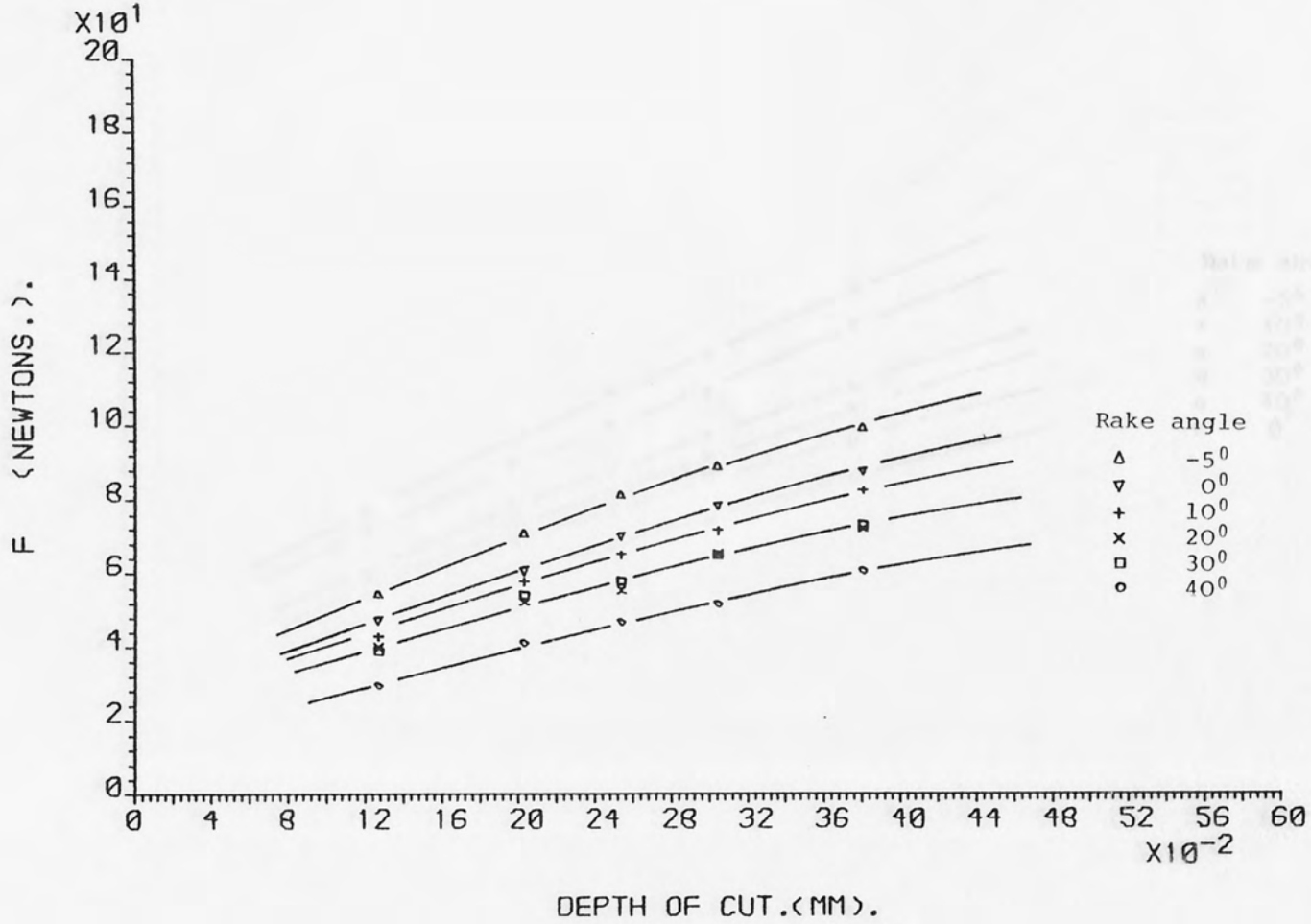

Fig. (7.31)

FIG. (7.31). F as a function of depth of cut for as-received Nylon, cutting speed 15.24 m/min.

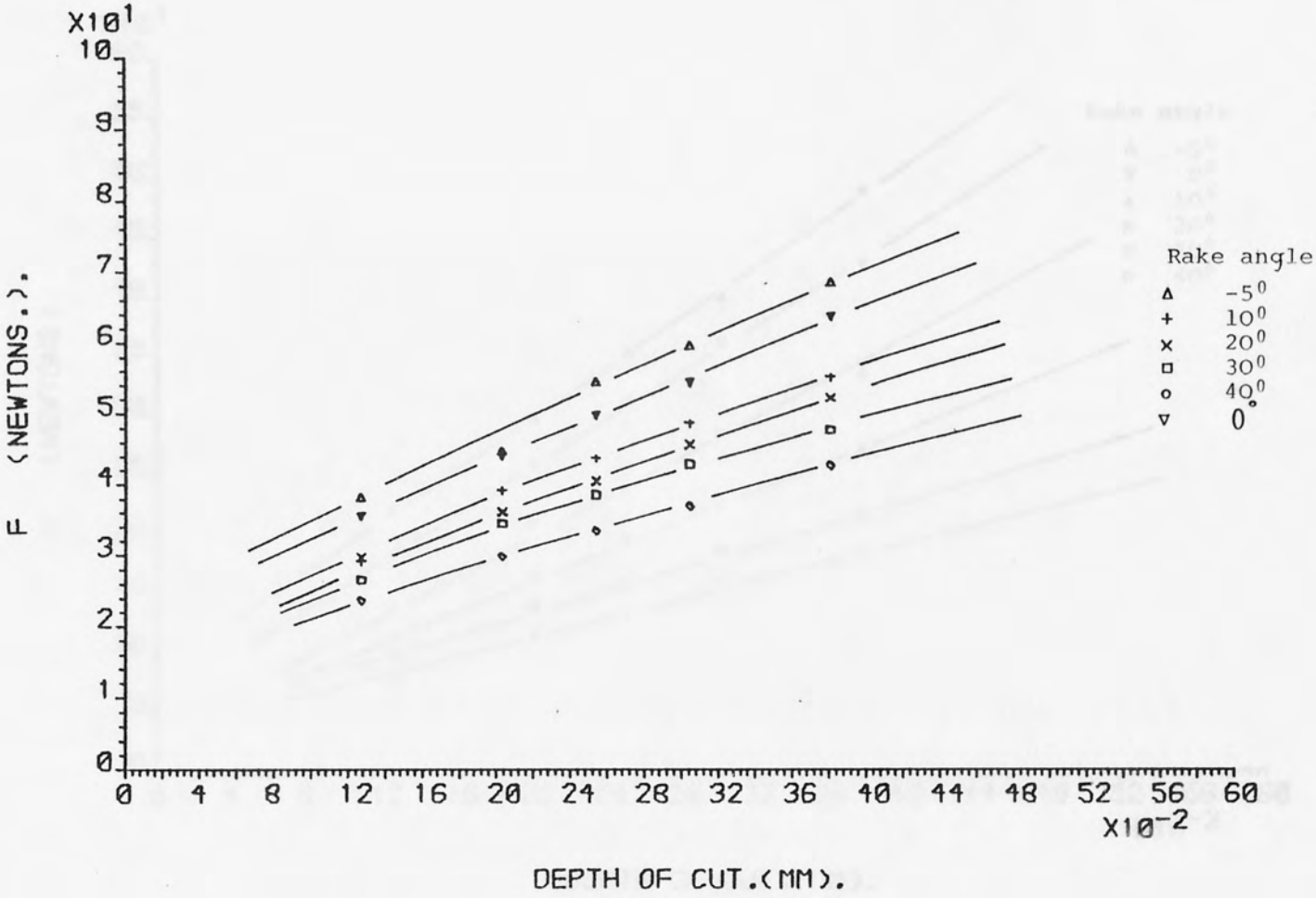

Fig. (7.32)

FIG. (7.32) F as a function of depth of cut for rolled Nylon, cutting speed 15.24 m/min.

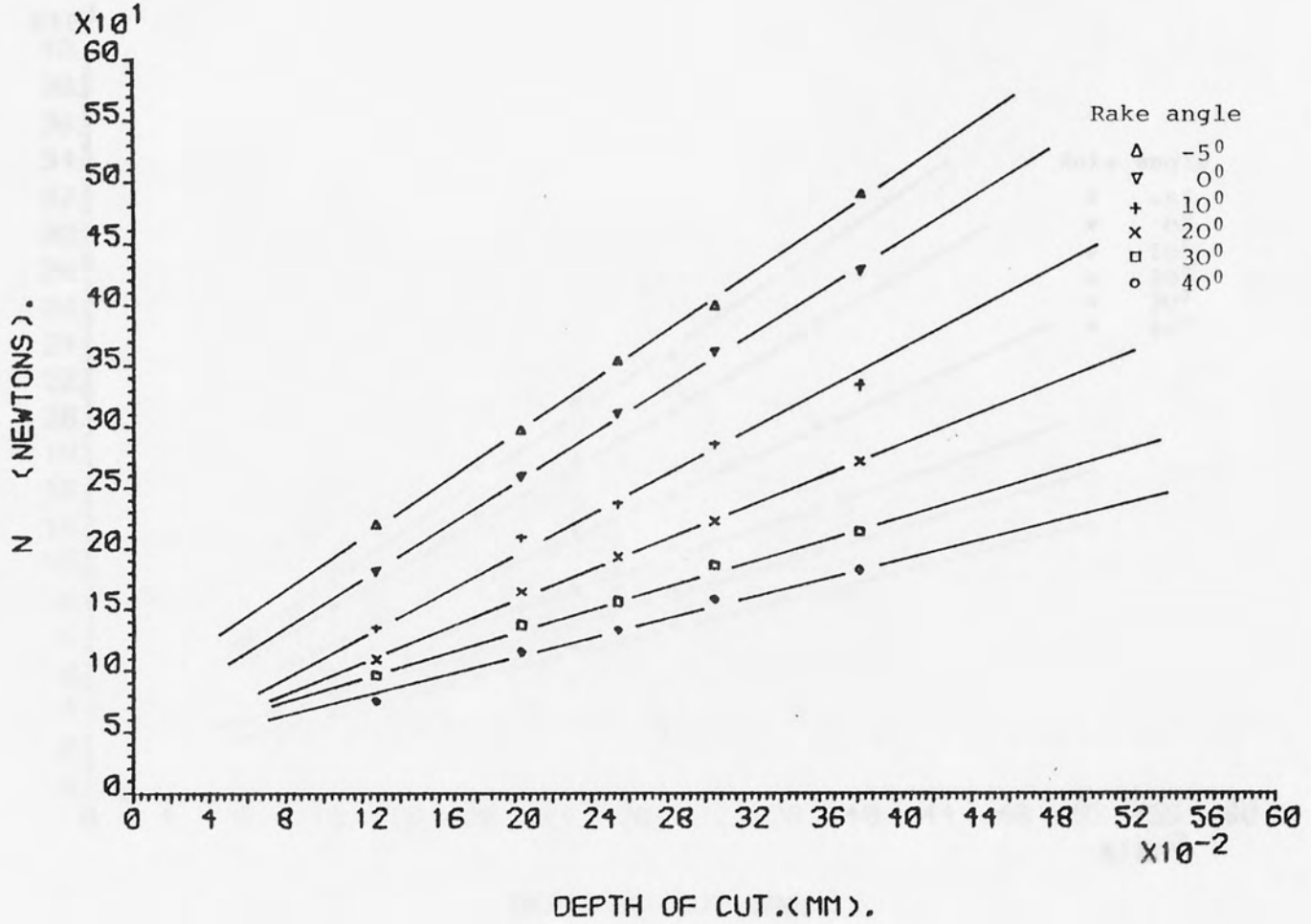

Fig. (7.33)

FIG. (7.33). N as a function of depth of cut for as-received polycarbonate, cutting speed 15.24 m/min.

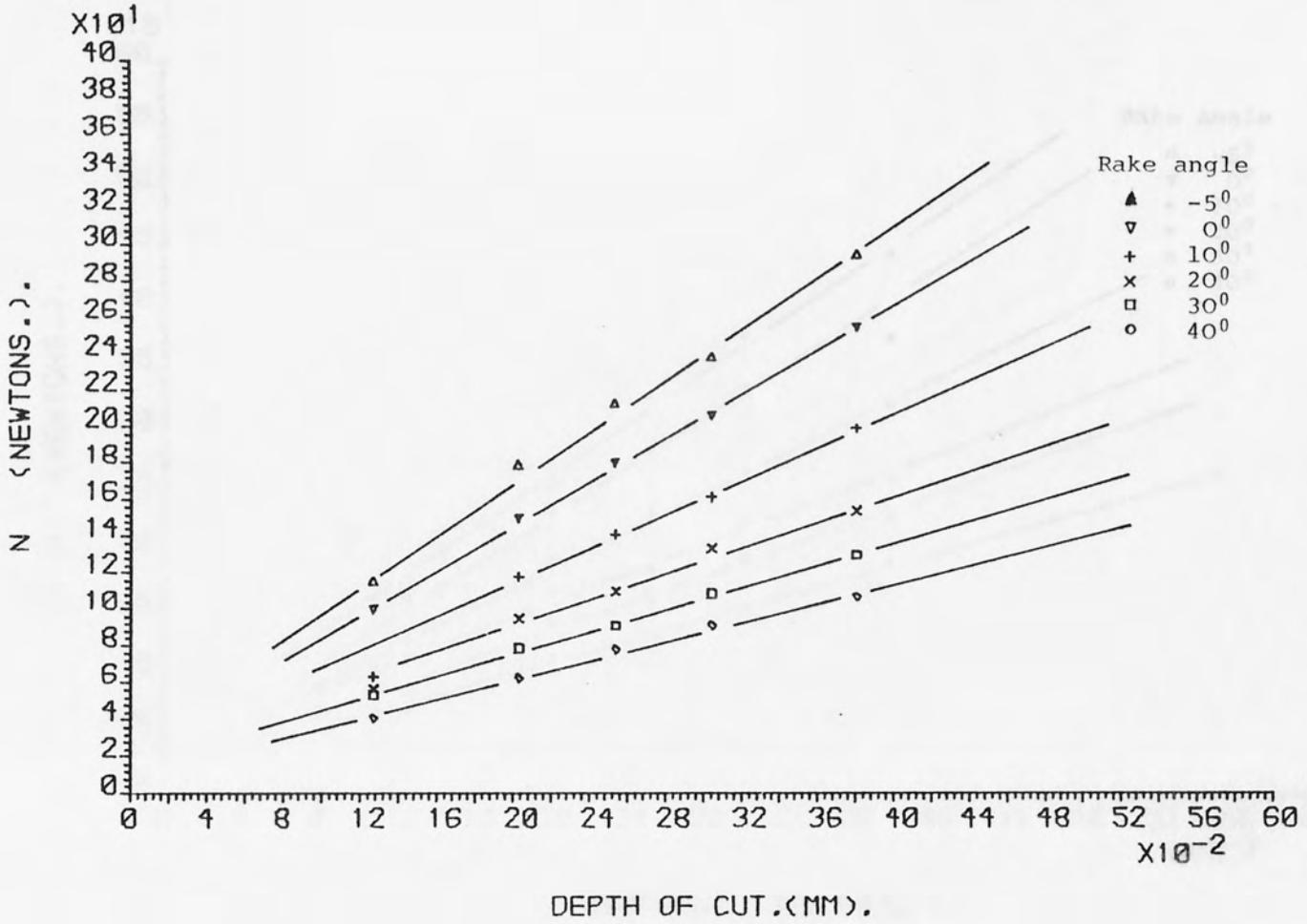

Fig. (7.34)

FIG. (7.34). N as a function of depth of cut for rolled polycarbonate, cutting speed 15.24 m/min.

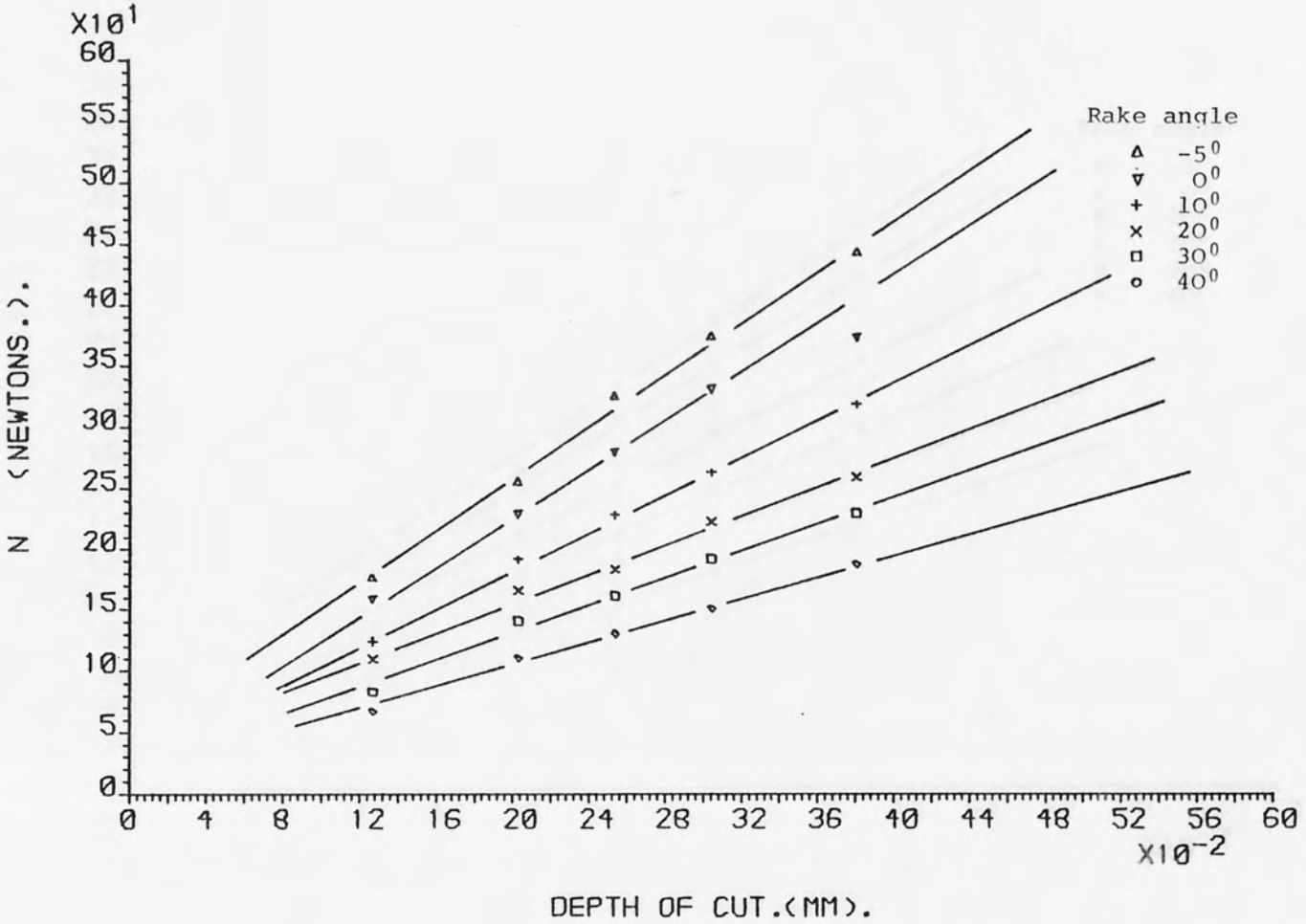

Fig. (7.35)

FIG. (7.35). N as a function of depth of cut for as-received Nylon, cutting speed 15.24 m/min.

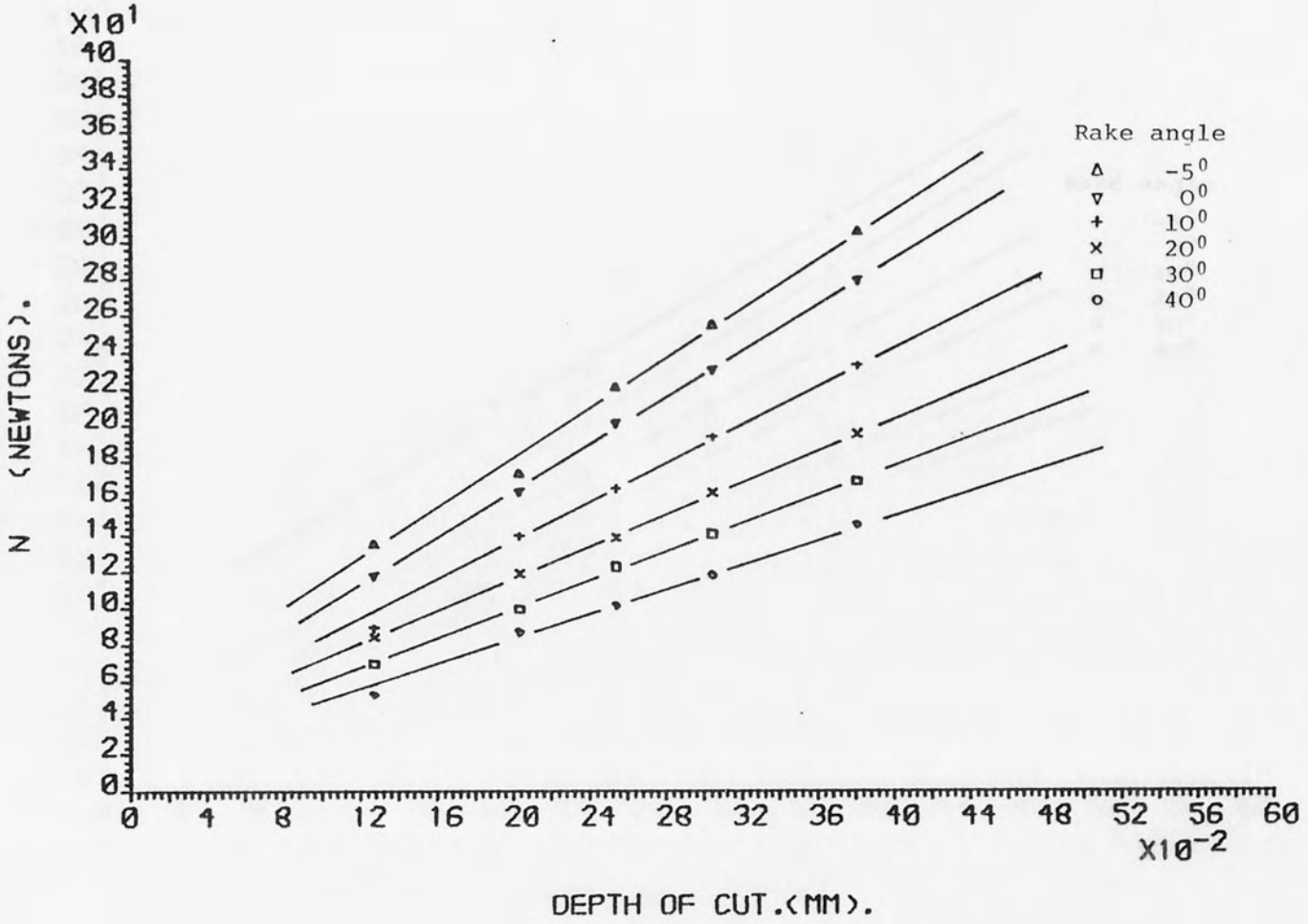

Fig. (7.36)

FIG. (7.36). N as a function of depth of cut for rolled Nylon, cutting speed 15.24 m/min.

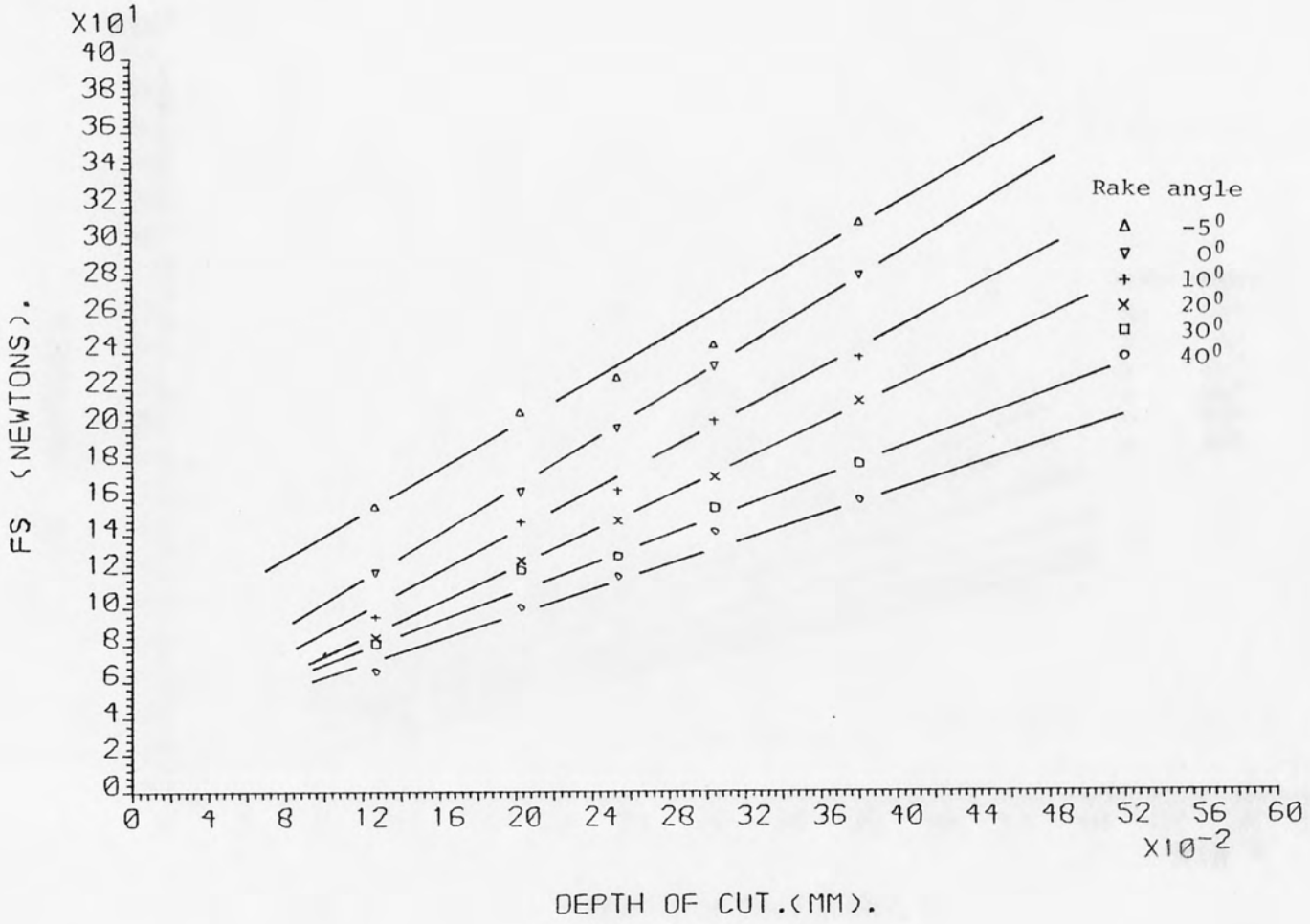

Fig. (7.37)

FIG. (7.37). F_s as a function of depth of cut for as-received polycarbonate, cutting speed 15.24 m/min.

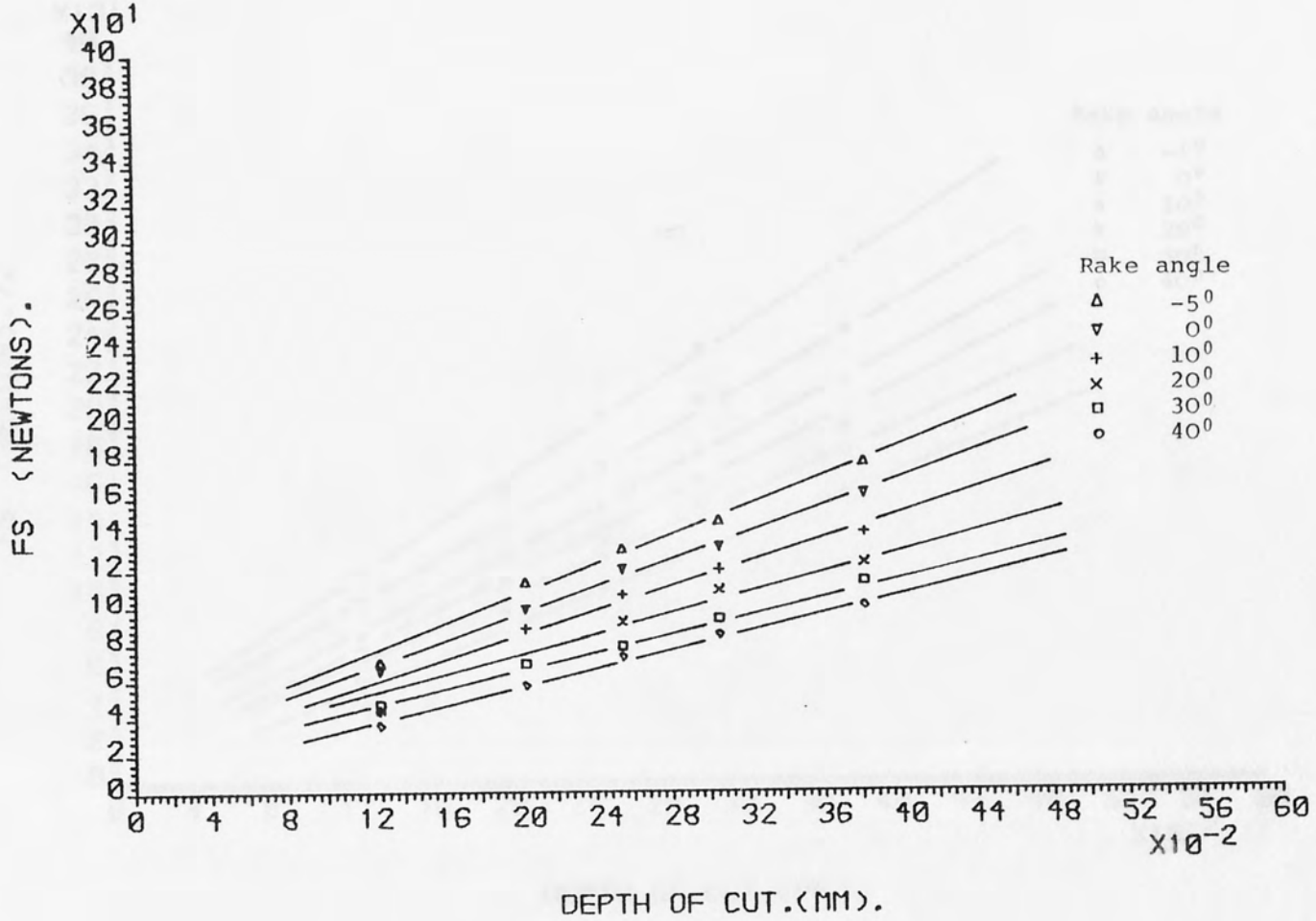

Fig. (7.38)

FIG. (7.38). F_s as a function of depth of cut for rolled polycarbonate, cutting speed 15.24 m/min.

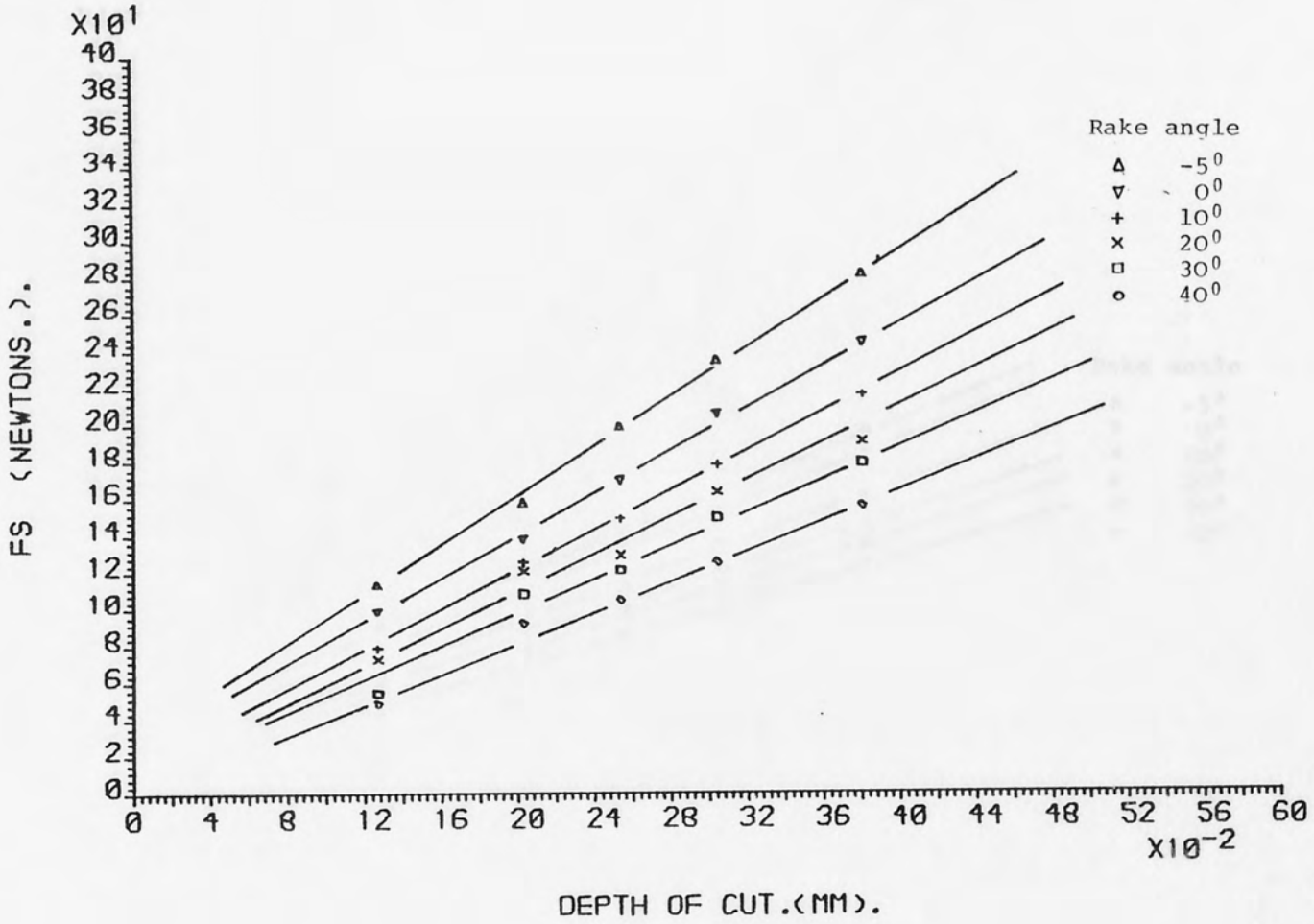

Fig. (7.39)

FIG. (7.39). F_s as a function of depth of cut for as-received Nylon, cutting speed 15.24 m/min.

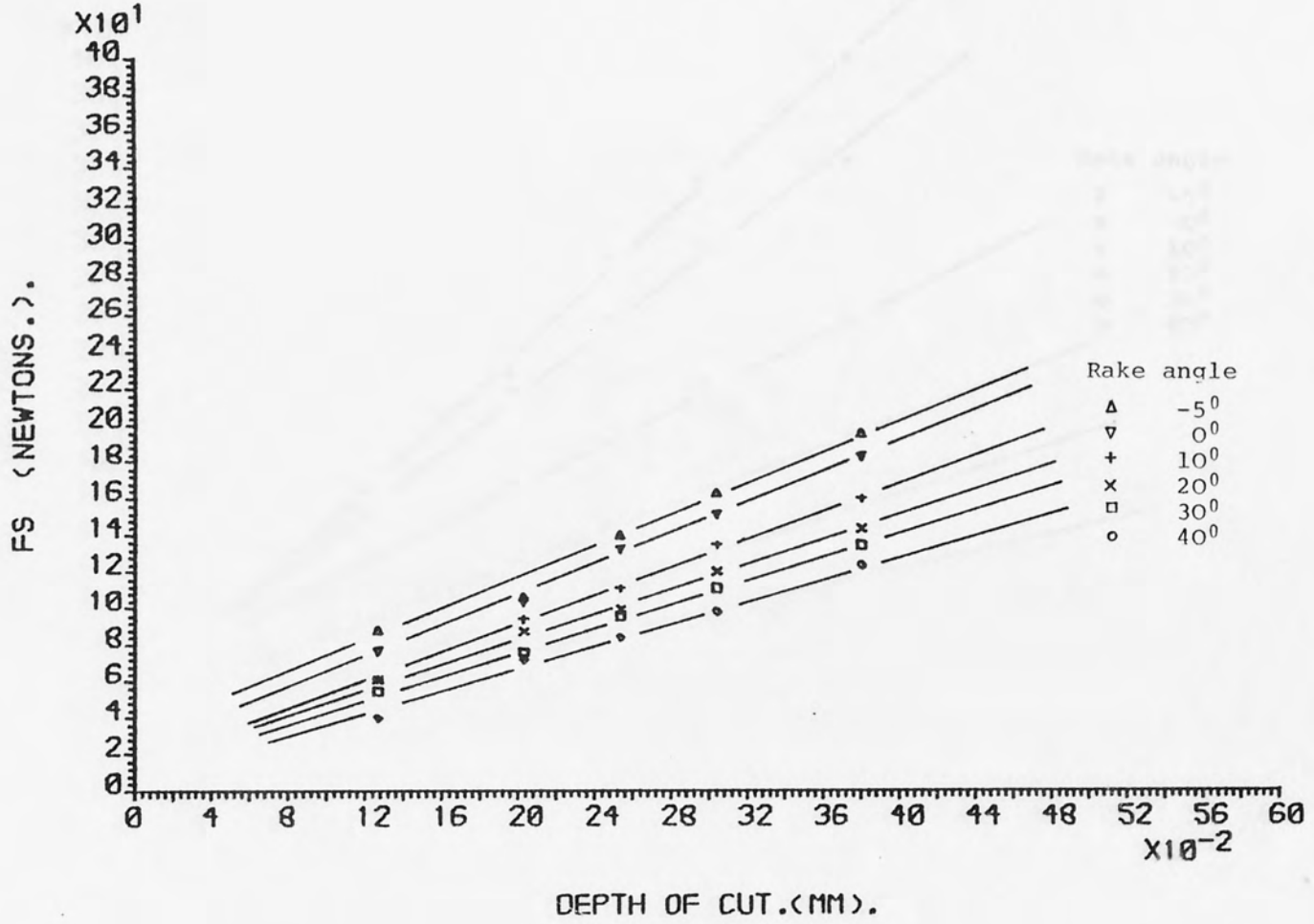

Fig. (7.40)

FIG. (7.40). F_s as a function of depth of cut for rolled Nylon, cutting speed 15.24 m/min.

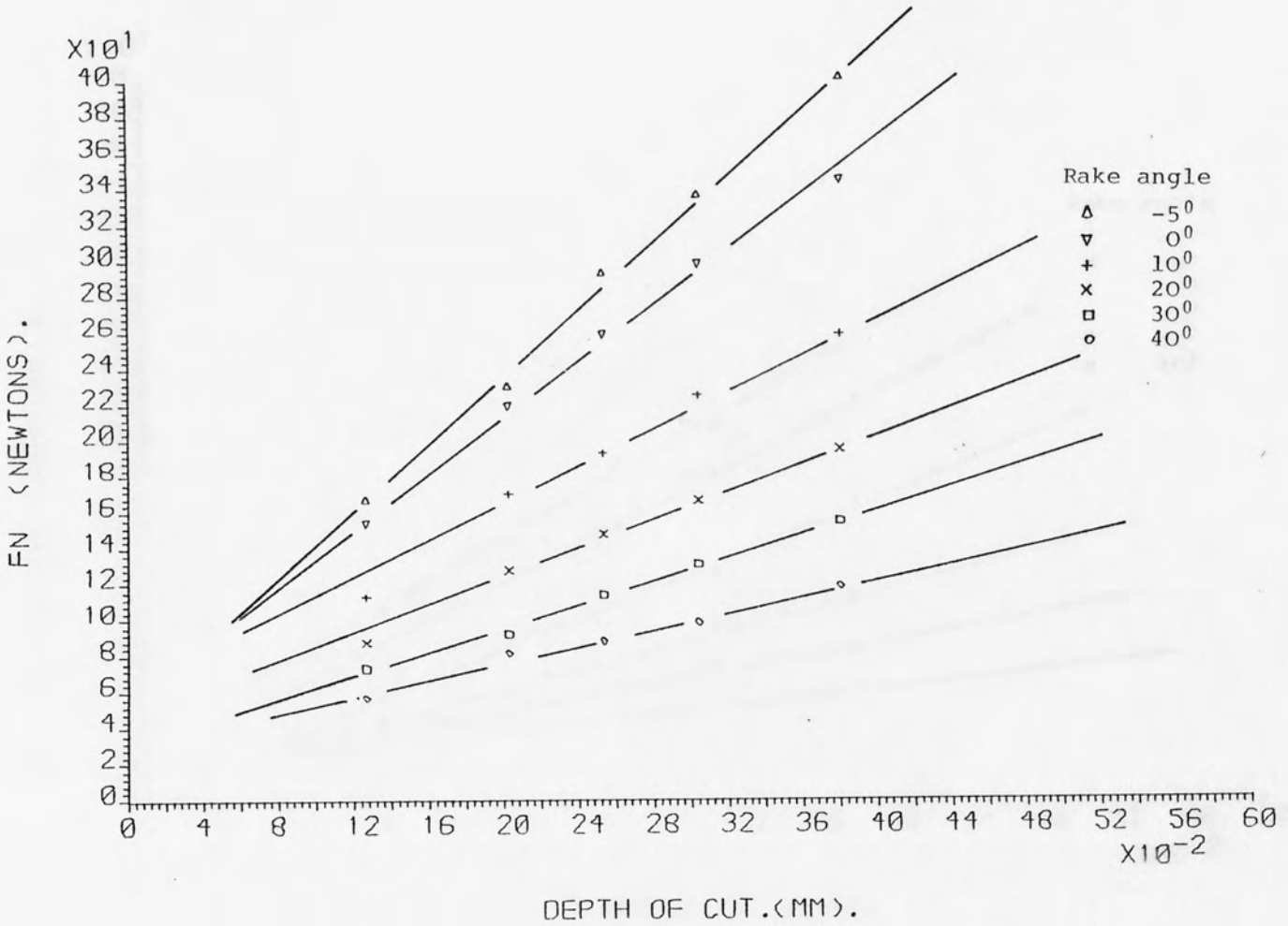

Fig. (7.41)

FIG. (7.41). F_n as a function of depth of cut for as-received polycarbonate, cutting speed 15.24 m/min.

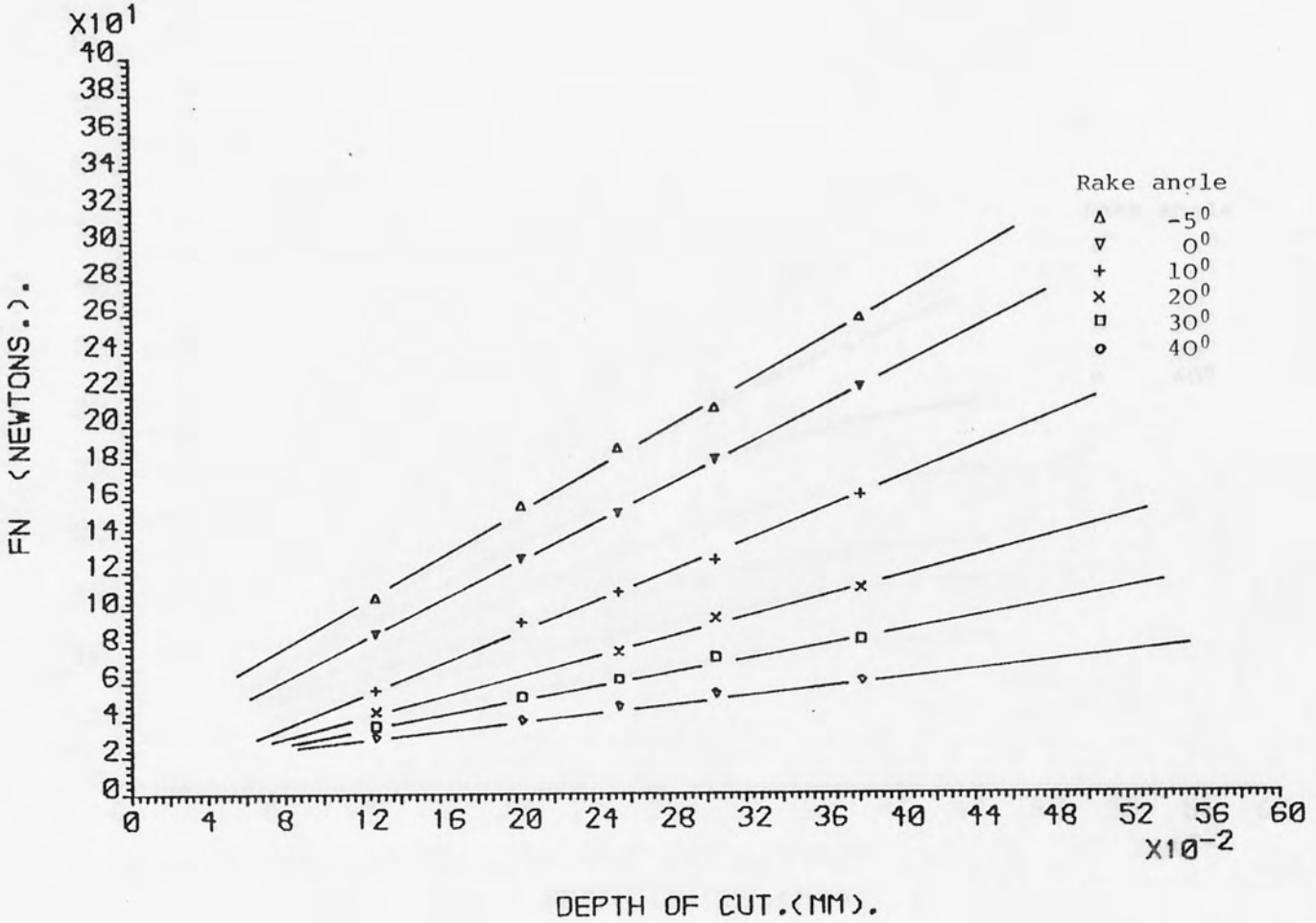

Fig. (7.42)

FIG. (7.42). F_n as a function of depth of cut for rolled polycarbonate, cutting speed 15.24 m/min.

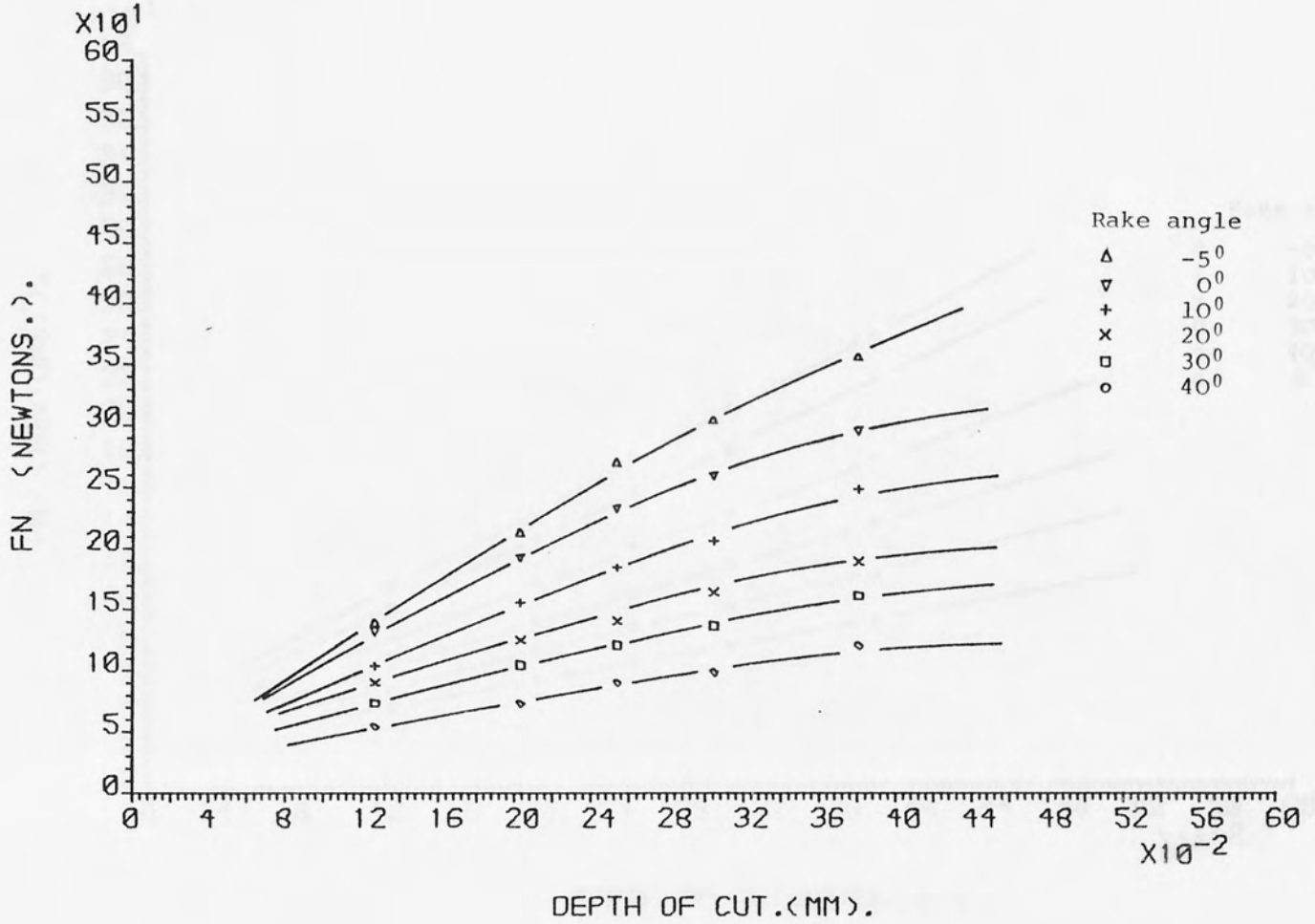

Fig. (7.43)

FIG. (7.43). F_n as a function of depth of cut for as-received Nylon, cutting speed 15.24 m/min.

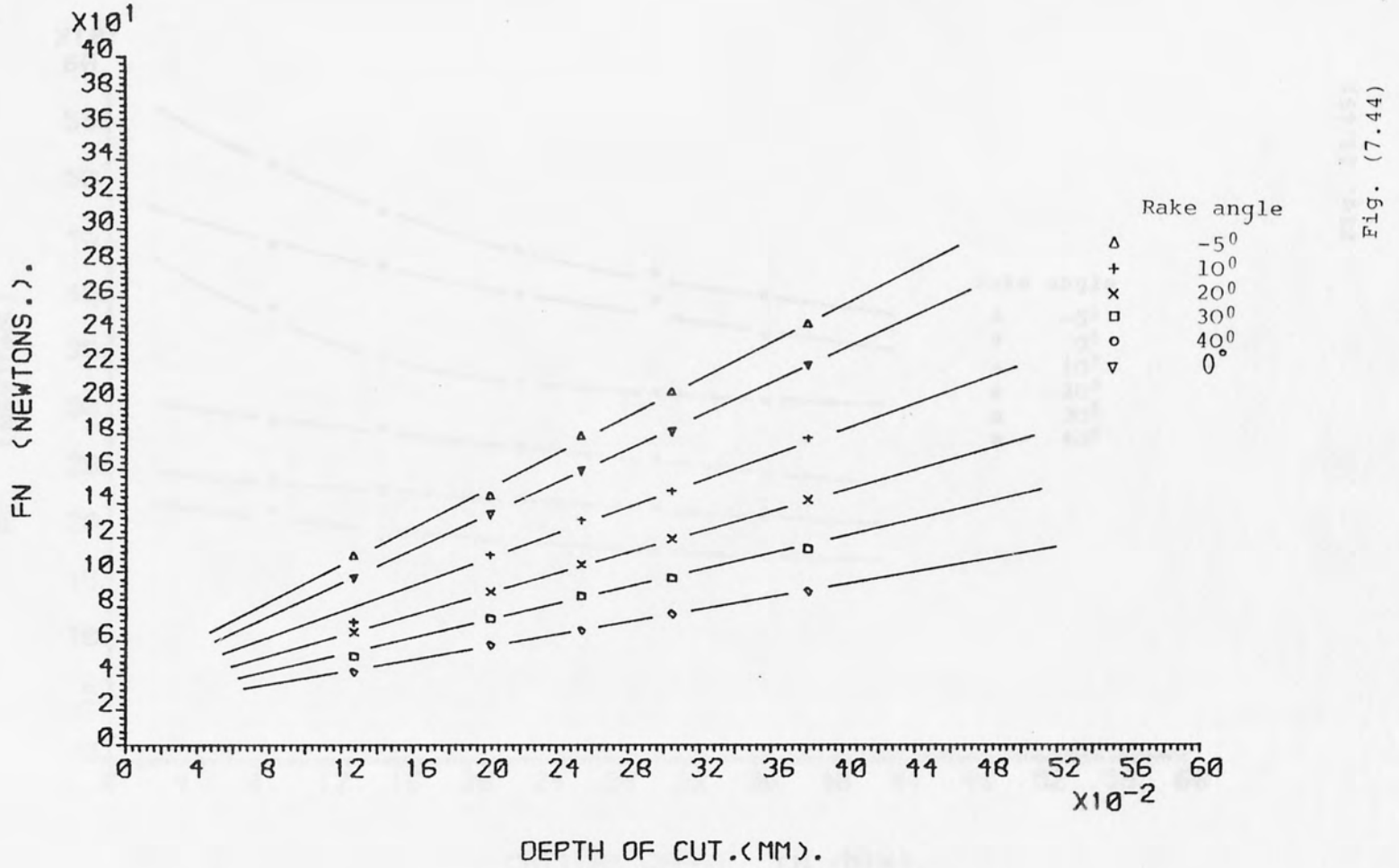

Fig. (7.44)

FIG. (7.44) F_n as a function of depth of cut for rolled Nylon, cutting speed 15.24 m/min.

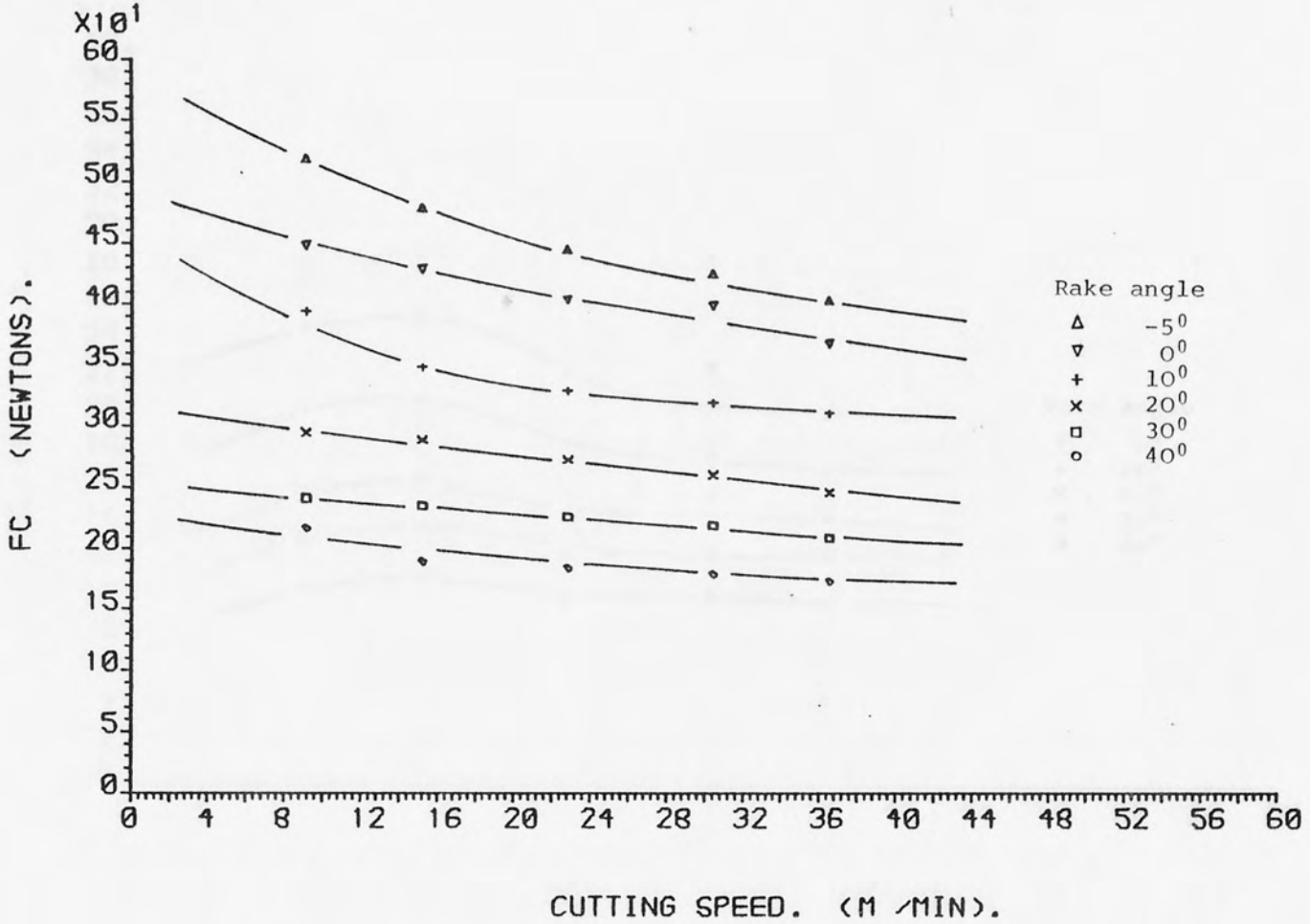

Fig. (7.45)

FIG. (7.45). F_c as a function of cutting speed for as-received polycarbonate, depth of cut 0.381 mm.

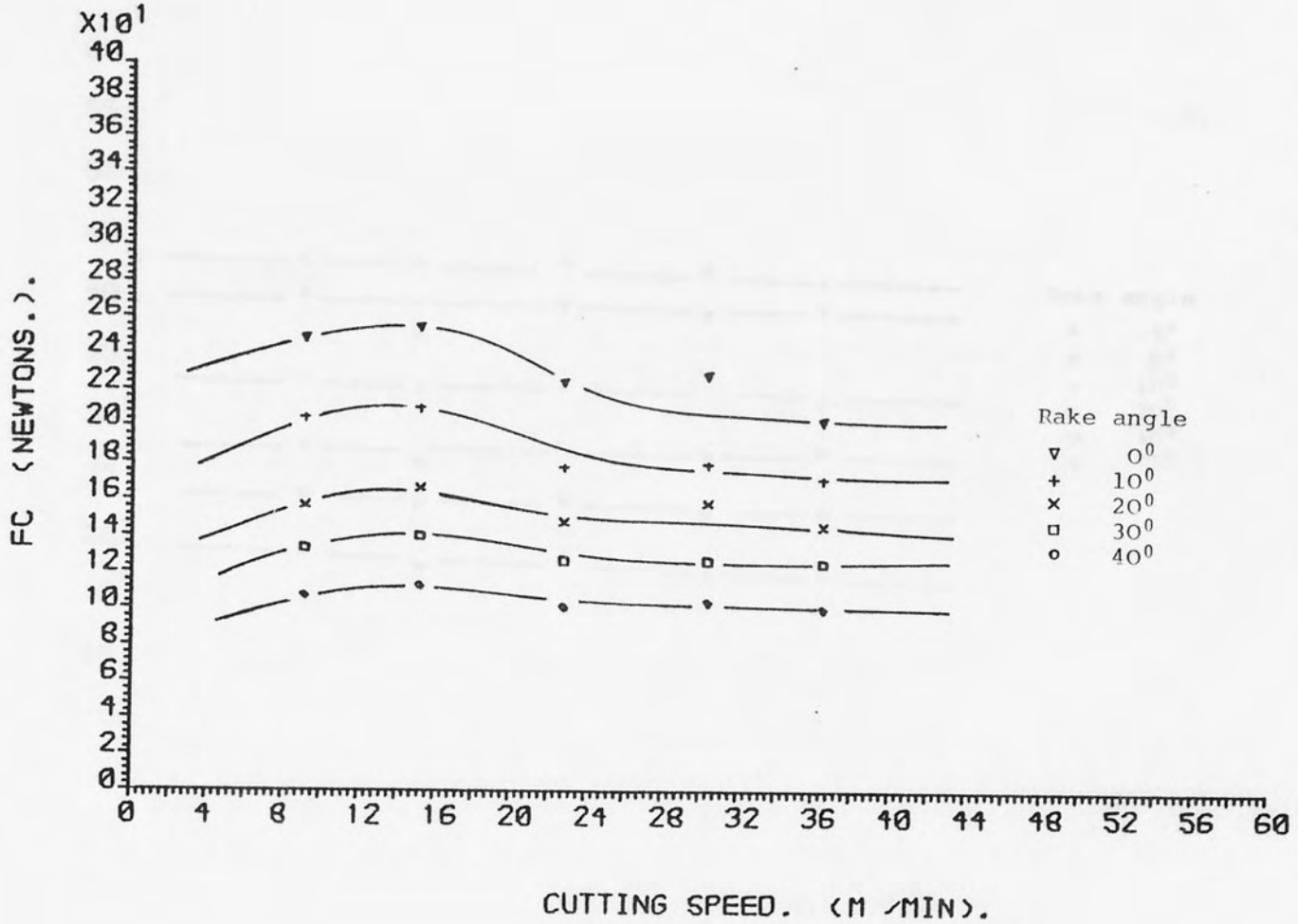

Fig. (7.46)

FIG. (7.46). F_c as a function of the cutting speed for rolled polycarbonate, depth of cut 0.381 mm.

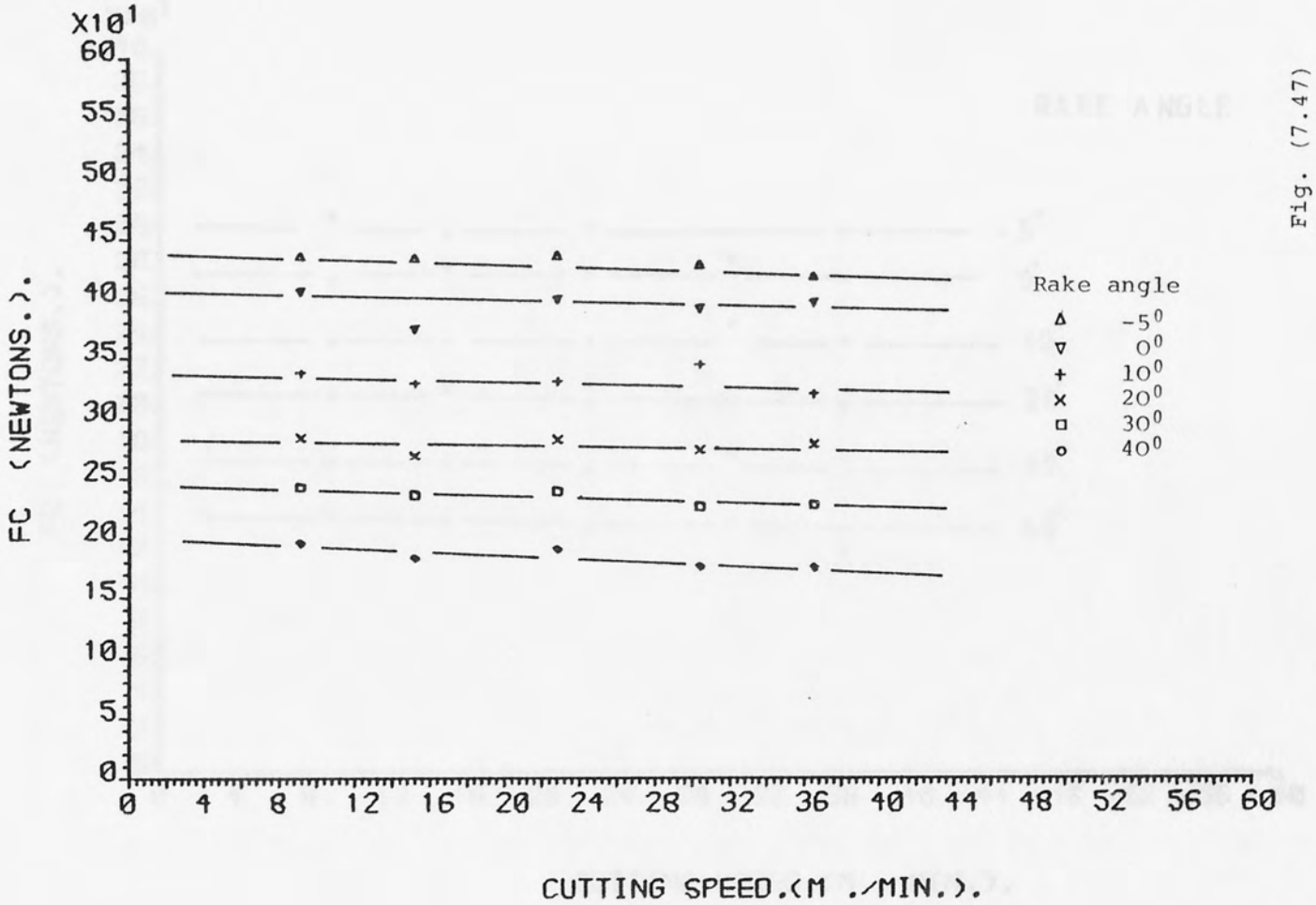

Fig. (7.47)

FIG. (7.47). F_c as a function of cutting speed for as-received Nylon, depth of cut 0.381 mm.

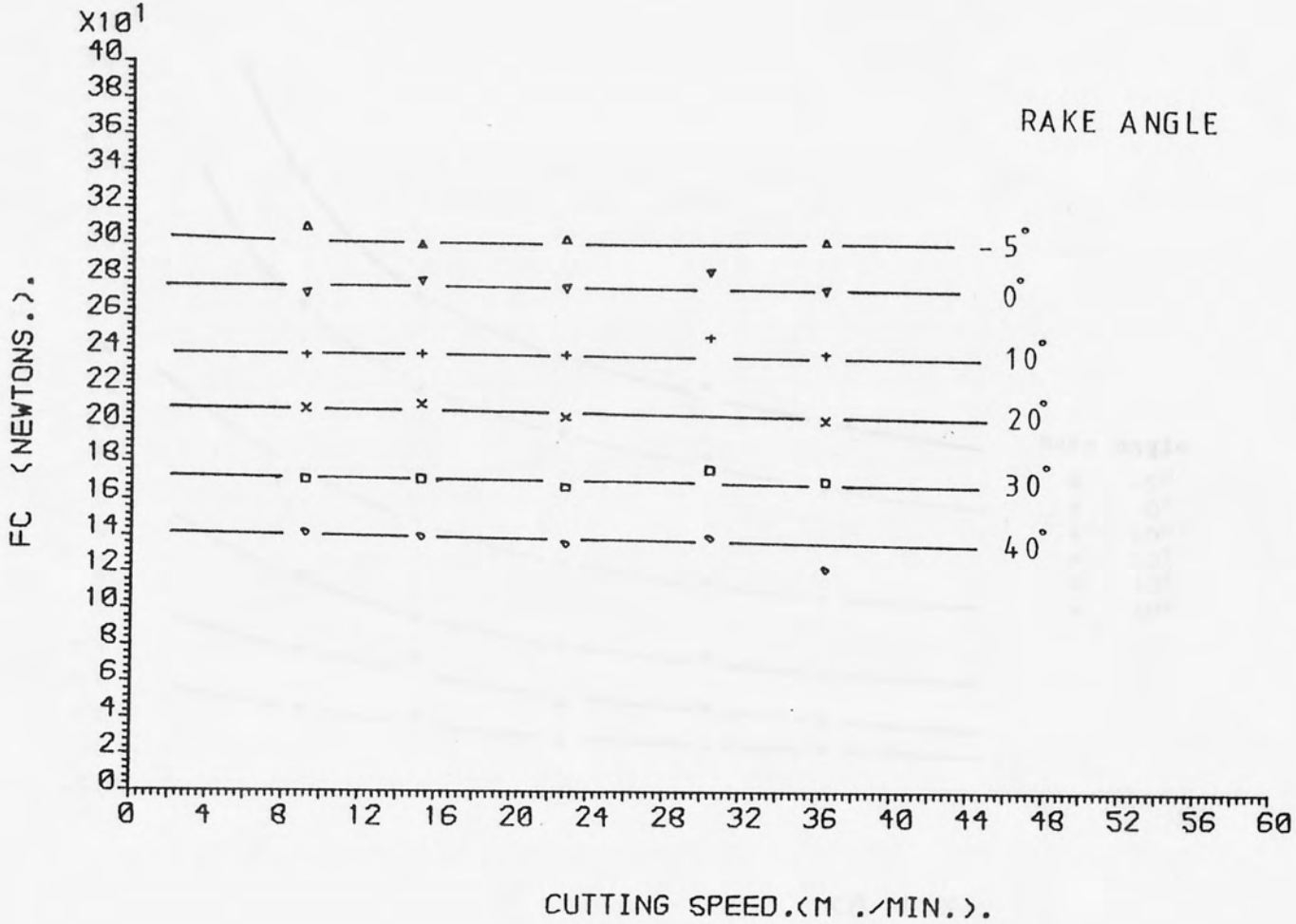

Fig. (7.48)

FIG. (7.48). F_c as a function of cutting speed for rolled Nylon, depth of cut 0.381 mm.

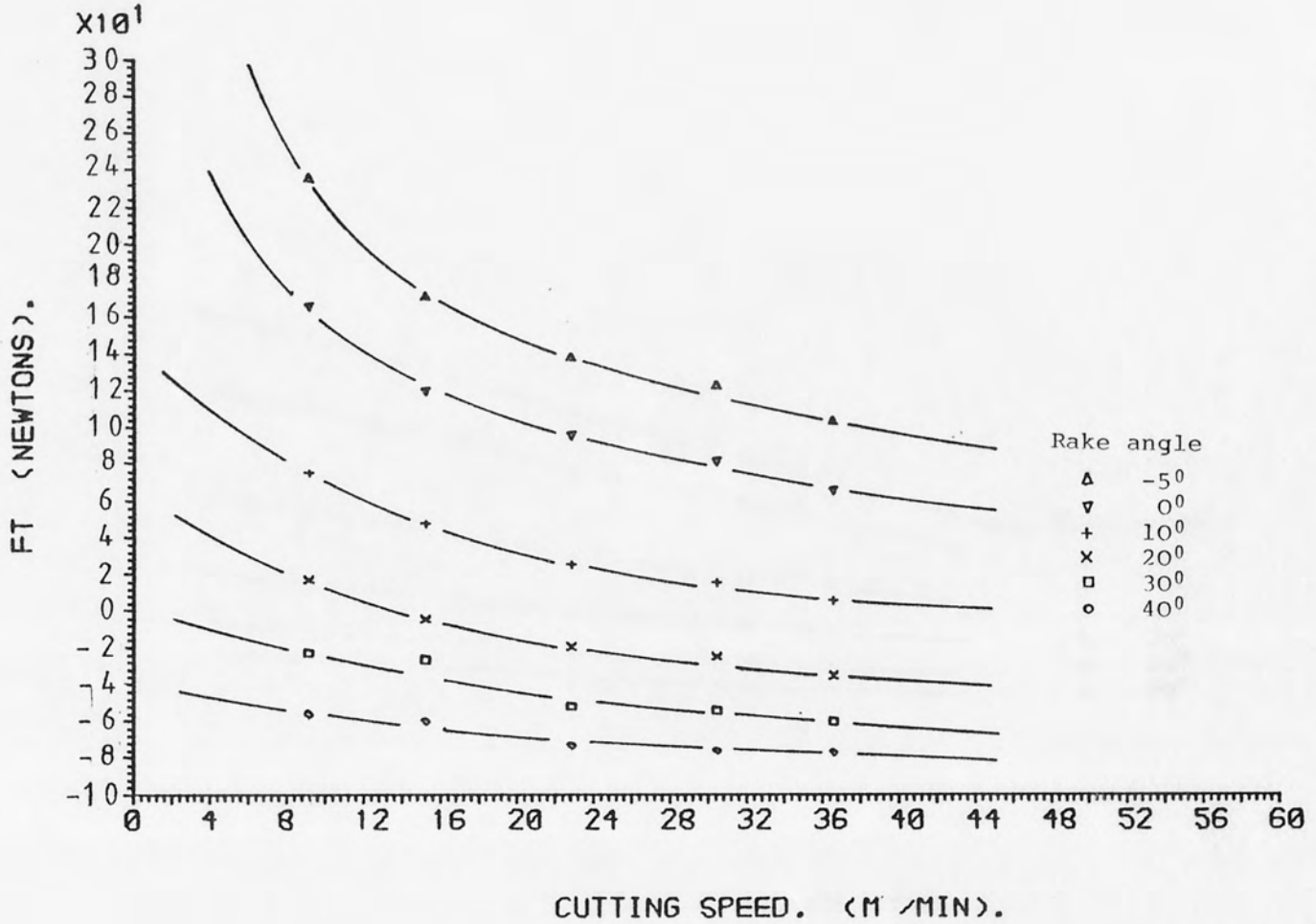

Fig. (7.49)

FIG. (7.49). F_t as a function of cutting speed for as-received polycarbonate, depth of cut 0.381 mm.

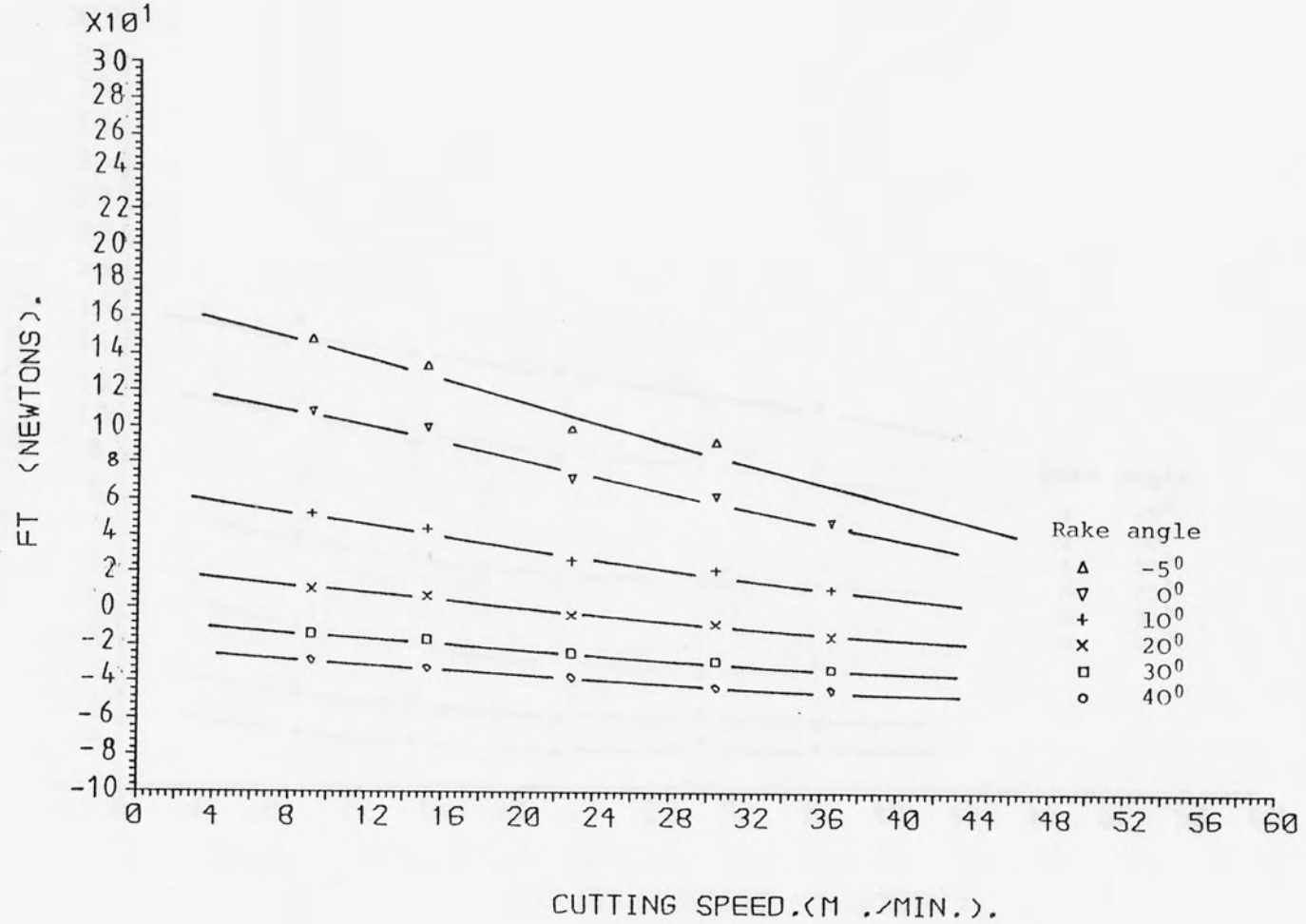

Fig. (7.50)

FIG. (7.50). F_t as a function of cutting speed for rolled polycarbonate, depth of cut 0.381 mm.

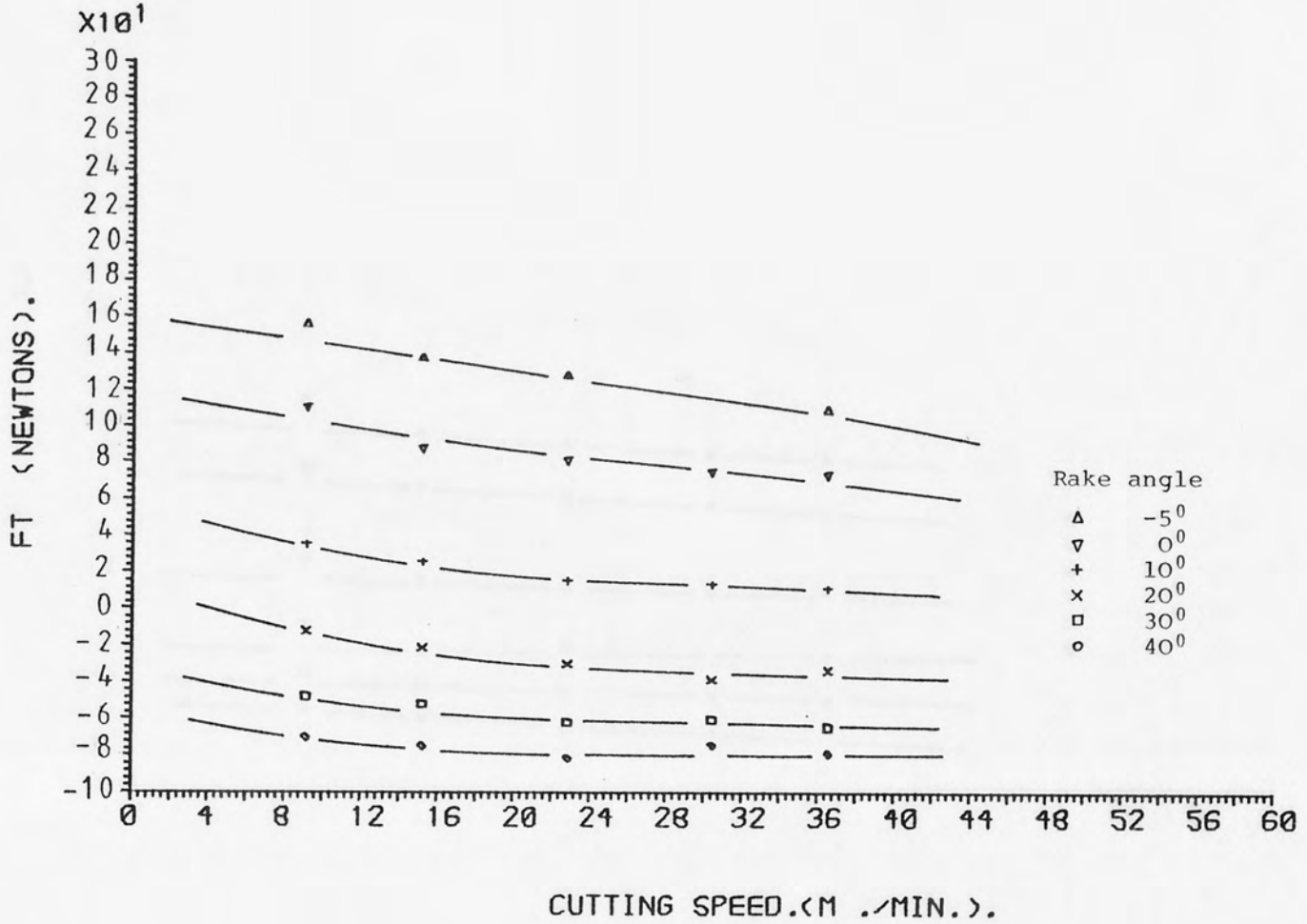

Fig. (7.51)

FIG. (7.51). F_t as a function of cutting speed for as-received Nylon, depth of cut 0.381 mm.

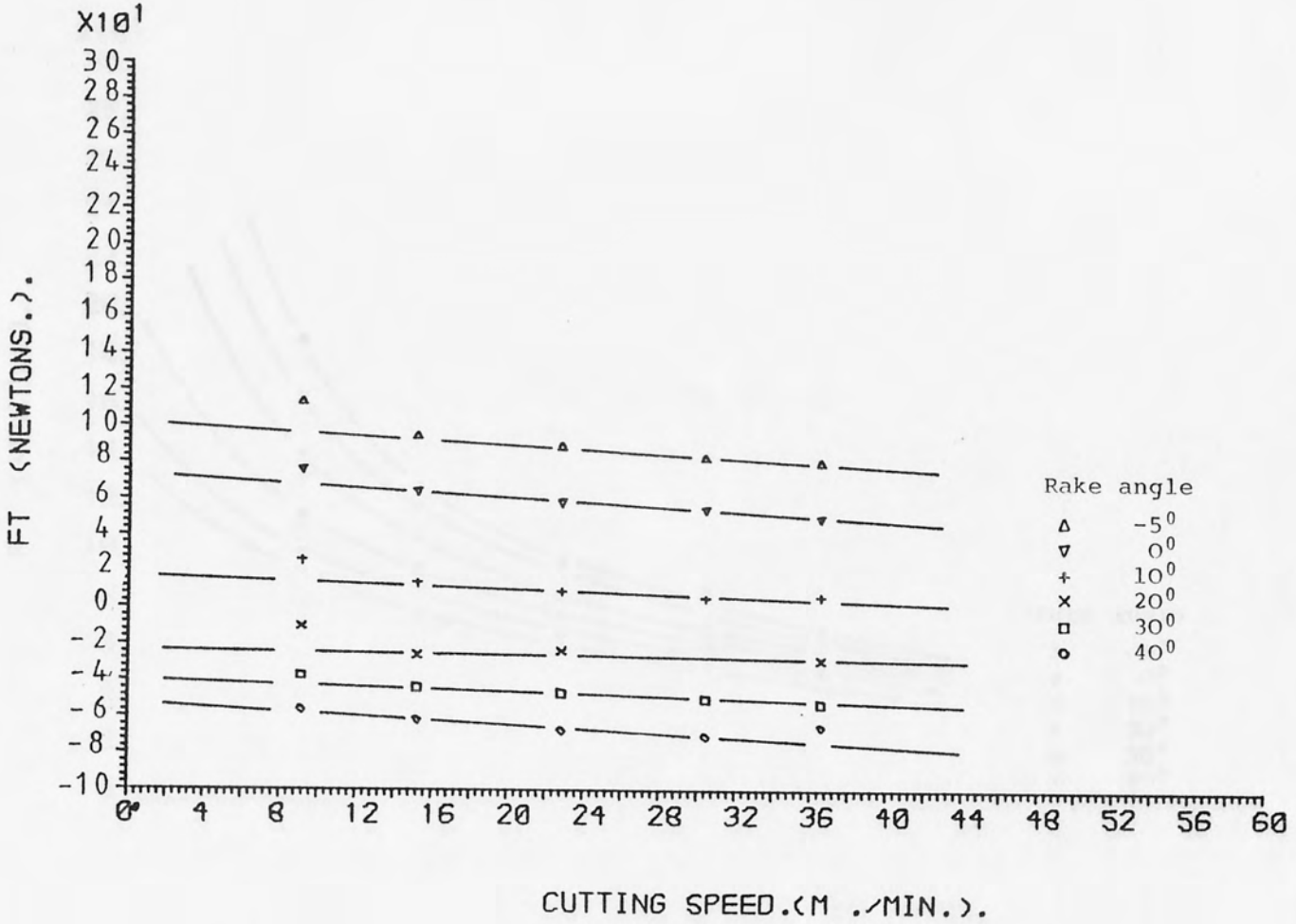

Fig. (7.52)

FIG. (7.52). F_t as a function of the cutting speed for rolled Nylon, depth of cut 0.381 mm.

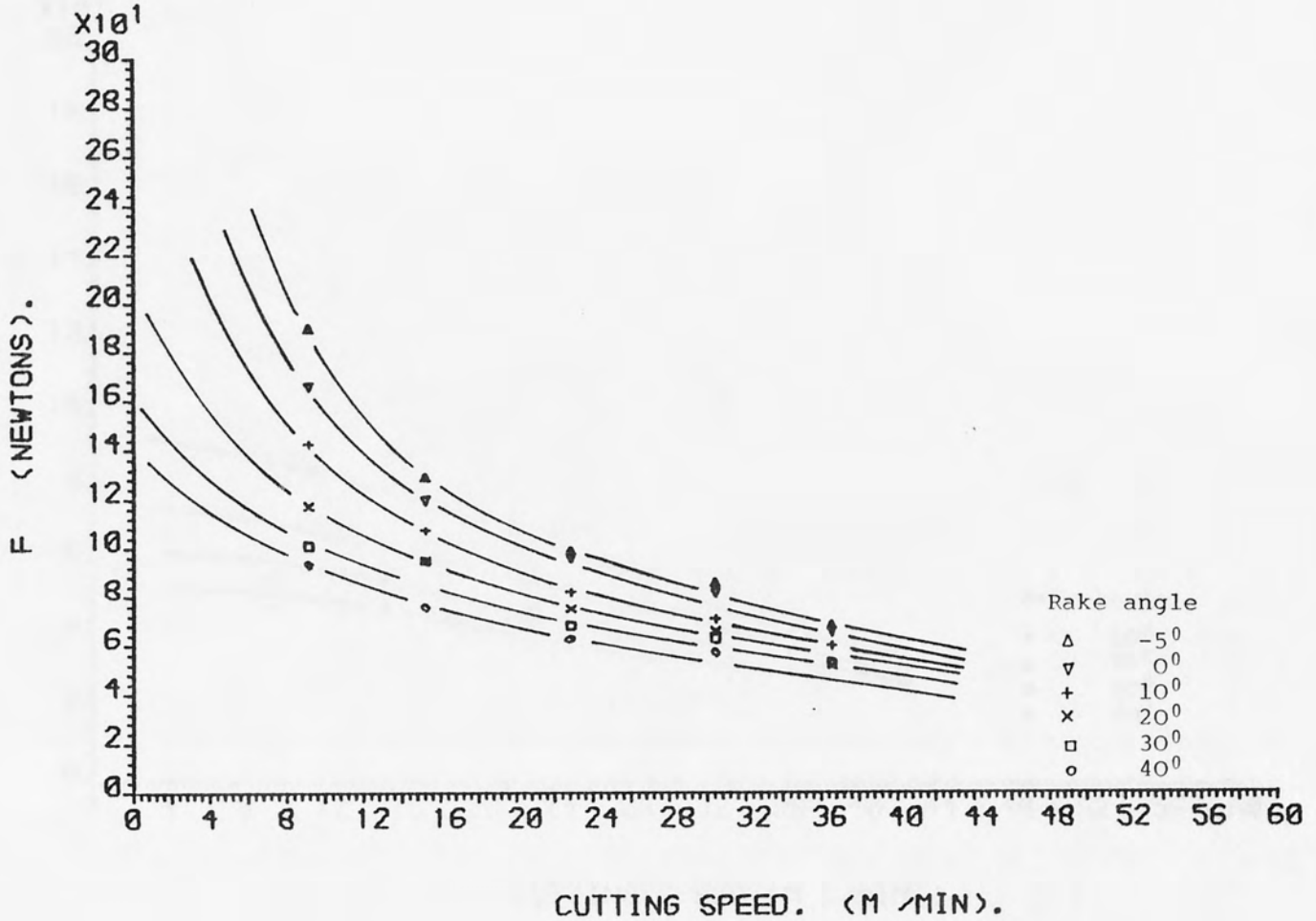

Fig. (7.53)

FIG. (7.53). F as a function of cutting speed for as-received polycarbonate, depth of cut 0.381 mm.

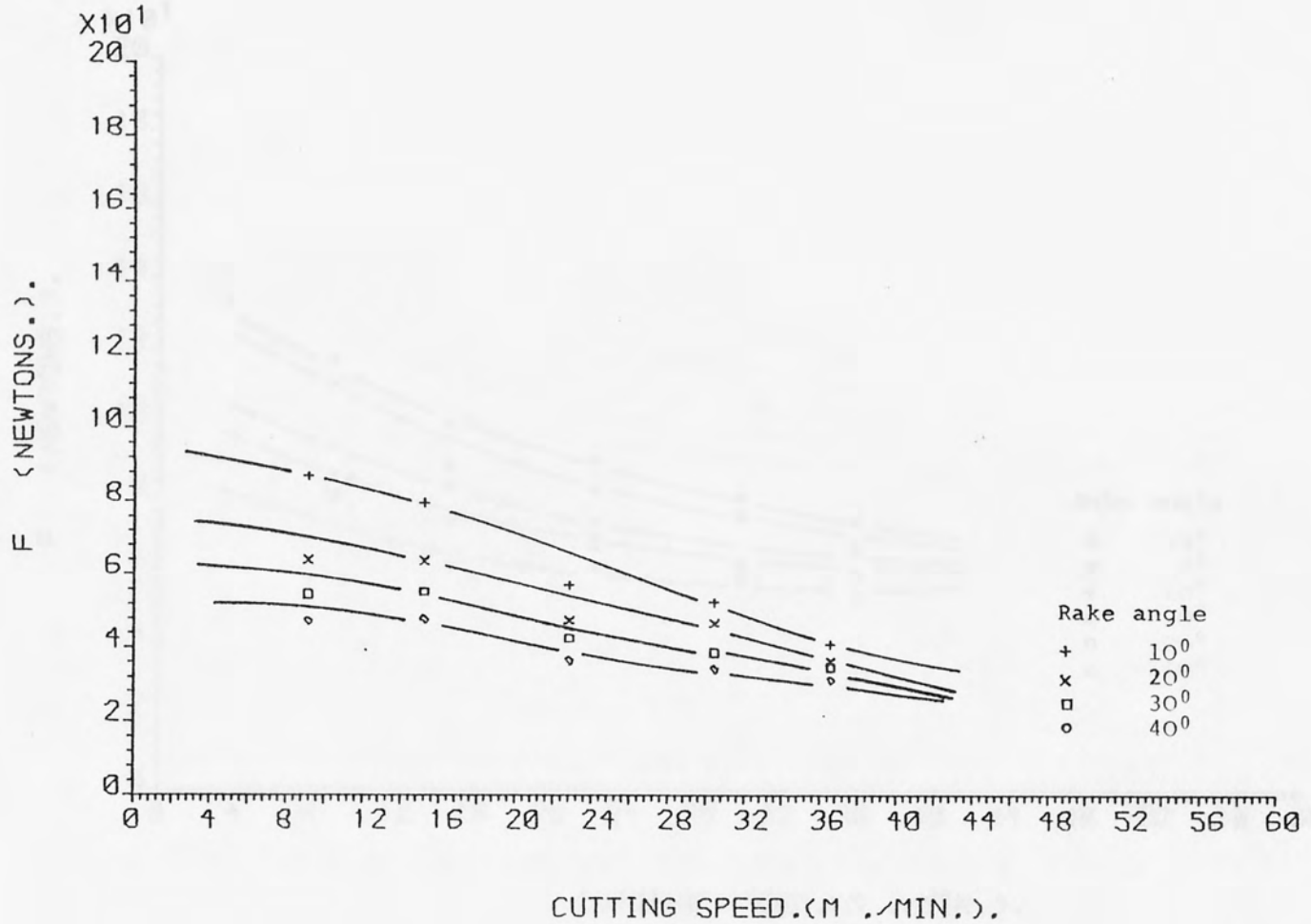

Fig. (7.54)

FIG. (7.54). F as a function of cutting speed for rolled polycarbonate, depth of cut 0.381 mm.

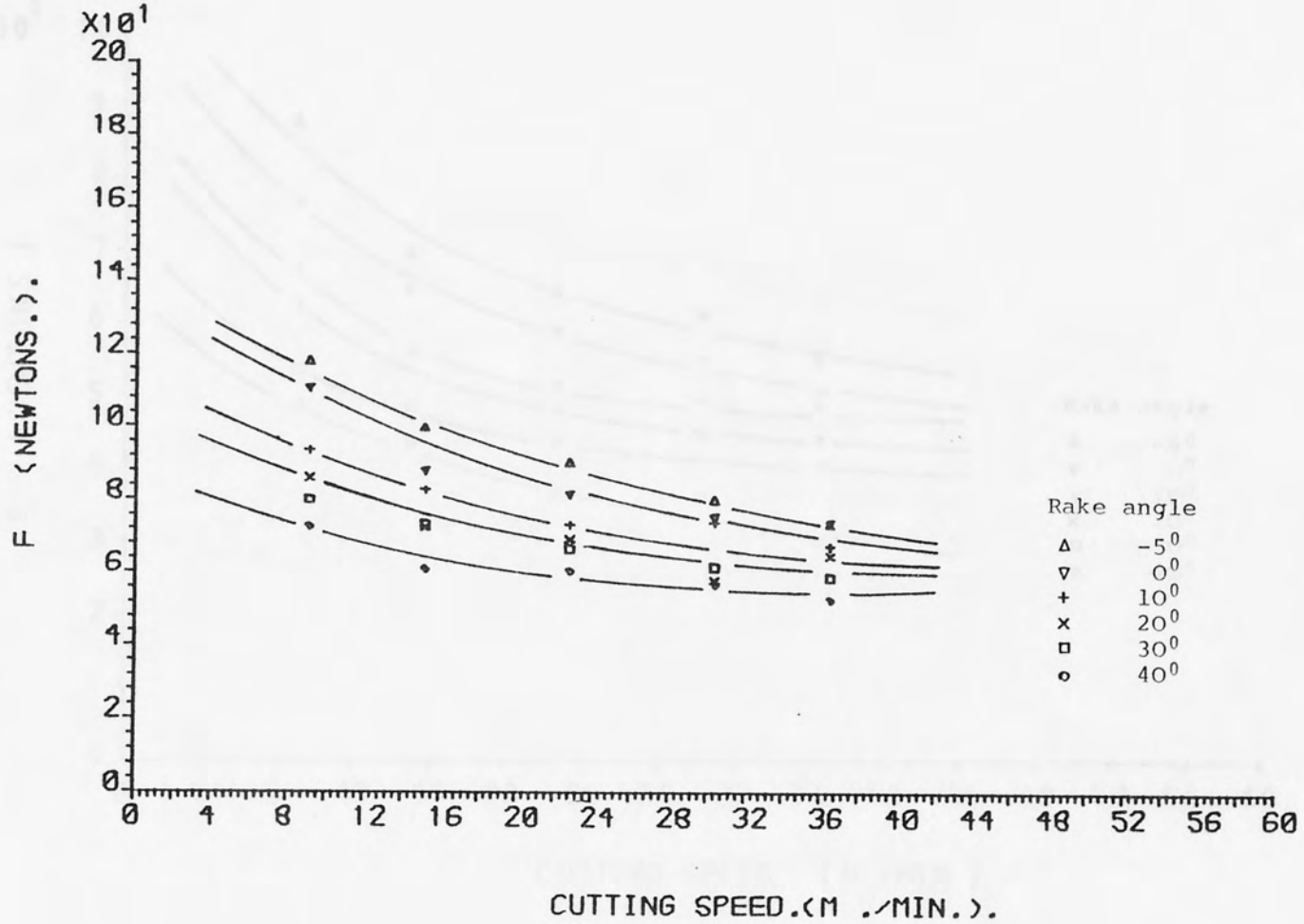

Fig. (7.55)

FIG. (7.55). F as a function of cutting speed for as-received Nylon, depth of cut 0.381 mm.

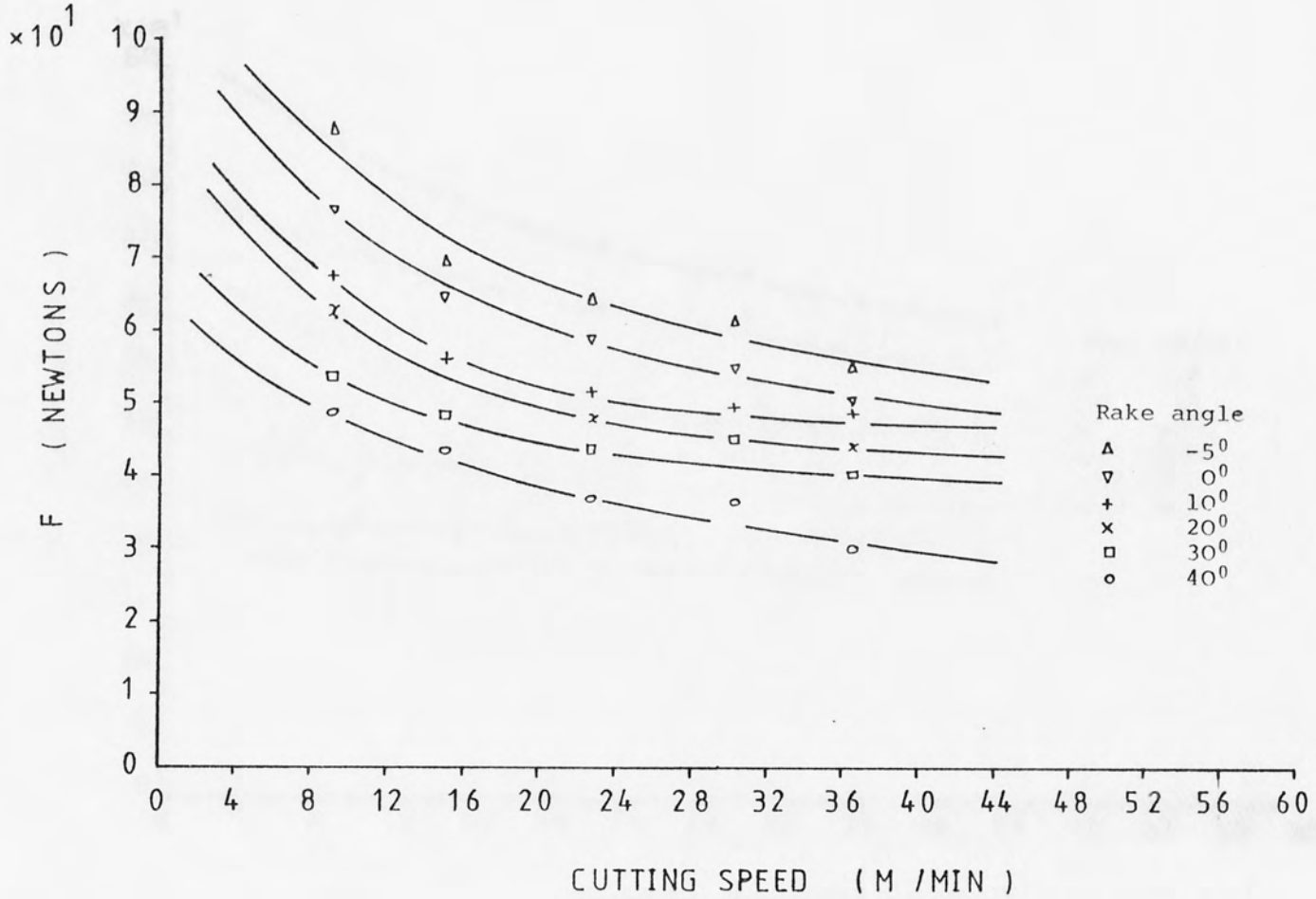

Fig. (7.56)

FIG. (7.56). F as a function of cutting speed for rolled Nylon, depth of cut 0.381 mm.

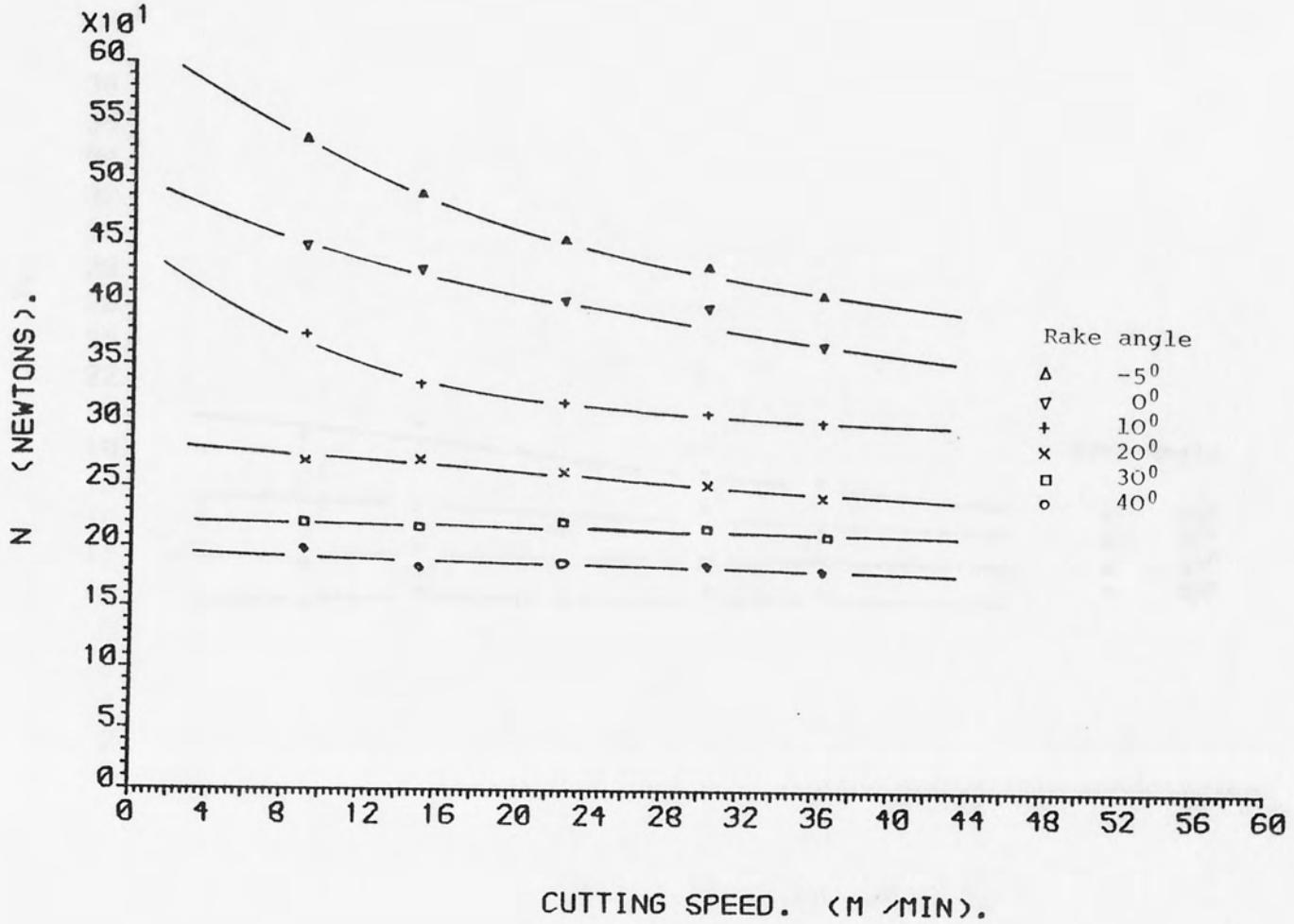

Fig. (7.57)

FIG. (7.57). N as a function of cutting speed for as-received polycarbonate, depth of cut 0.381 mm.

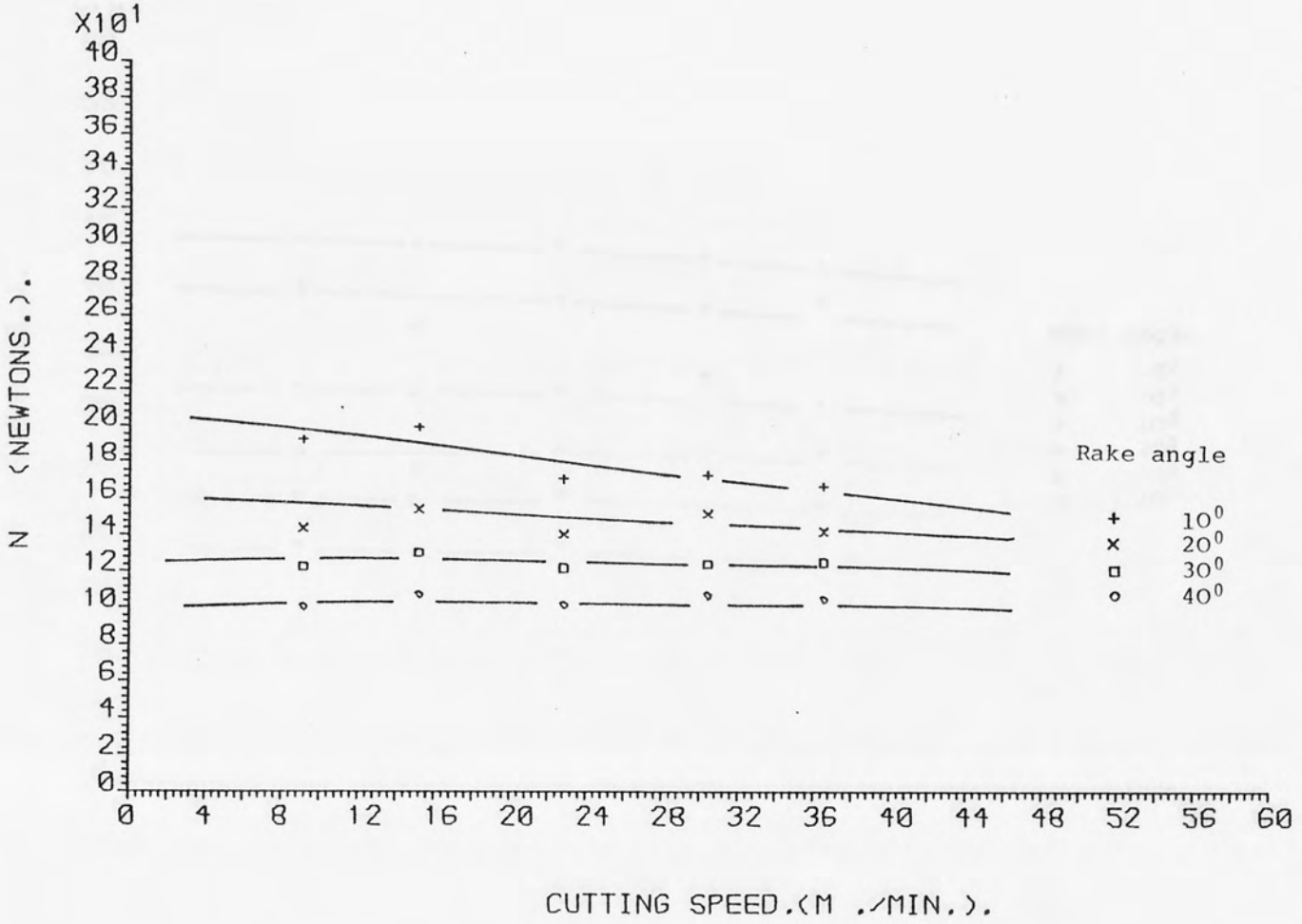

Fig. (7.58)

FIG. (7.58). N as a function of cutting speed for rolled polycarbonate, depth of cut 0.381 mm.

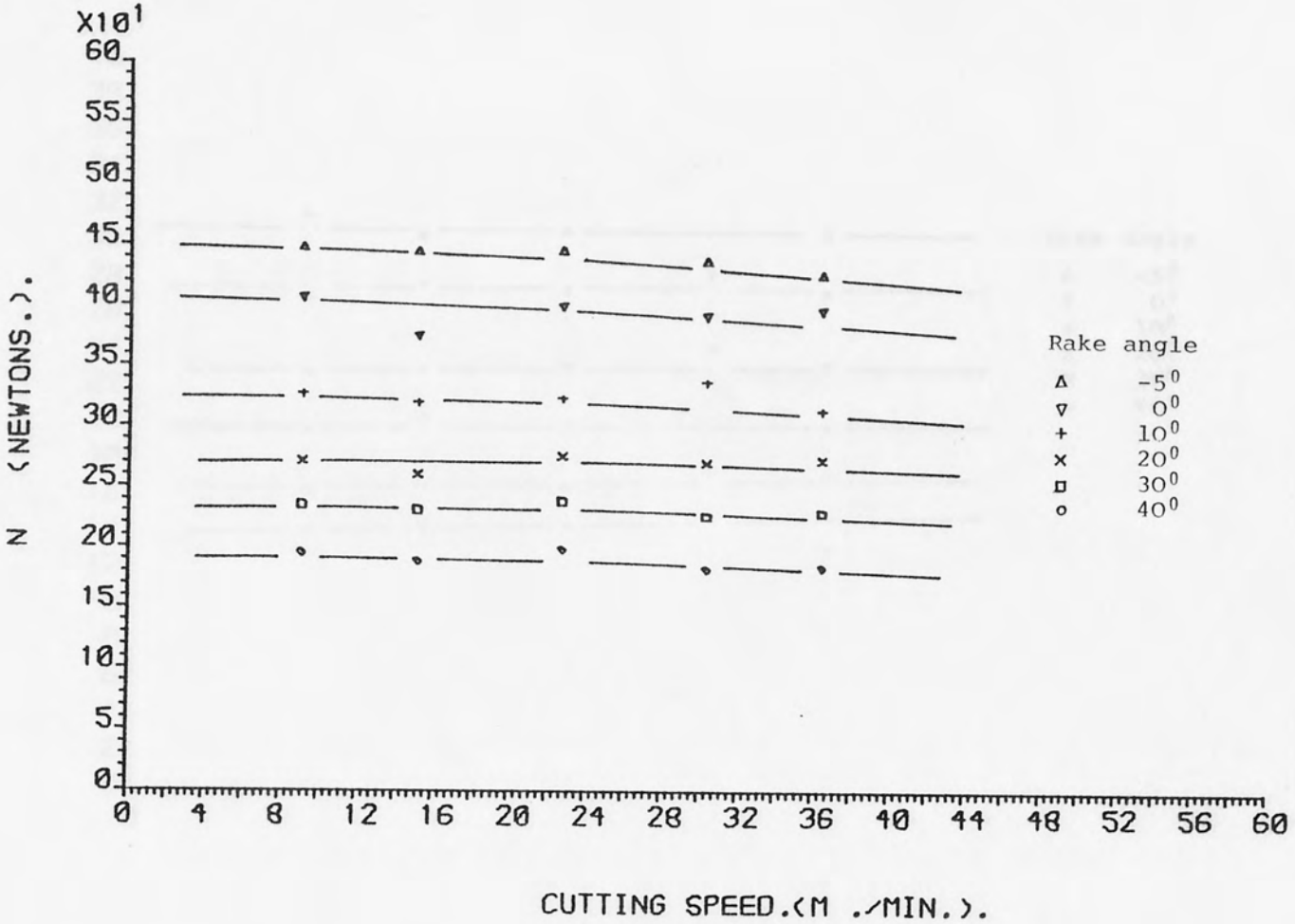

Fig. (7.59)

FIG. (7.59). N as a function of cutting speed for as-received Nylon, depth of cut 0.381 mm.

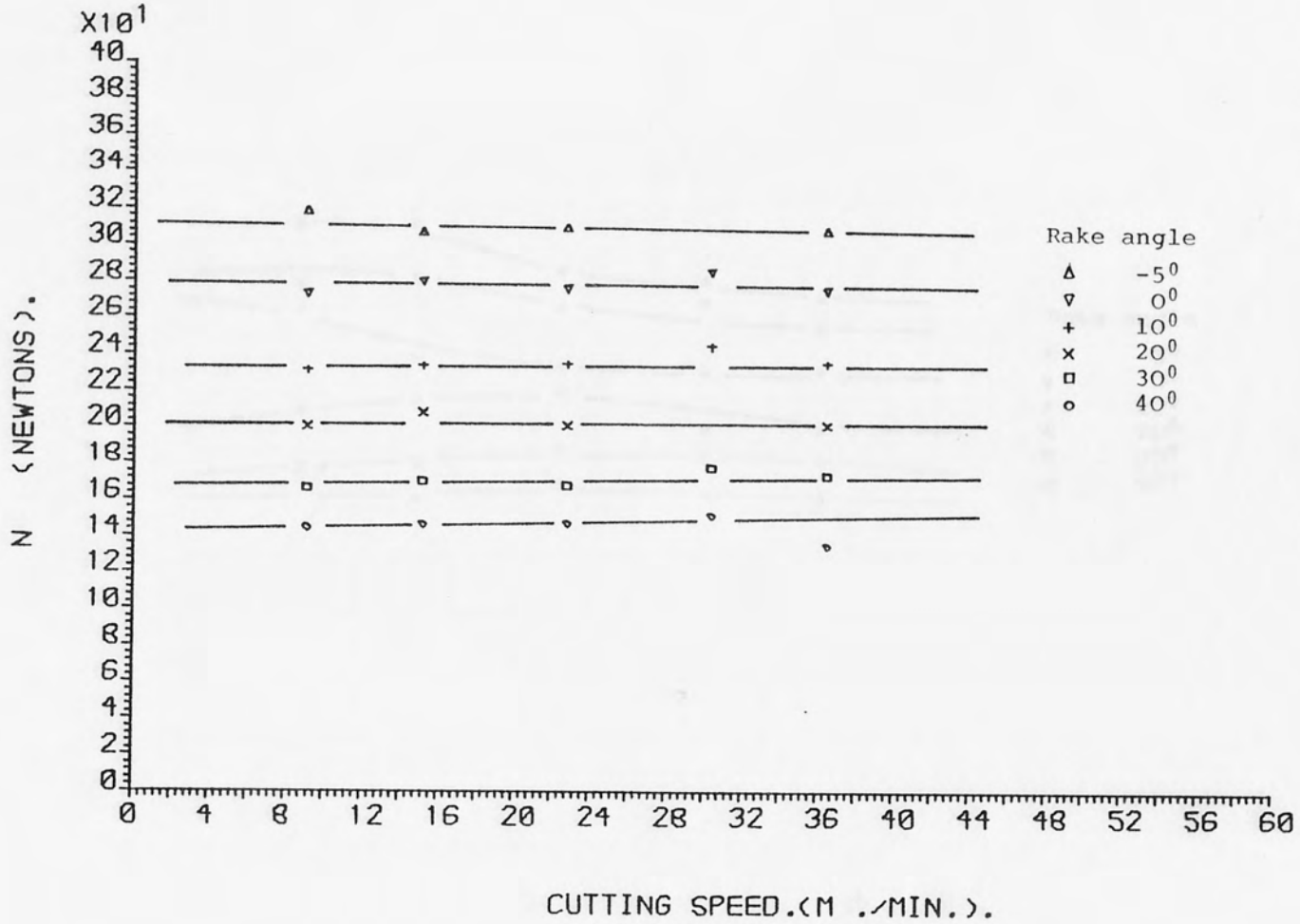

Fig. (7.60)

FIG. (7.60). N as a function of cutting speed for rolled Nylon, depth of cut 0.381 mm.

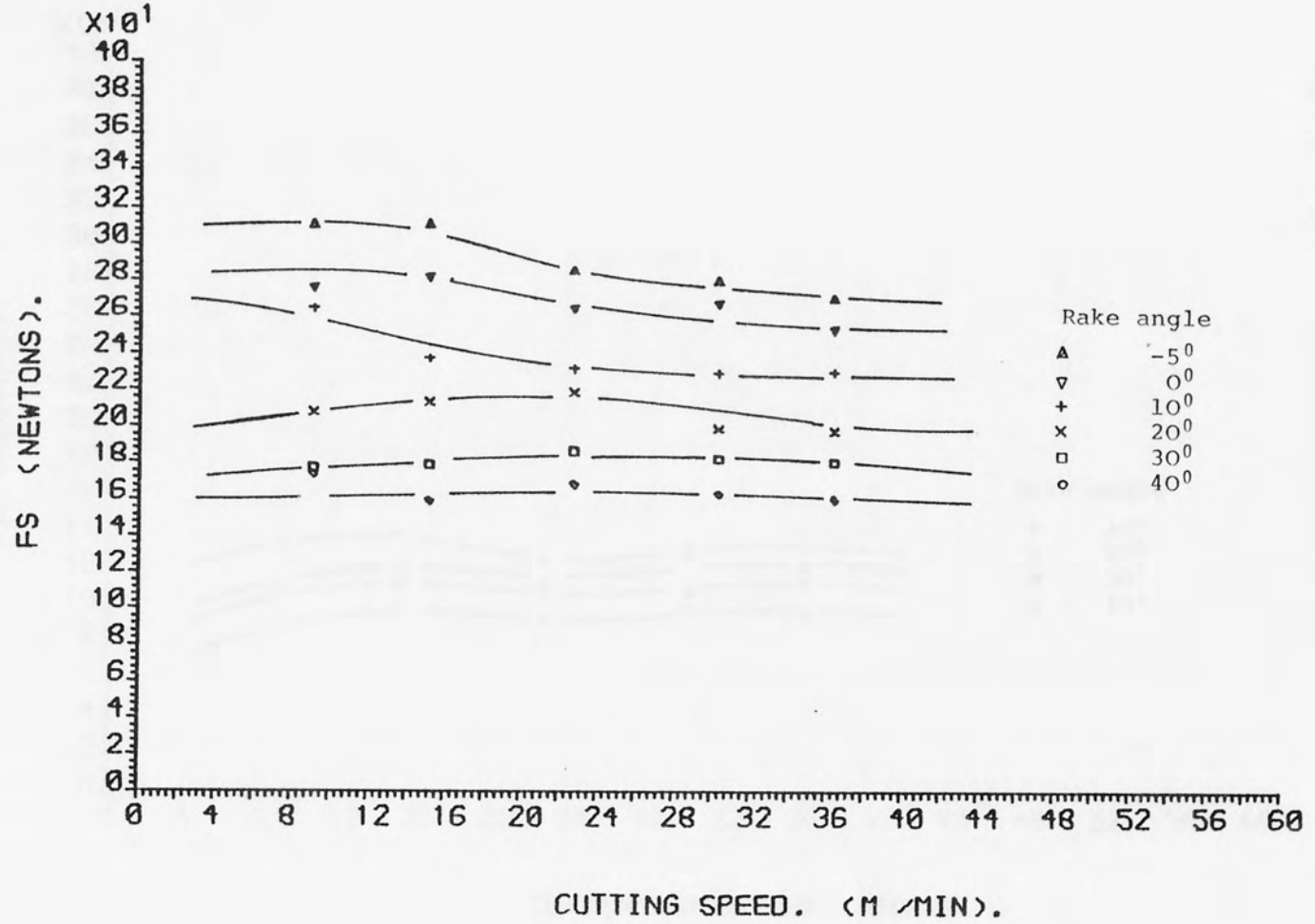

Fig. (7.61)

FIG. (7.61). F_s as a function of cutting speed for as-received polycarbonate, depth of cut 0.381 mm.

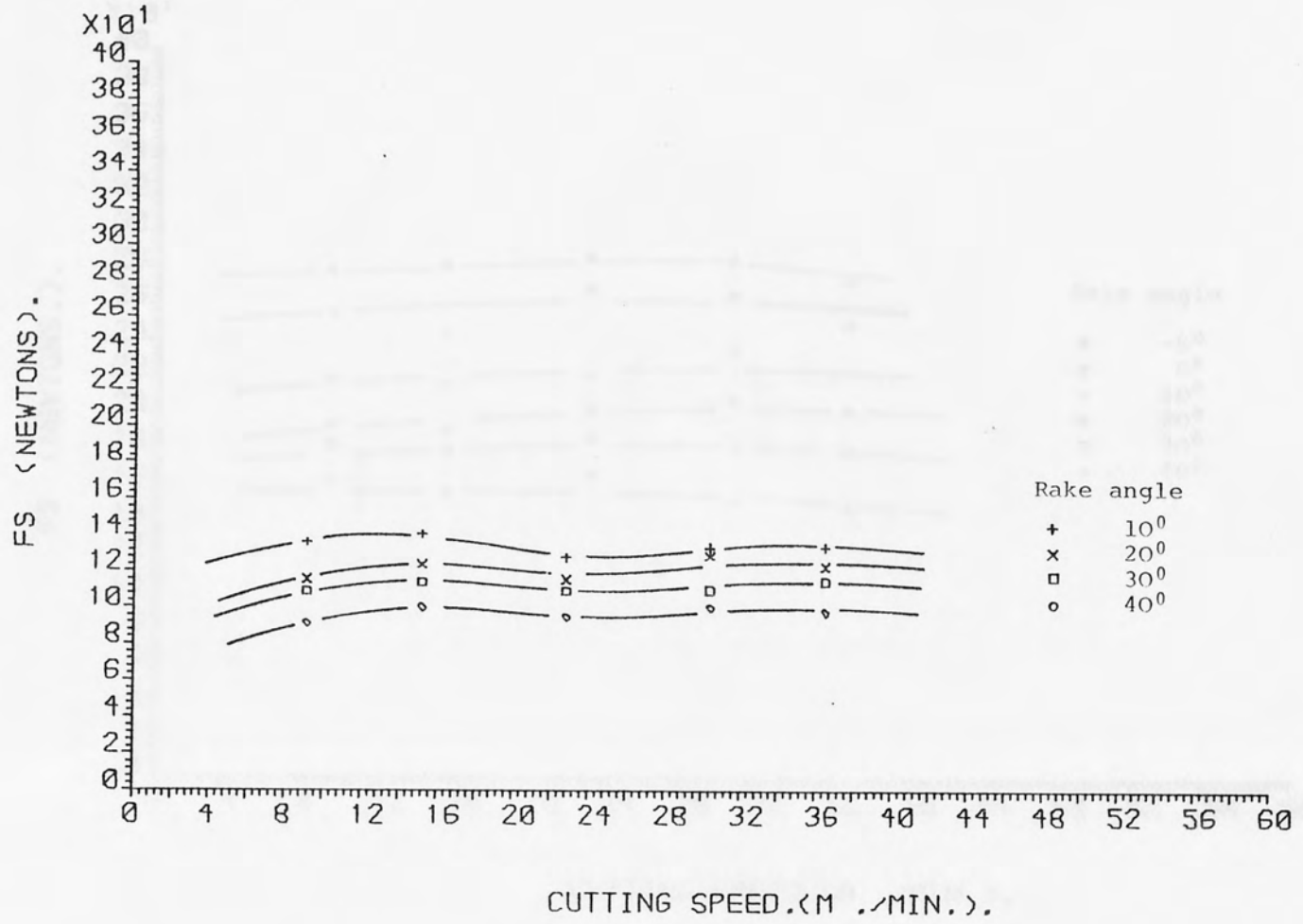

Fig. (7.62)

FIG. (7.62). F_s as a function of cutting speed for polycarbonate, depth of cut 0.381 mm.

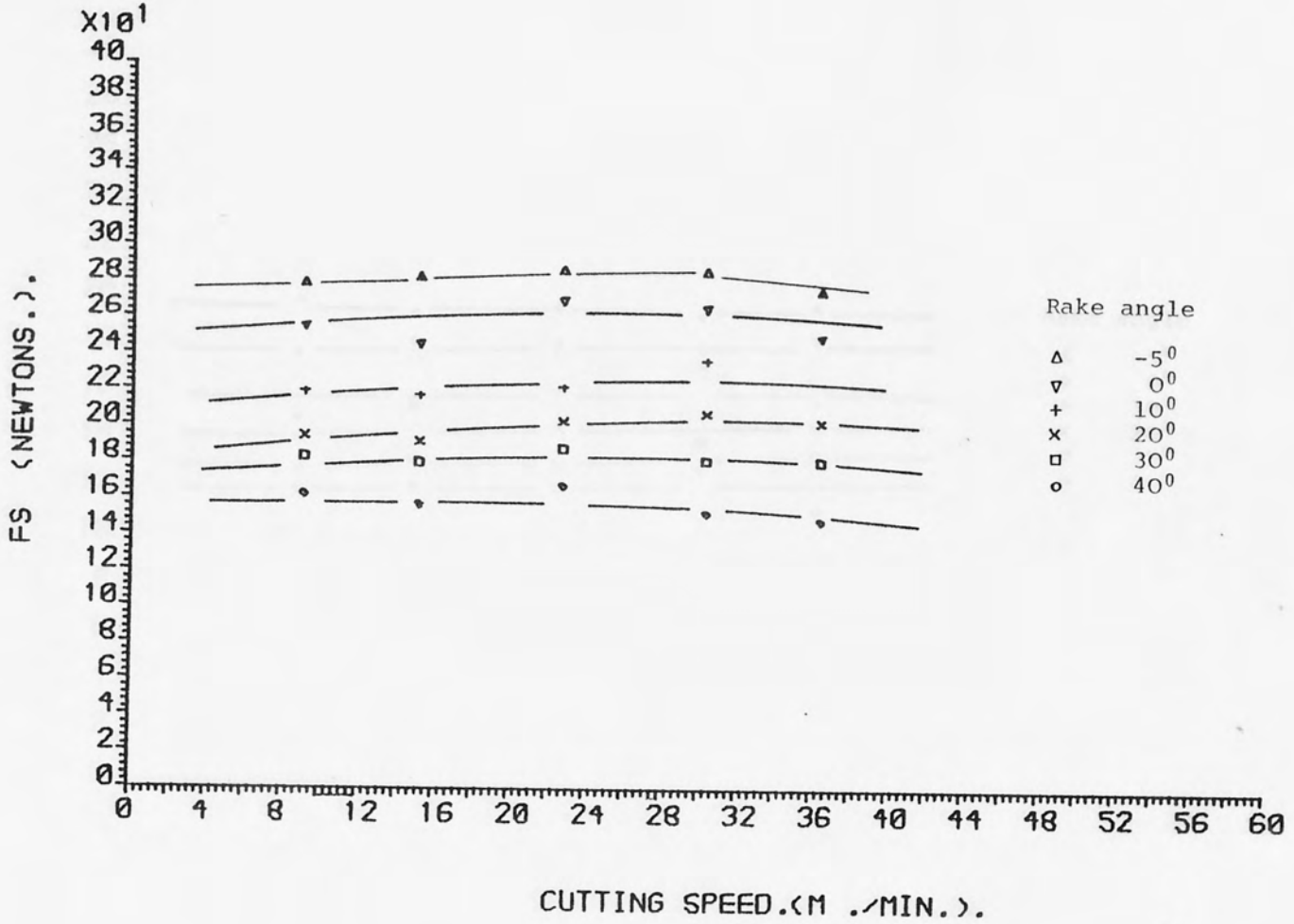

Fig. (7.63)

FIG. (7.63). F_s as a function of cutting speed for as-received Nylon, depth of cut 0.381 mm.

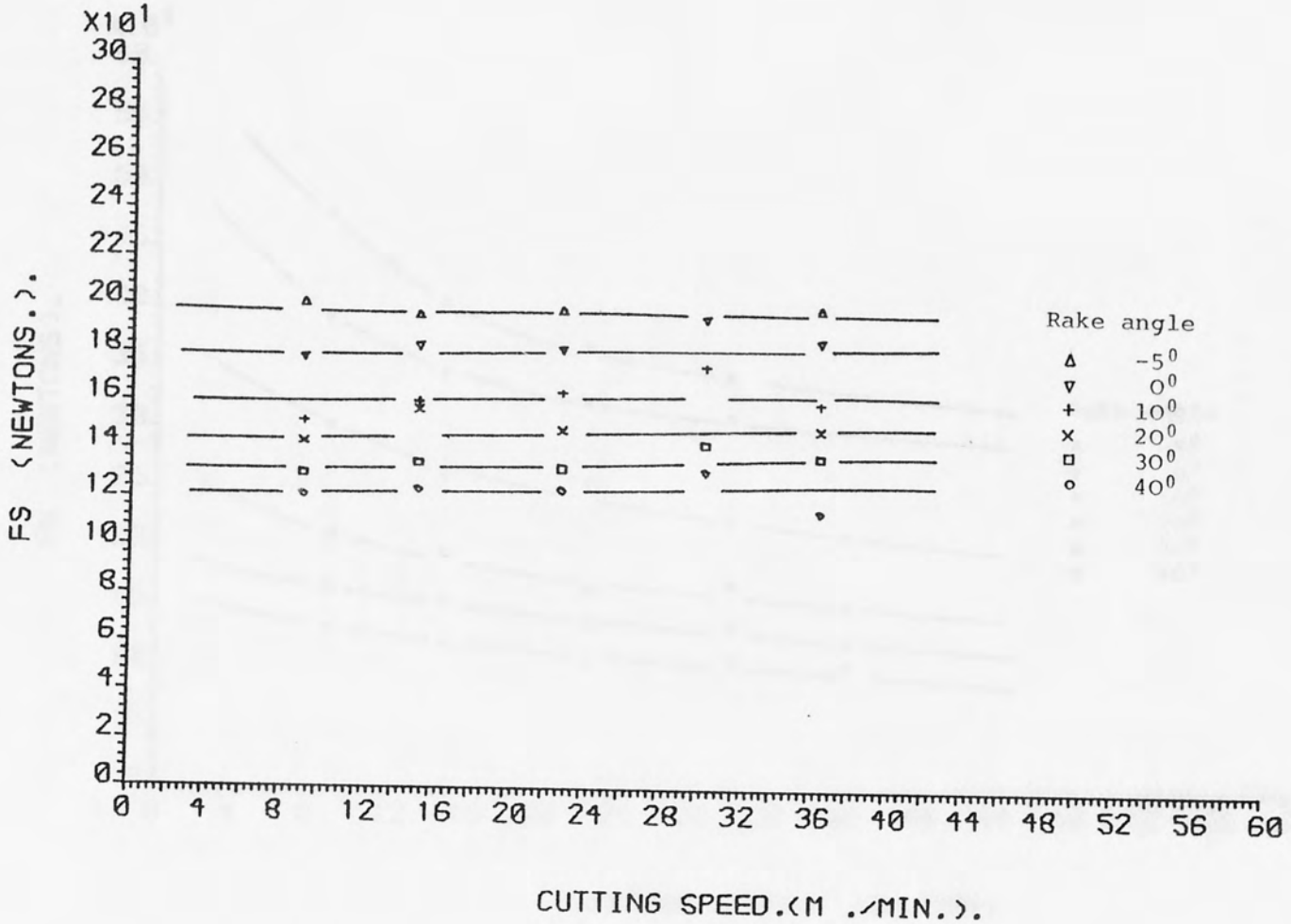

Fig. (7.64)

FIG. (7.64). F_s as a function of the cutting speed for rolled Nylon, depth of cut 0.381 mm.

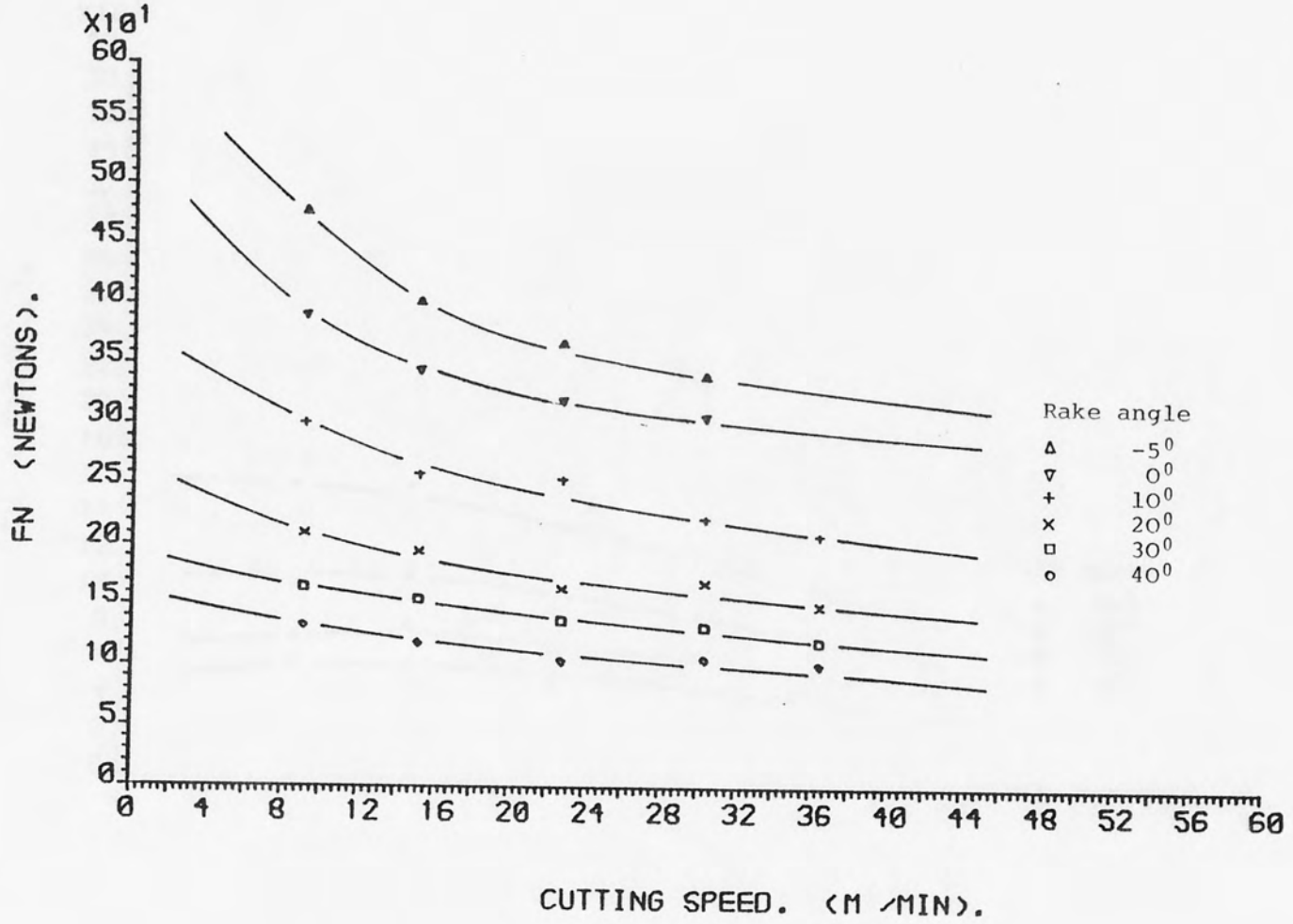

Fig. (7.65)

FIG. (7.65). F_n as a function of cutting speed for as-received polycarbonate, depth of cut 0.381 mm.

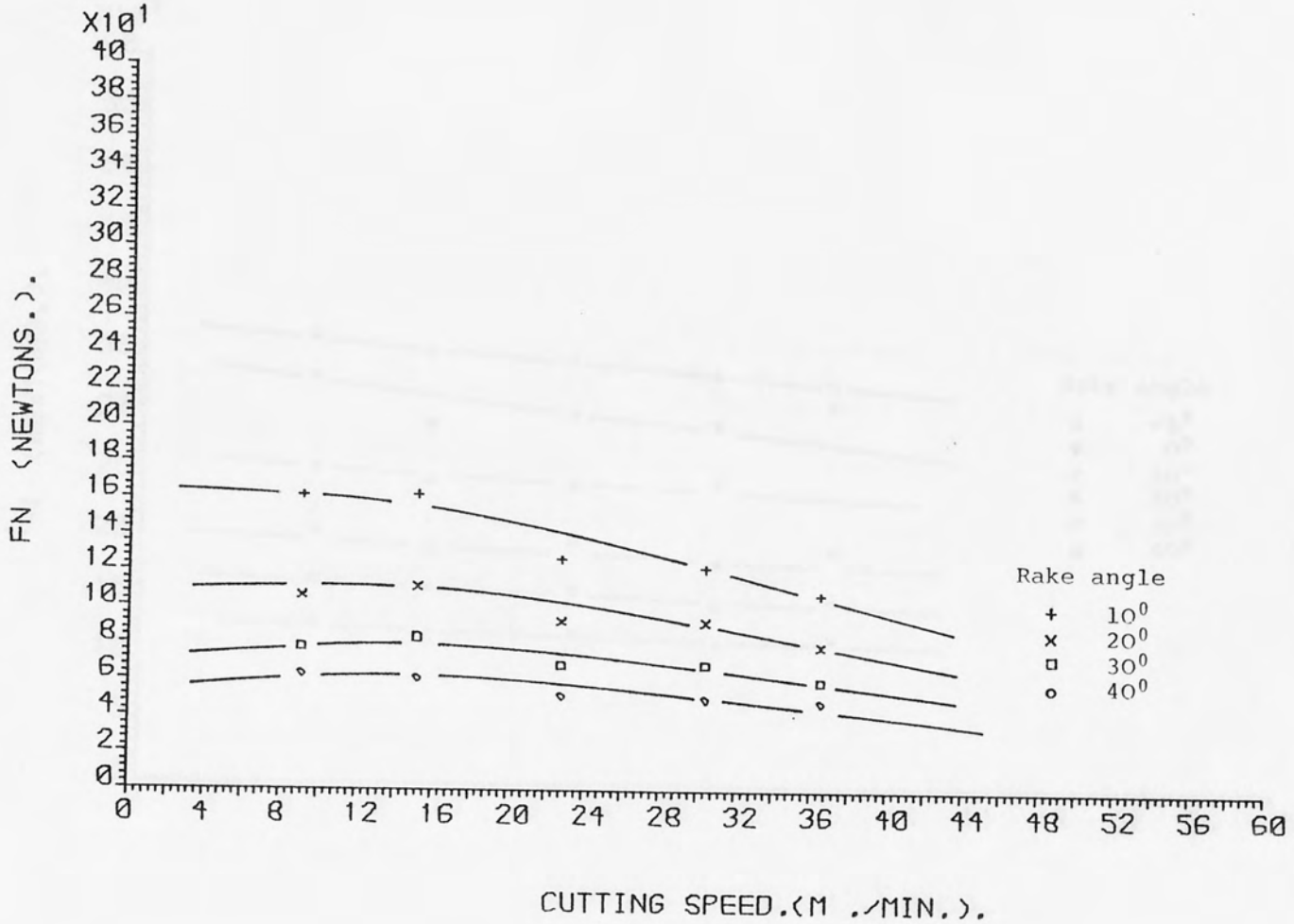

Fig. (7.66)

FIG. (7.66). F_n as a function of cutting speed for rolled polycarbonate, depth of cut 0.381 mm.

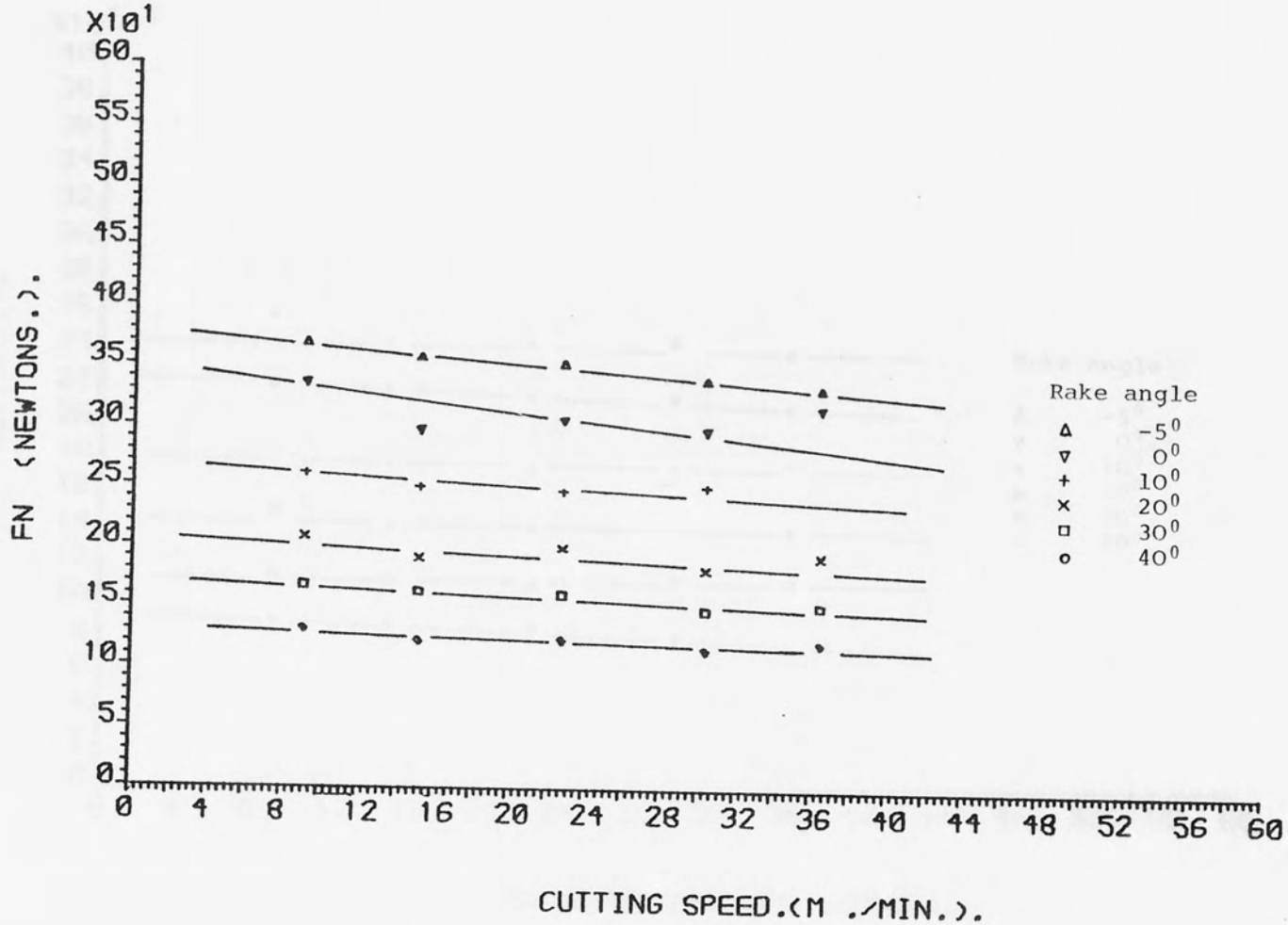

Fig. (7.67)

FIG. (7.67). F_n as a function of cutting speed for as-received Nylon, depth of cut 0.381 mm.

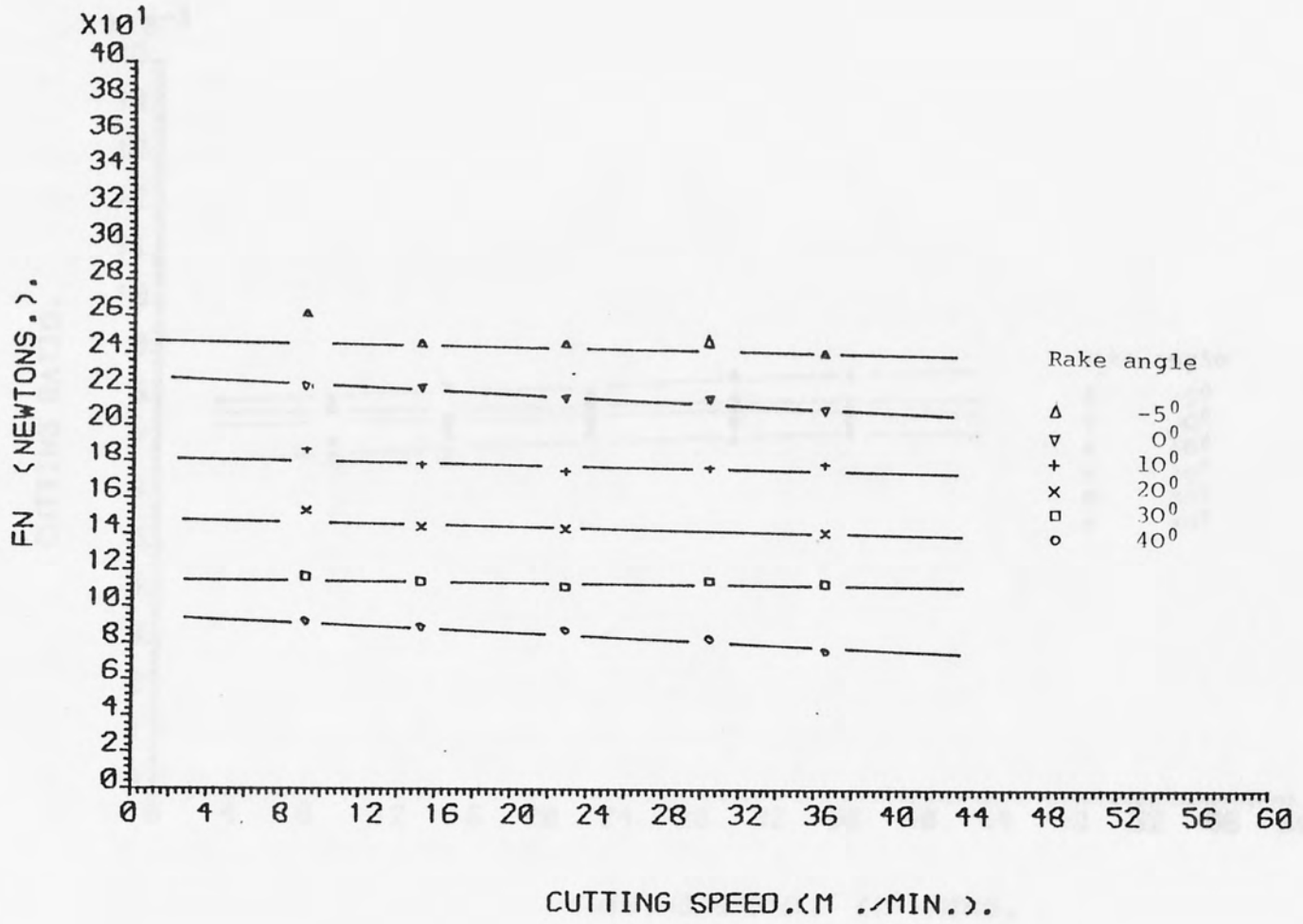

Fig. (7.68)

FIG. (7.68). F_n as a function of the cutting speed for rolled Nylon, depth of cut 0.381 mm.

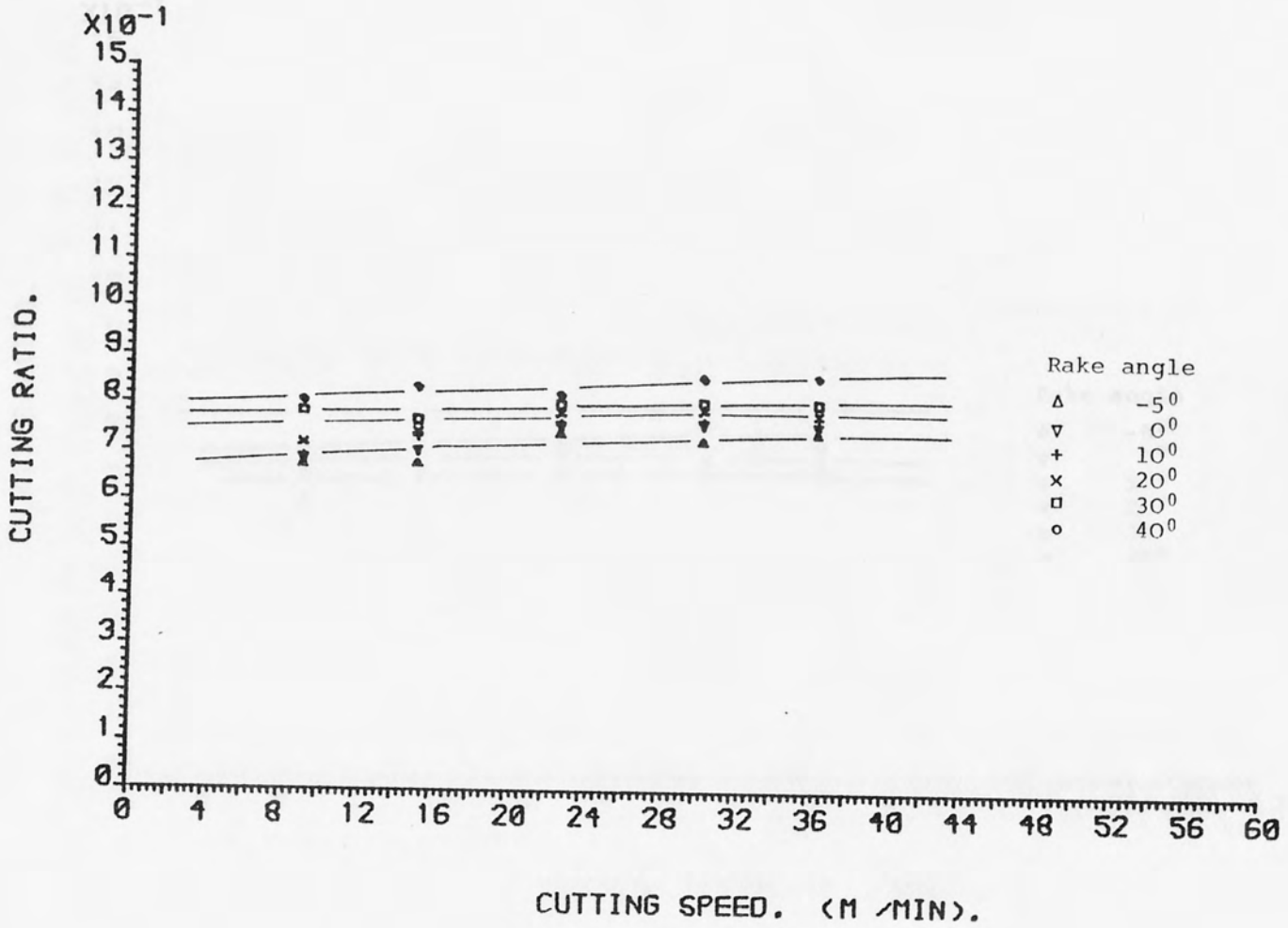

Fig. (7.69)

FIG. (7.69). r_c as a function of cutting speed for as-received polycarbonate, depth of cut 0.381 mm.

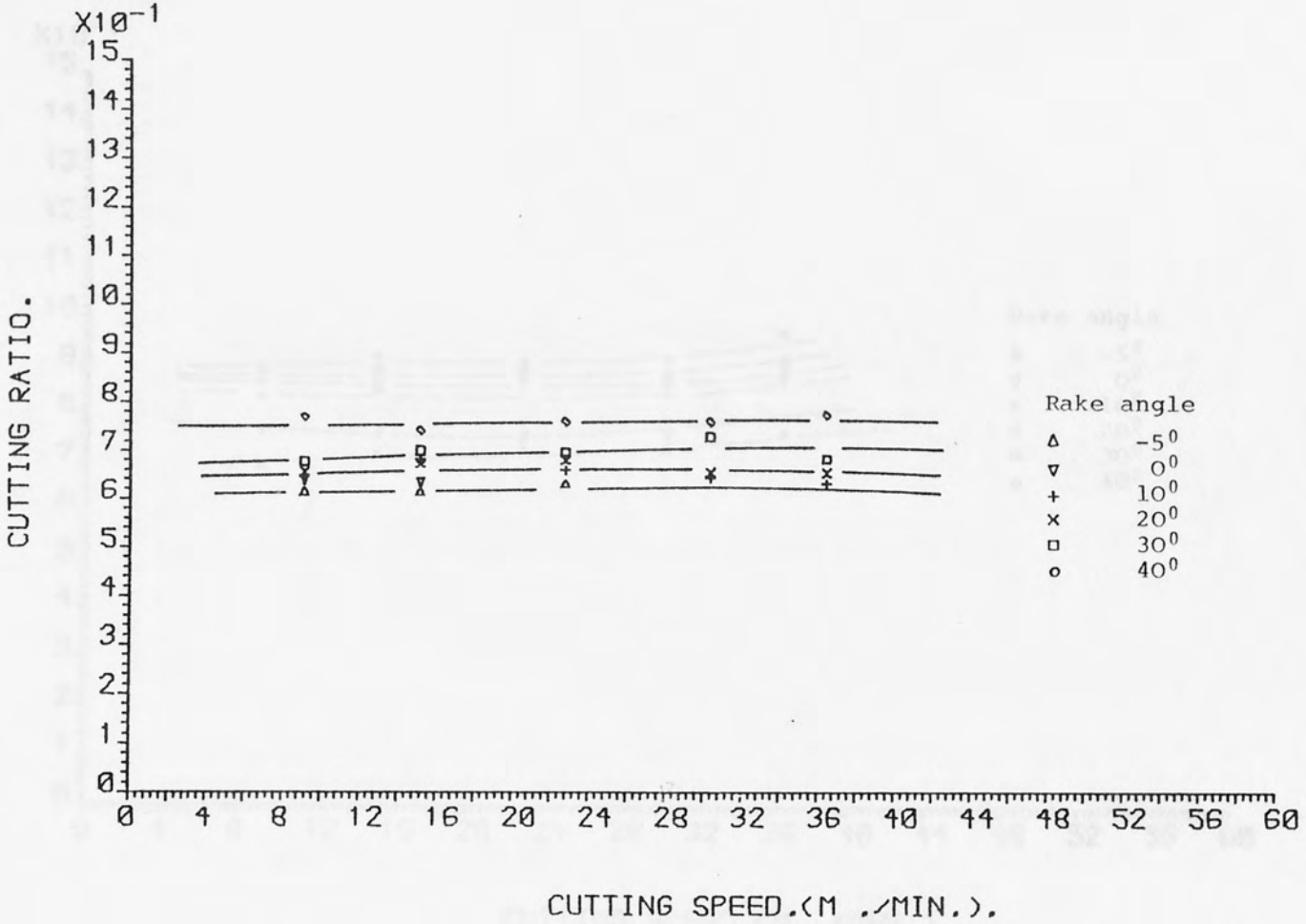

Fig. (7.70)

FIG. (7.70). r_c as a function of cutting speed for rolled polycarbonate, depth of cut 0.381 mm.

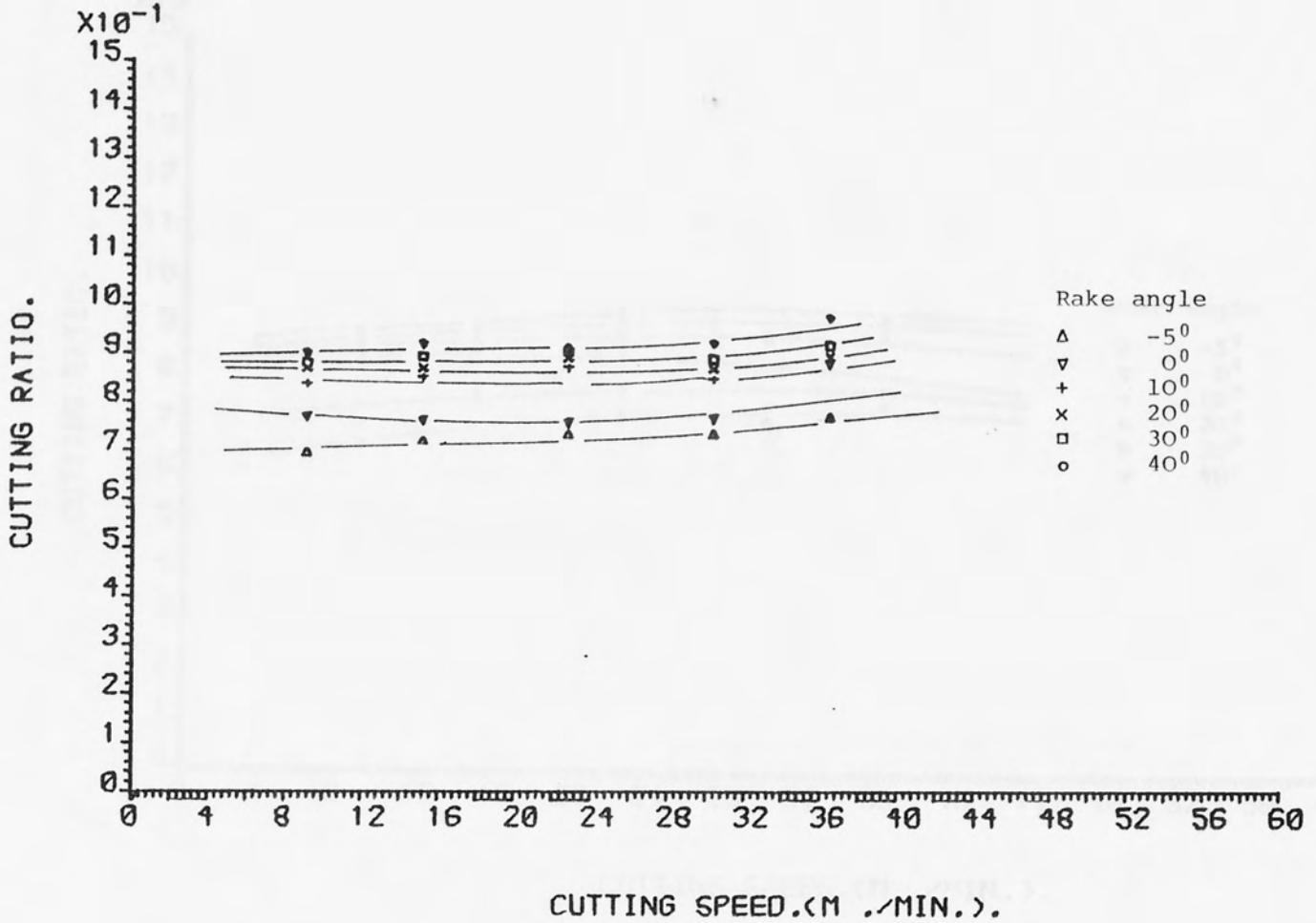

Fig. (7.71)

FIG. (7.71). r_c as a function of cutting speed for as-received Nylon, depth of cut 0.381 mm.

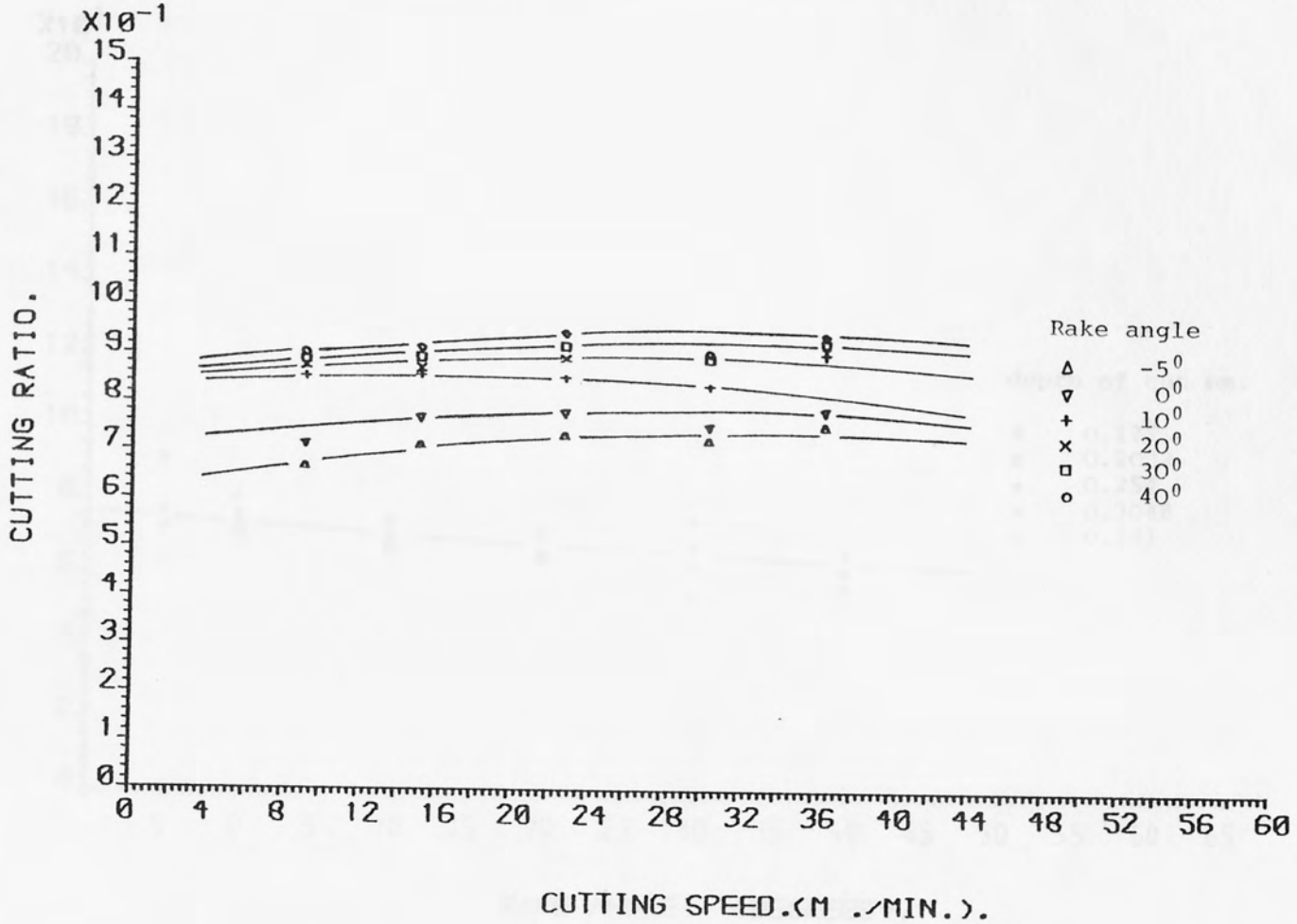

Fig. (7.72)

FIG. (7.72) r_c as a function of the cutting speed for rolled Nylon, depth of cut 0.381 mm.

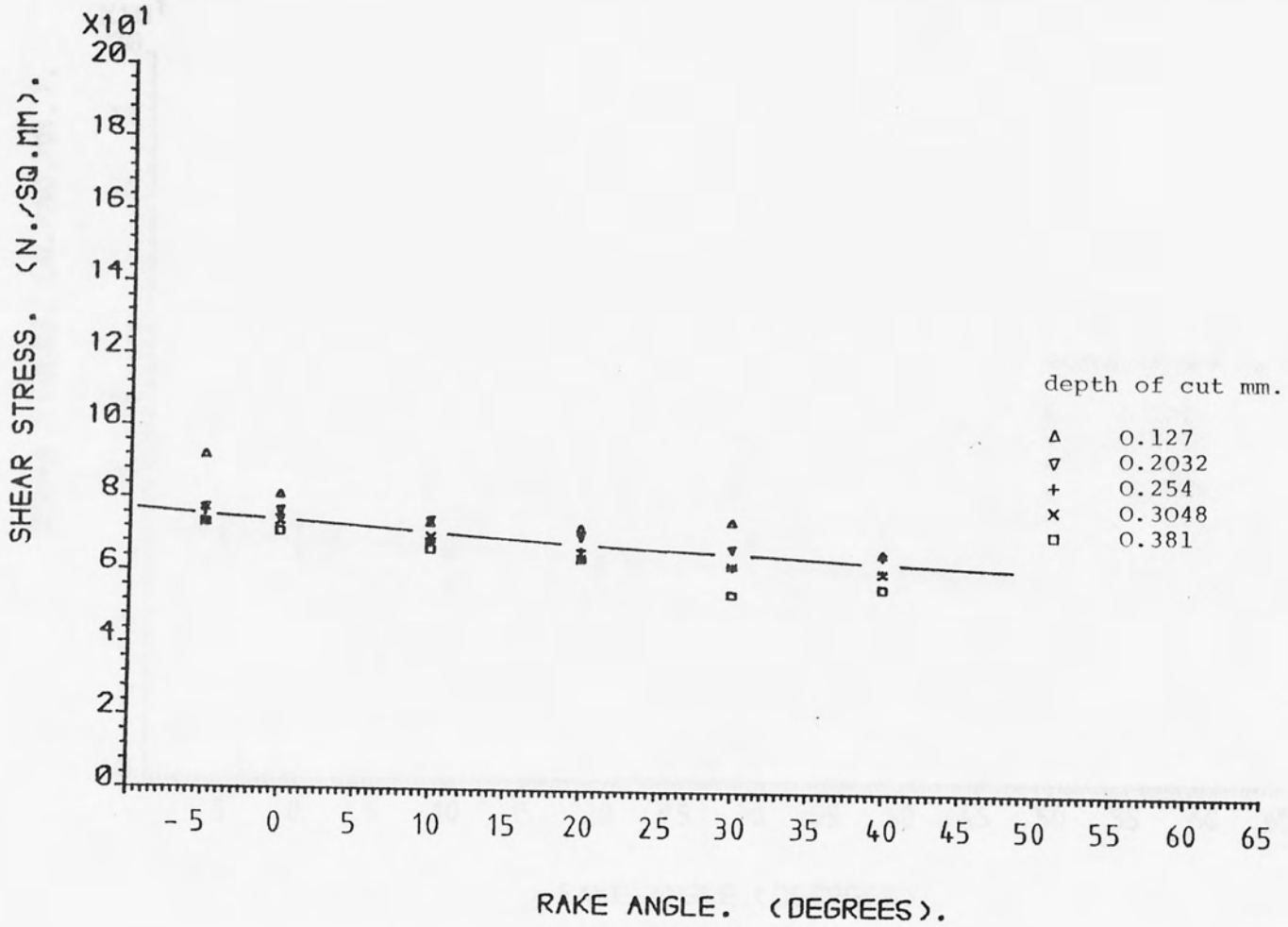

Fig. (7.73)

FIG. (7.73). τ_s as a function of rake angle for as-received polycarbonate, cutting speed 15.24 m/min.

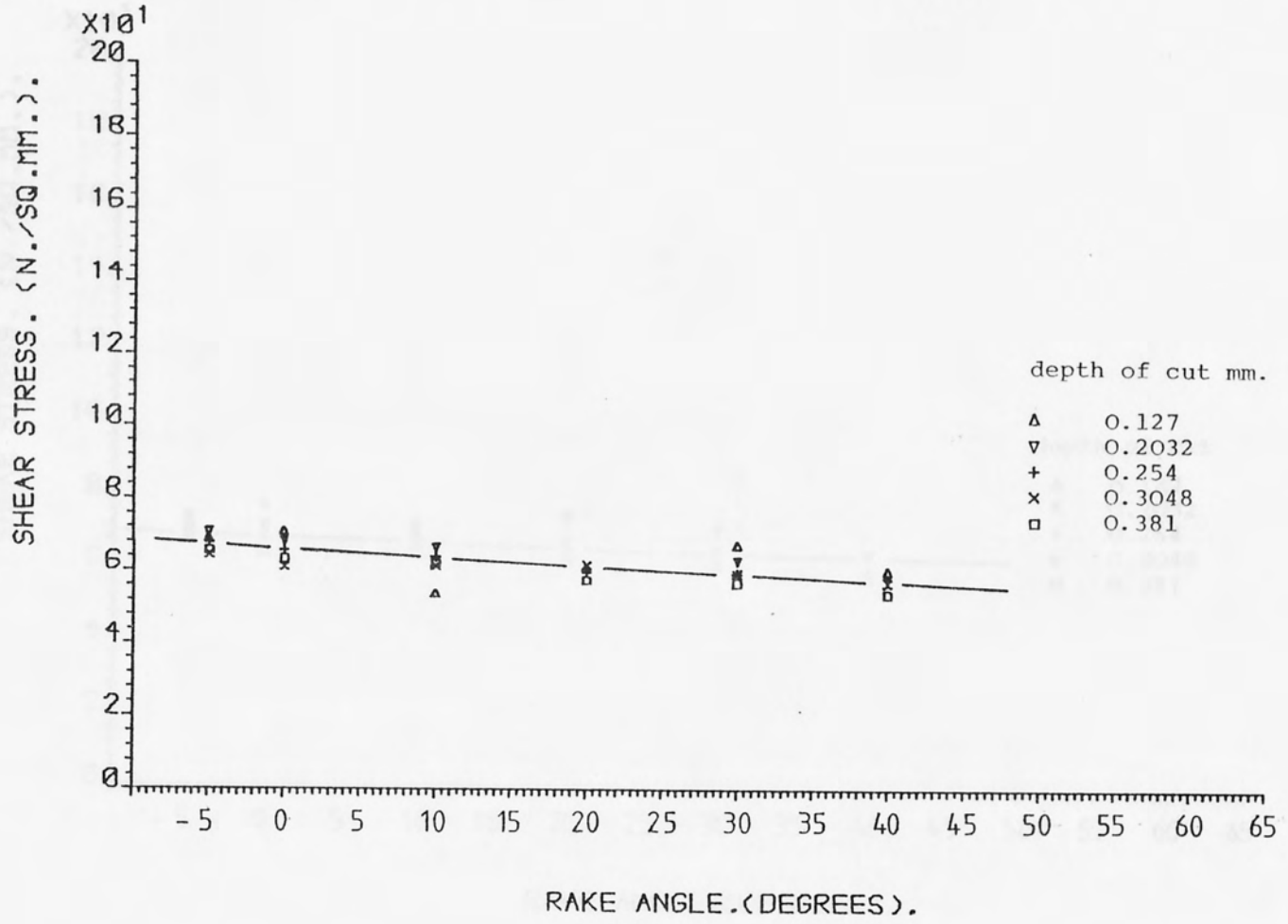

Fig. (7.74)

FIG. (7.74). τ_s as a function of rake angle for rolled polycarbonate, cutting speed 15.24 m/min.

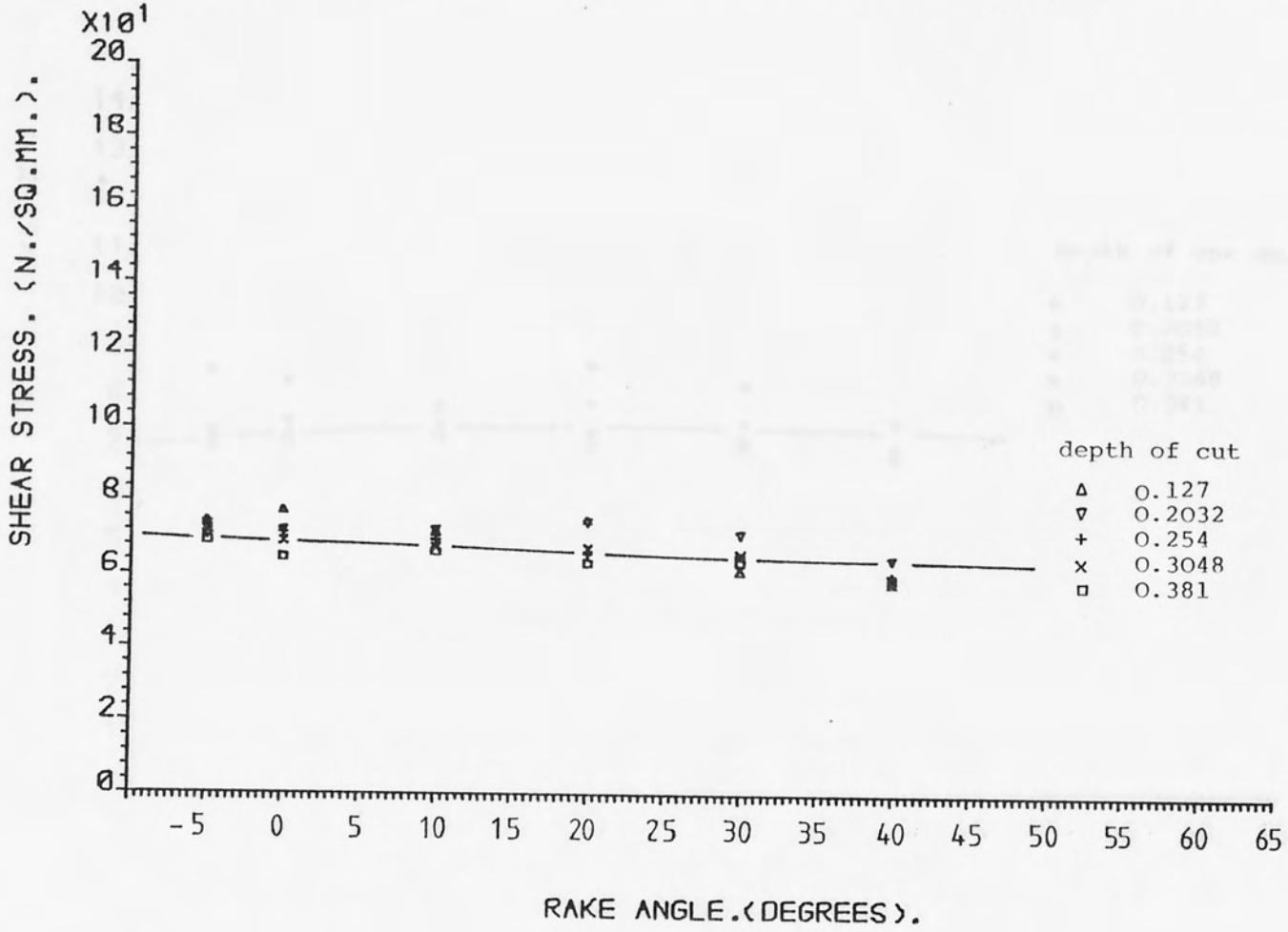

Fig. (7.75)

FIG. (7.75). τ_s as a function of rake angle for as-received Nylon, cutting speed 15.24 m/min.

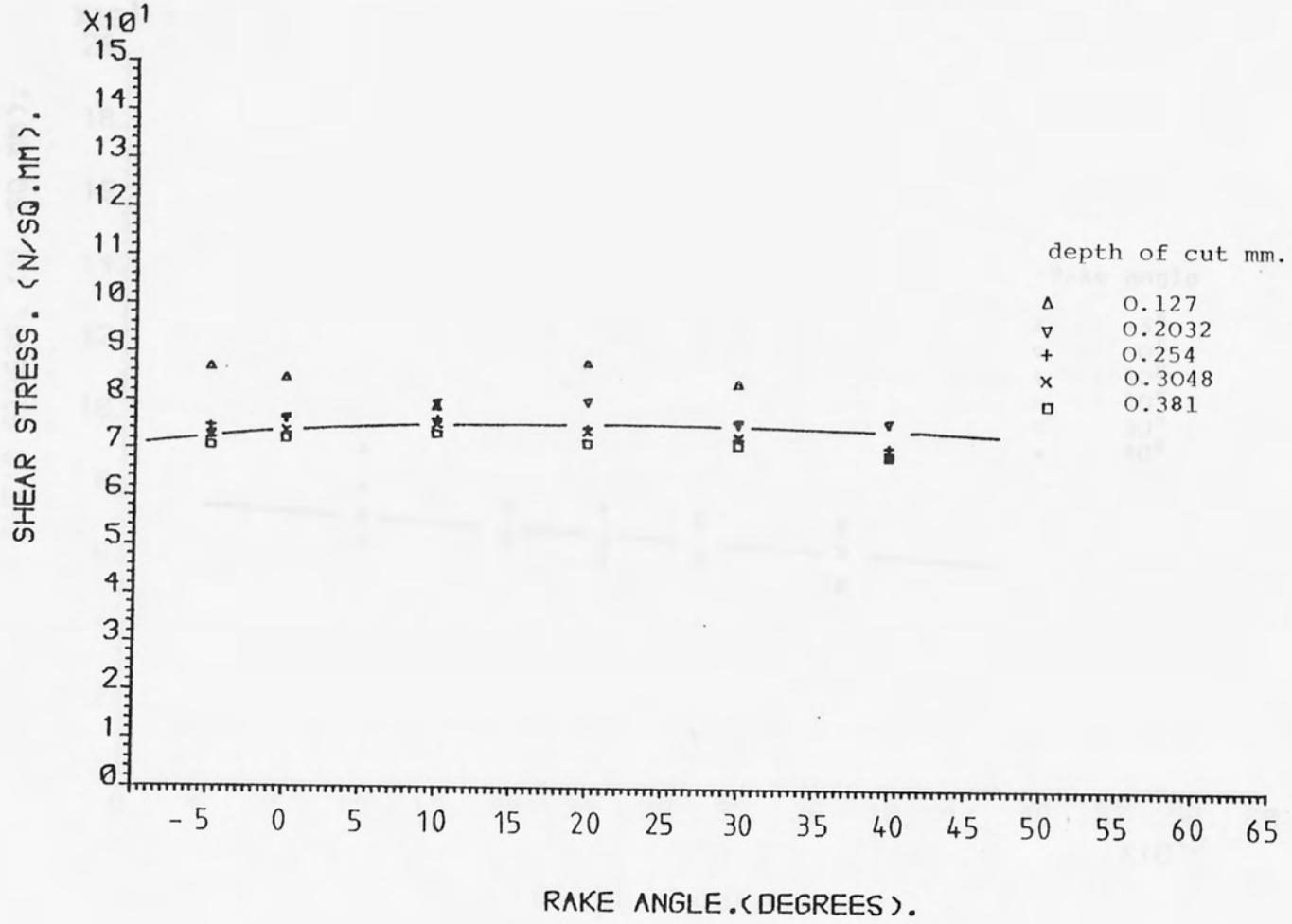

Fig. (7.76)

FIG. (7.76). τ_s as a function of rake angle for rolled Nylon, cutting speed 15.24 m/min.

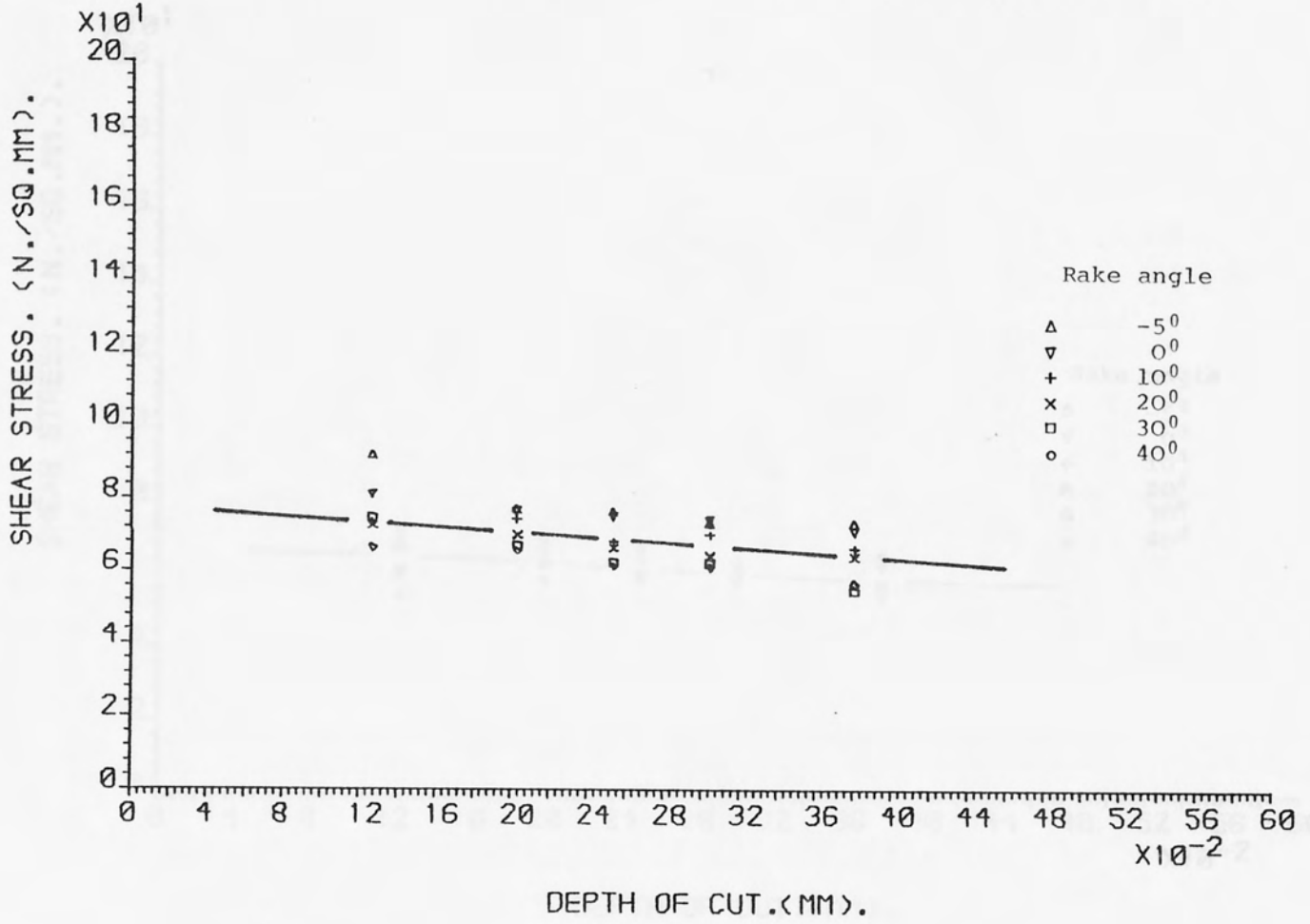

Fig. (7.77)

FIG. (7.77). τ_s as a function of depth of cut for as-received polycarbonate, cutting speed 15.24 m/min.

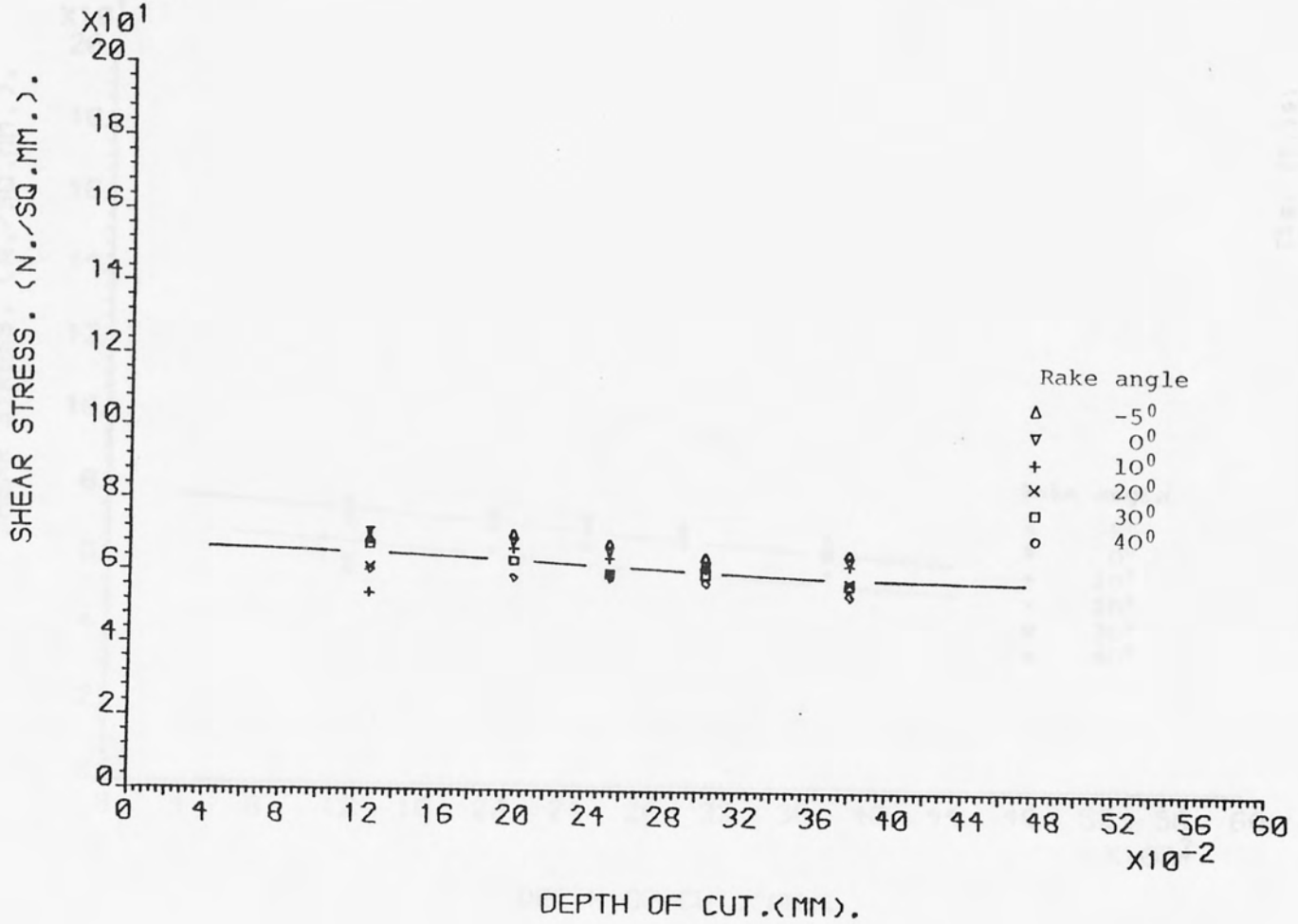

Fig. (7.78)

FIG. (7.78). τ_s as a function of depth of cut for rolled polycarbonate, cutting speed 15.24 m/min.

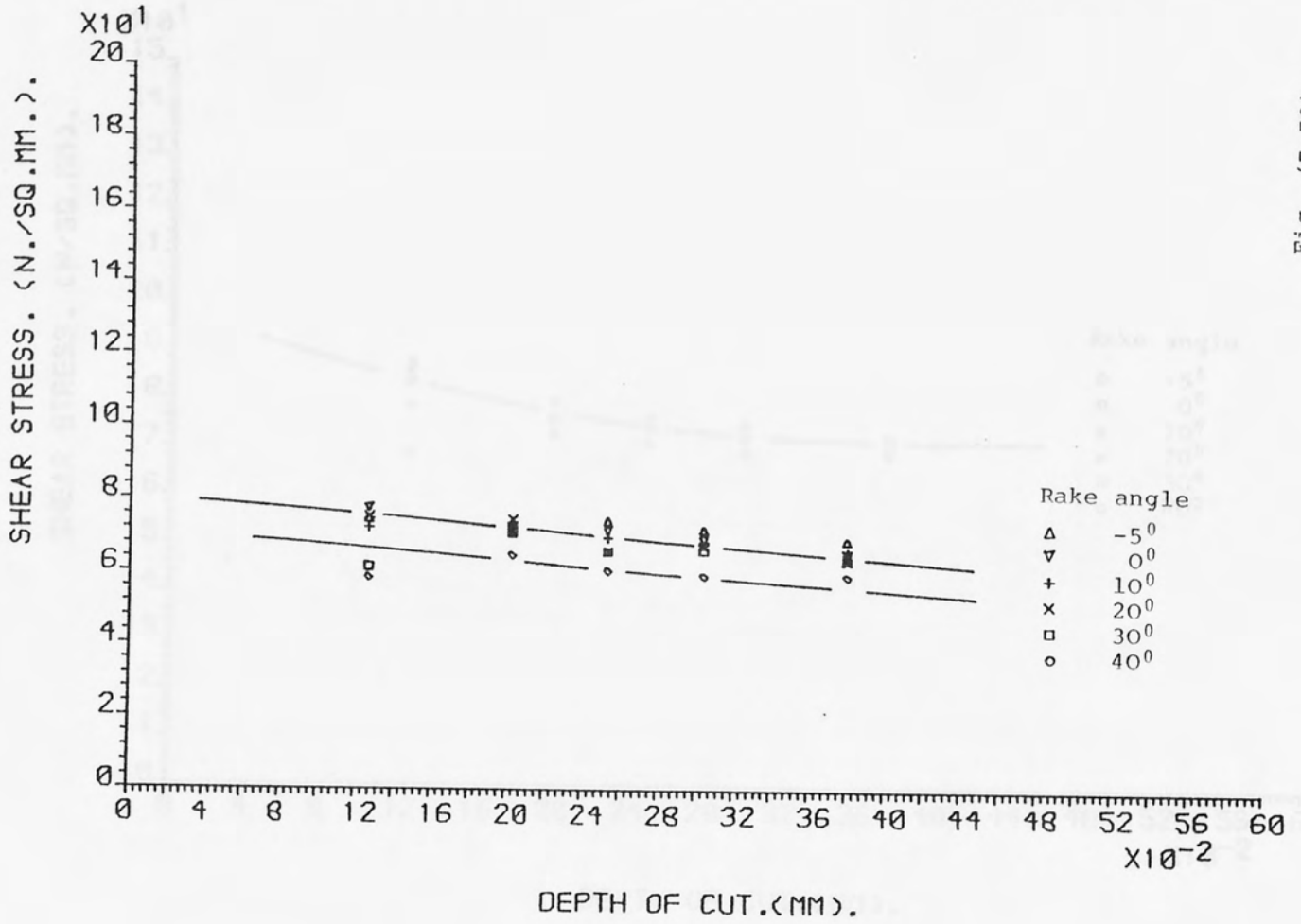

Fig. (7.79)

FIG. (7.79). τ_s as a function of depth of cut for as-received Nylon, cutting speed 15.24 m/min.

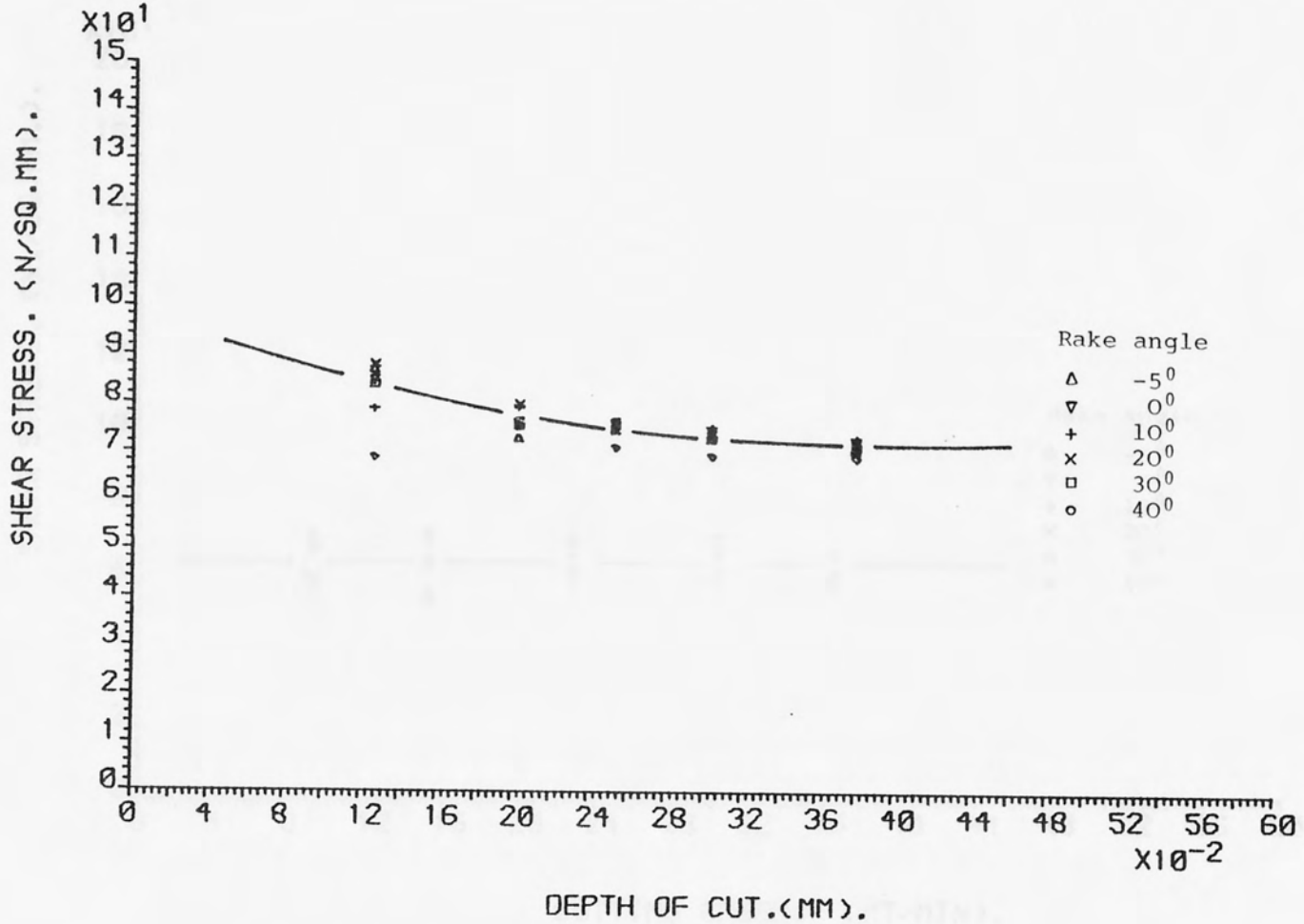

Fig. (7.80)

FIG. (7.80). τ_s as a function of depth of cut for rolled Nylon, cutting speed 15.24 m/min.

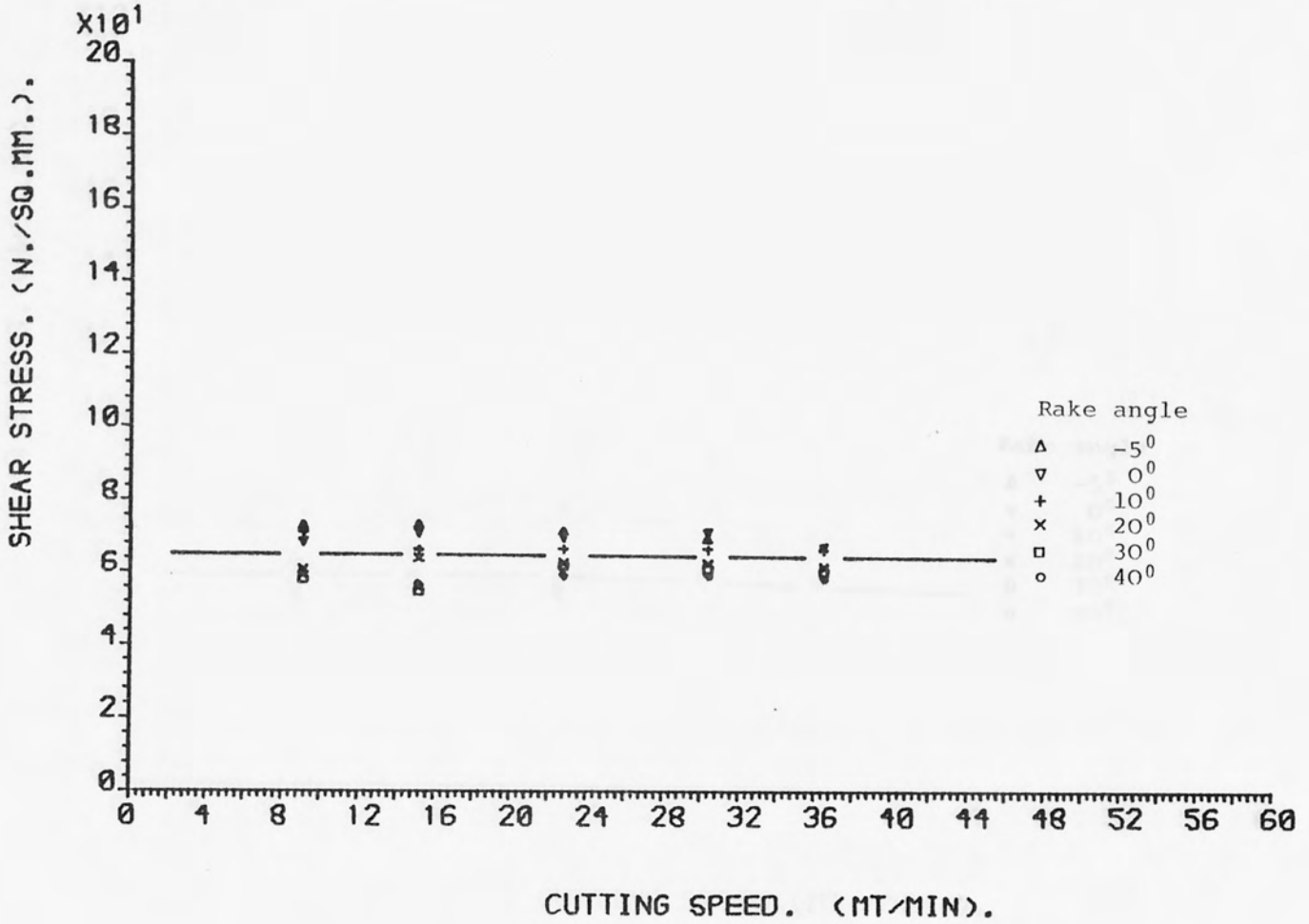

Fig. (7.81)

FIG. (7.81). τ_s as a function of cutting speed for as-received polycarbonate, depth of cut 0.381 mm.

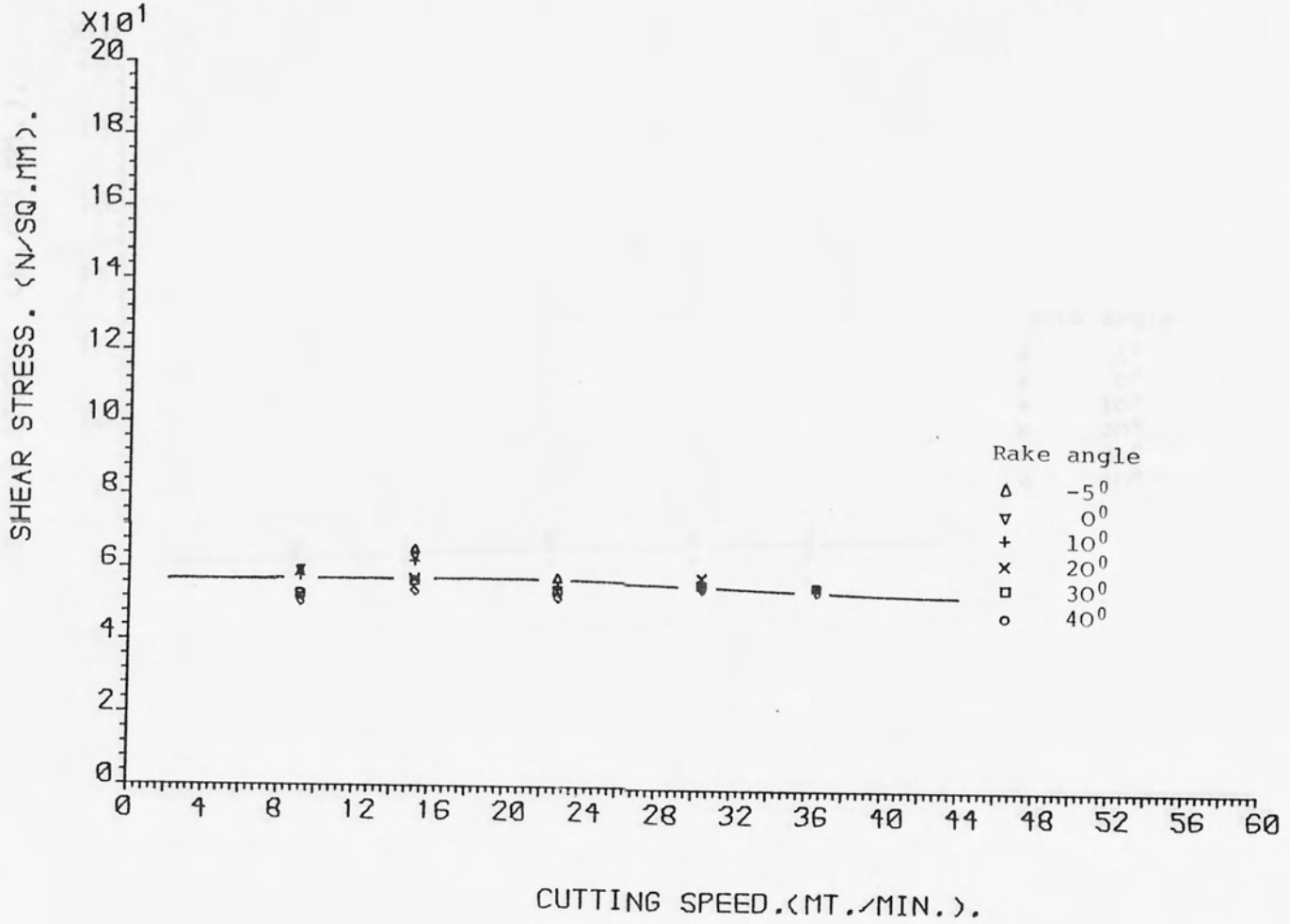

Fig. (7.82)

FIG. (7.82). τ_s as a function of cutting speed for rolled polycarbonate, depth of cut 0.381 mm.

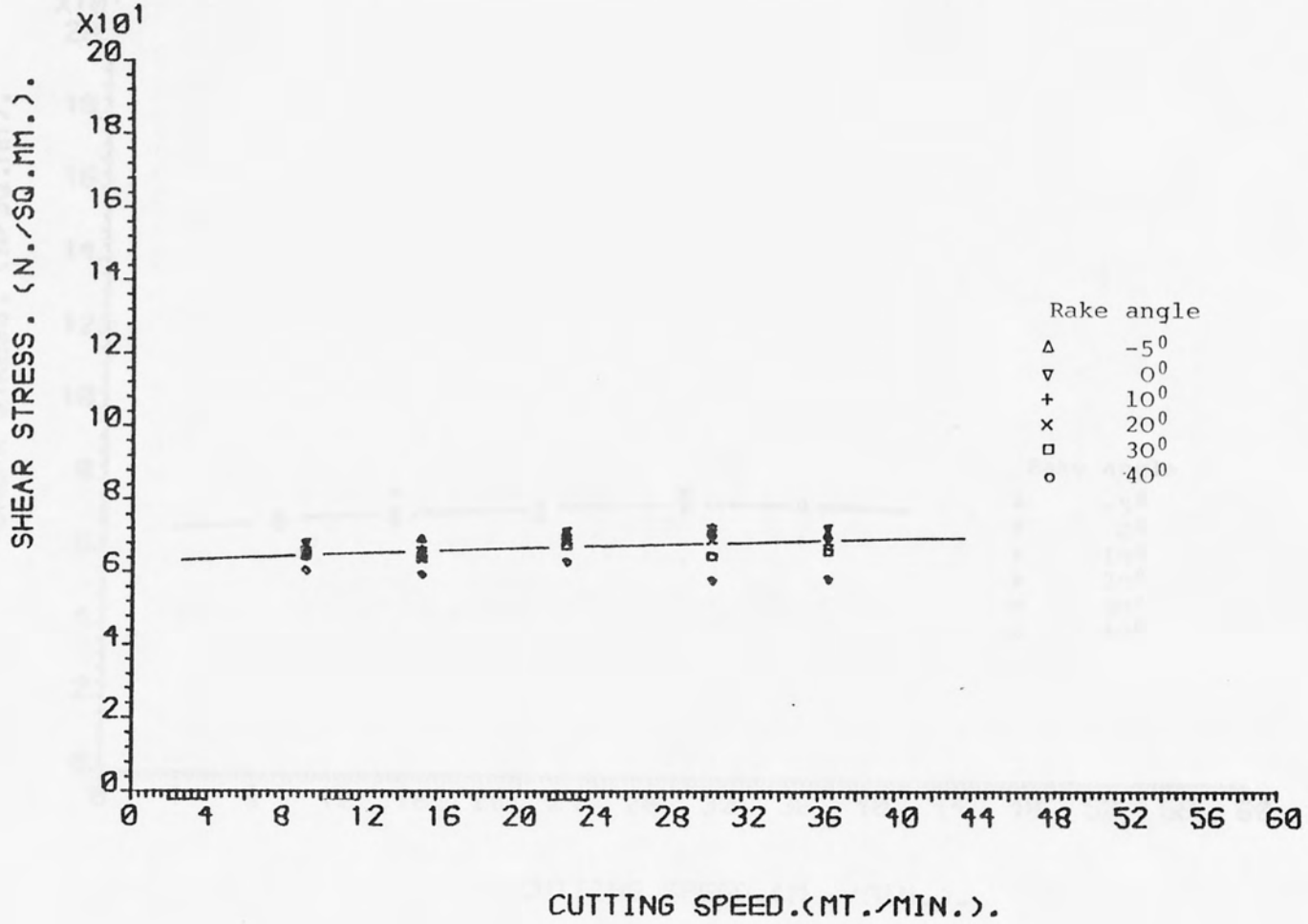

Fig. (7.83)

FIG. (7.83). τ_s as a function of cutting speed for as-received Nylon, depth of cut 0.381 mm.

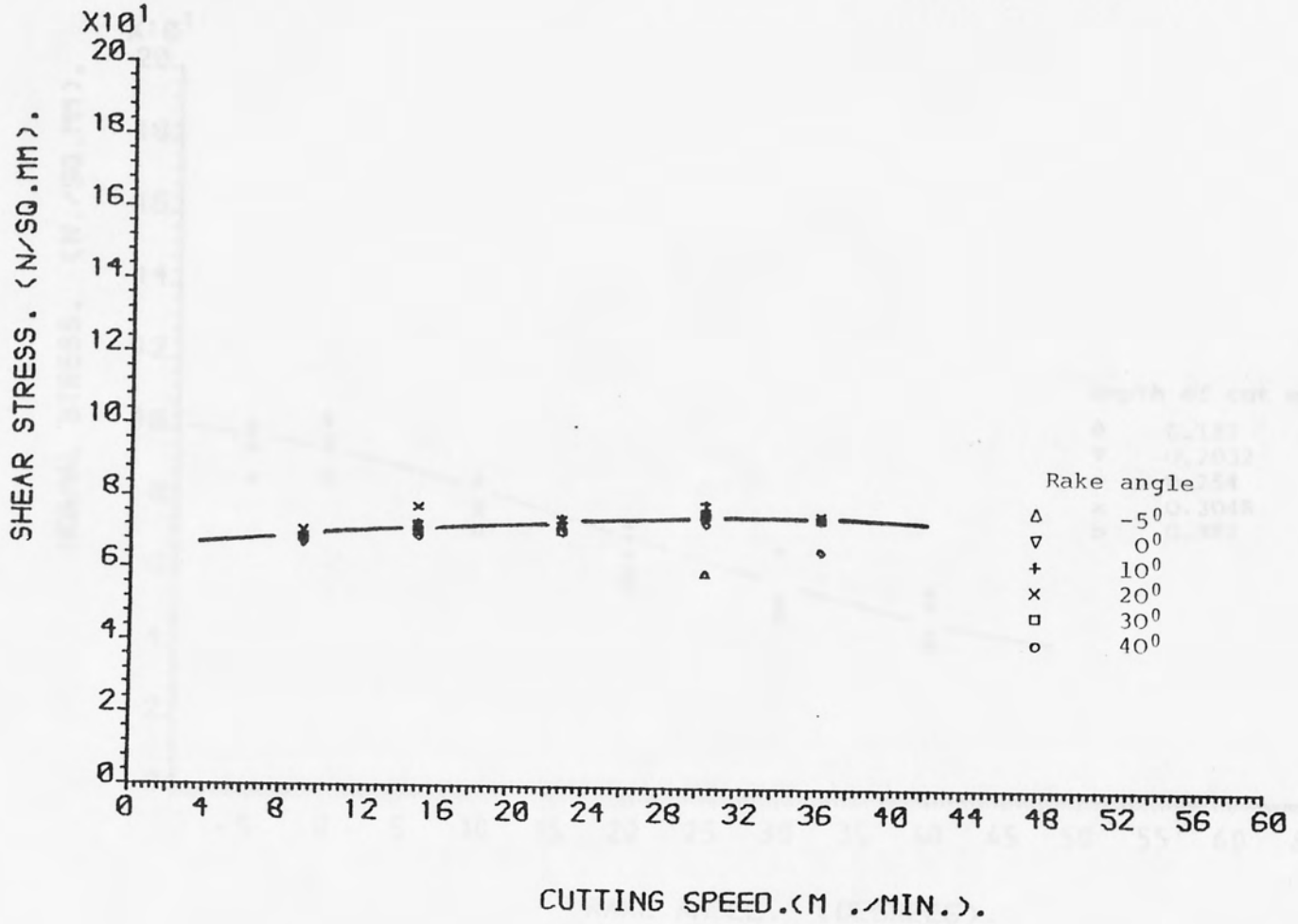

Fig. (7.84)

FIG. (7.84). τ_s as a function of the cutting speed for rolled Nylon, depth of cut 0.381 mm.

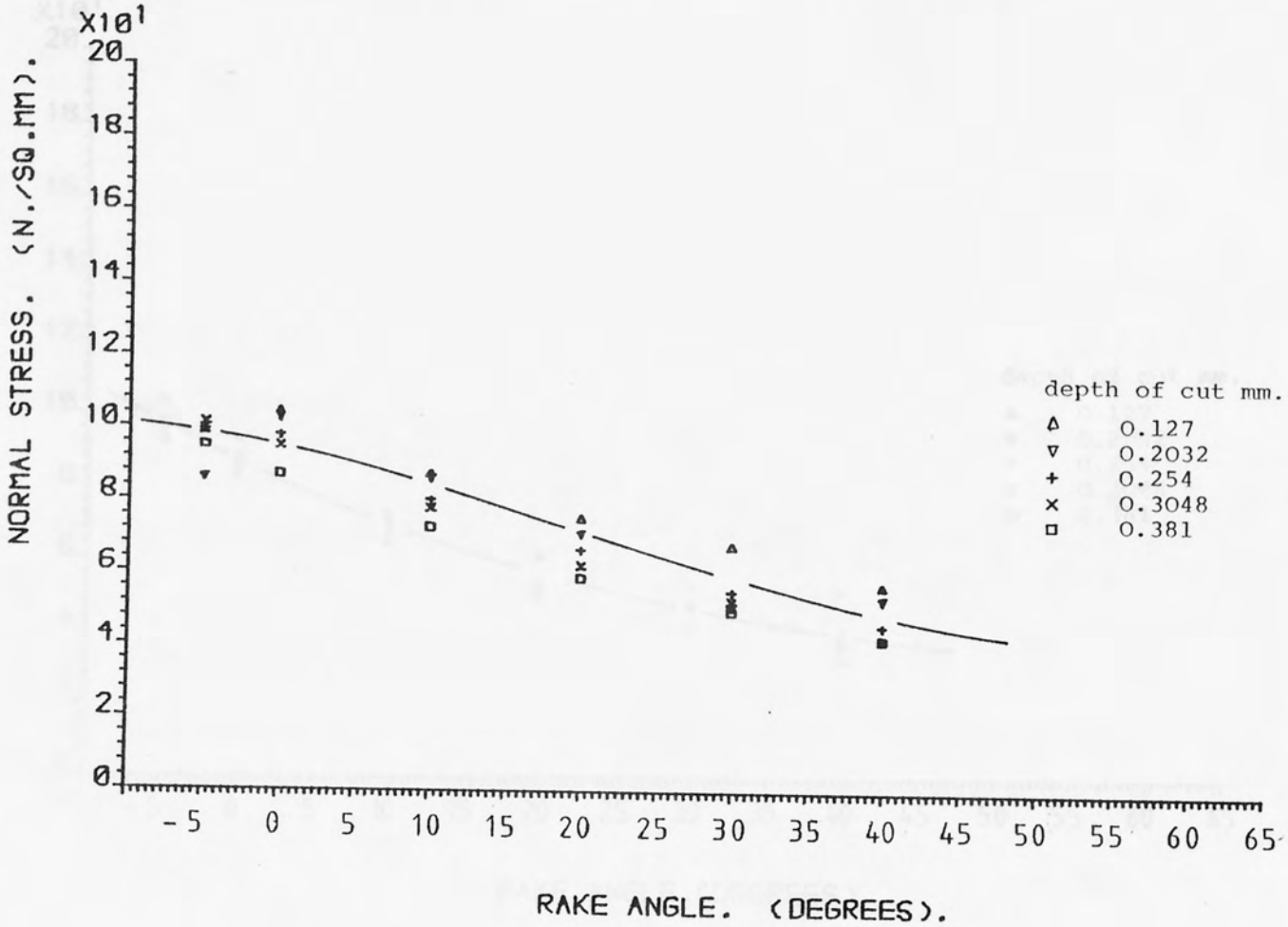

Fig. (7.85)

FIG. (7.85). σ_s as a function of rake angle for as-received polycarbonate, cutting speed 15.24 m/min.

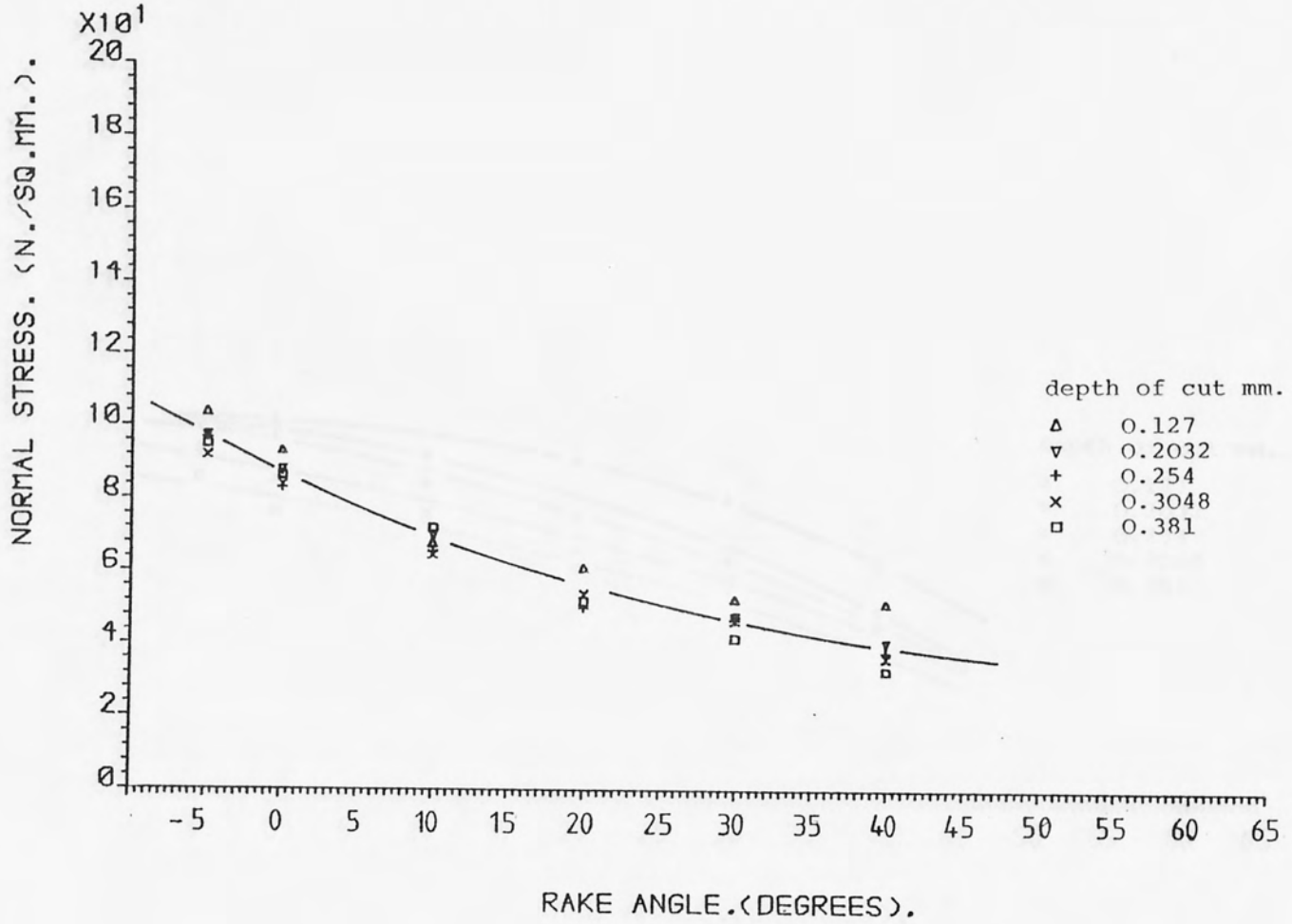

Fig. (7.86)

FIG. (7.86). σ_s as a function of rake angle for rolled polycarbonate, cutting speed 15.24 m/min.

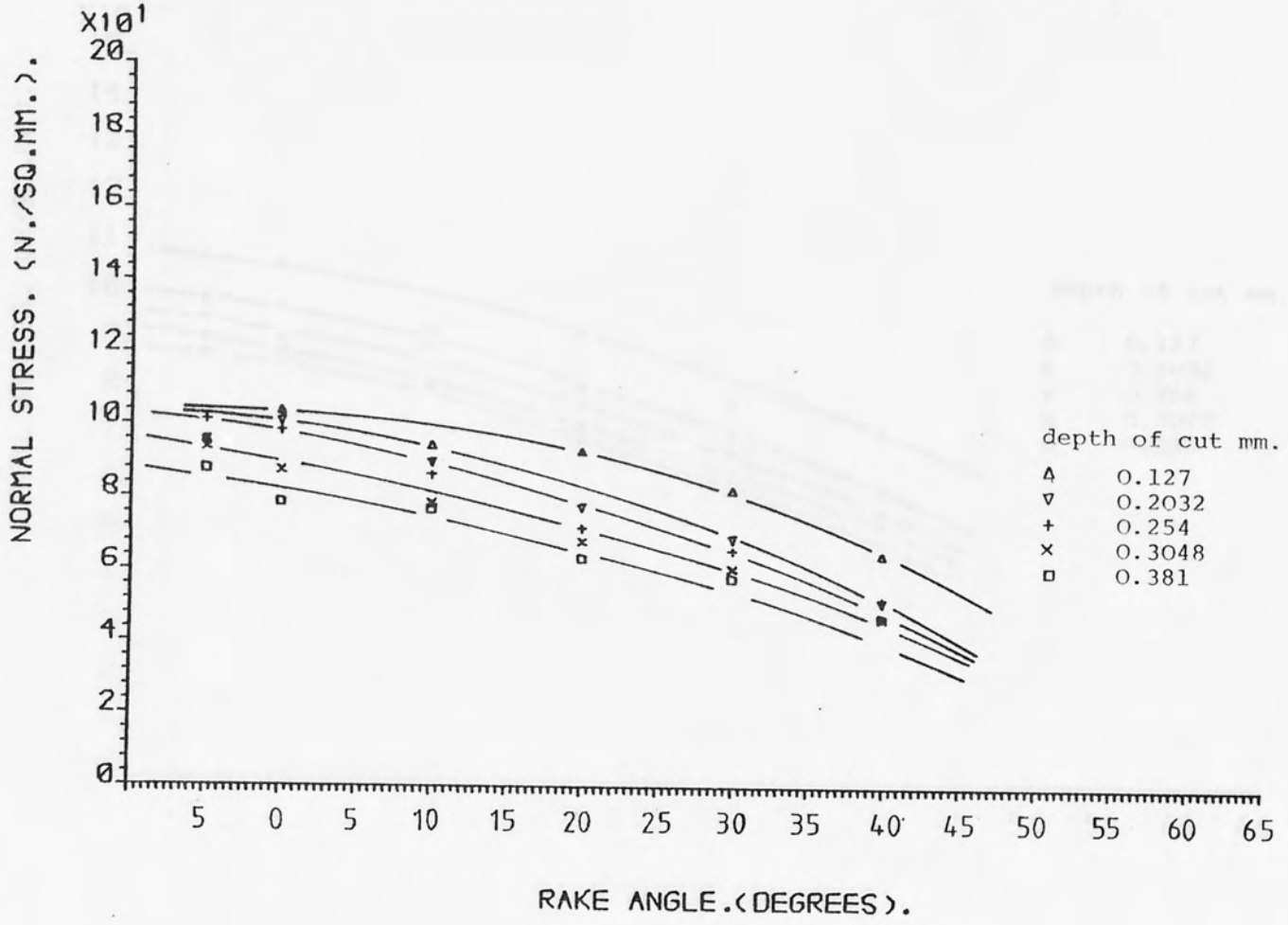

Fig. (7.87)

FIG. (7.87). σ_s as a function of rake angle for as-received Nylon, cutting speed 15.24 m/min.

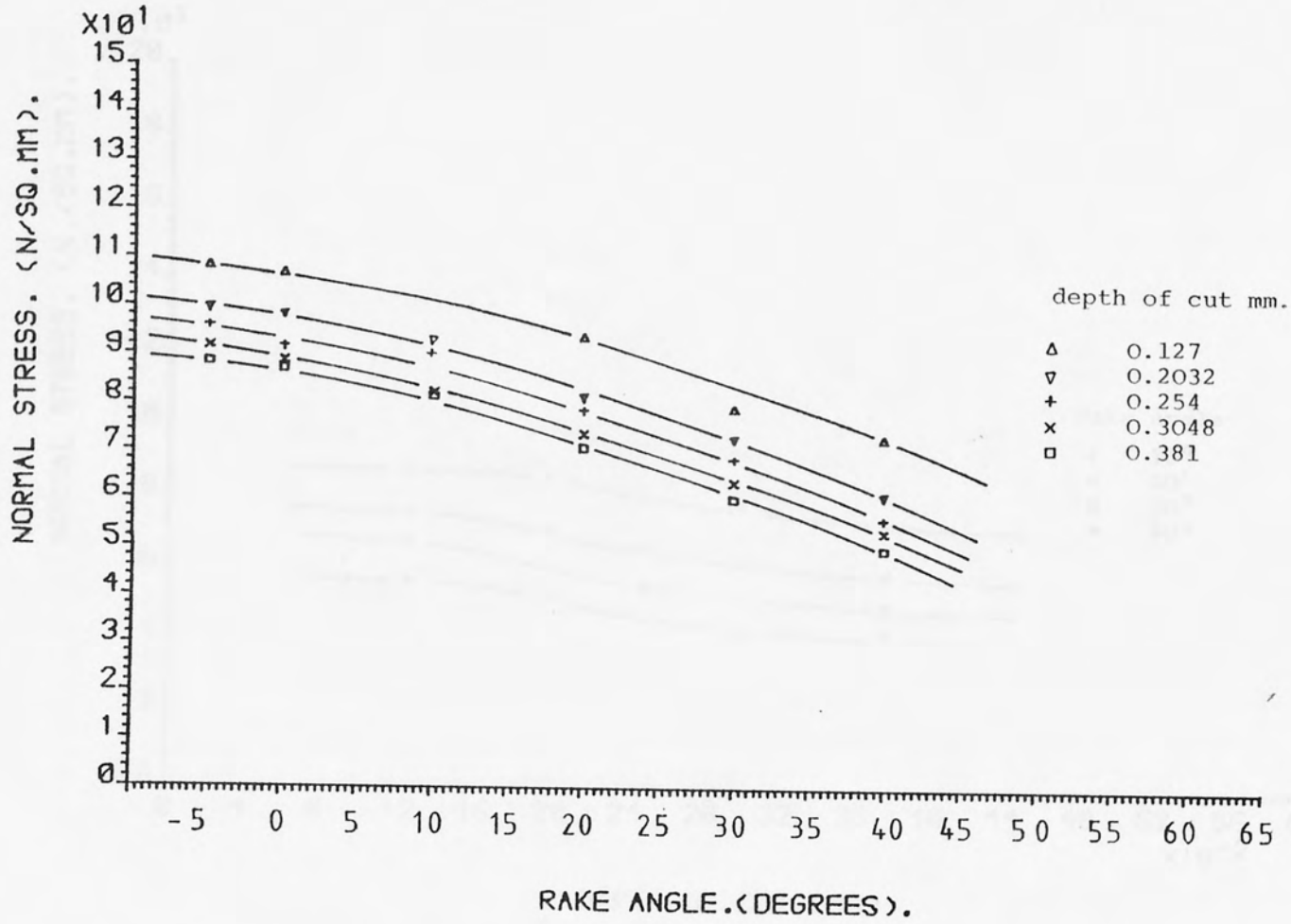

Fig. (7.88)

FIG. (7.88). σ_s as a function of rake angle for rolled Nylon, cutting speed 15.24 m/min.

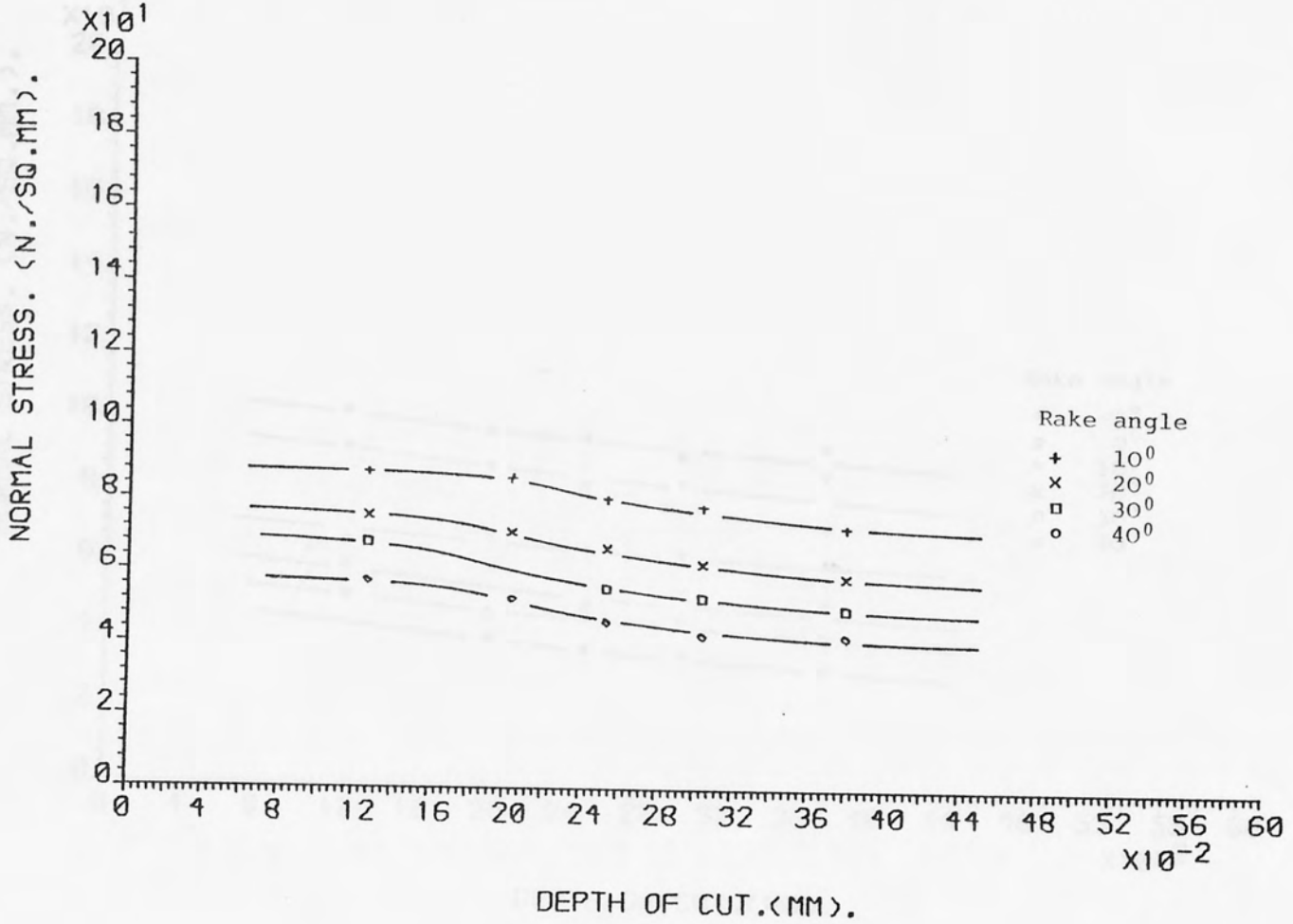

Fig. (7.89)

FIG. (7.89). σ_s as a function of depth of cut for as-received polycarbonate, cutting speed 15.24 m/min.

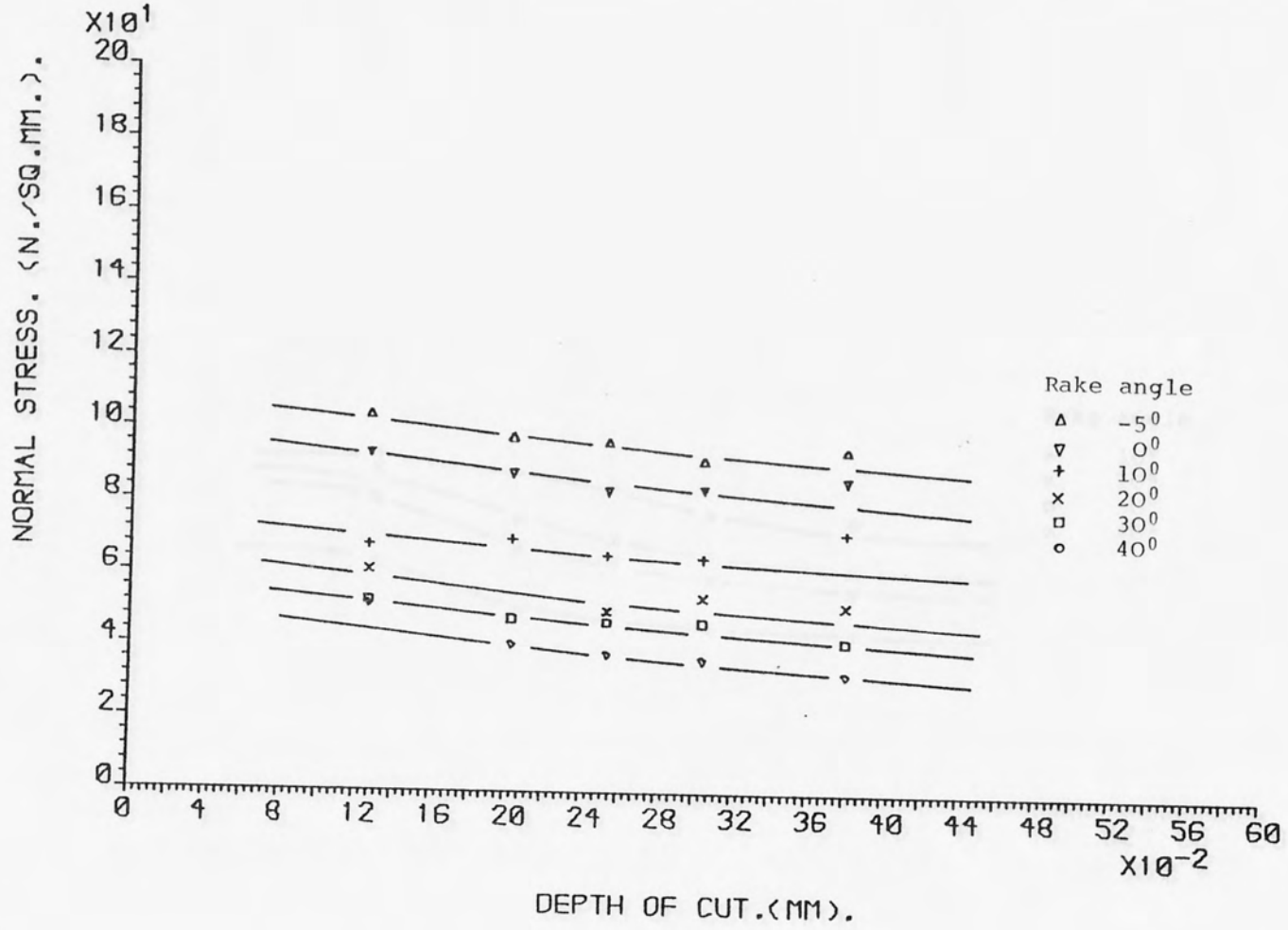

Fig. (7.90)

FIG. (7.90). σ_s as a function of depth of cut for rolled polycarbonate, cutting speed 15.24 m/min.

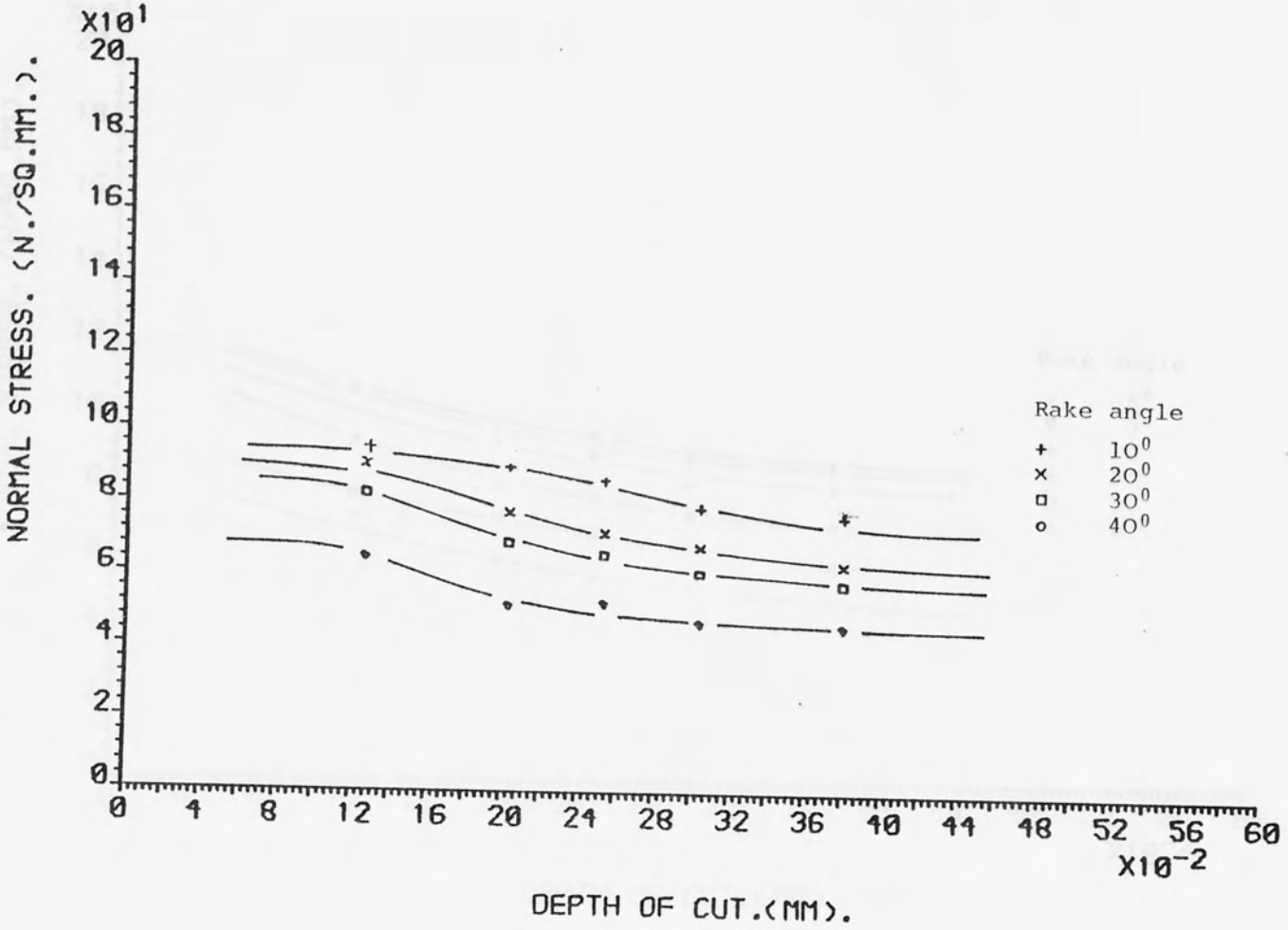

Fig. (7.91)

FIG. (7.91) σ_s as a function of depth of cut for as-received Nylon, cutting speed 15.24 m/min.

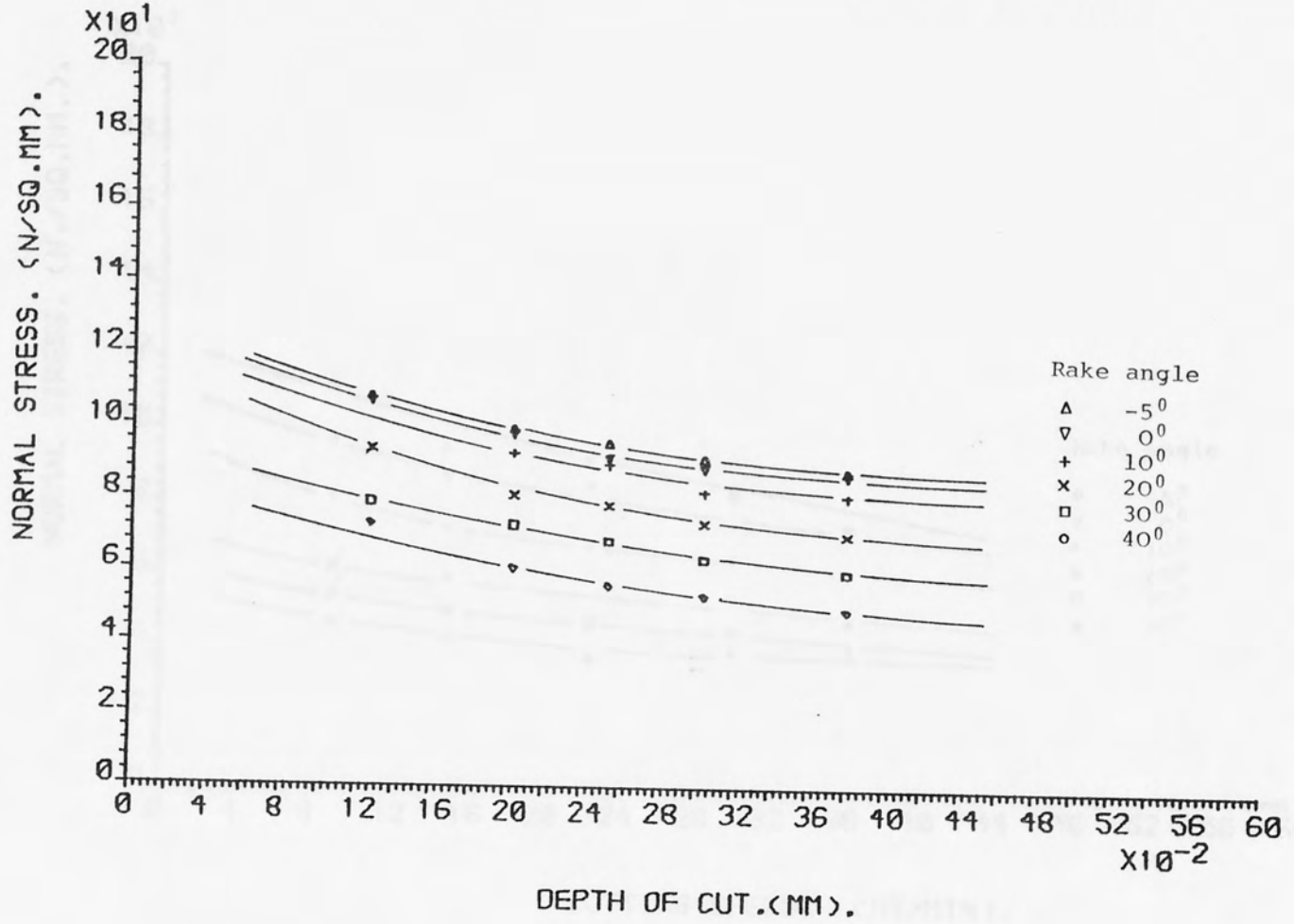

Fig. (7.92)

FIG. (7.92). σ_s as a function of depth of cut for rolled Nylon, cutting speed 15.24 m/min.

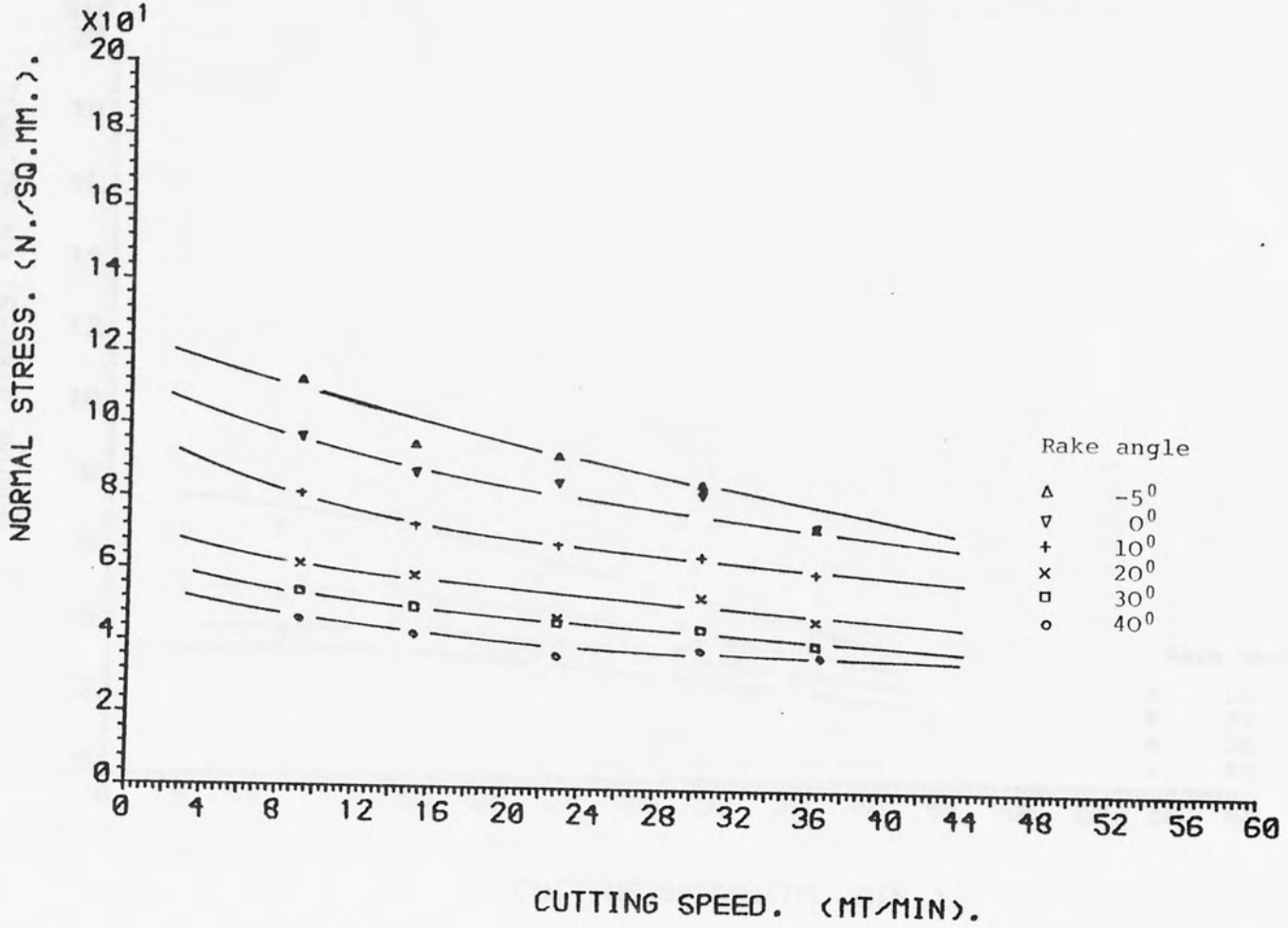

Fig. (7.93)

FIG. (7.93). σ_s as a function of cutting speed for as-received polycarbonate, depth of cut 0.381 mm.

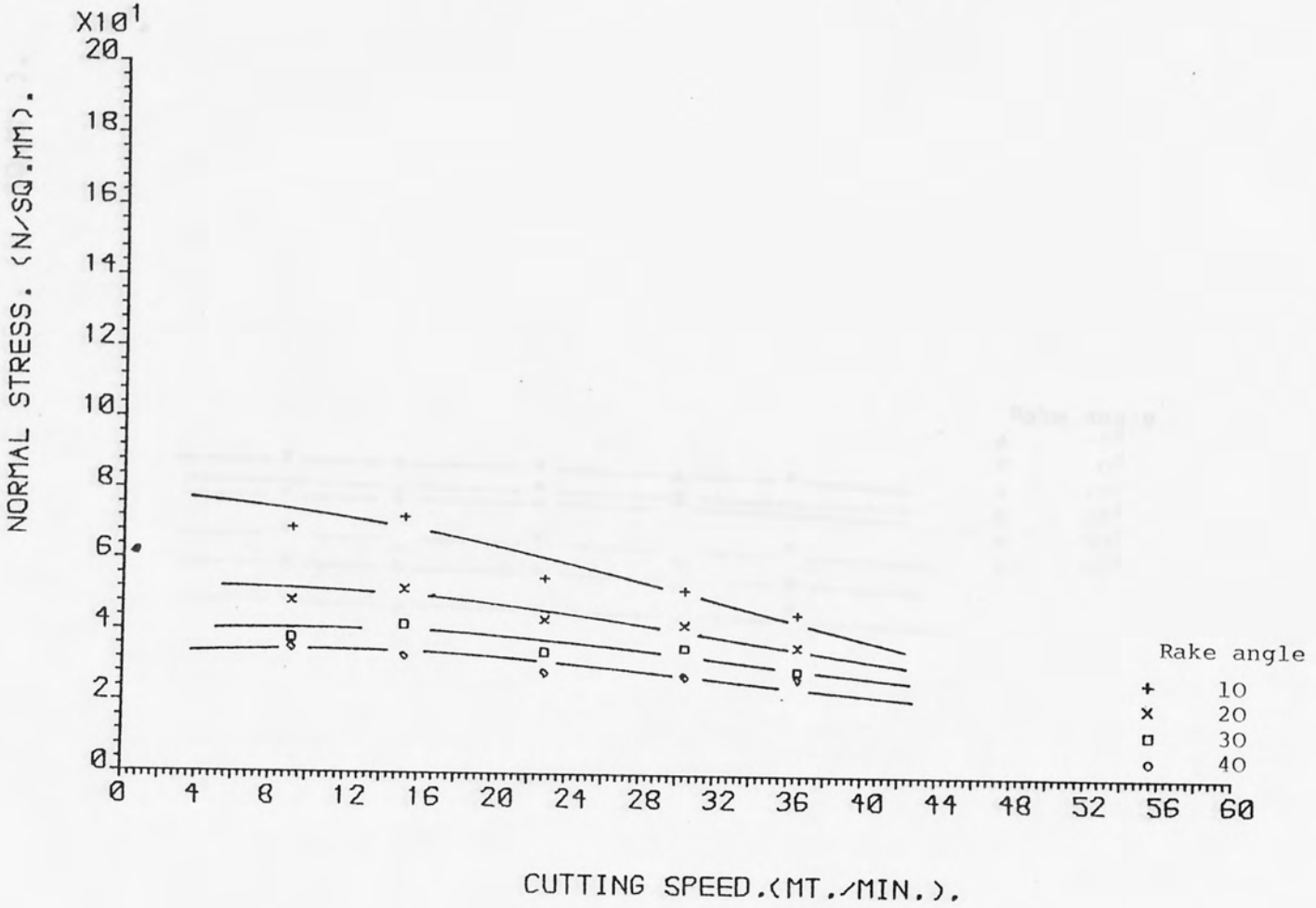

Fig. (7.94)

FIG. (7.94). σ_s as a function of cutting speed for rolled polycarbonate, depth of cut 0.381 mm.

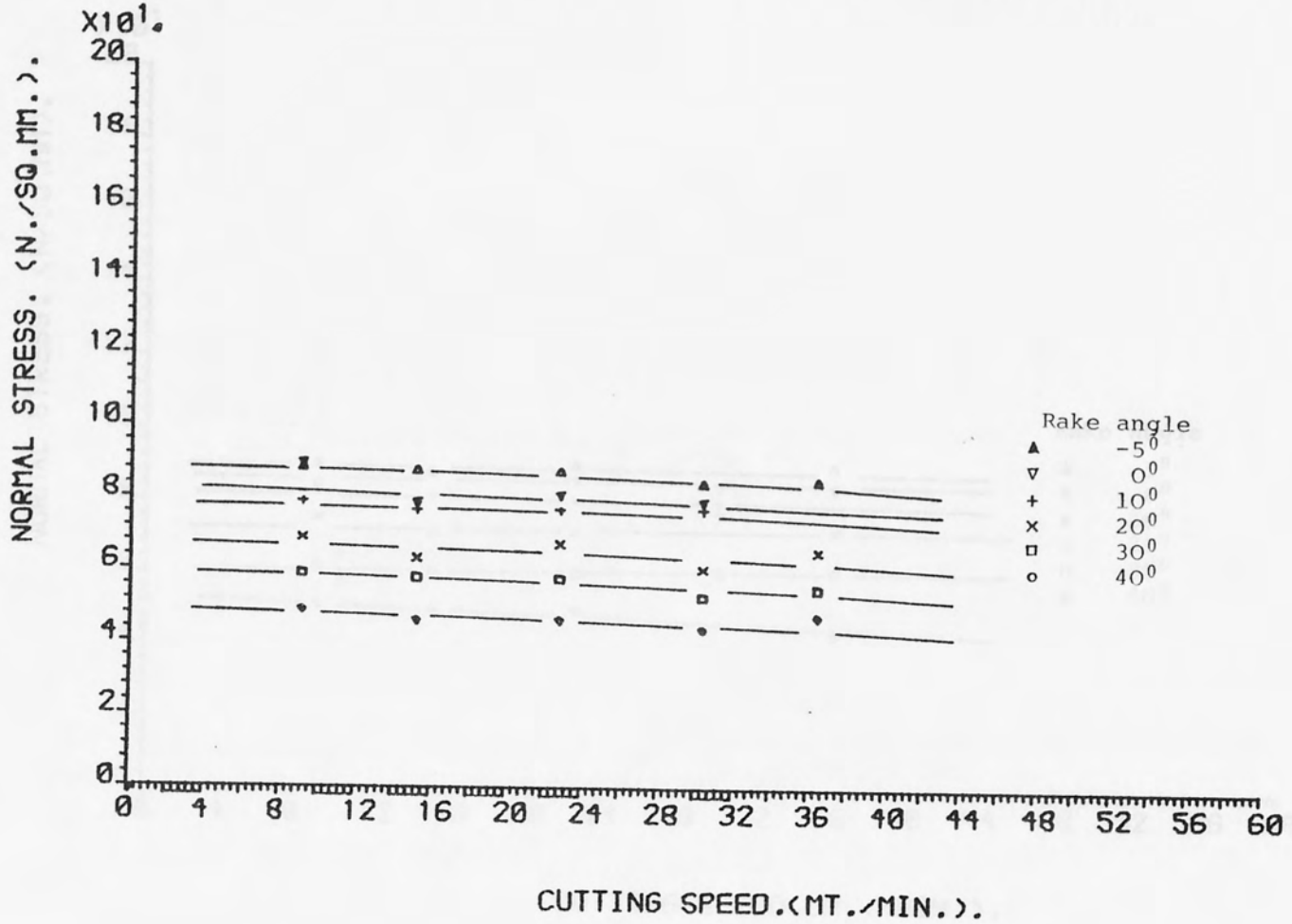

Fig. (7.95)

FIG. (7.95). σ_s as a function of cutting speed for as-received Nylon, depth of cut 0.381 mm.

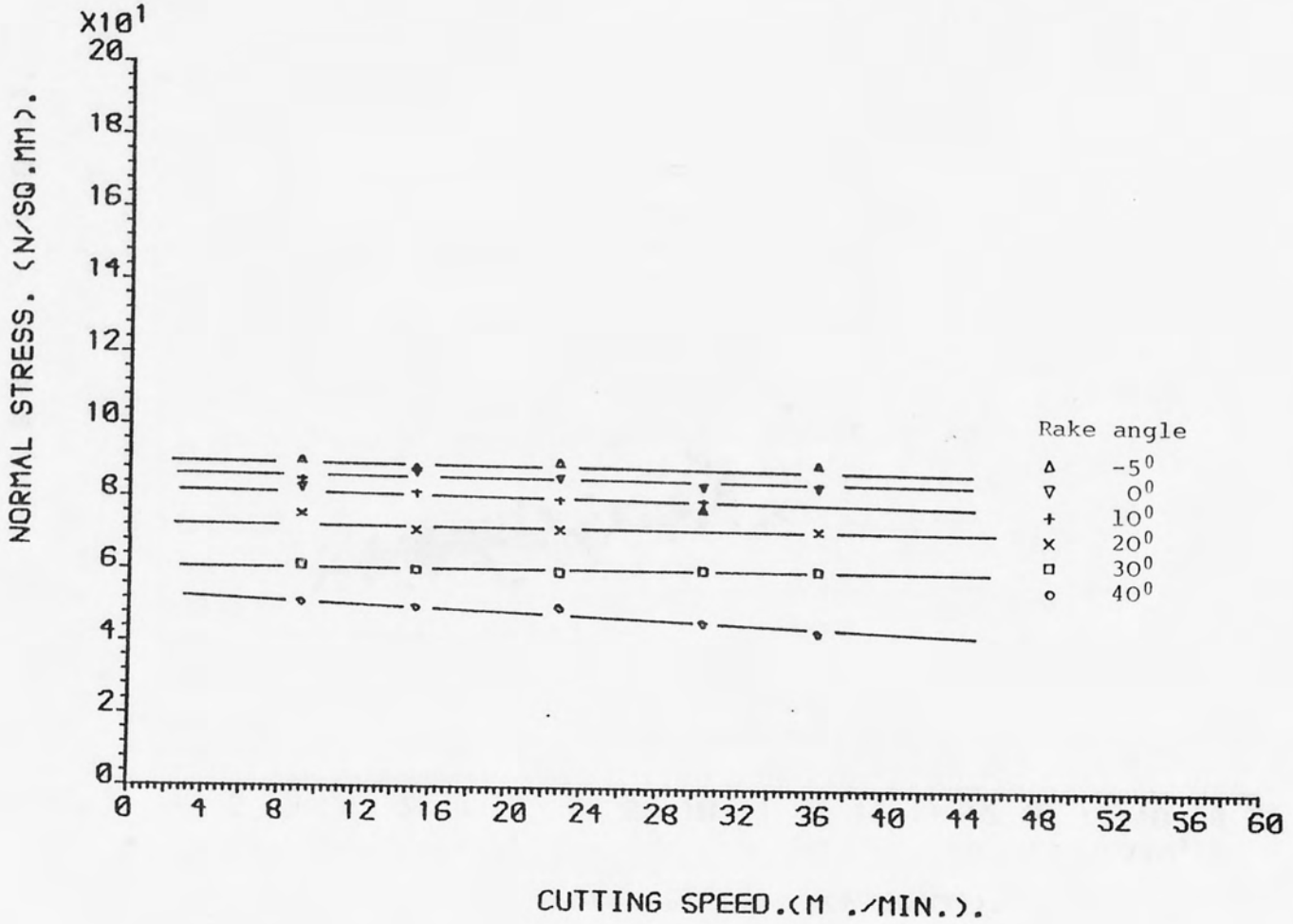

Fig. (7.96)

FIG. (7.96). σ_s as a function of the cutting speed for rolled Nylon, depth of cut 0.381 mm.

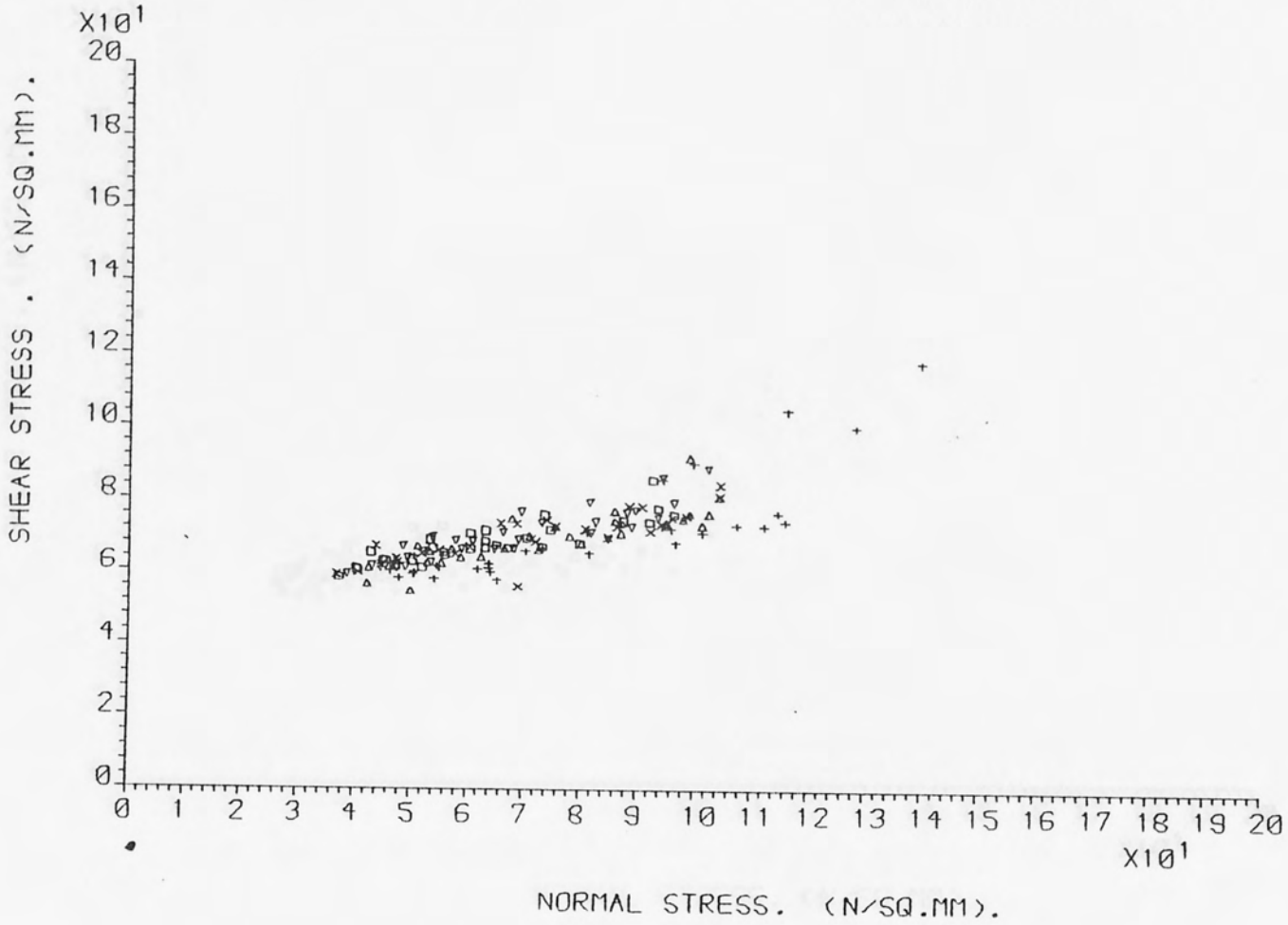

Fig. (7.97)

FIG. (7.97). σ_s and τ_s relationship for as-received polycarbonate, cutting conditions table [1]

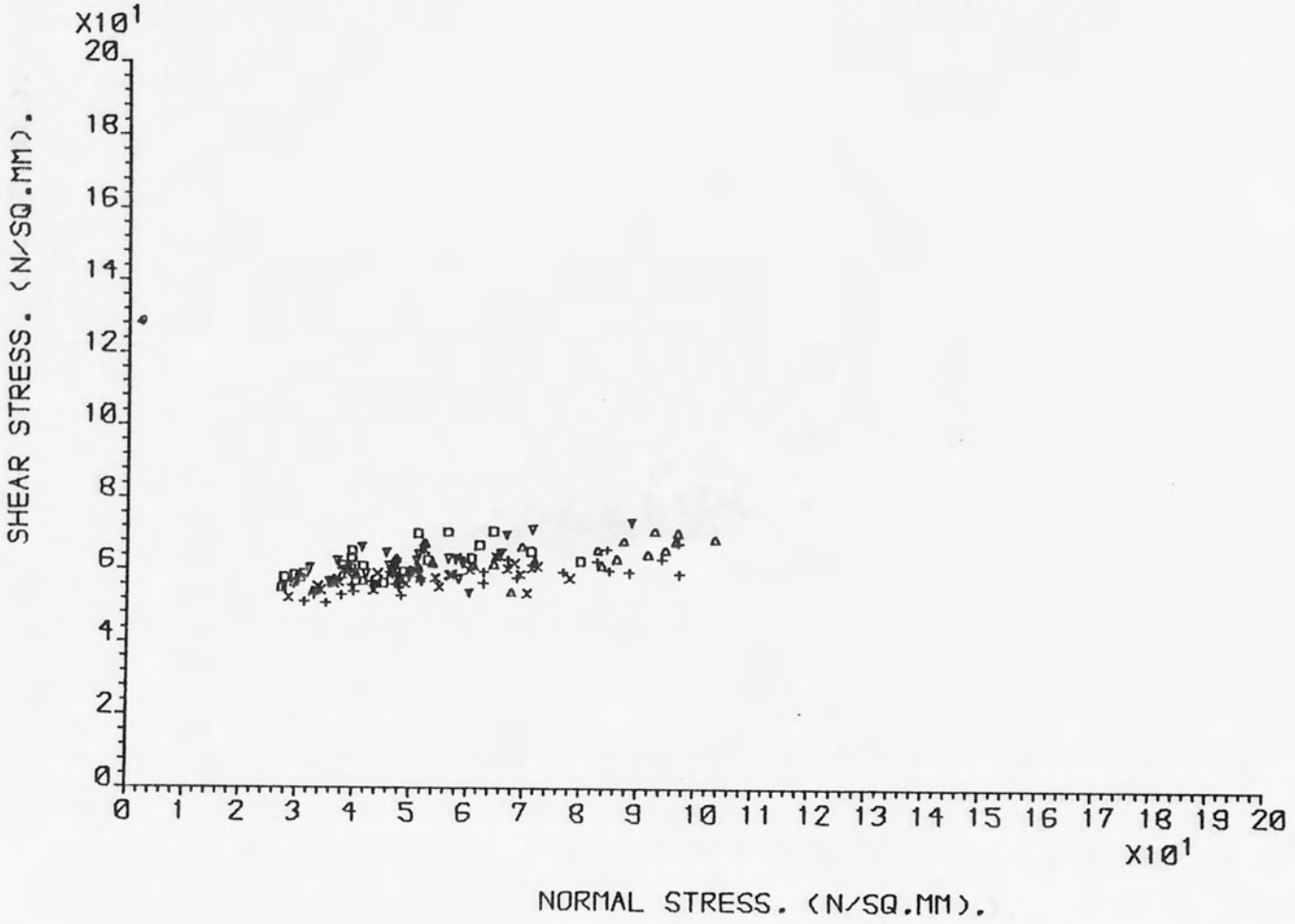

Fig. (7.98)

FIG. (7.98). σ_s and τ_s relationship for rolled polycarbonate, cutting conditions in table [2]

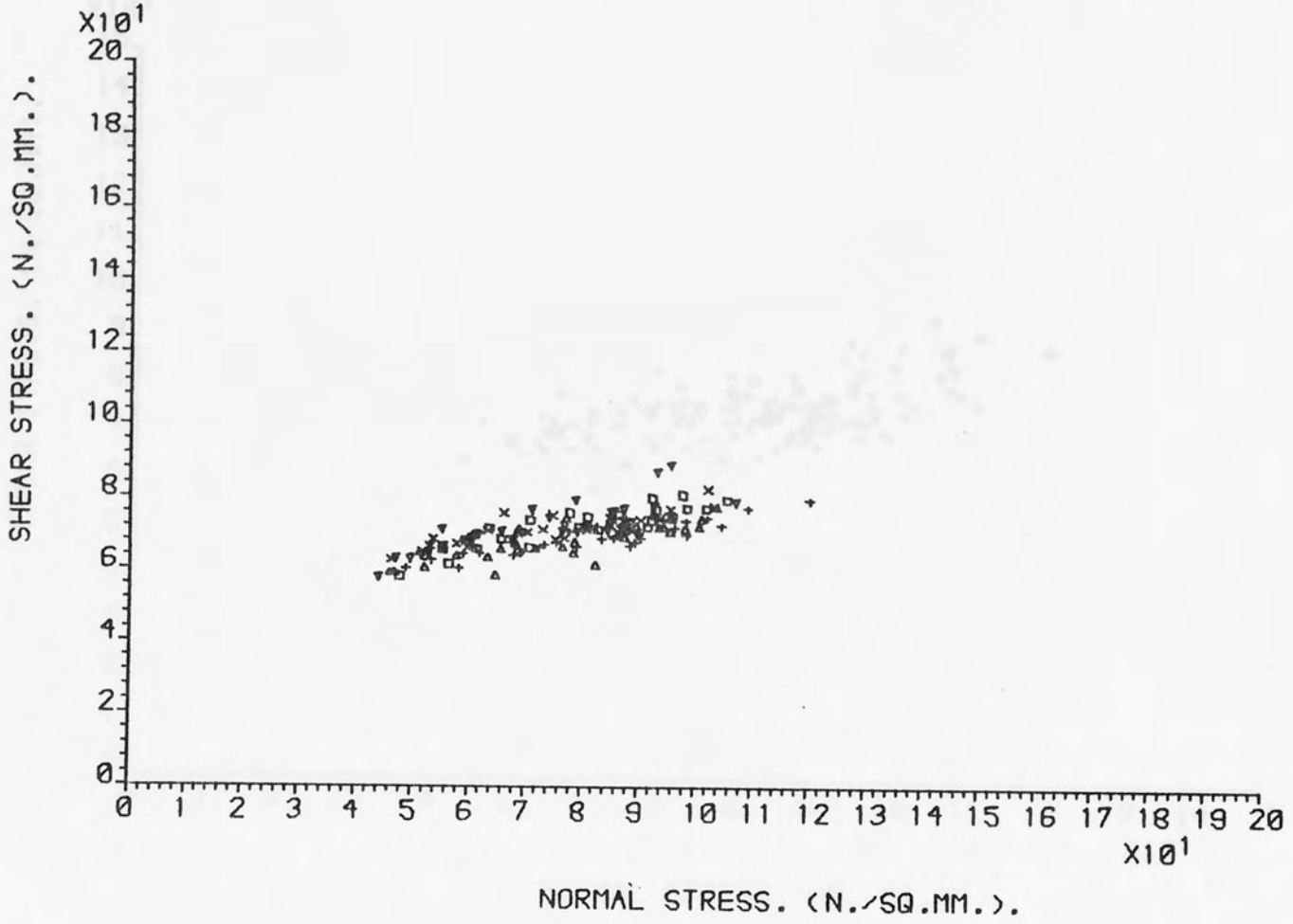

Fig. (7.99)

FIG. (7.99). σ_s and τ_s relationship for as-received Nylon, cutting conditions table [3]

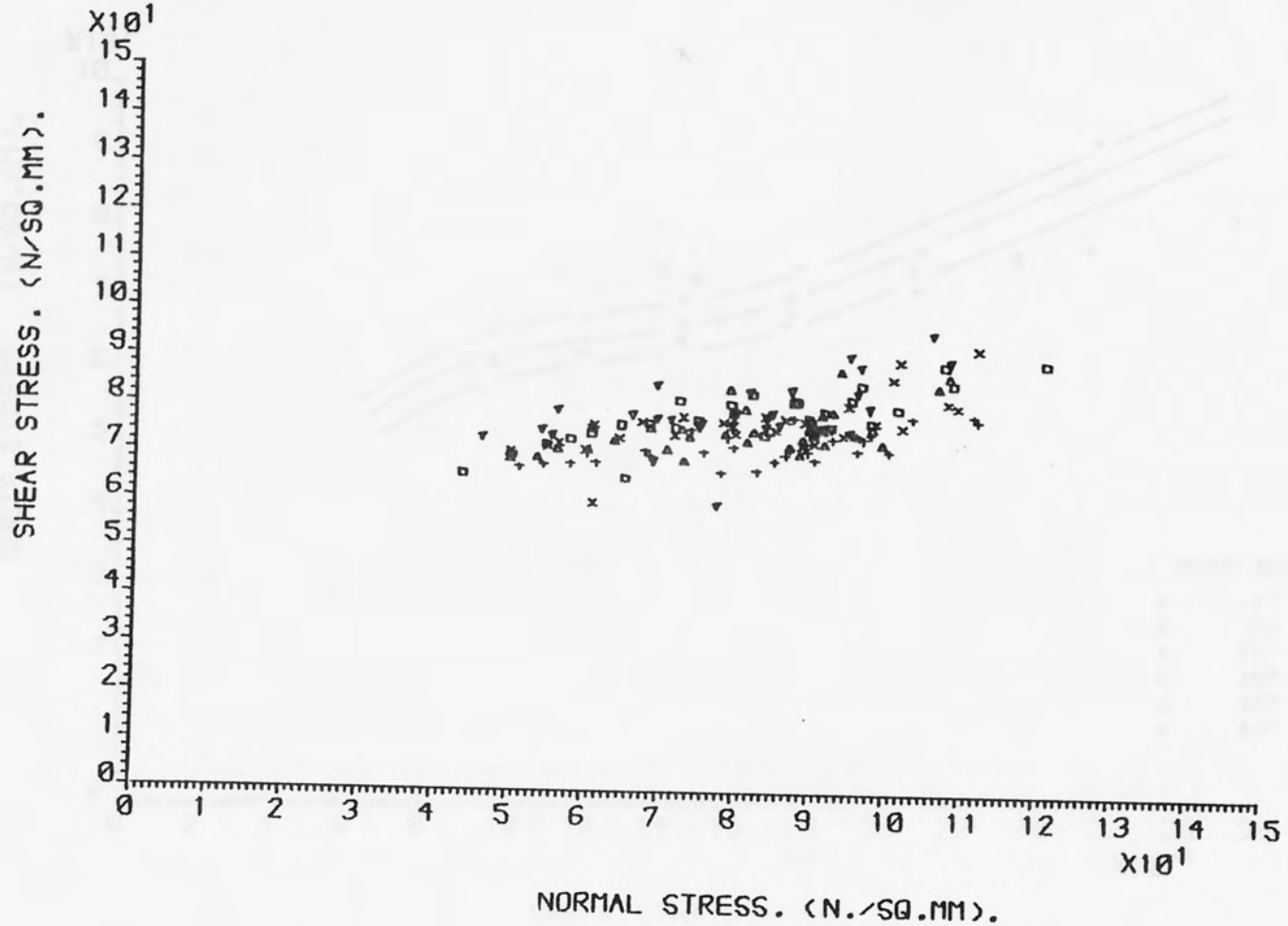

Fig. (7.100)

FIG. (7.100). σ_s and τ_s relationship for rolled Nylon, cutting conditions table [4]

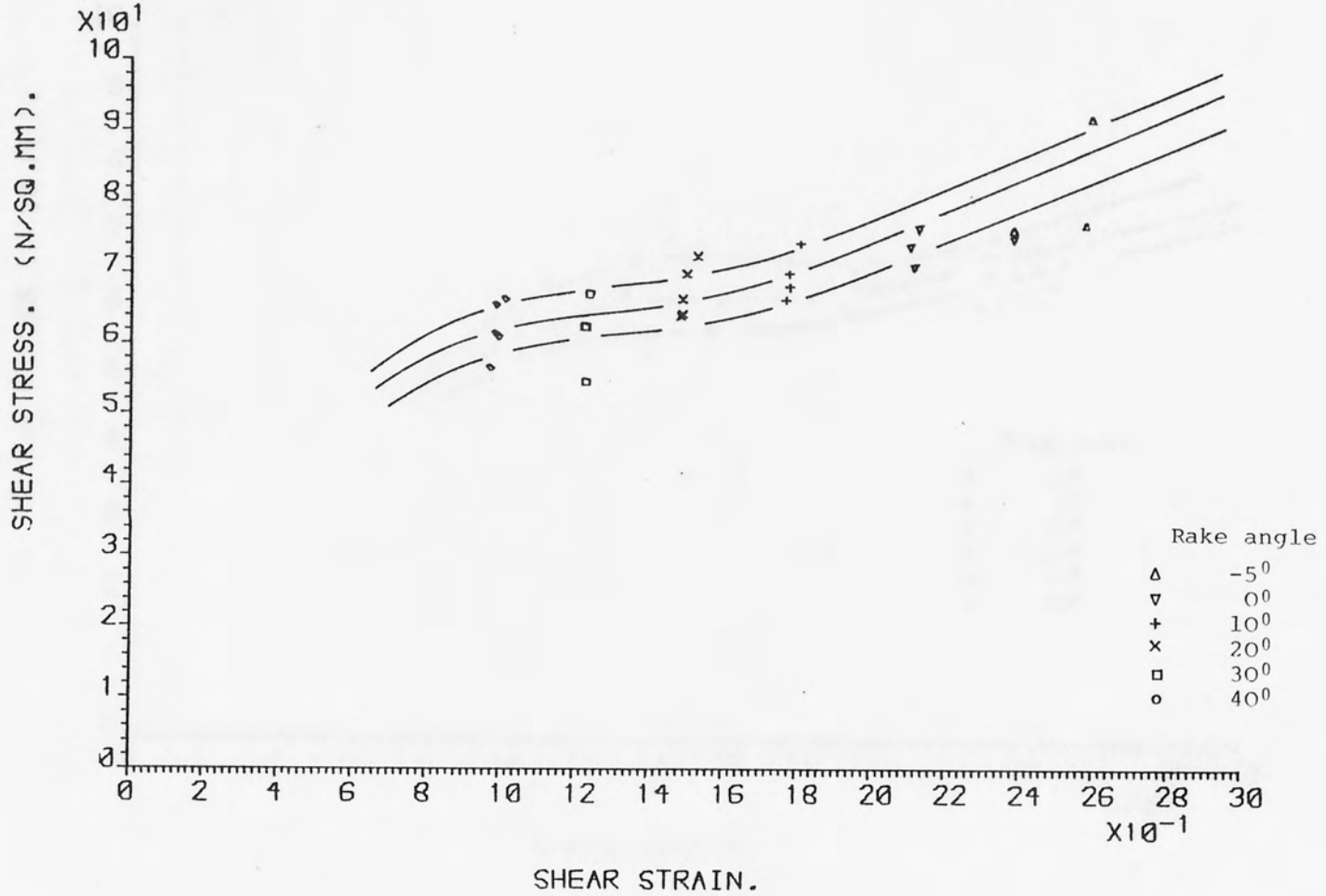

Fig.(7.101)

FIG. (7.101) τ_s and γ_s relationship for as-received polycarbonate, cutting speed 15.24 m/min.

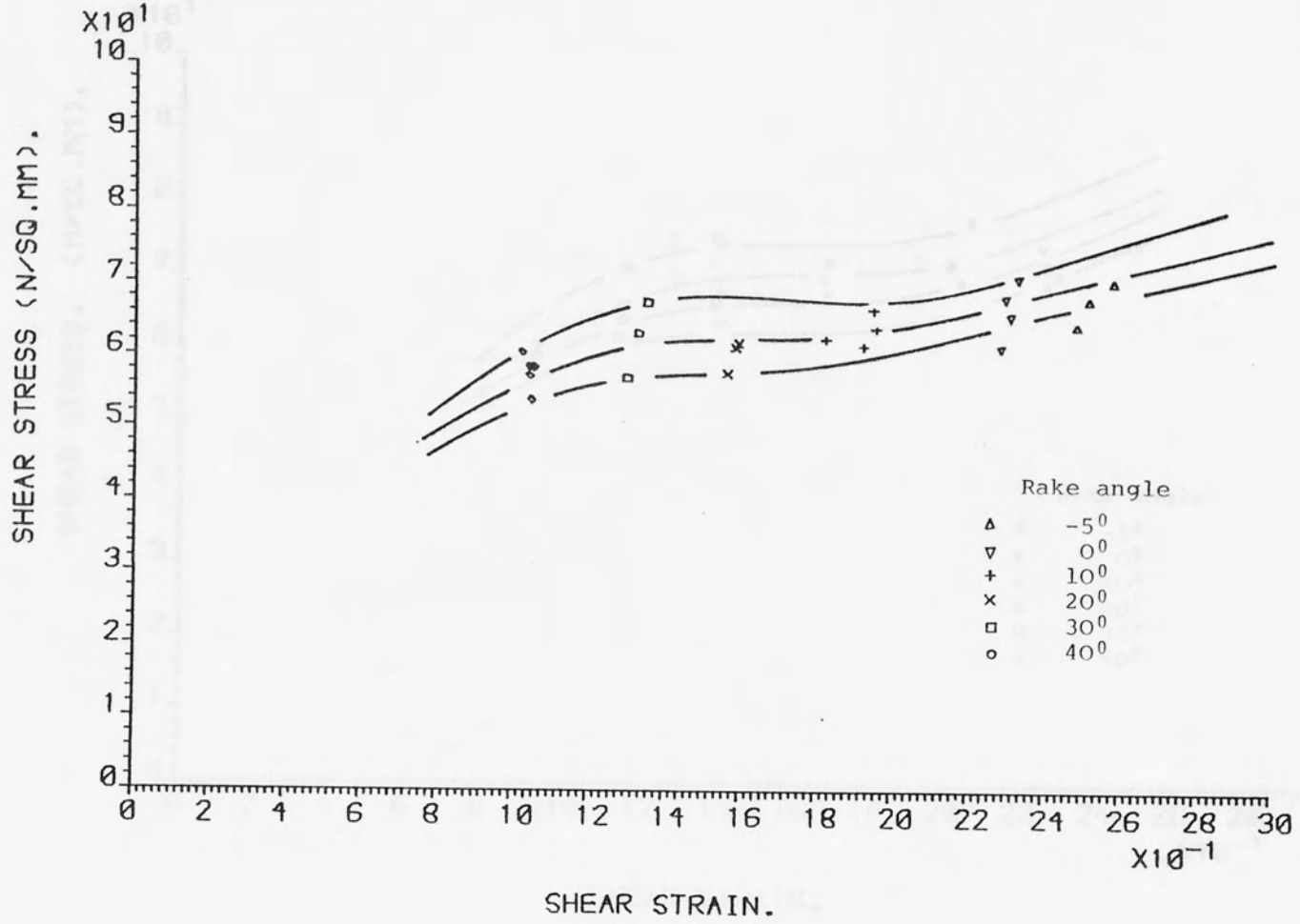

Fig. (7.102)

FIG. (7.102) τ_s and γ_s relationship for rolled polycarbonate, cutting speed 15.24 m/min.

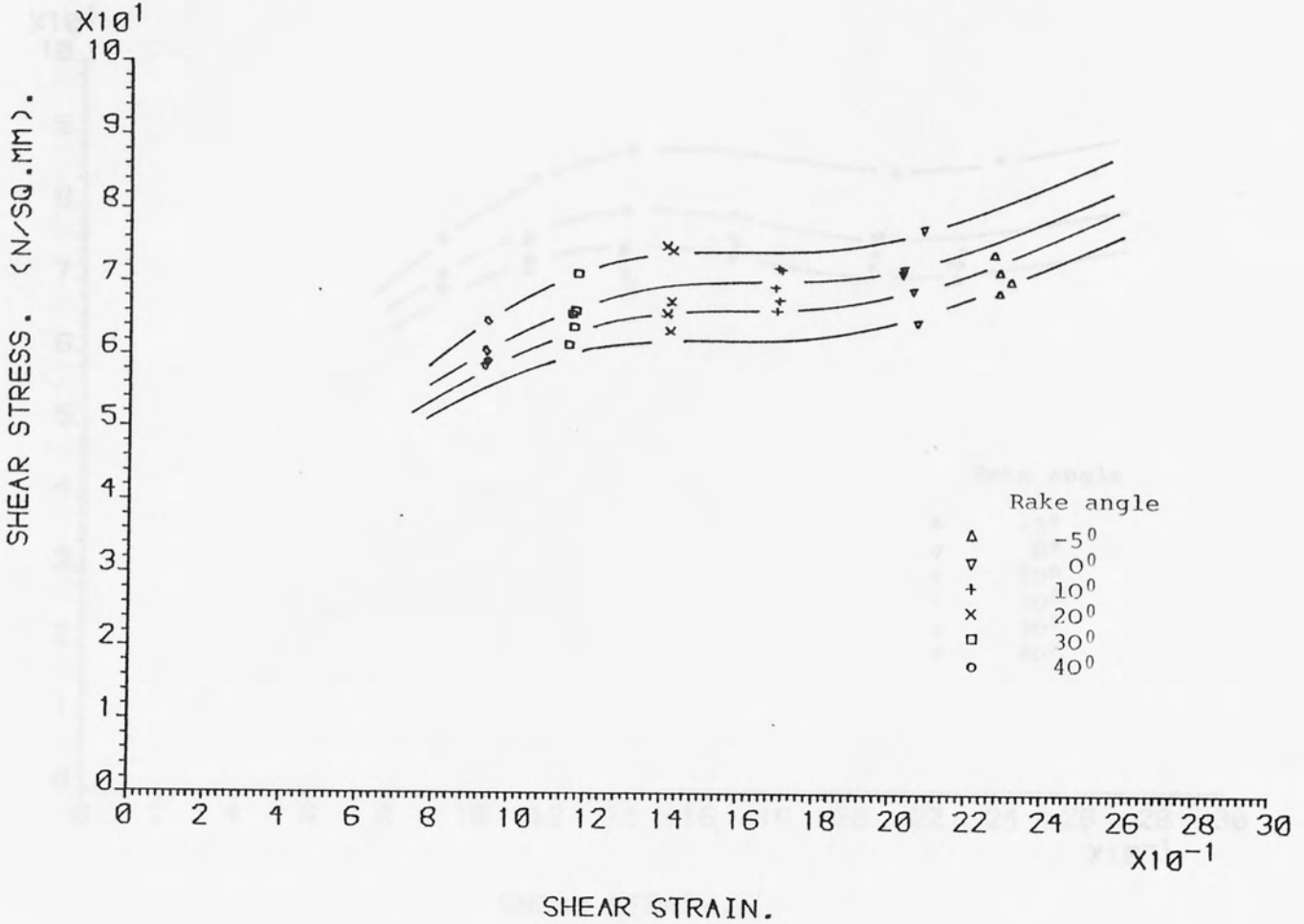

Fig. (7.103)

FIG. (7.103) τ_s and γ_s relationship for as-received Nylon, cutting speed 15.24 m/min.

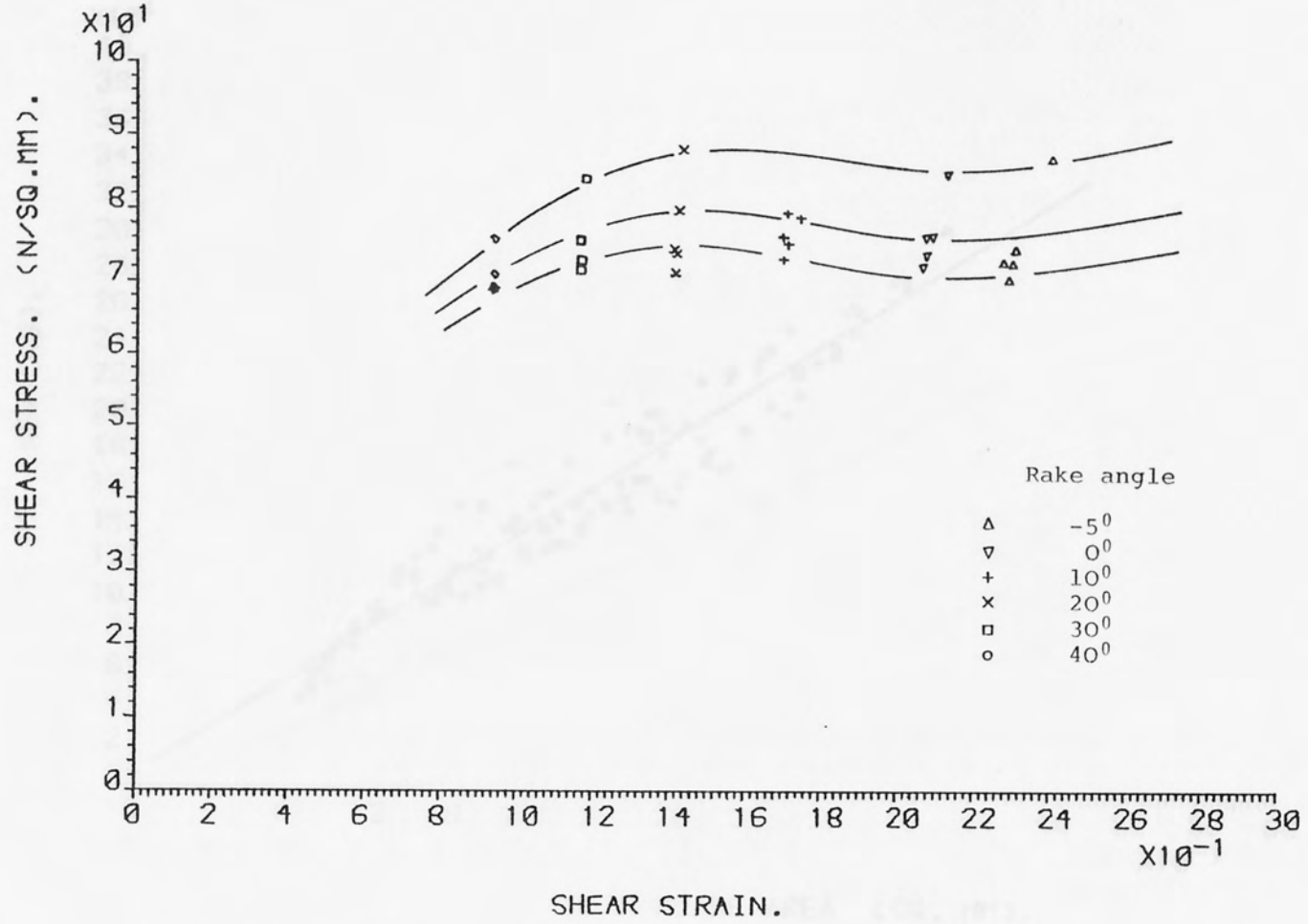

Fig. (7.104)

FIG. (7.104) τ_s and γ_s relationship for rolled Nylon cutting speed 15.24 m/min.

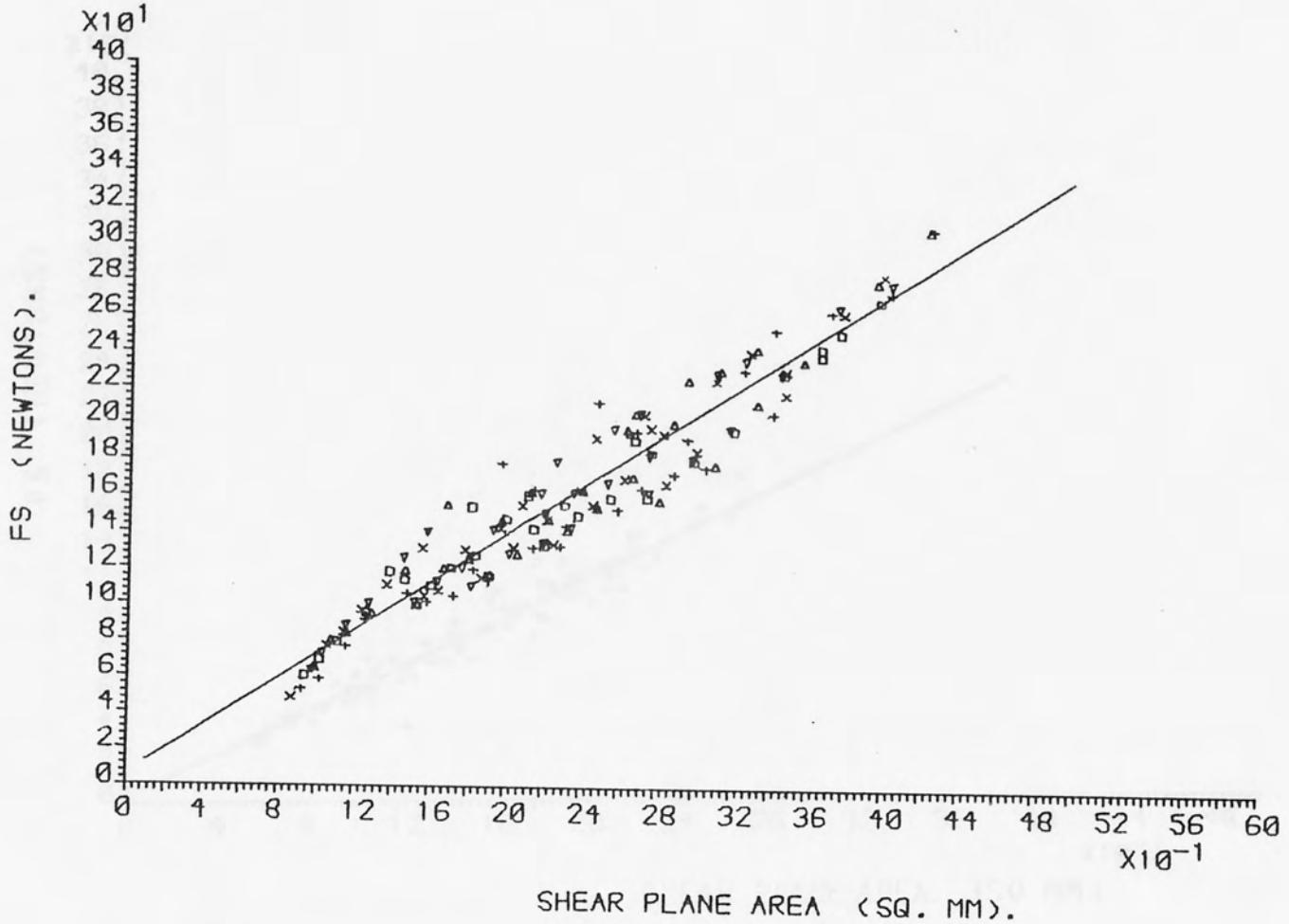

Fig. (7.105)

FIG. (7.105) A_s and F_s relationship for as-received polycarbonate, cutting conditions in table [1]

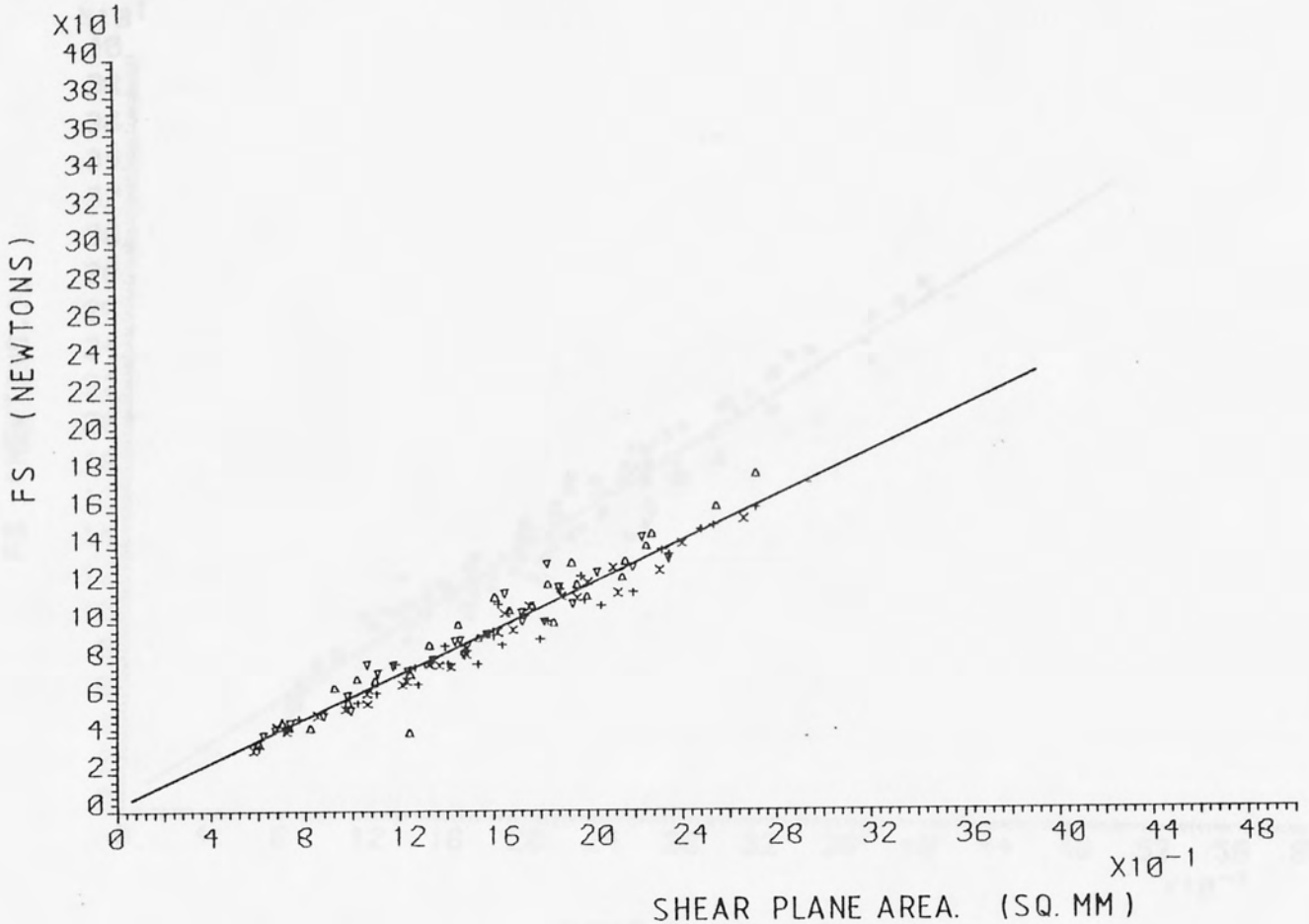

Fig. (7.106)

FIG. (7.106). A_s and F_s relationship for rolled polycarbonate, cutting conditions in table [2]

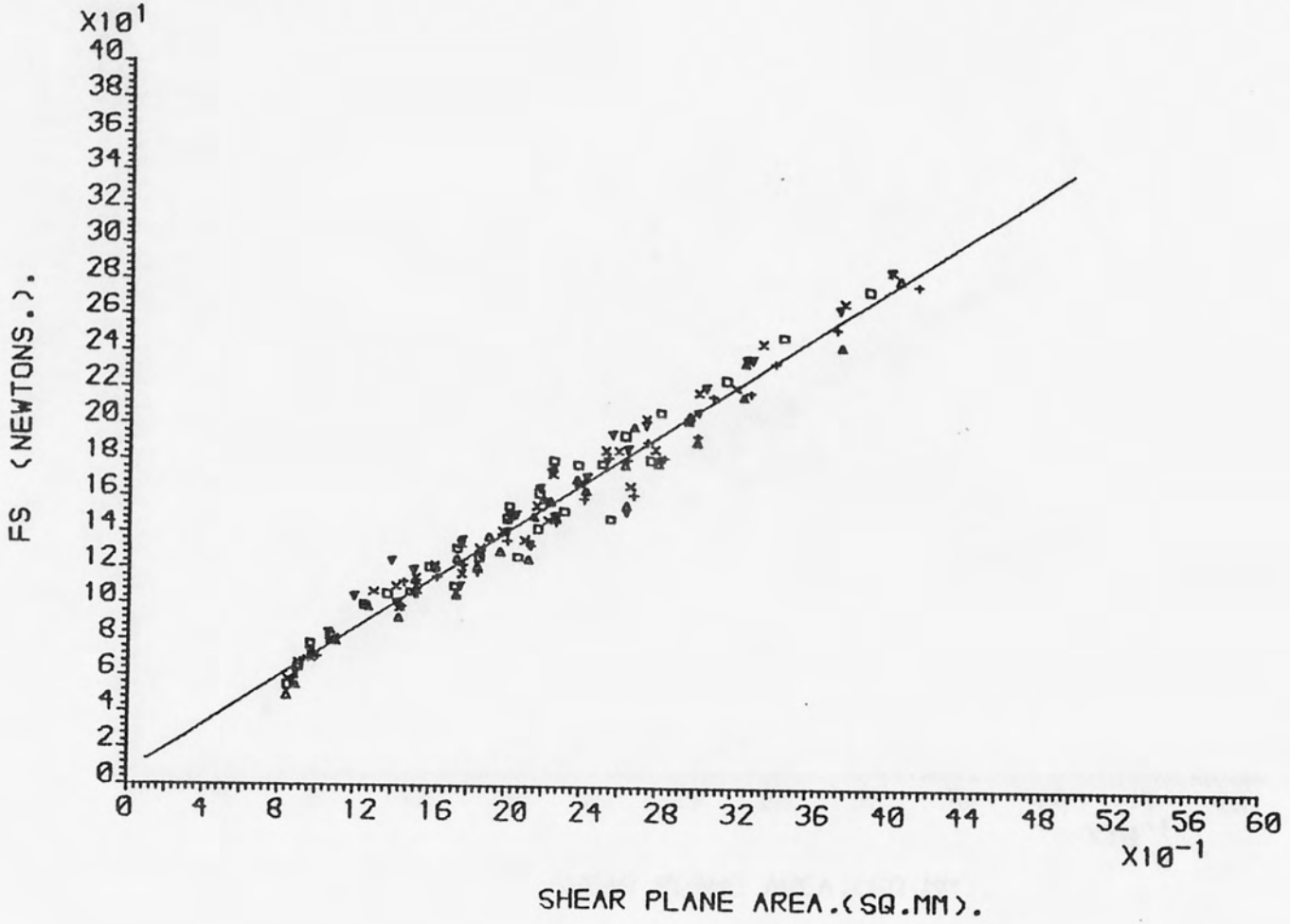

Fig. (7.107)

FIG. (7.107). A_s and F_s relationship for as-received Nylon, cutting conditions in table [3]

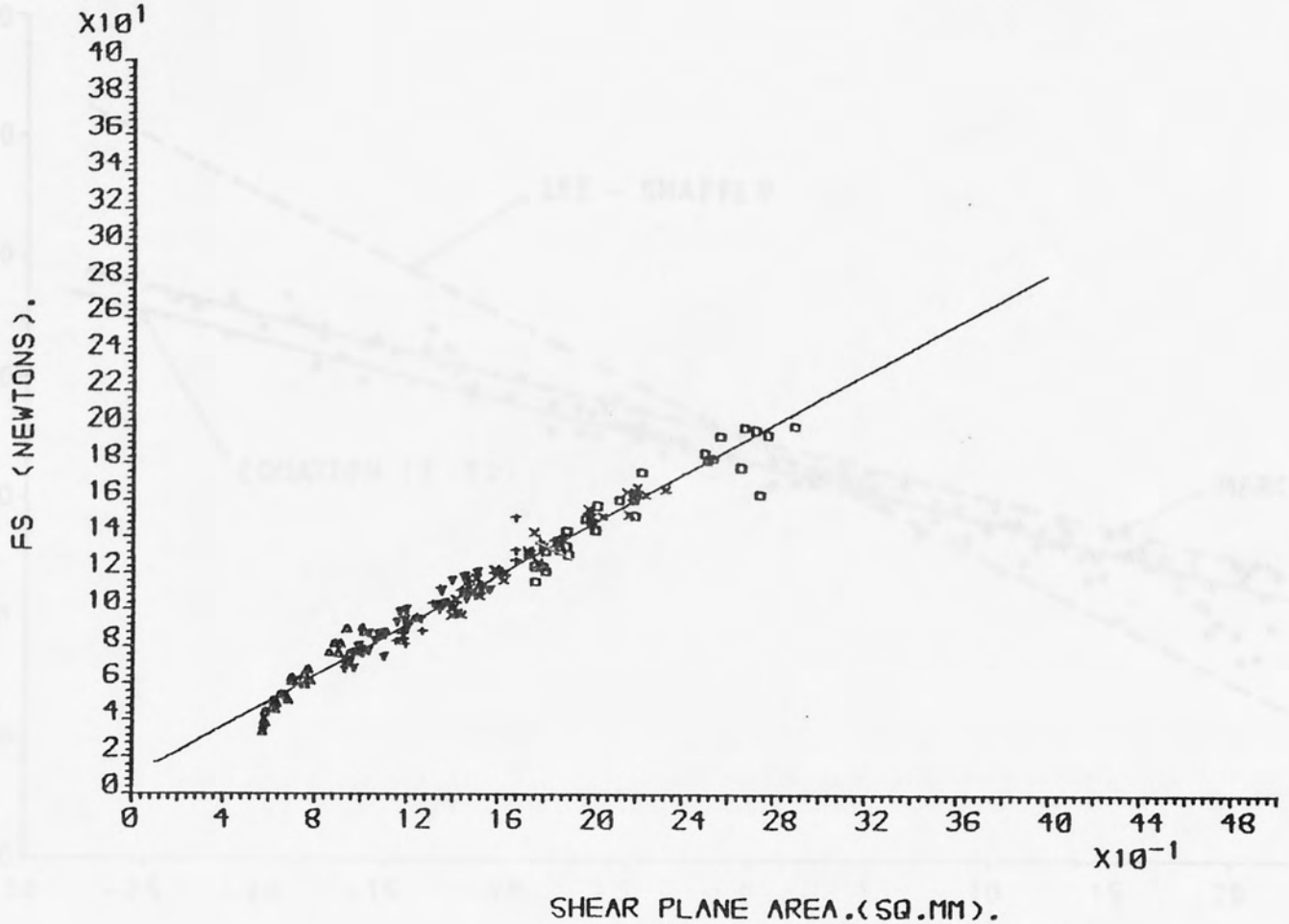

Fig. (7.108)

FIG. (7.10[8]). F_s and A_s relationship for rolled Nylon, cutting conditions in table [4]

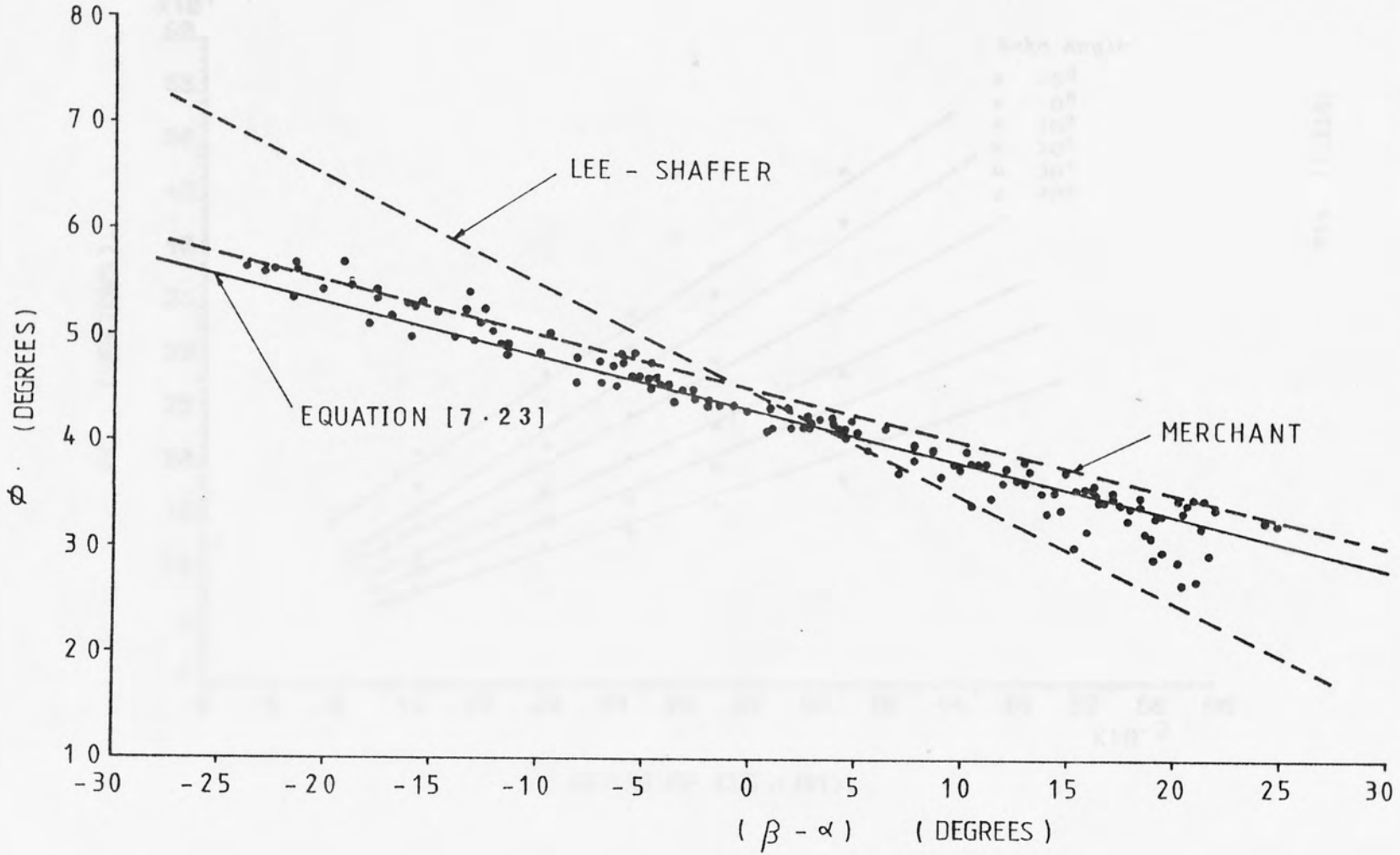

Fig. (7.109)

FIG. (7.109) ϕ and (β - α) relationship for as-received polycarbonate, cutting conditions table (1), solid line represents equation [7.23]

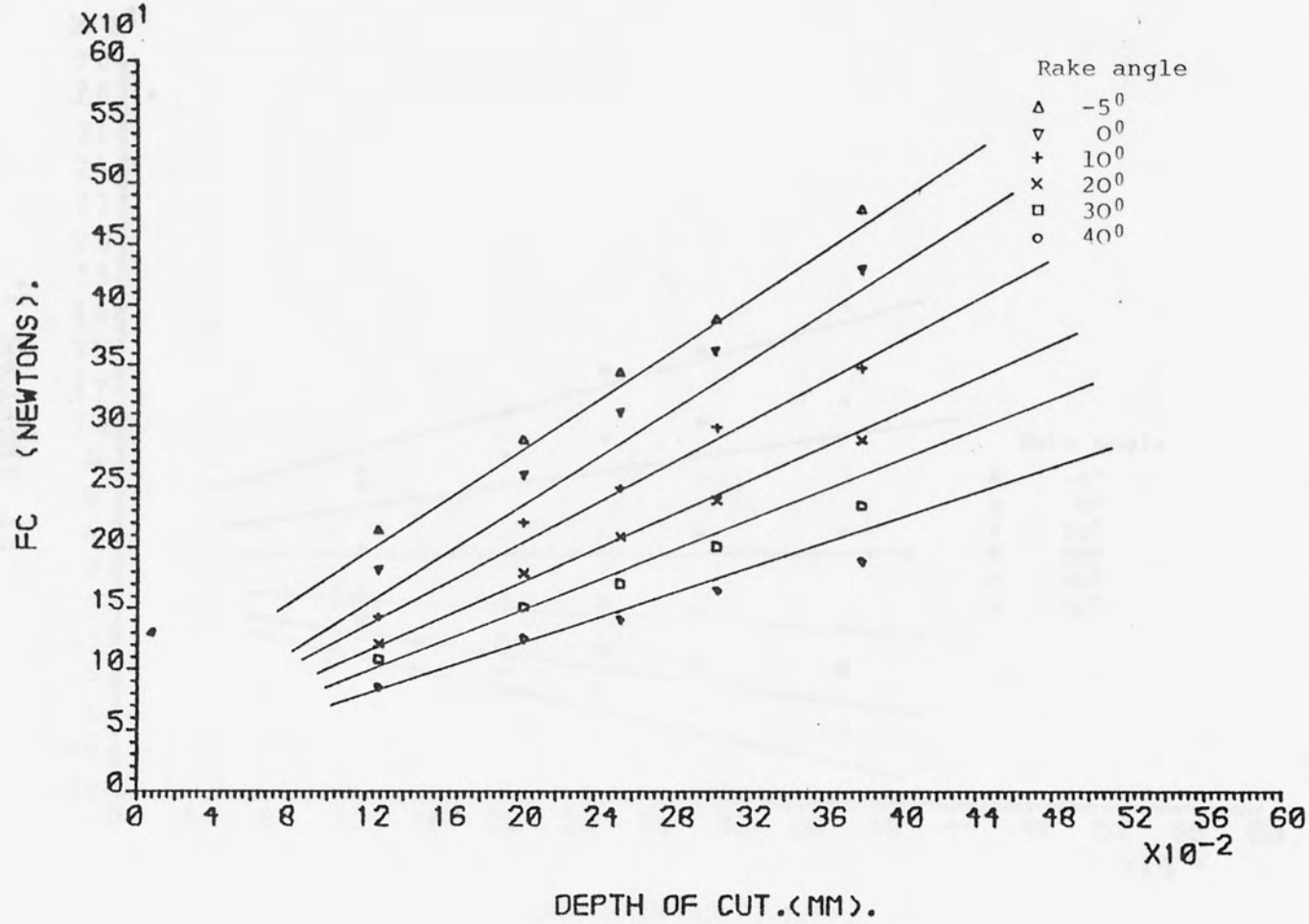

Fig. (7.110)

FIG. (7.110) F_c as a function of depth of cut for as-received polycarbonate, cutting speed 15.24 m/min. solid lines represent the predicted values of F_c

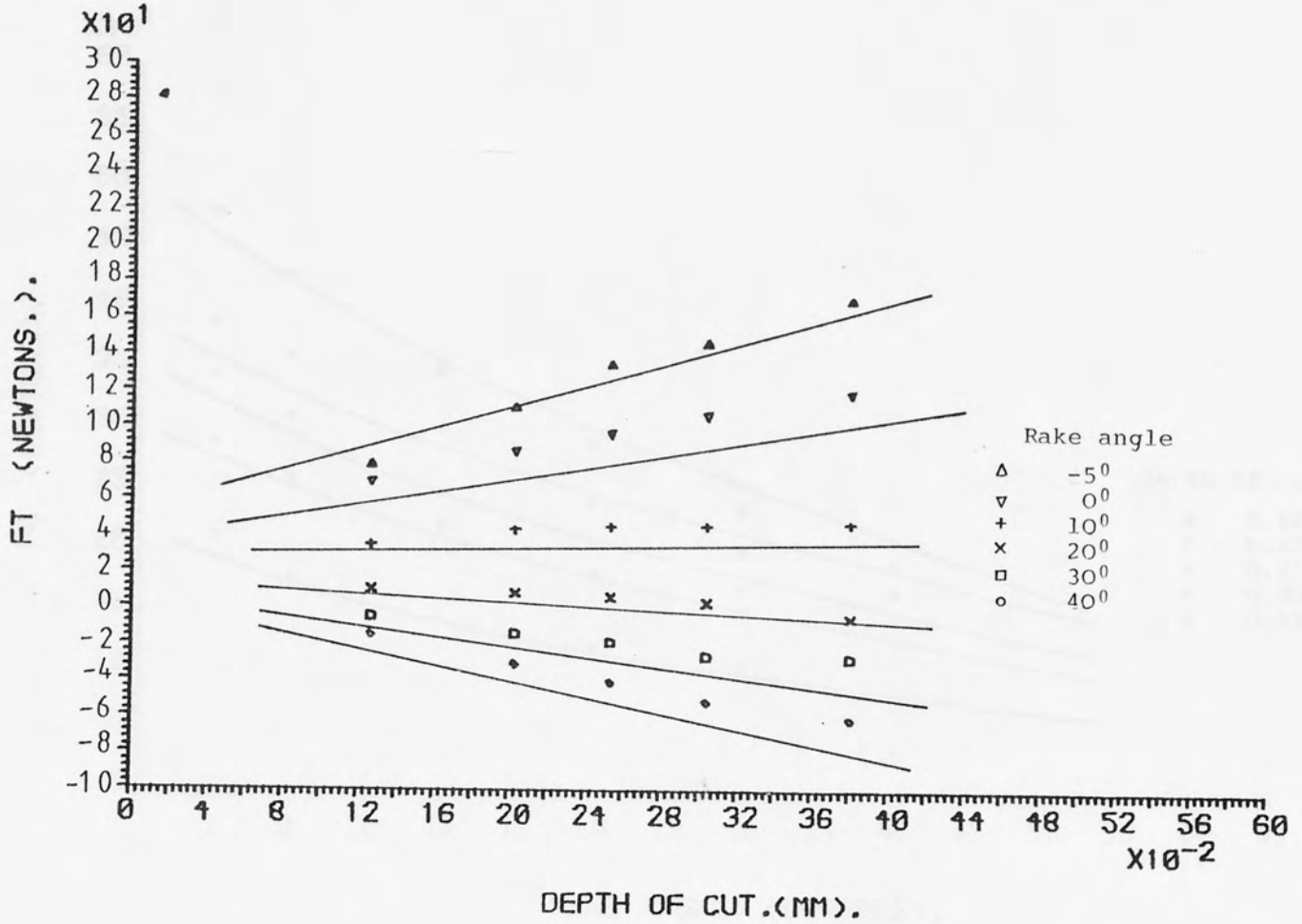

Fig. (7.111)

FIG. (7.111) F_t as a function of depth of cut for as-received polycarbonate, cutting speed 15.24 m/min. solid lines represent the predicted values of F_t

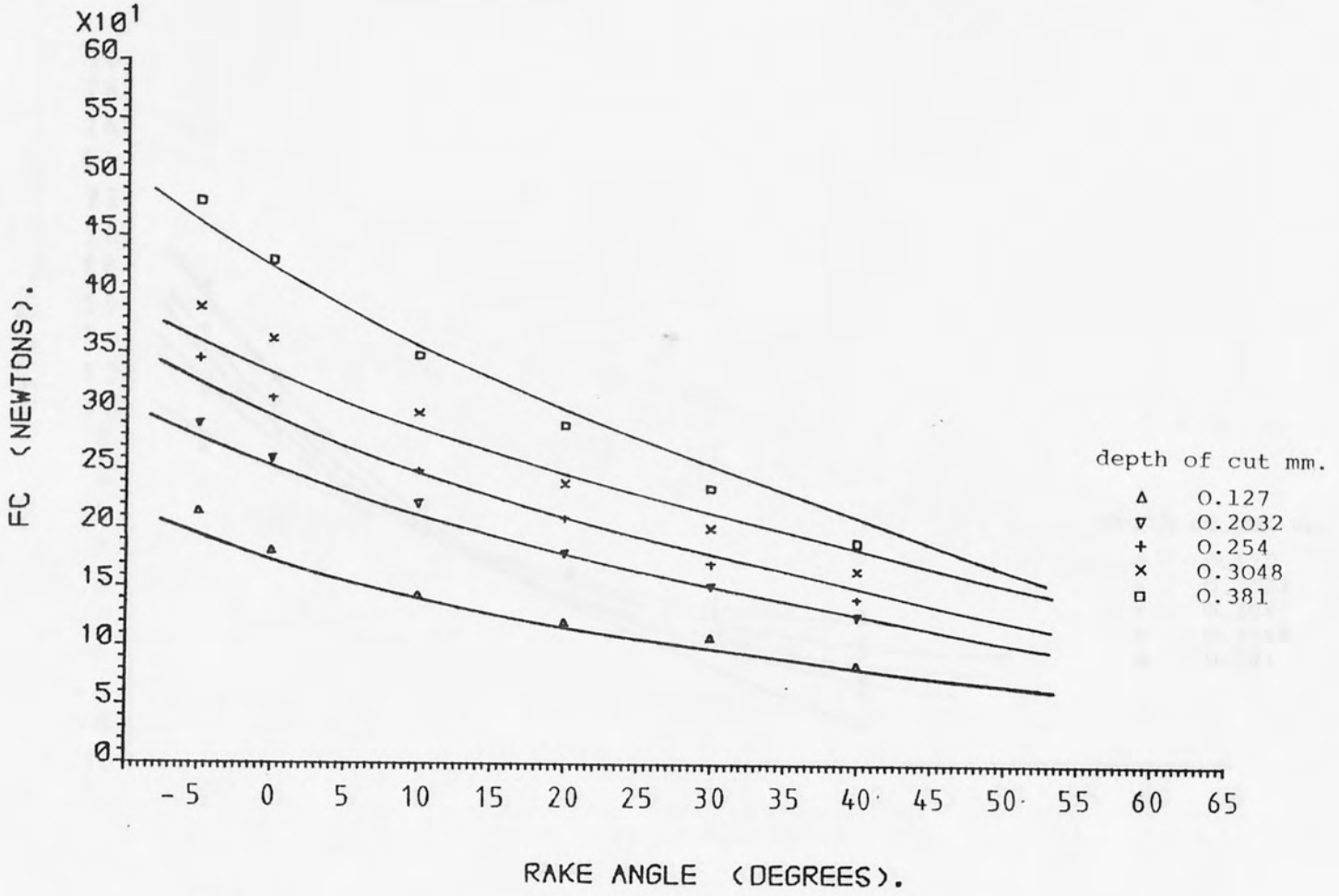

Fig. (7.112)

FIG. (7.112) F_c as a function of rake angle for as-received polycarbonate, cutting speed 15.24 m/min. solid lines represent the predicted values of F_c

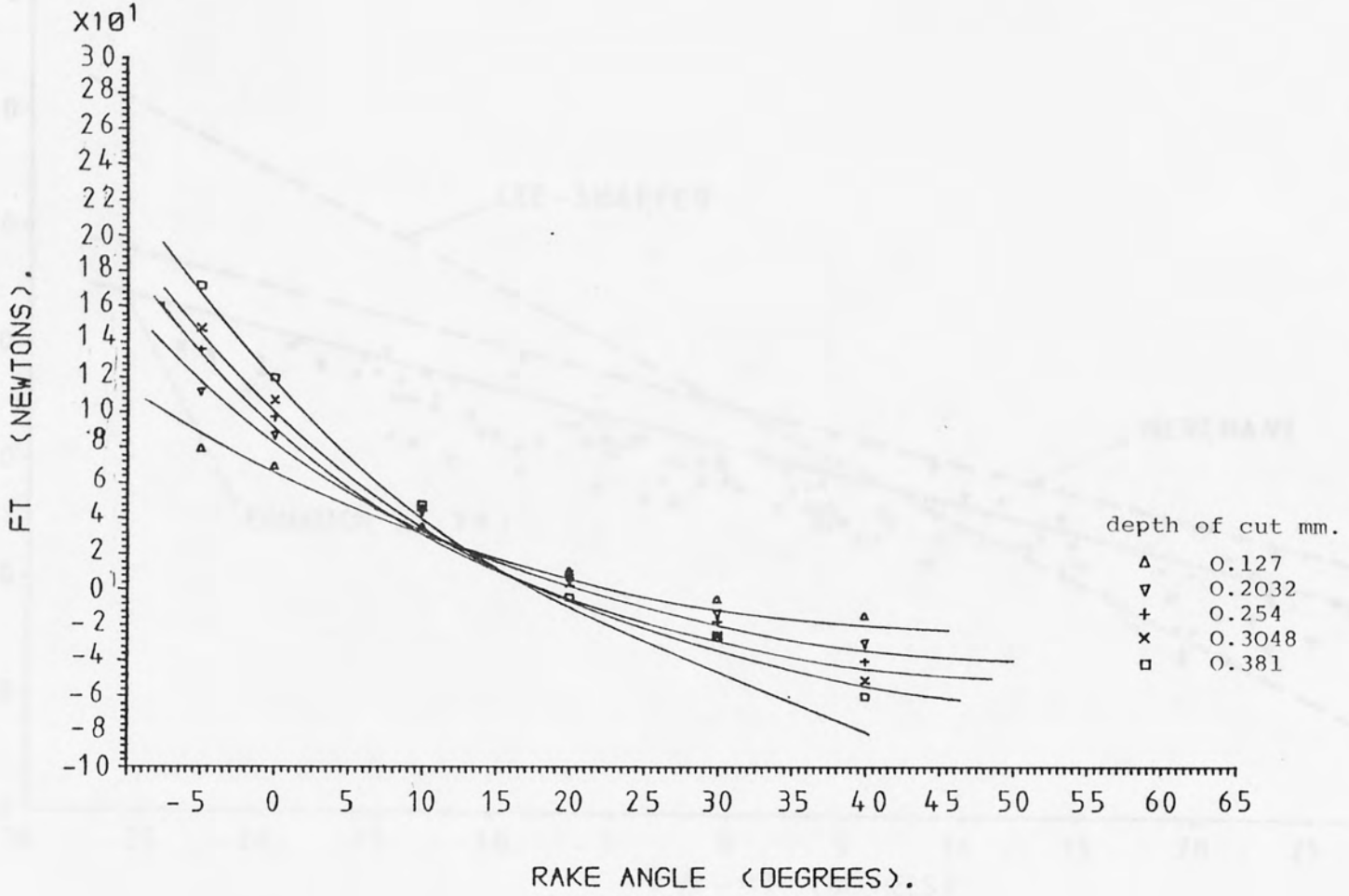

Fig. (7.113)

FIG. (7.113) F_t as a function of rake angle for as-received polycarbonate, cutting speed 15.24 m/min. solid lines represent the predicted values of F_t

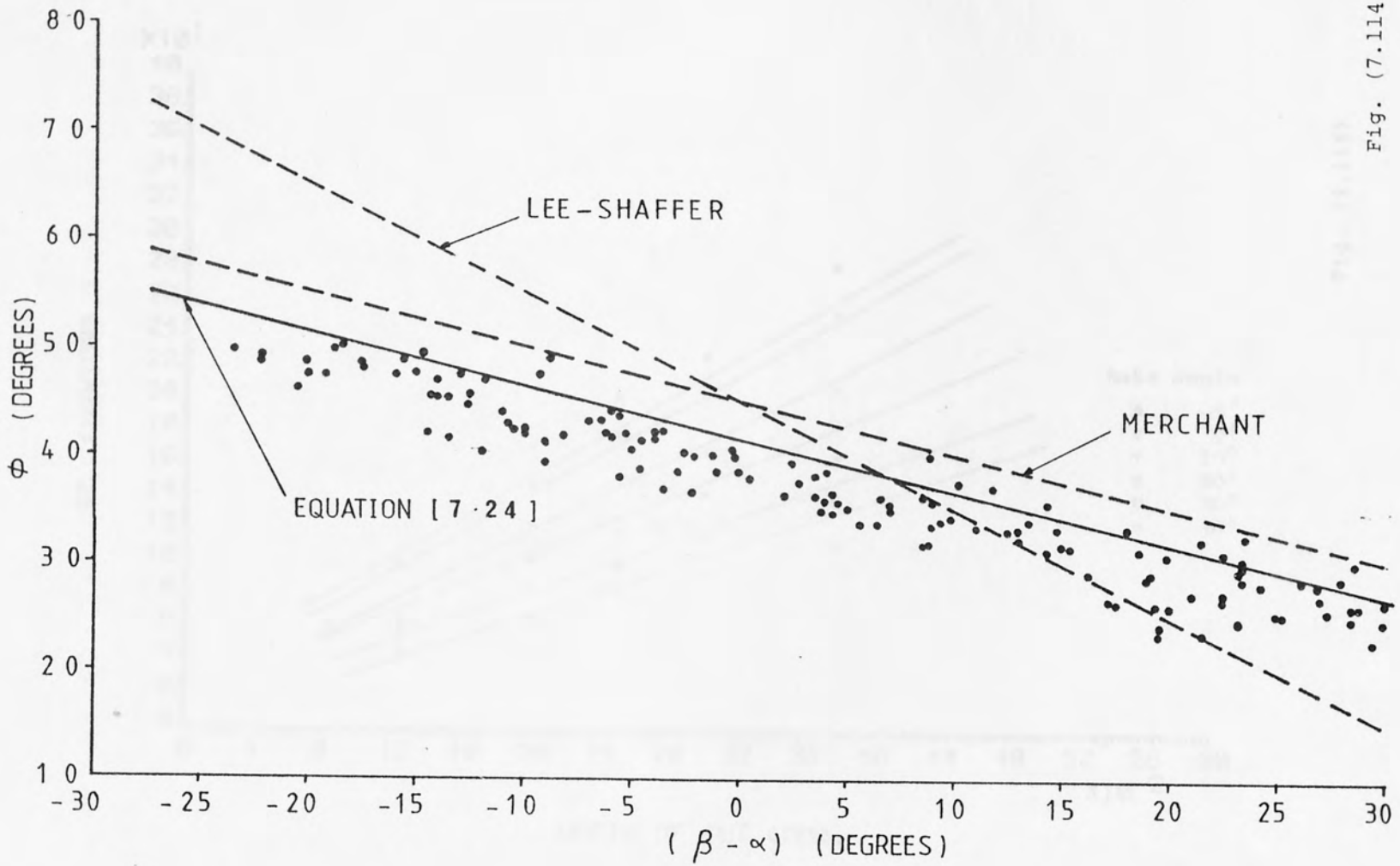

Fig. (7.114)

Fig. (7.114) ϕ and (β - α) relationship for rolled polycarbonate, cutting conditions table (2), solid line represents equation [7.24]

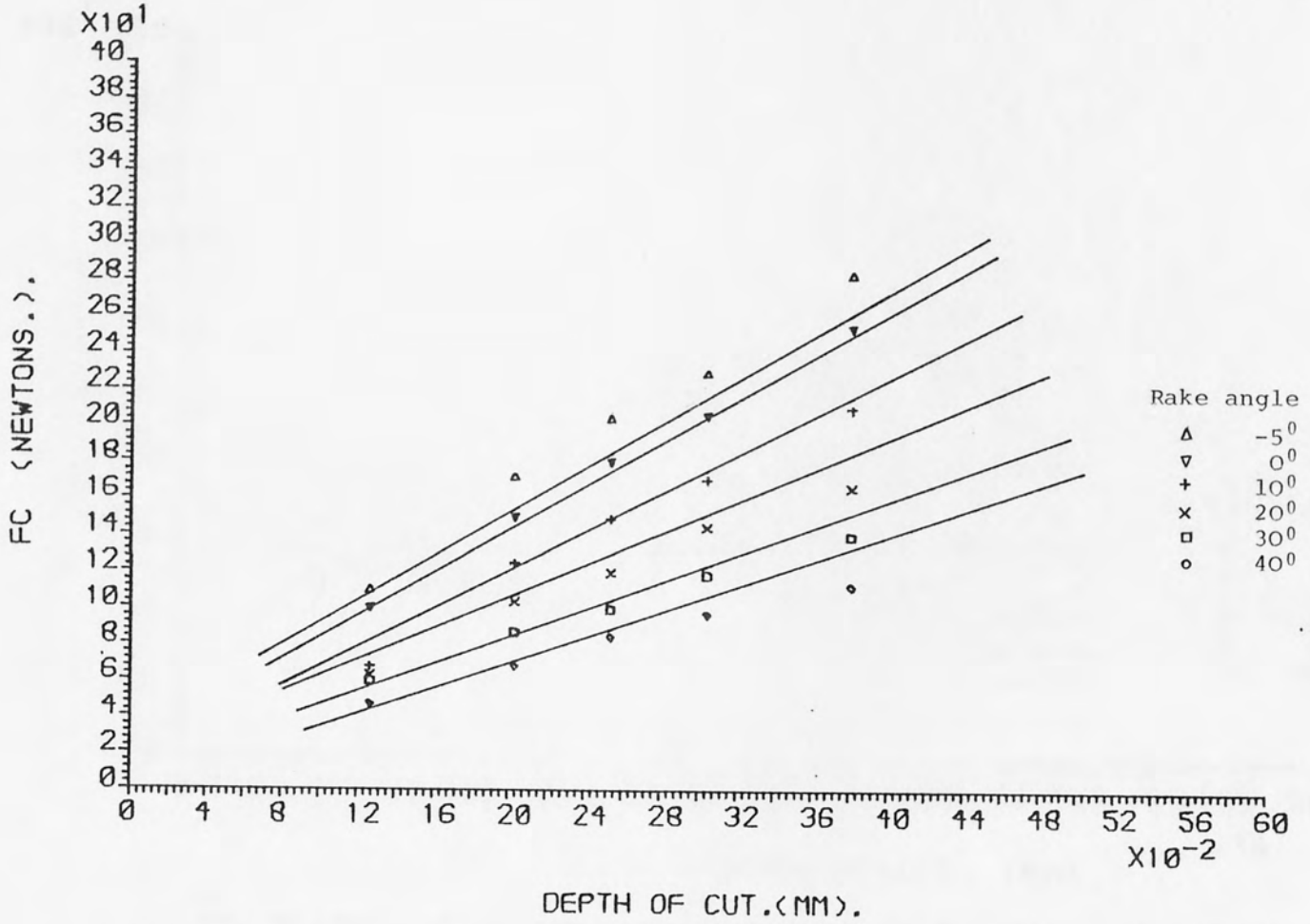

Fig. (7.115)

FIG. (7.115) F_c as a function of depth of cut for rolled polycarbonate, cutting speed 15.24 m/min solid lines represent the predicted values of F_c

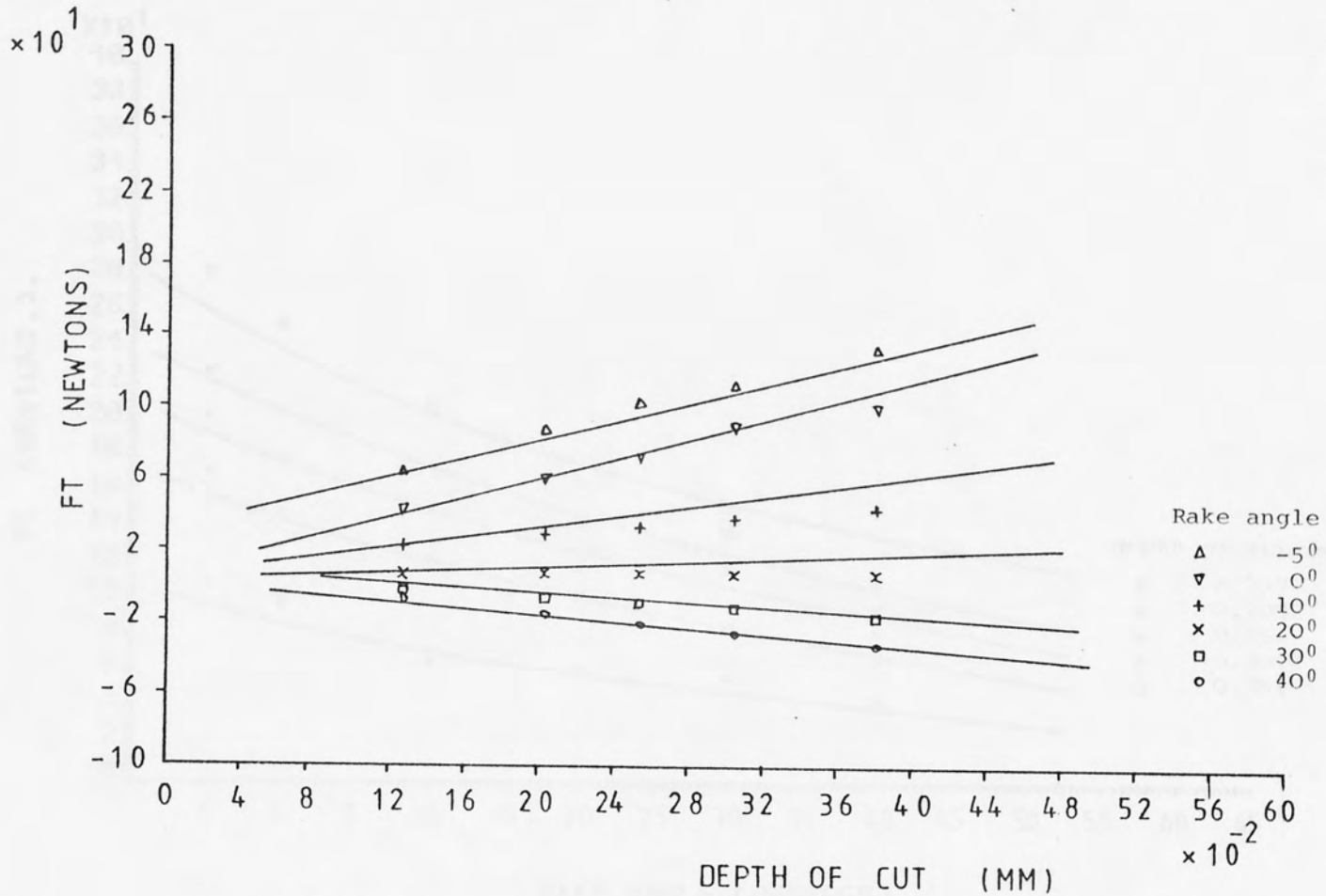

FIG. (7.116) F_t as a function of depth of cut for rolled polycarbonate, cutting speed 15.24 m/min. solid lines represent the predicted values of F_t

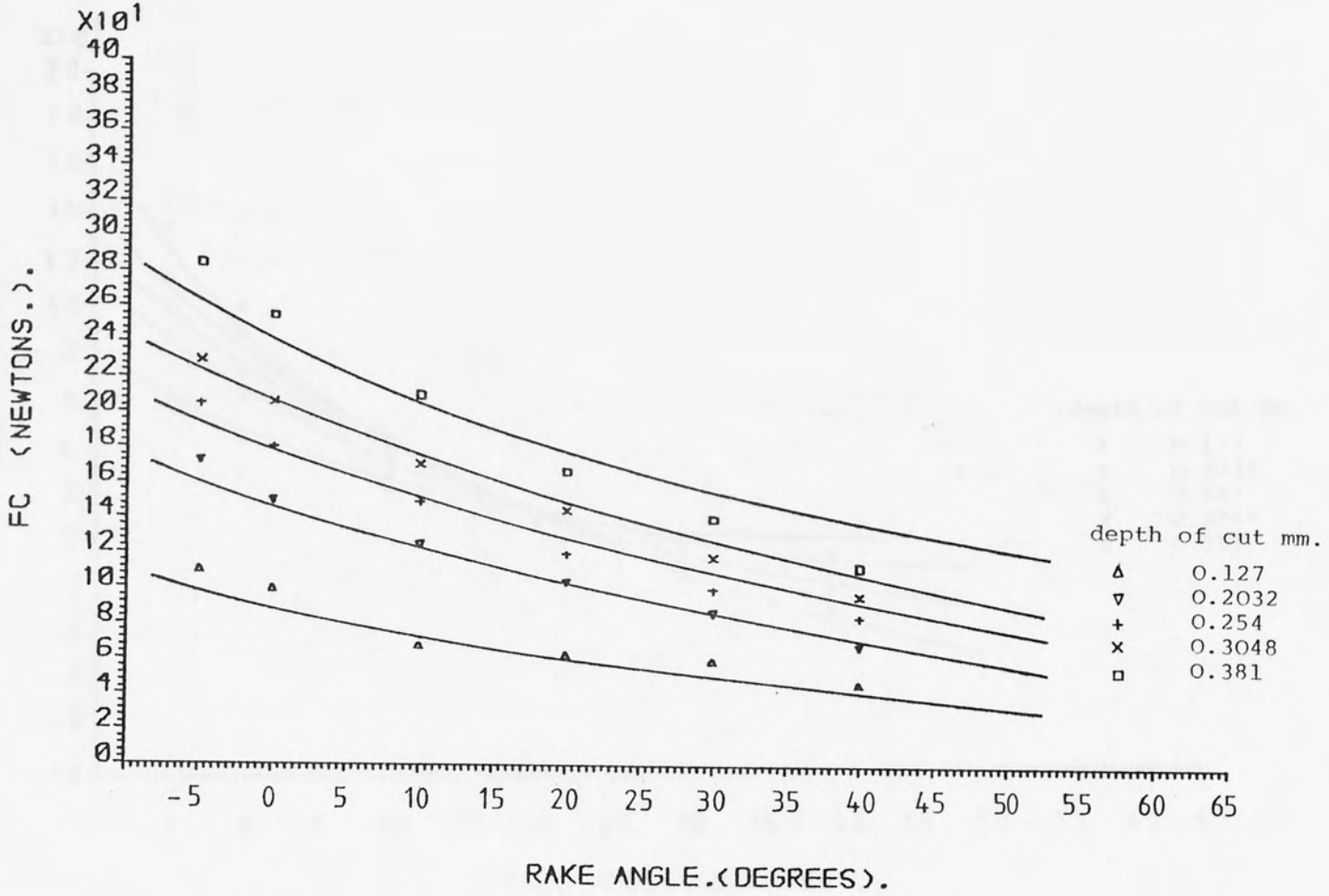

Fig. (7.117)

FIG. (7.117) F_c as a function of rake angle for rolled polycarbonate, cutting speed 15.24 m/min. solid lines represent the predicted values of F_c

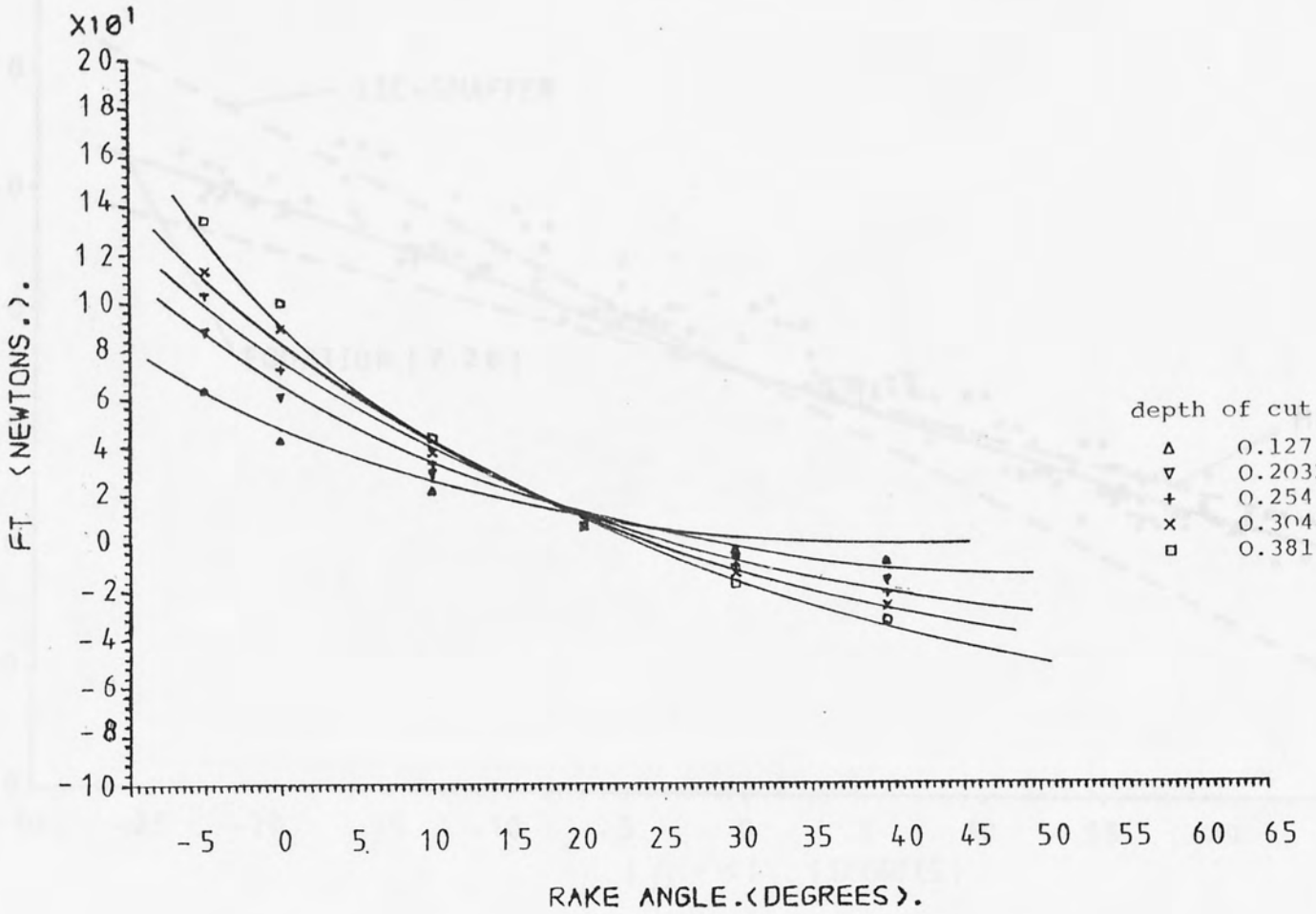

Fig. (7.118)

FIG. (7.118) F_t as a function of rake angle for rolled polycarbonate, cutting speed 15.24 m/min. solid lines represent the predicted values of F_c

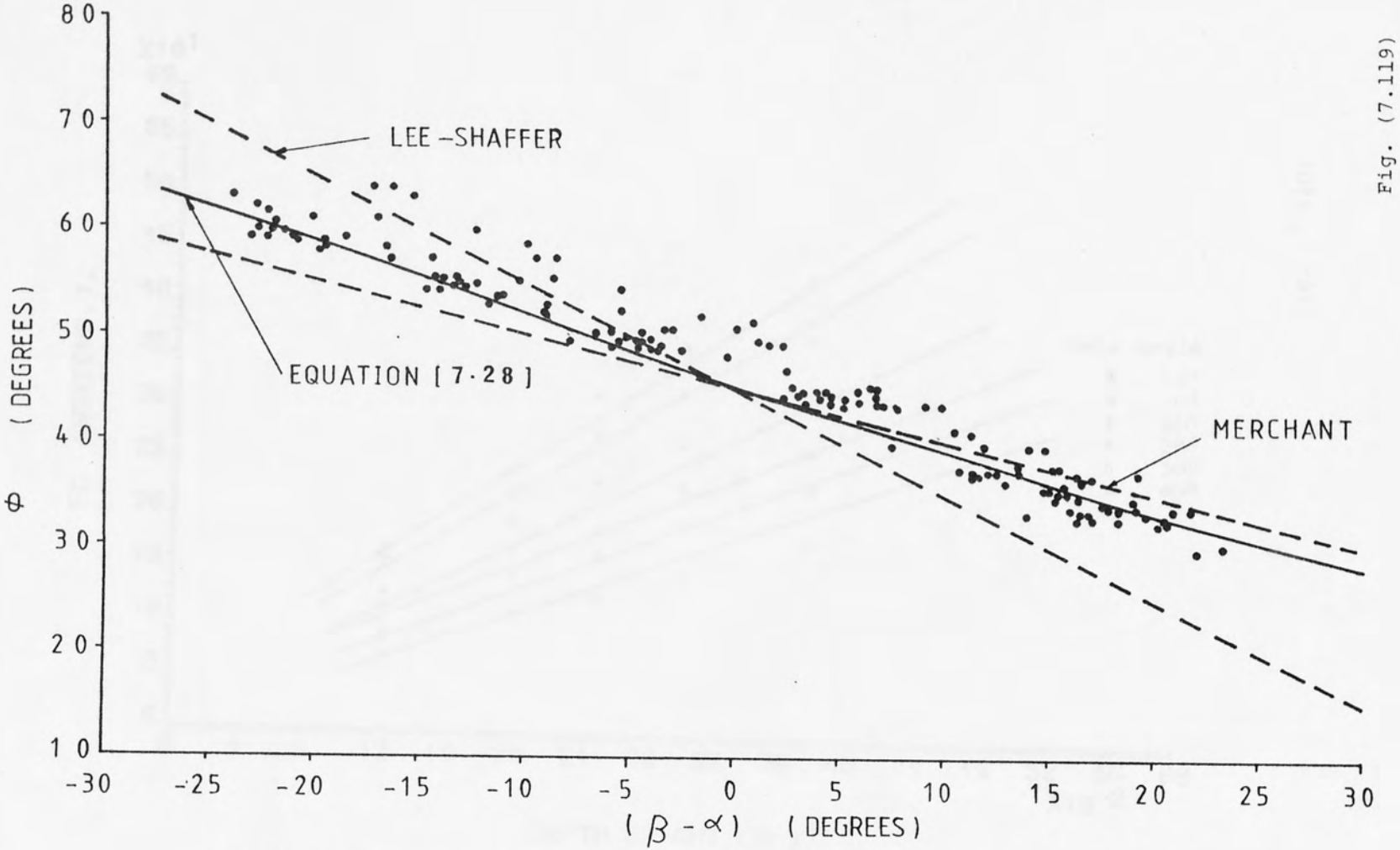

Fig. (7.119)

FIG. (7.119) ϕ and (β - α) relationship for as-received Nylon, cutting conditions table (3), solid lines represent the equation [7.28]

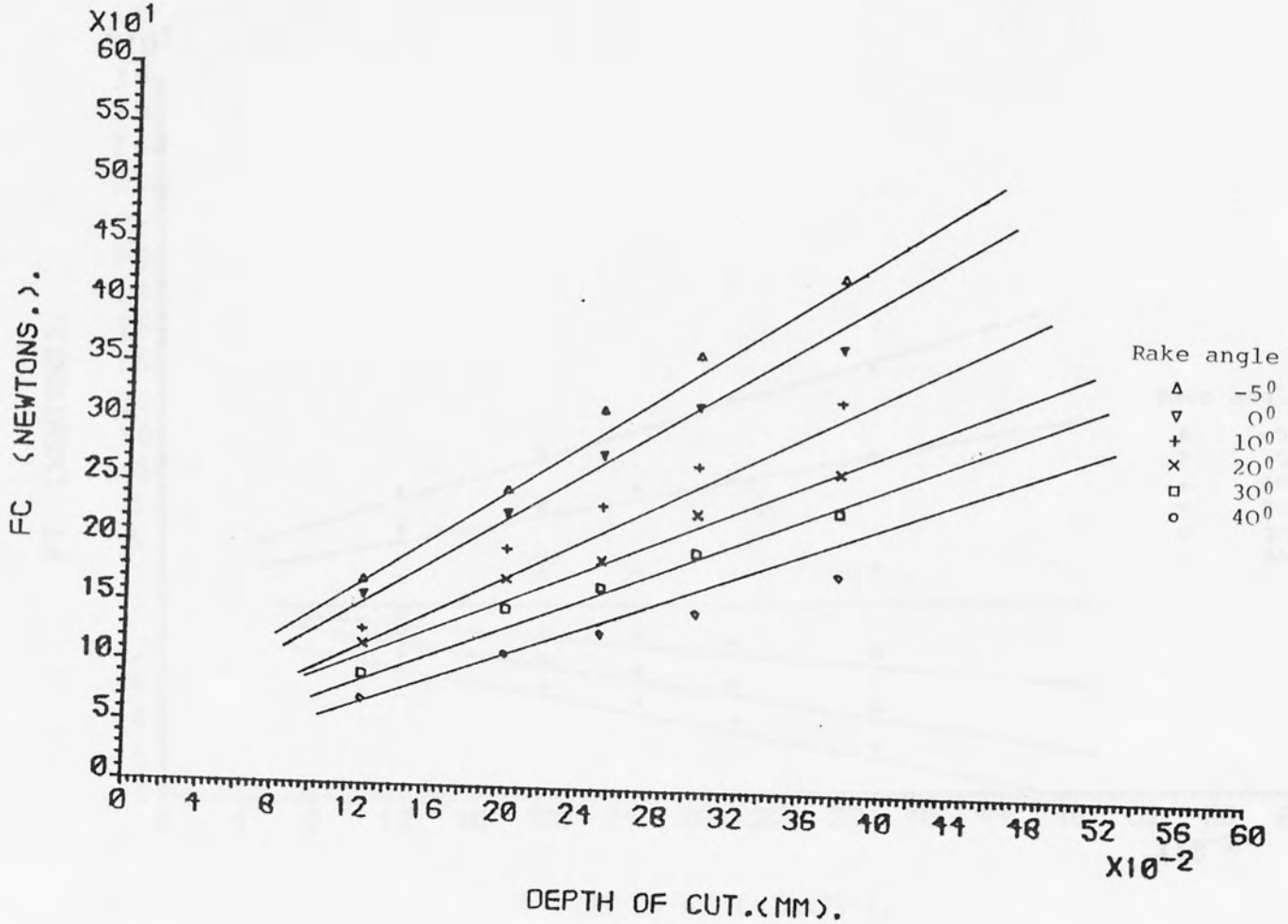

Fig. (7.120)

FIG. (7.120) F_c as a function of depth of cut for as-received Nylon, cutting speed 15.24 m/min, solid lines represent the predicted values of F_c

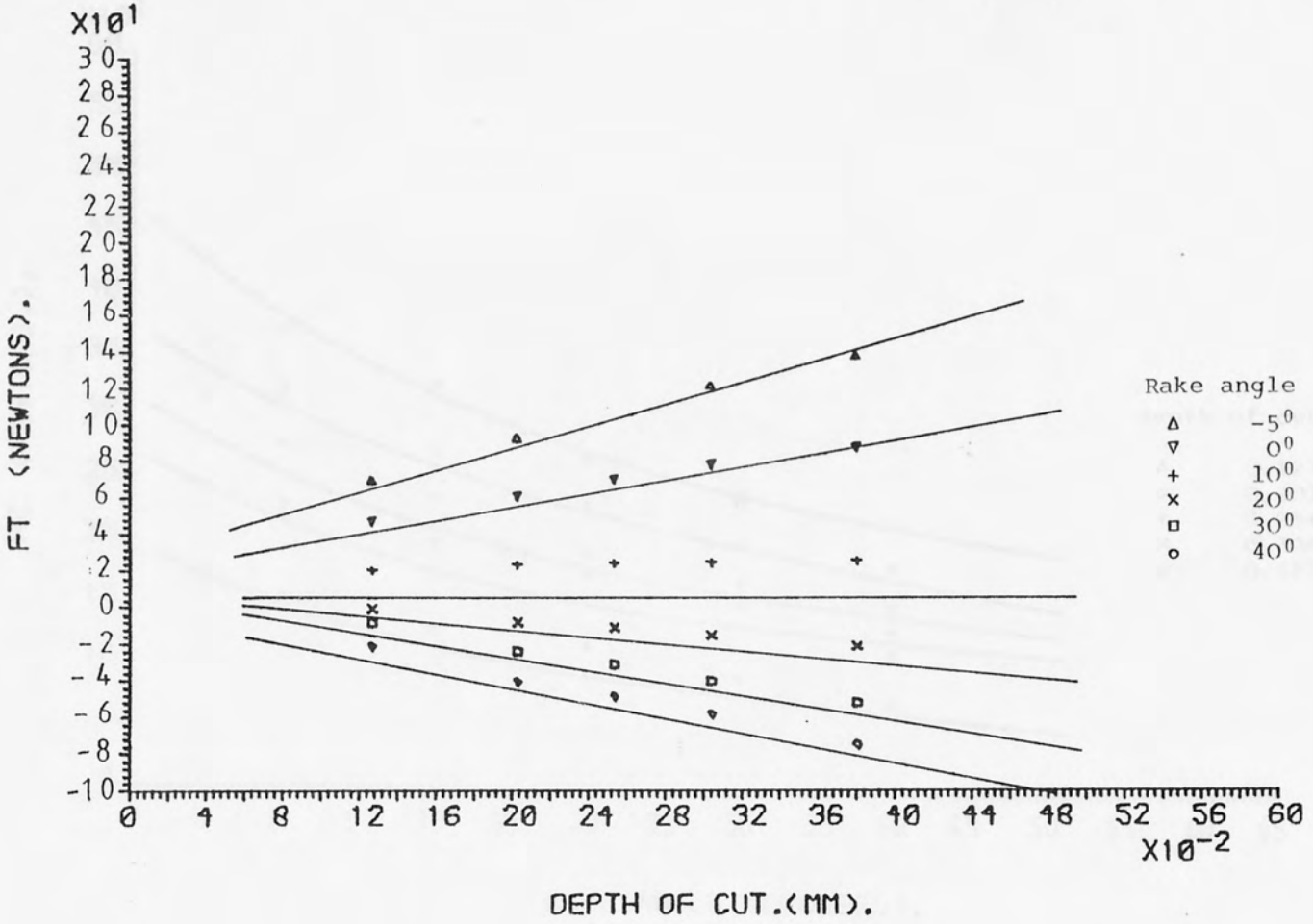

Fig. (7.121)

FIG. (7.121) F_t as a function of depth of cut for as-received Nylon, cutting speed 15.24 m/min. solid lines represent the predicted values of F_t

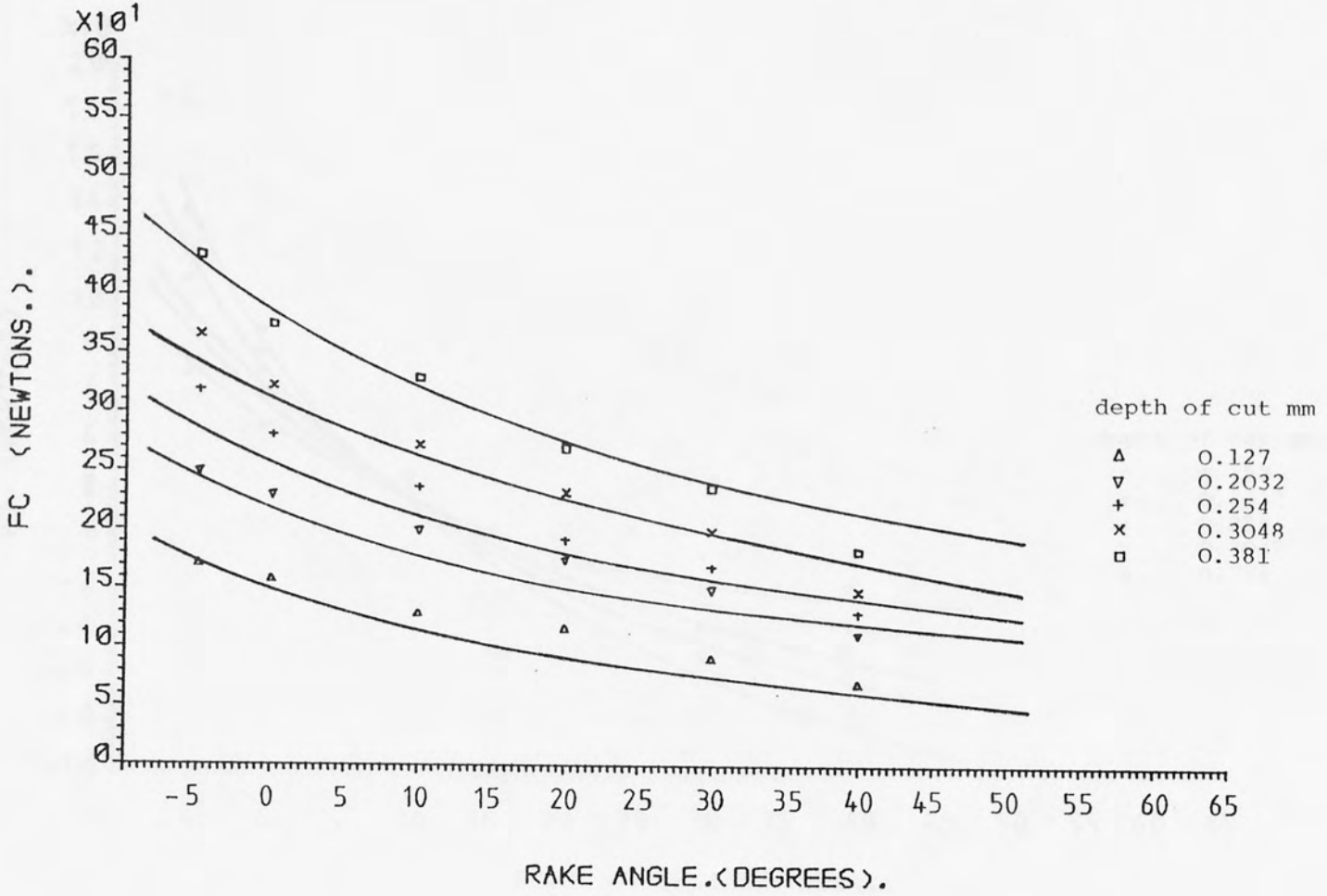

Fig. (7.122)

FIG. (7.122) F_c as a function of rake angle for as-received Nylon, cutting speed 15.24 m/min. solid lines represent the predicted values of F_c

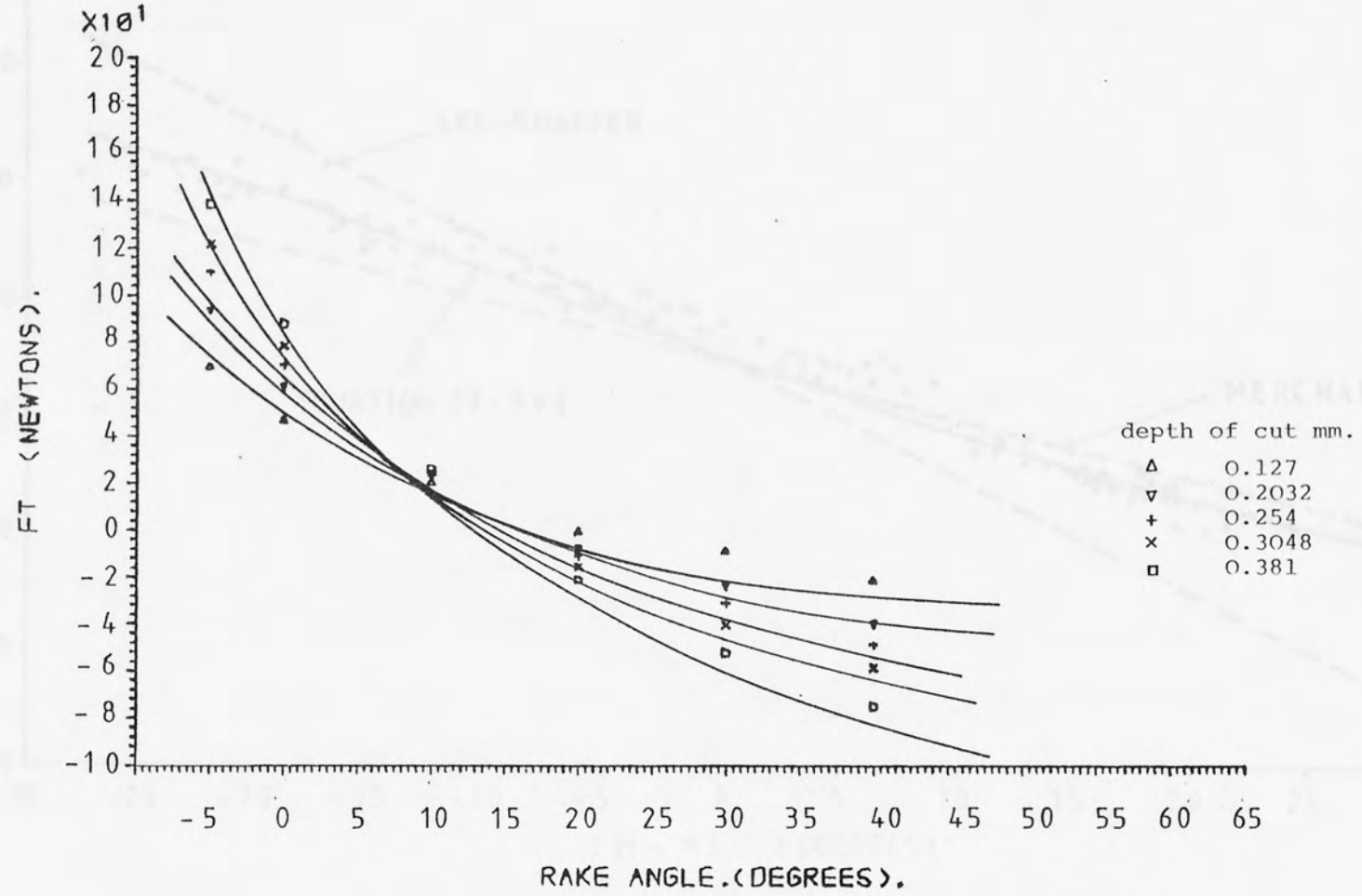

Fig. (7.123)

FIG. (7.123) F_t as a function of rake angle for as-received Nylon, cutting speed 15.24 m/min., solid lines represent the predicted values of F_t

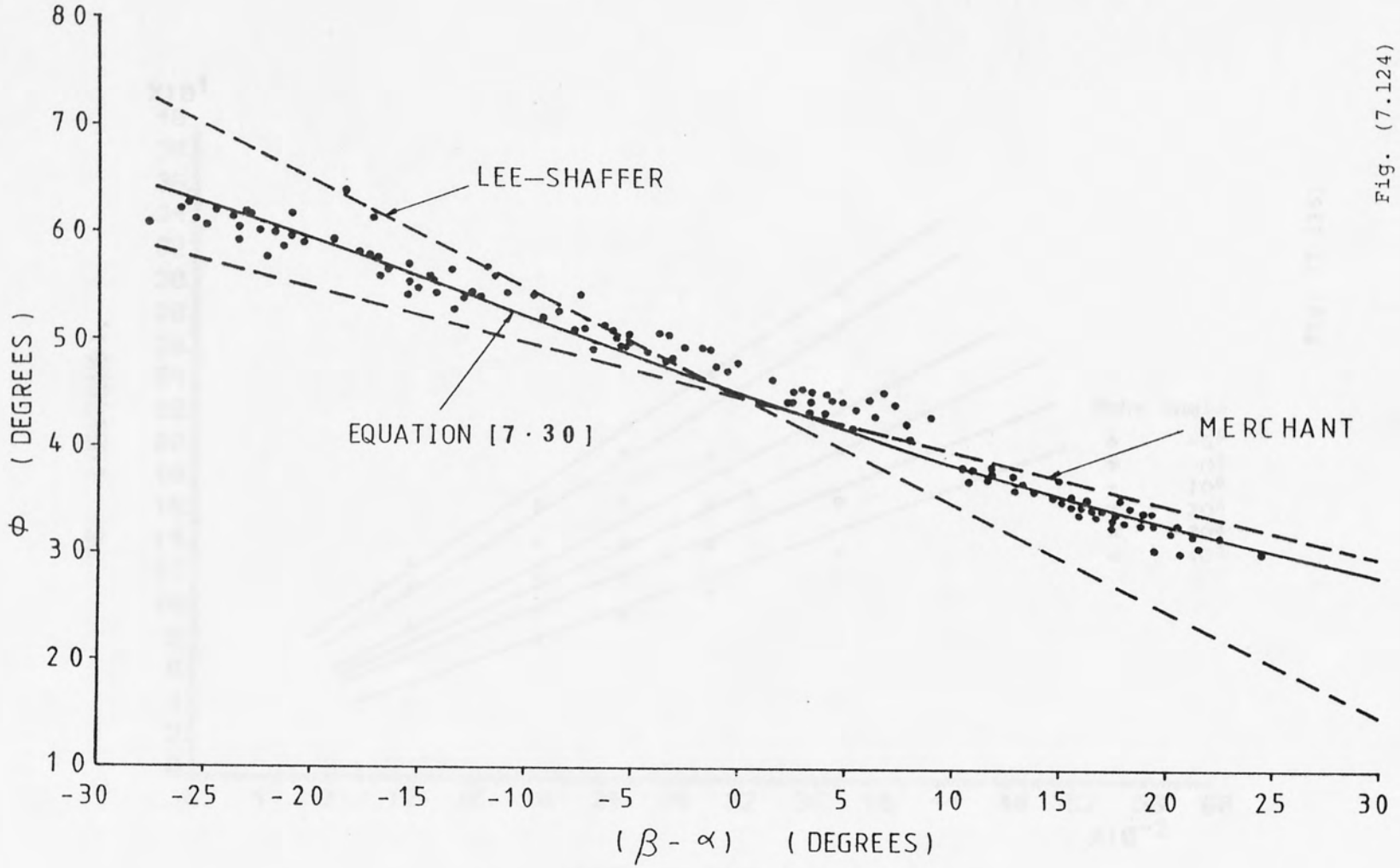

Fig. (7.124)

FIG. (7.124) ϕ and (β - α) relationship for rolled Nylon, cutting conditions Table (4), solid lines represent equation [7.30]

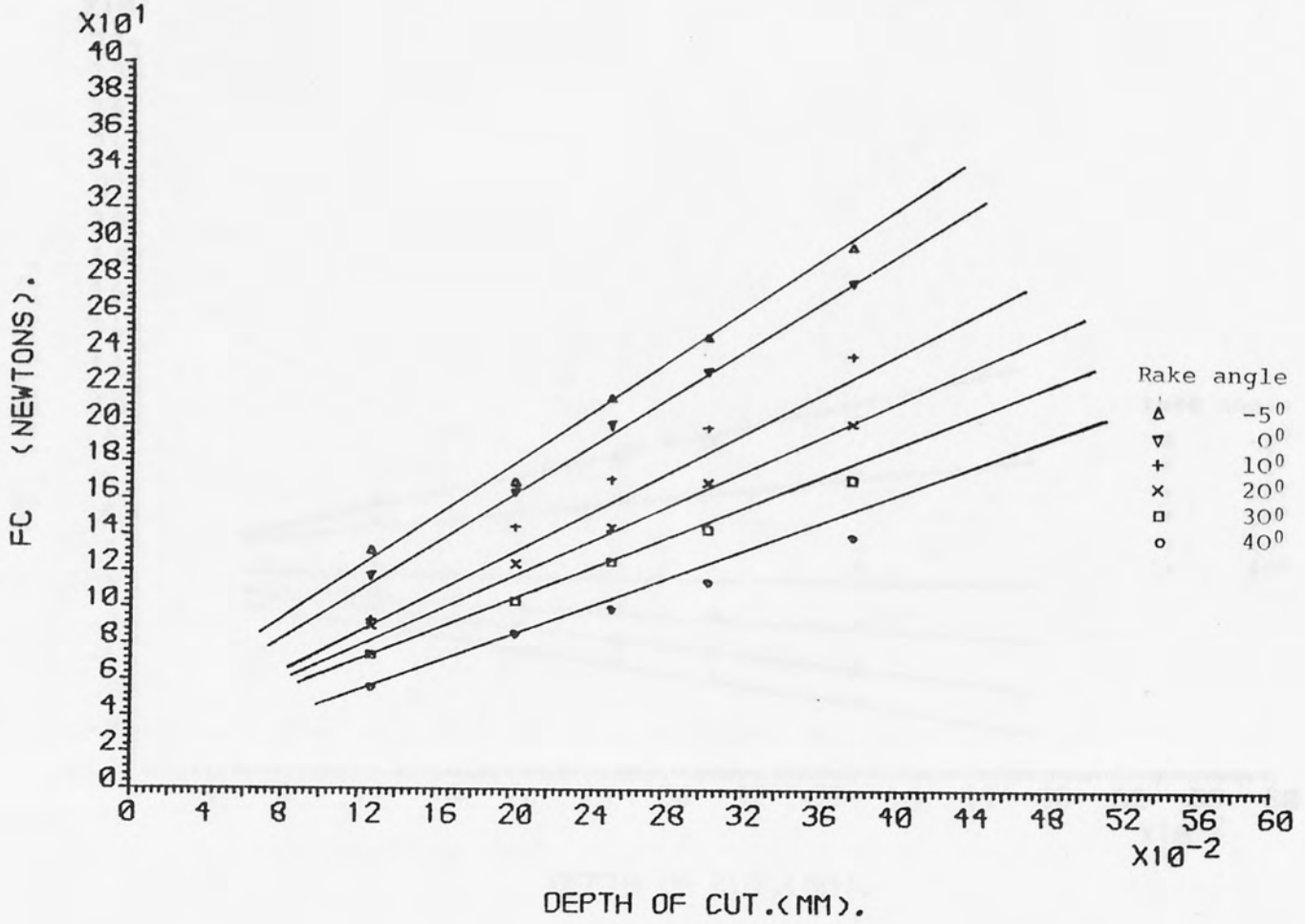

Fig. (7.125)

FIG. (7.125) F_c as a function of depth of cut for rolled Nylon, cutting speed 15.24 m/min. solid lines represent the predicted values of F_c

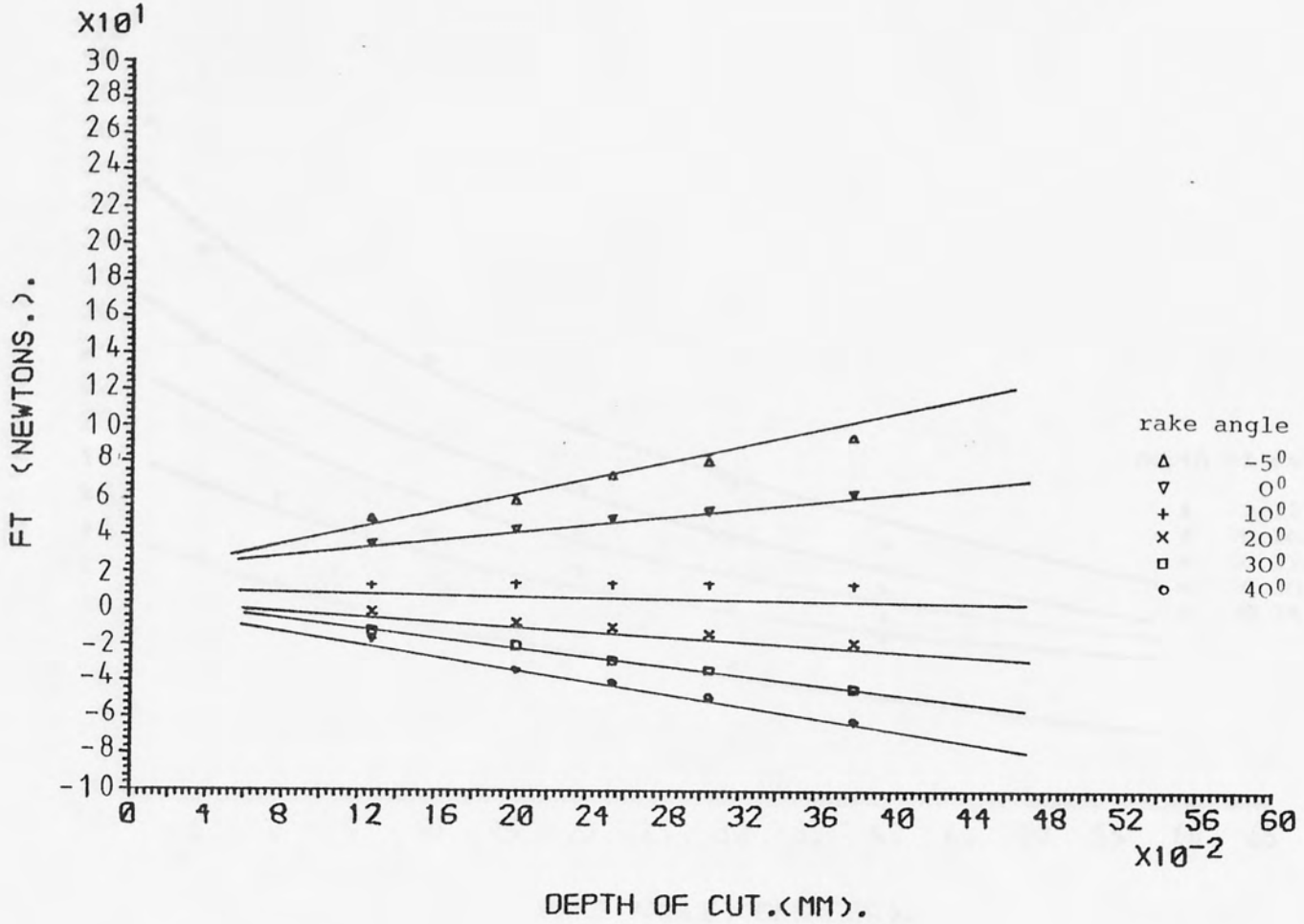

Fig. (7.126)

FIG. (7.126) F_t as a function of depth of cut for rolled Nylon, cutting speed 15.24 m/min, solid lines represent the predicted values of F_t

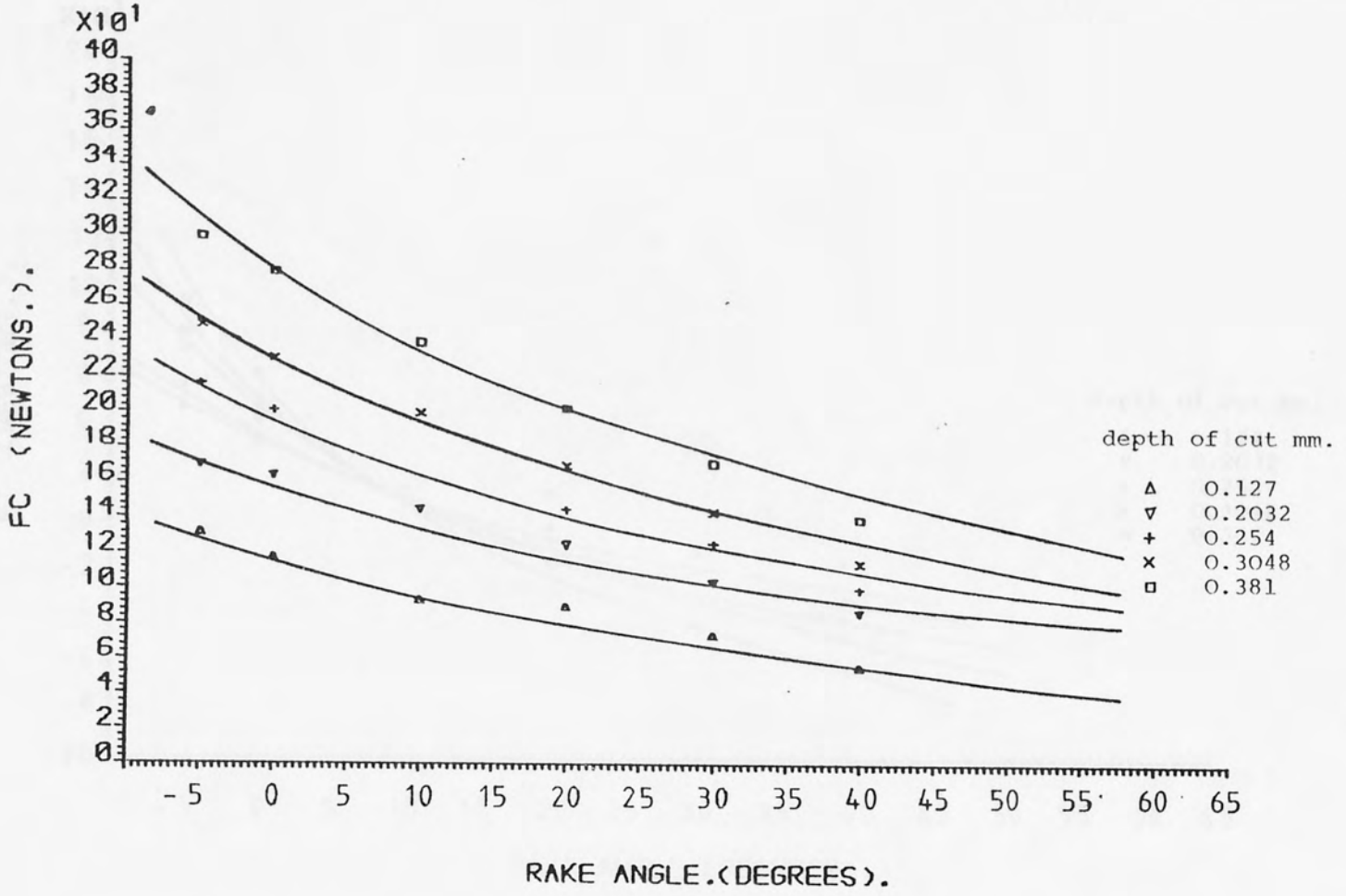

Fig. (7.127)

FIG. (7.127) F_c as a function of rake angle for rolled Nylon, cutting speed 15.24 m/min. solid lines represent the predicted values of F_c

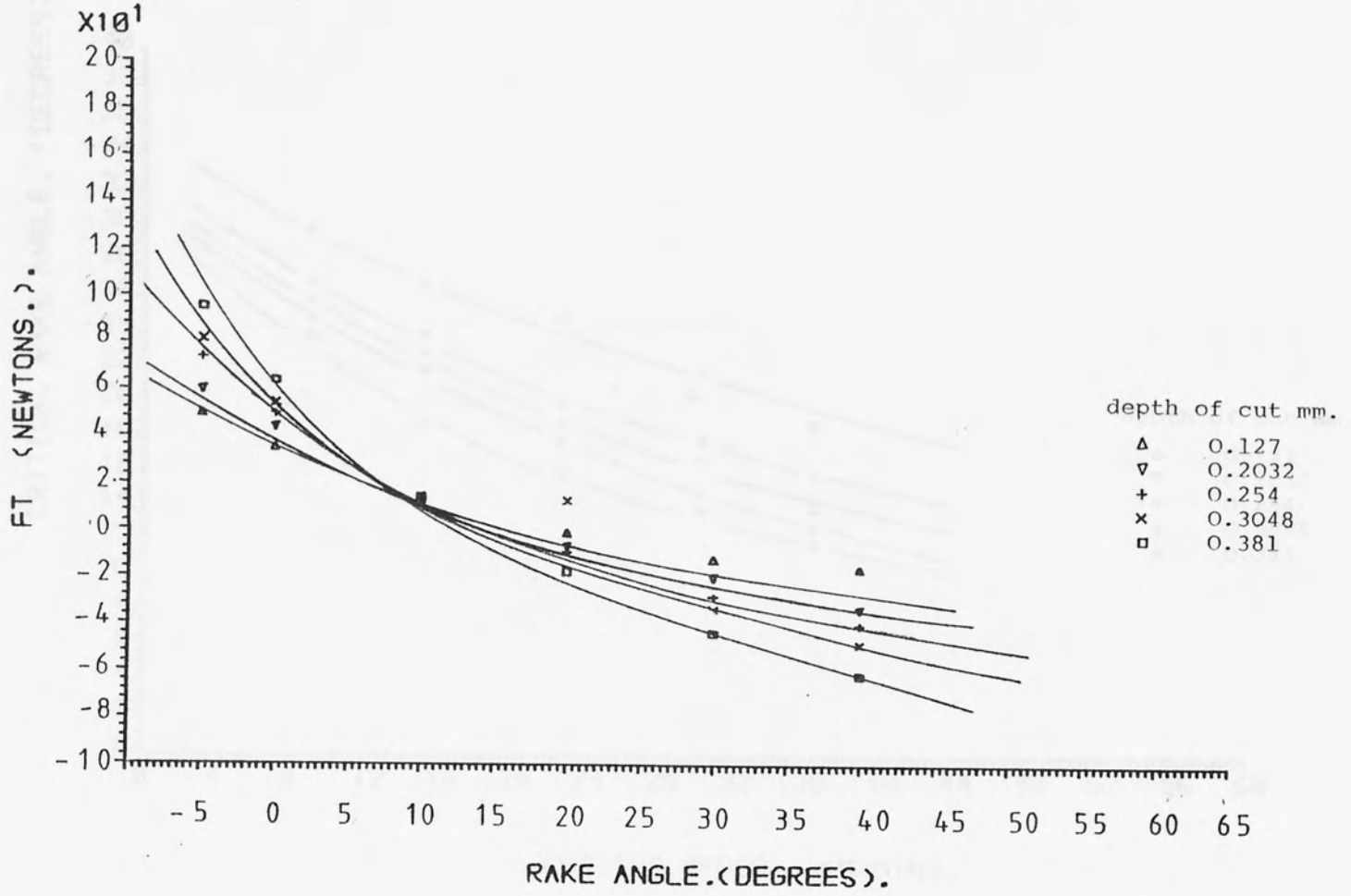

Fig. (7.128)

FIG. (7.128) F_t as a function of rake angle for rolled Nylon, cutting speed 15.24 m/min. solid lines represent the predicted values of F_t

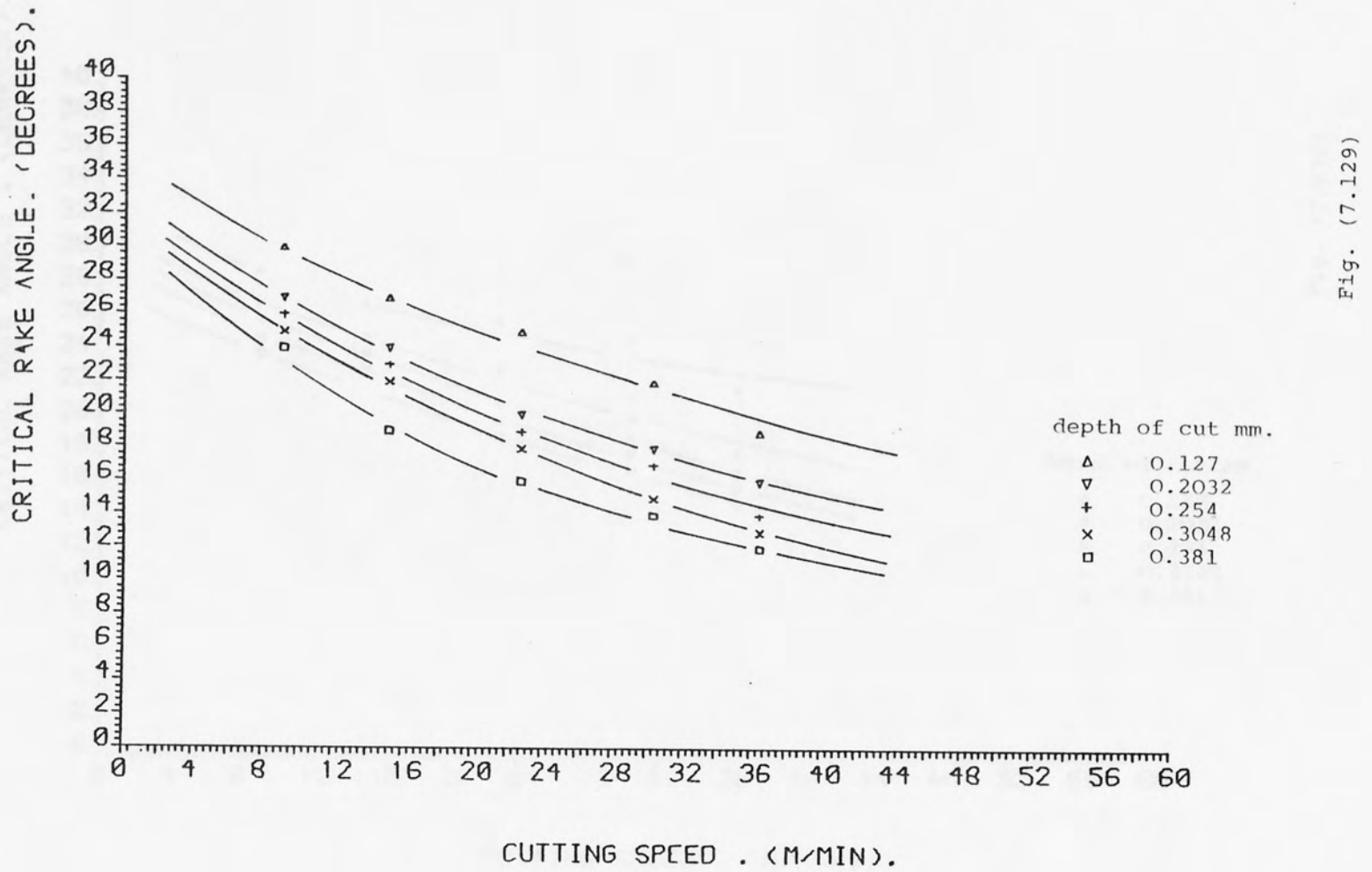

Fig. (7.129)

FIG. (7.129) Critical rake angle as a function of cutting speed and depth of cut for as-received polycarbonate

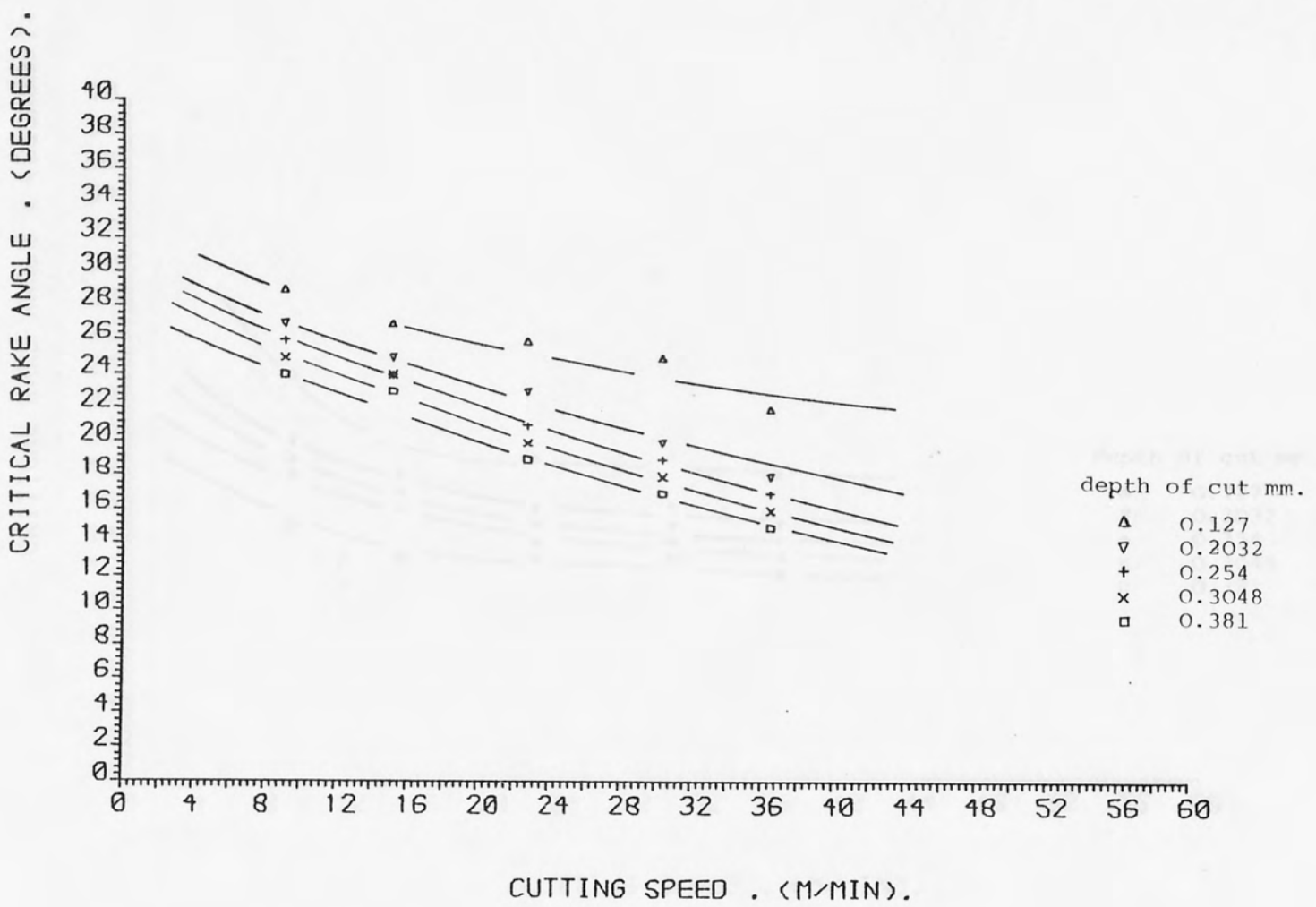

Fig. (7.130)

FIG. (7.130) Critical rake angle as a function of cutting speed and depth of cut for rolled polycarbonate

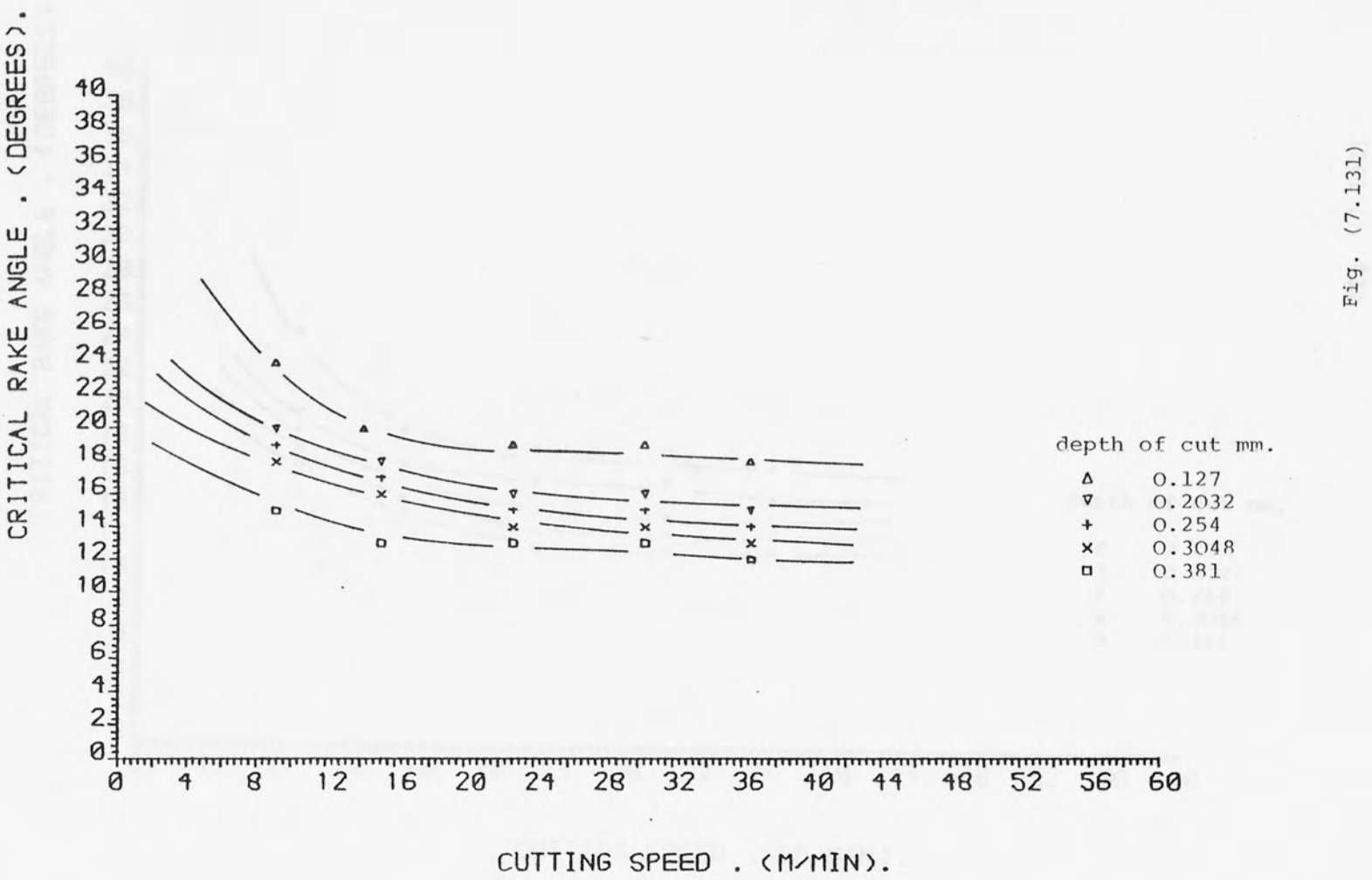

Fig. (7.131)

FIG. (7.131) Critical rake angle as a function of cutting speed and depth of cut for as-received Nylon

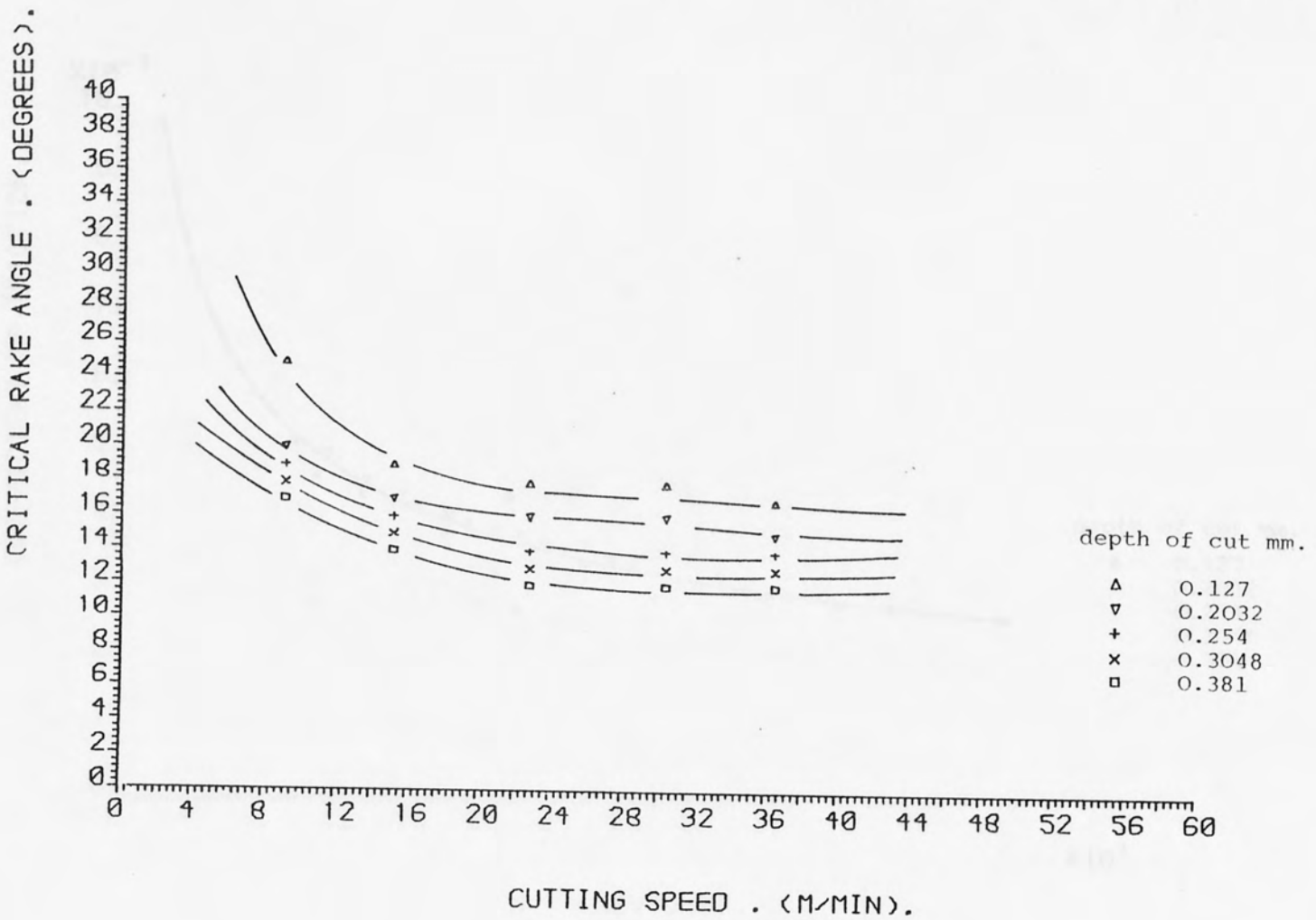

Fig. (7.132)

FIG. (7.132) Critical rake angle as a function of cutting speed and depth of cut for rolled Nylon

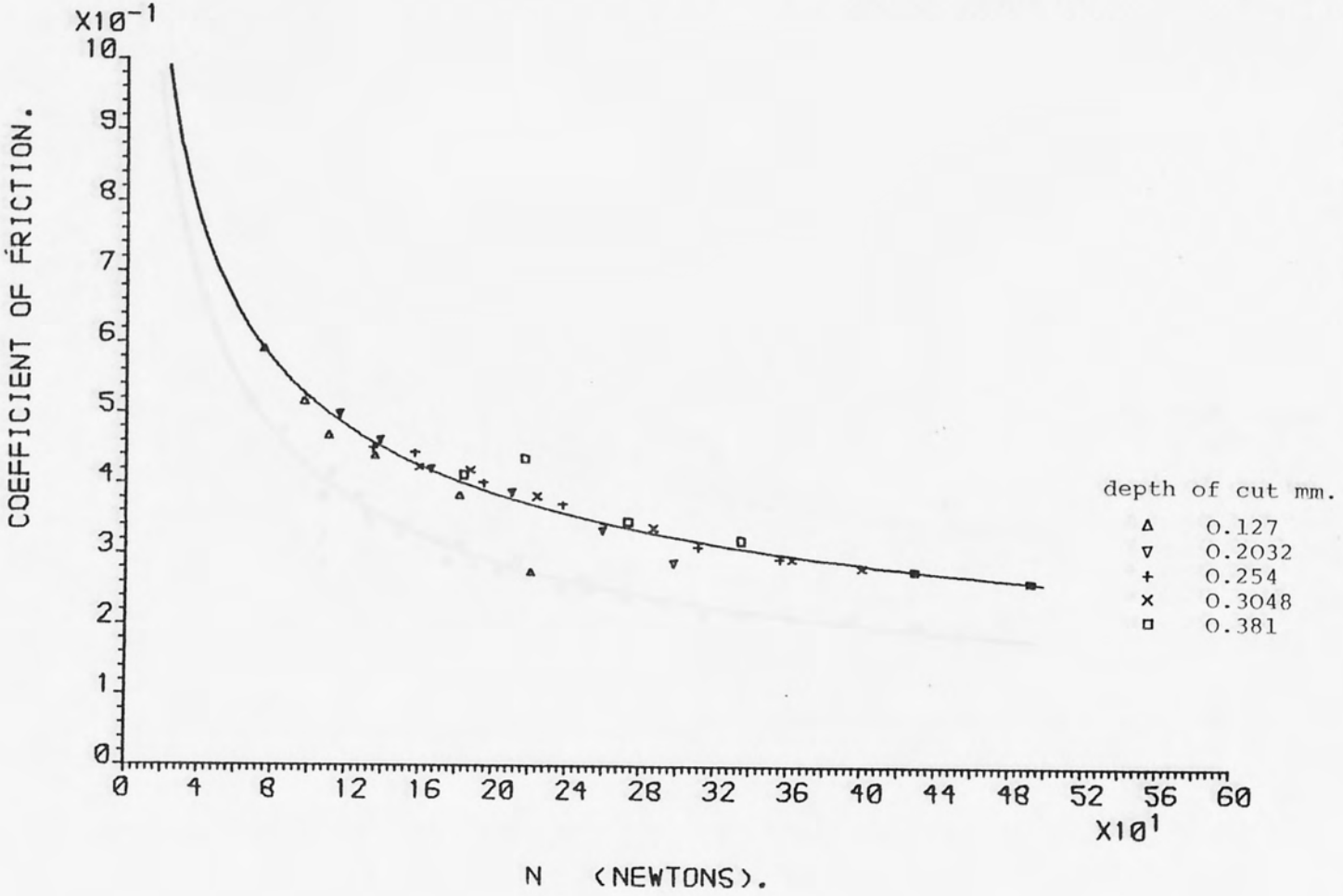

Fig. (7.133)

FIG. (7.133) μ and N relationship for as-received polycarbonate, cutting speed 15.24 m/min.

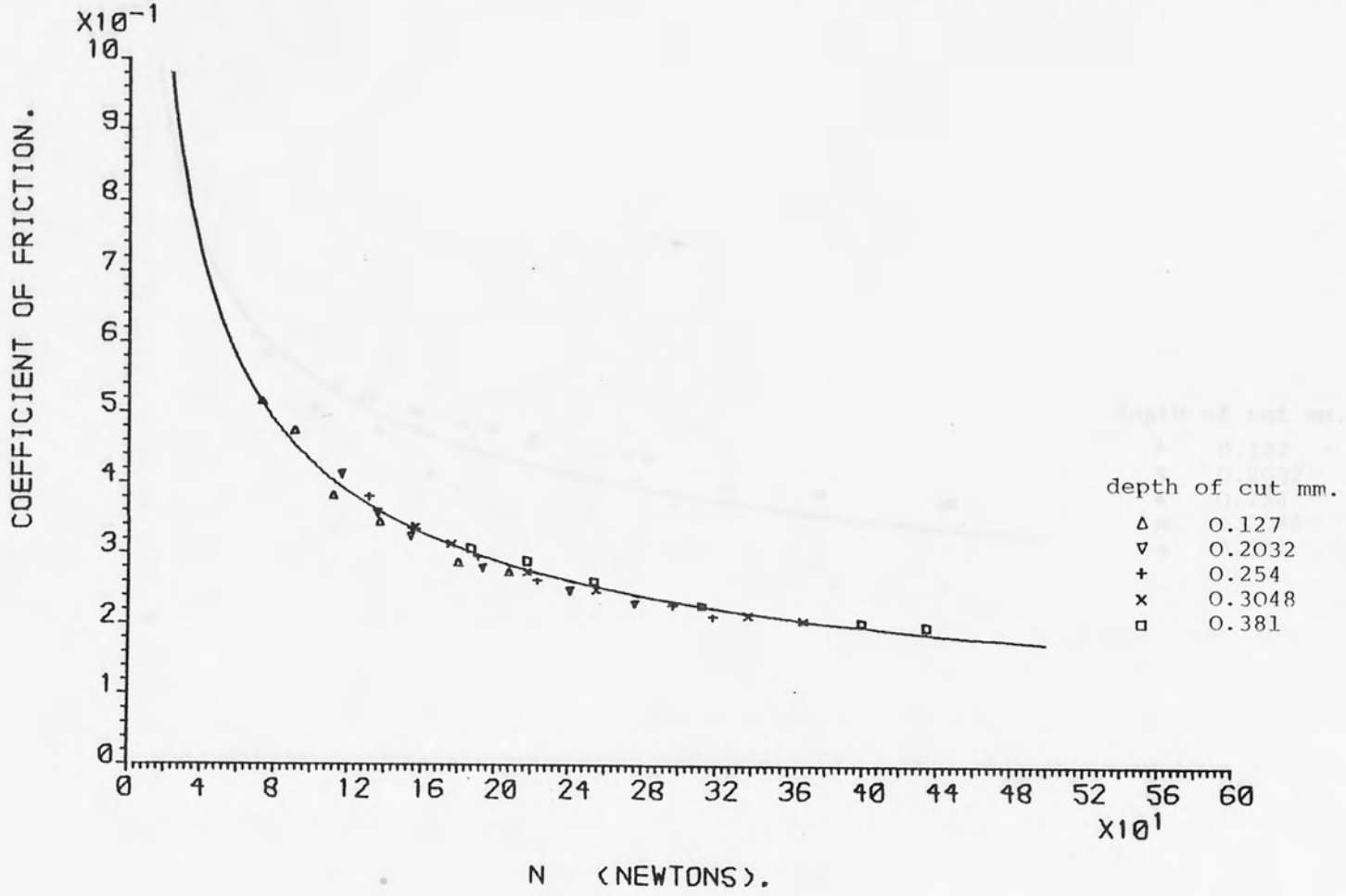

Fig. (7.134)

FIG. (7.134) μ and N relationship for as-received polycarbonate, cutting speed 30.48 m/min.

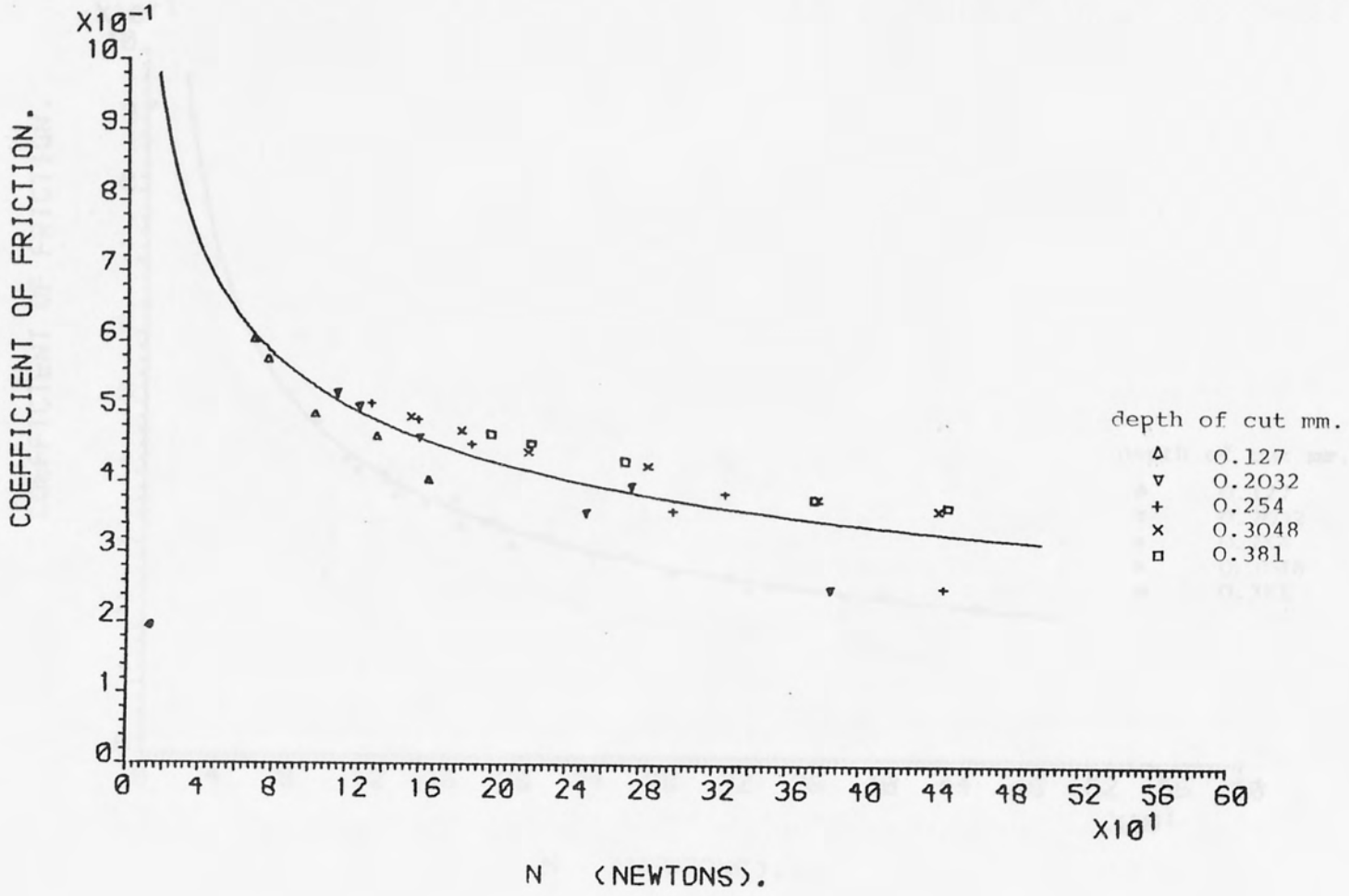

Fig. (7.135)

FIG. (7.135) μ and N relationship for as-received polycarbonate, cutting speed 9.14 m/min.

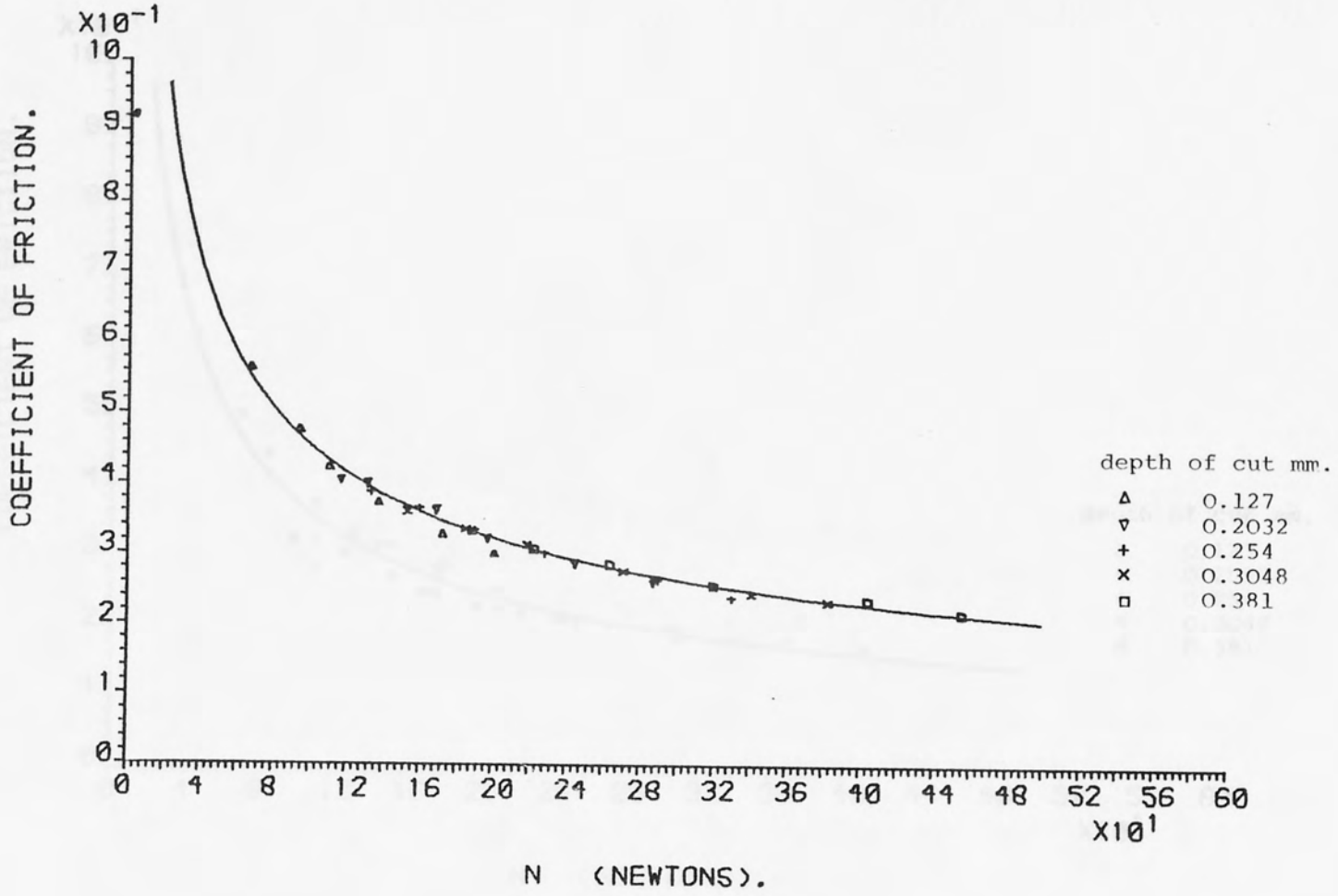

Fig. (7.136)

FIG. (7.136) μ and N relationship for as-received polycarbonate, cutting speed 22.86 m/min.

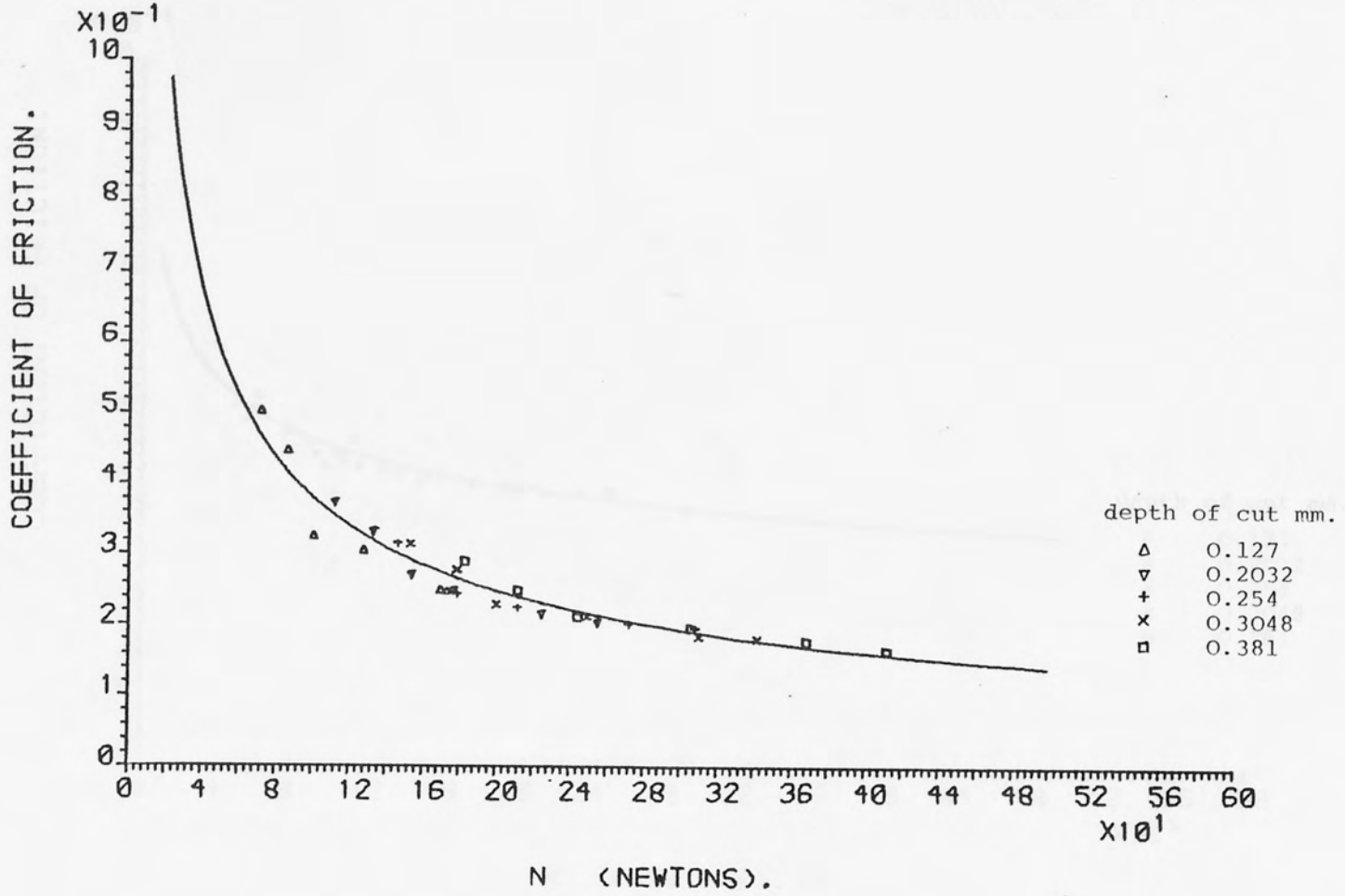

Fig. (7.137)

FIG. (7.137) μ and N relationship for as-received polycarbonate, cutting speed 36.58 m/min.

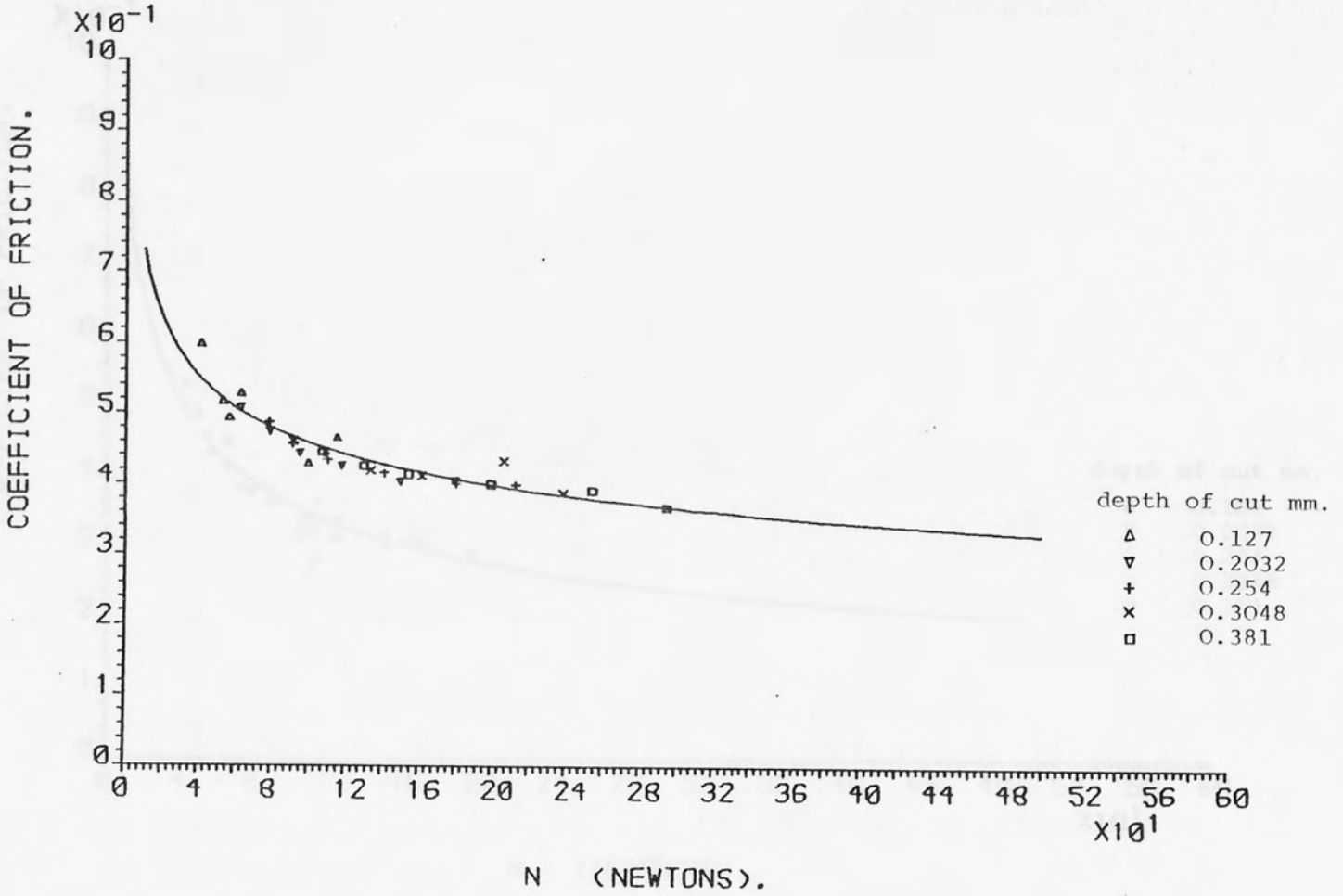

Fig. (7.138)

FIG. (7.138) μ and N relationship for rolled polycarbonate, cutting speed 15.24 m/min.

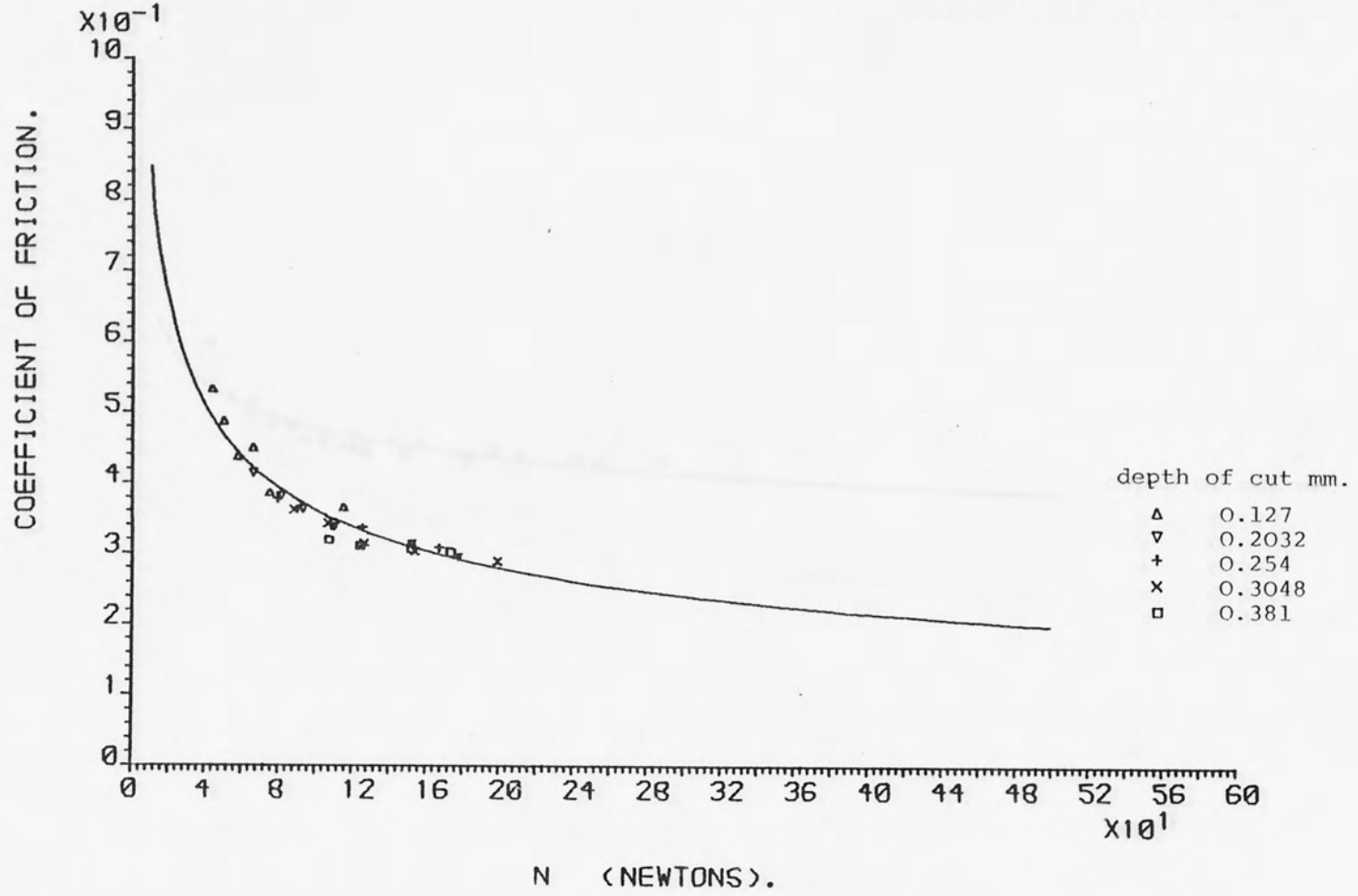

Fig. (7.139)

FIG. (7.139) μ and N relationship for rolled polycarbonate, cutting speed 30.48 m/min.

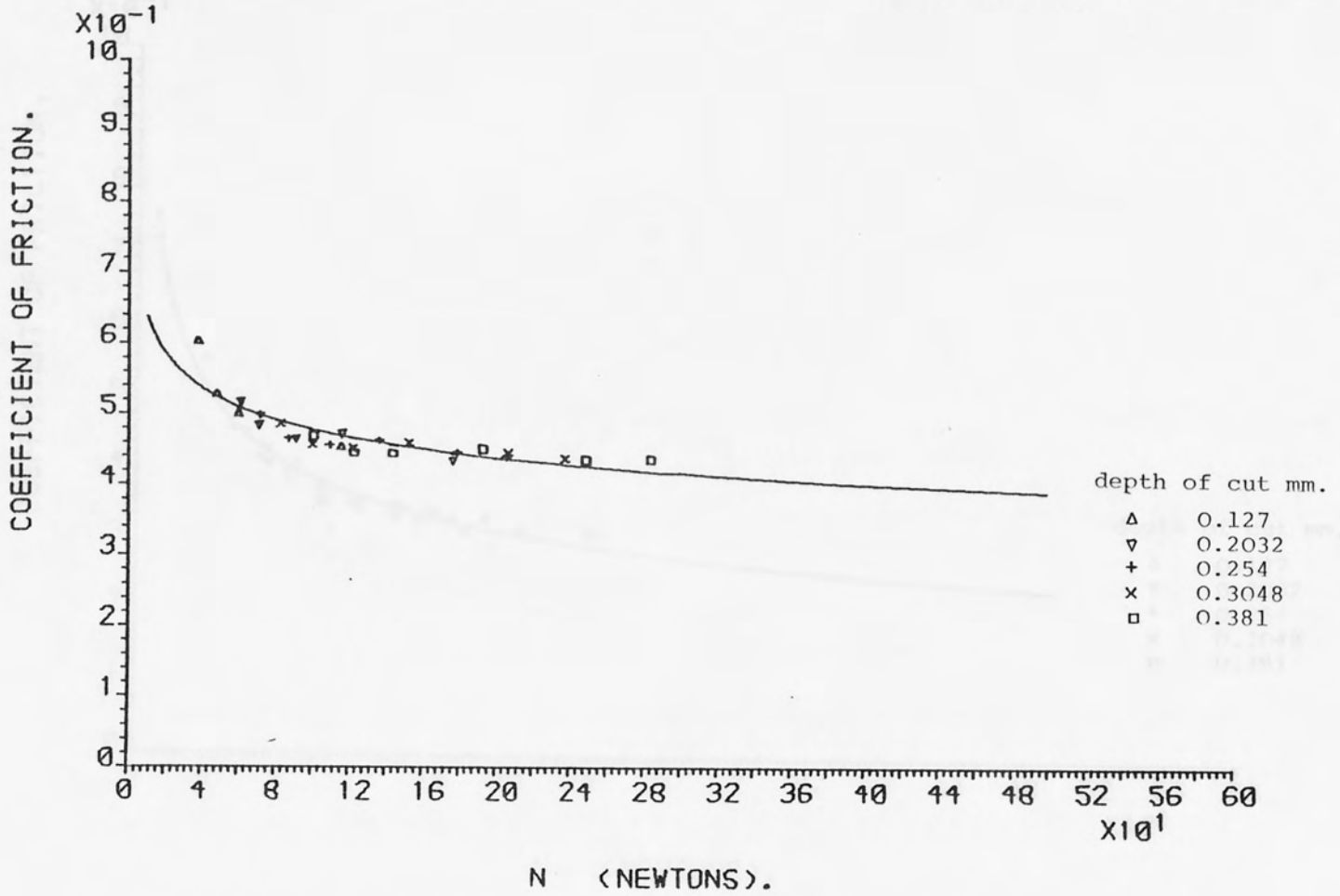

Fig. (7.140)

FIG. (7.140) μ and N relationship for rolled polycarbonate, cutting speed 9.14 m/min.

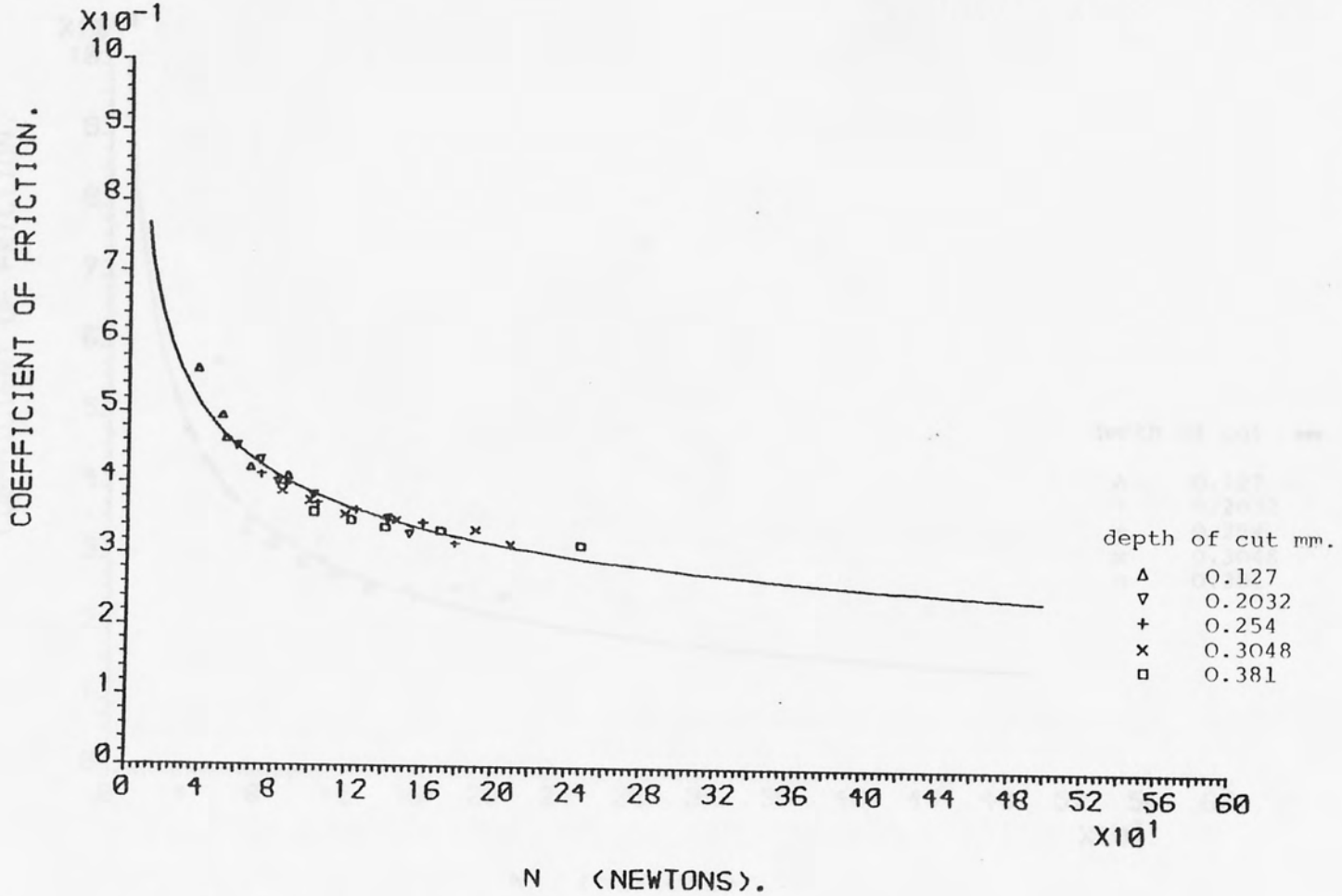

Fig. (7.141)

FIG. (7.141) μ and N relationship for rolled polycarbonate, cutting speed 22.86 m/min.

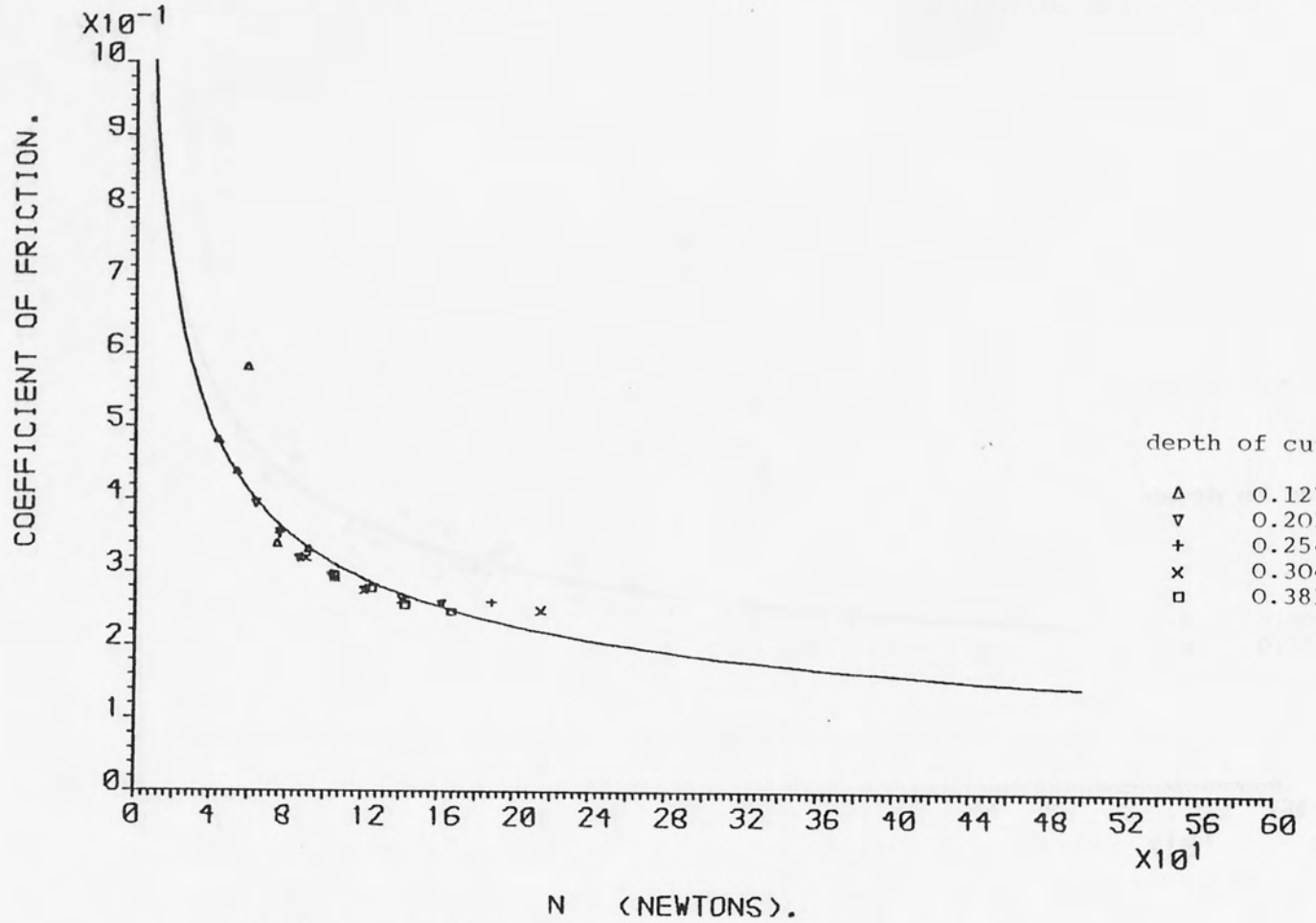

Fig. (7.142)

FIG. (7.142) μ and N relationship for rolled polycarbonate, cutting speed 36.58 m/min

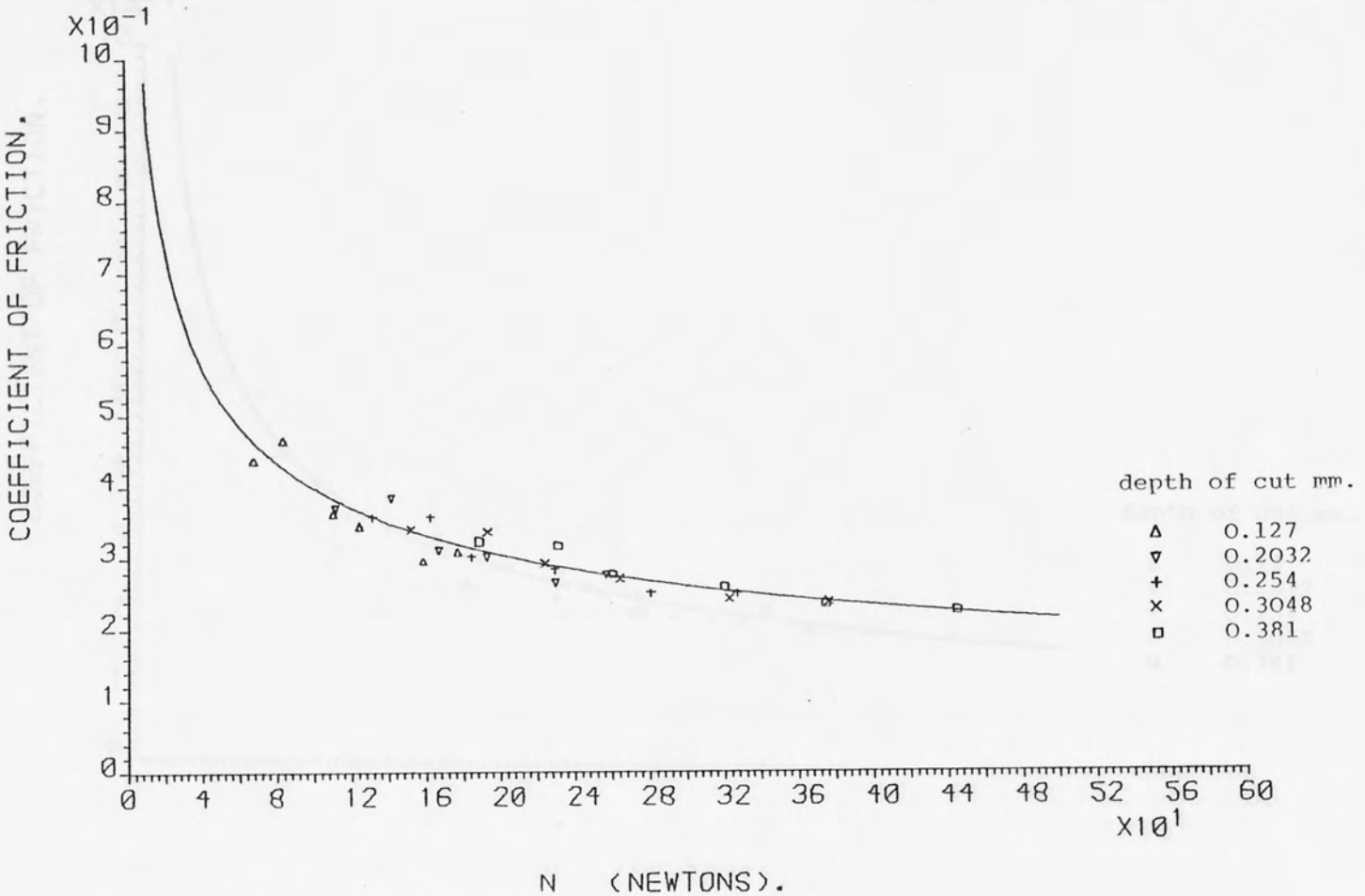

Fig. (7.143)

FIG. (7.143) μ and N relationship for as-received Nylon, cutting speed 15.24 m/min.

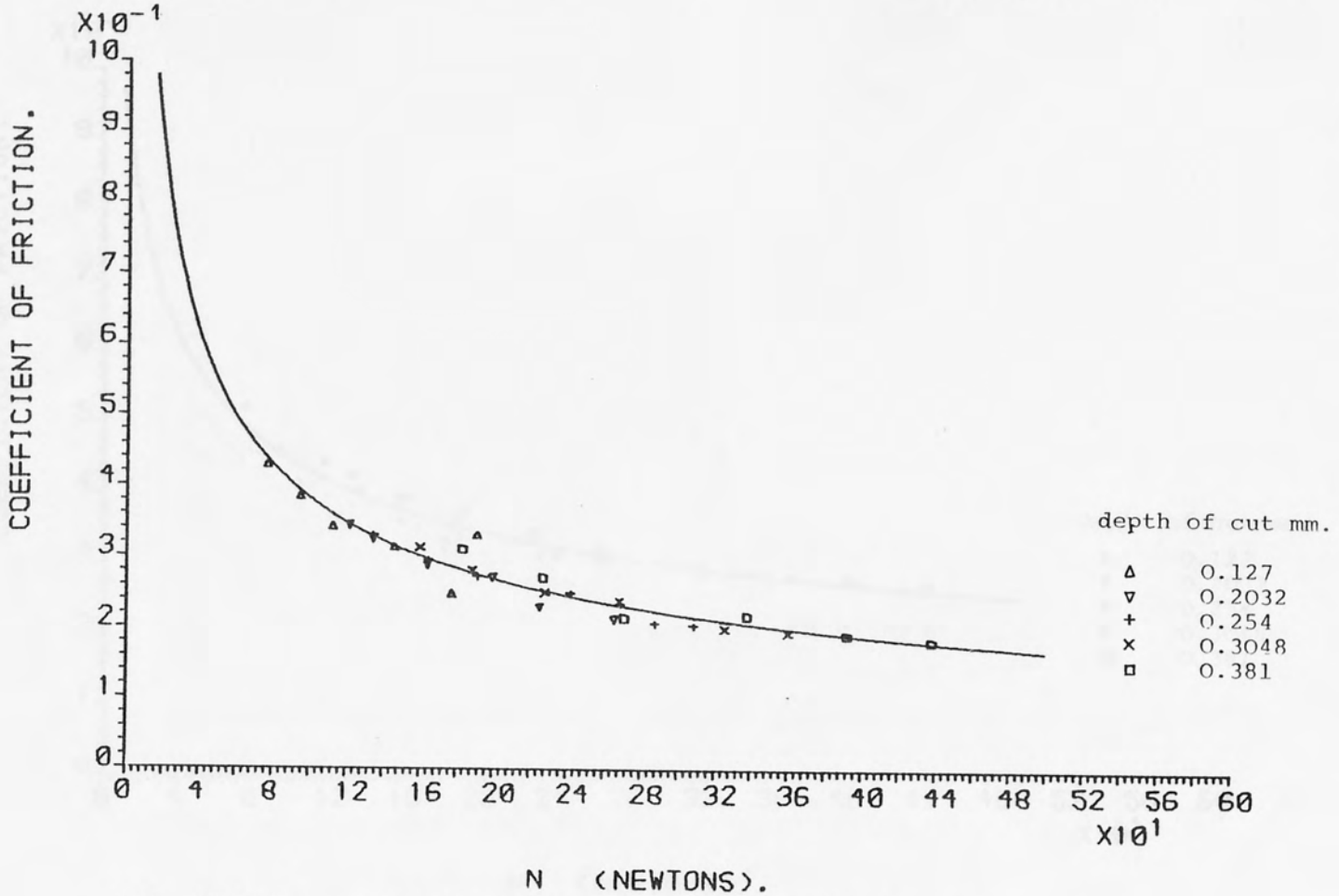

Fig. (7.144)

FIG. (7.144) μ and N relationship for as-received Nylon, cutting speed 30.48 m/min.

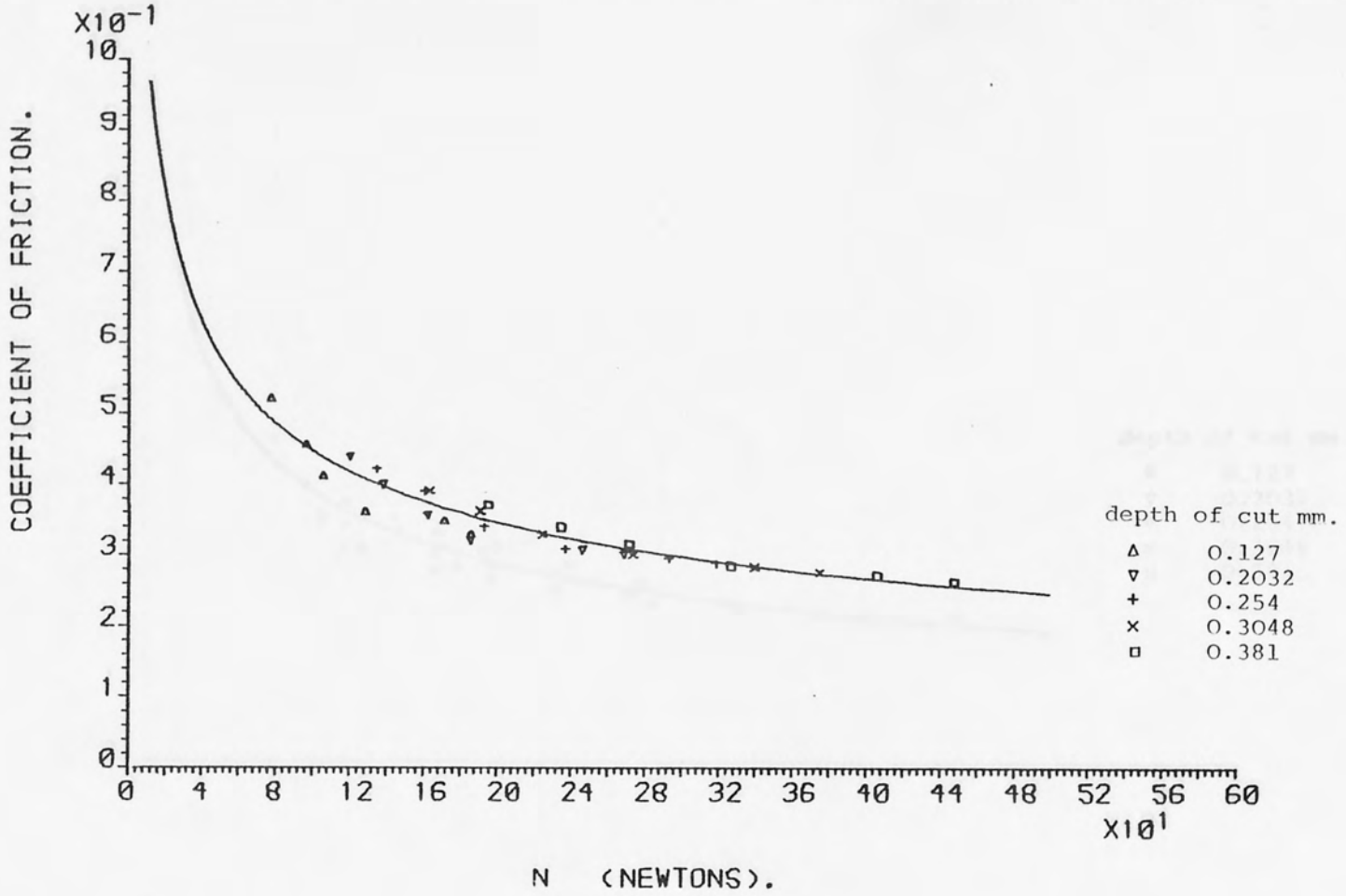

Fig. (7.145)

FIG. (7.145) μ and N relationship for as-received Nylon, cutting speed 9.14 m/min.

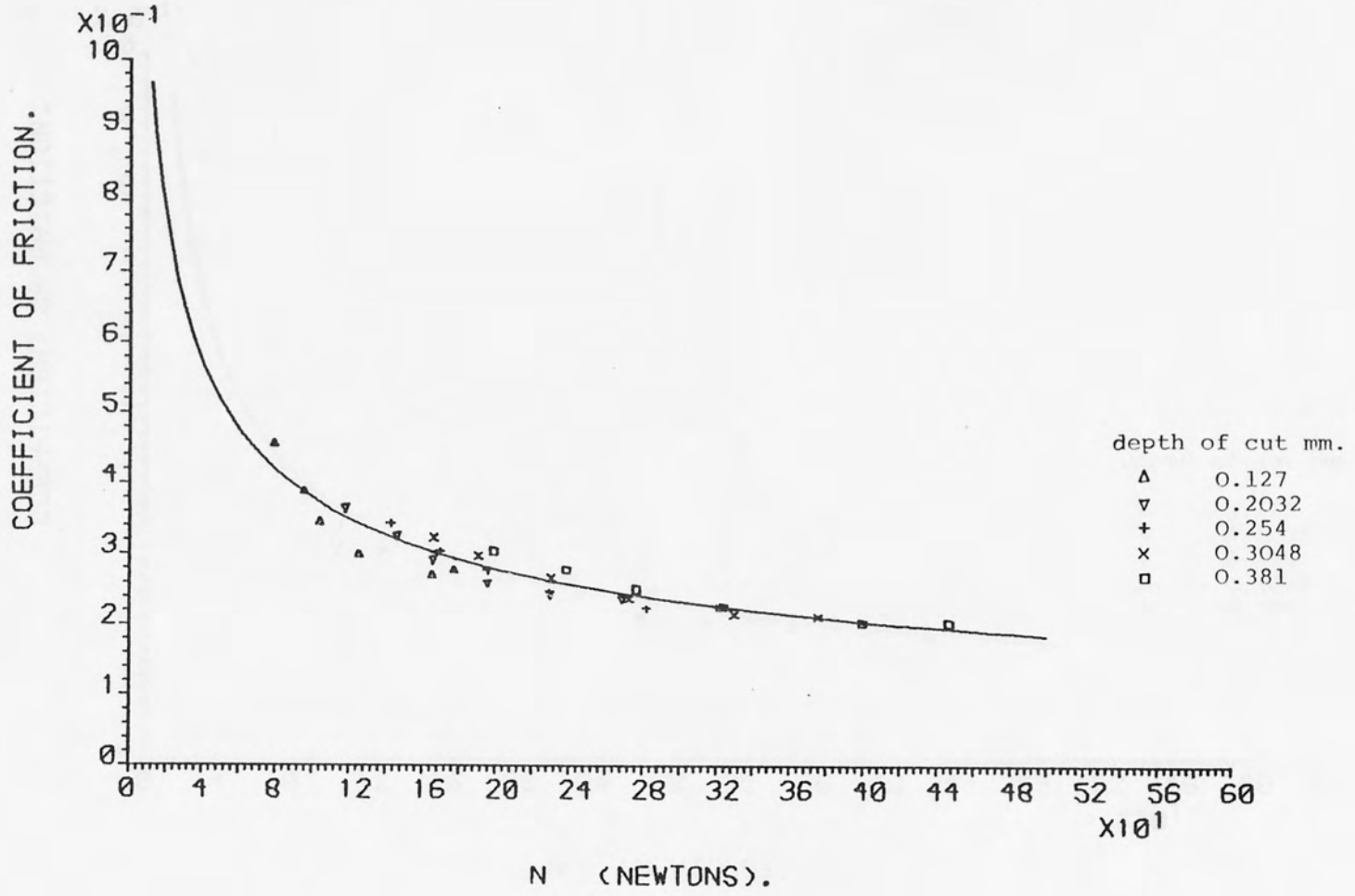

Fig. (7.146)

FIG. (7.146) μ and N relationship for as-received Nylon, cutting speed 22.86 m/min.

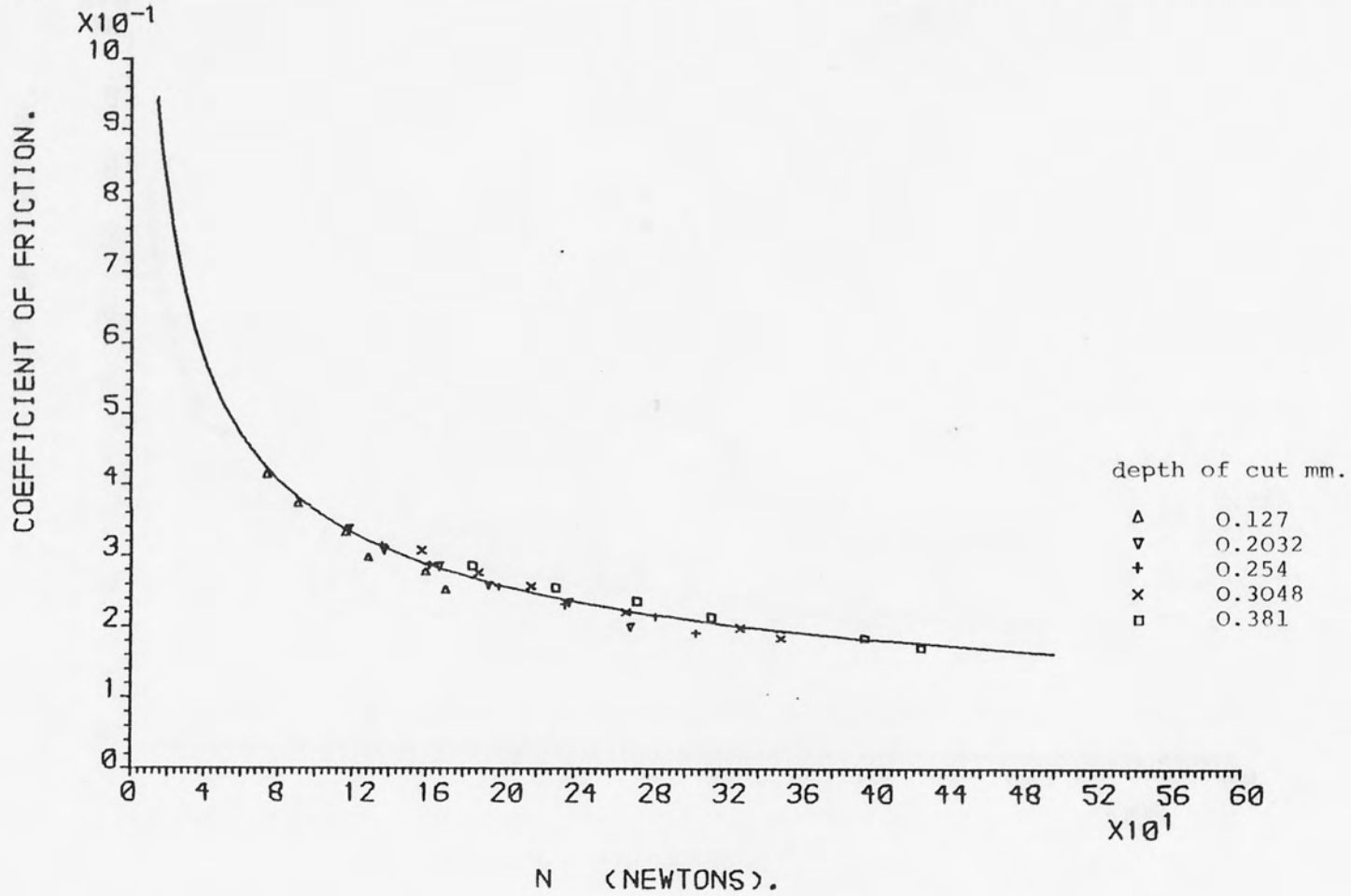

Fig. (7.147)

FIG. (7.147) μ and N relationship for as-received Nylon, cutting speed 36.58 m/min.

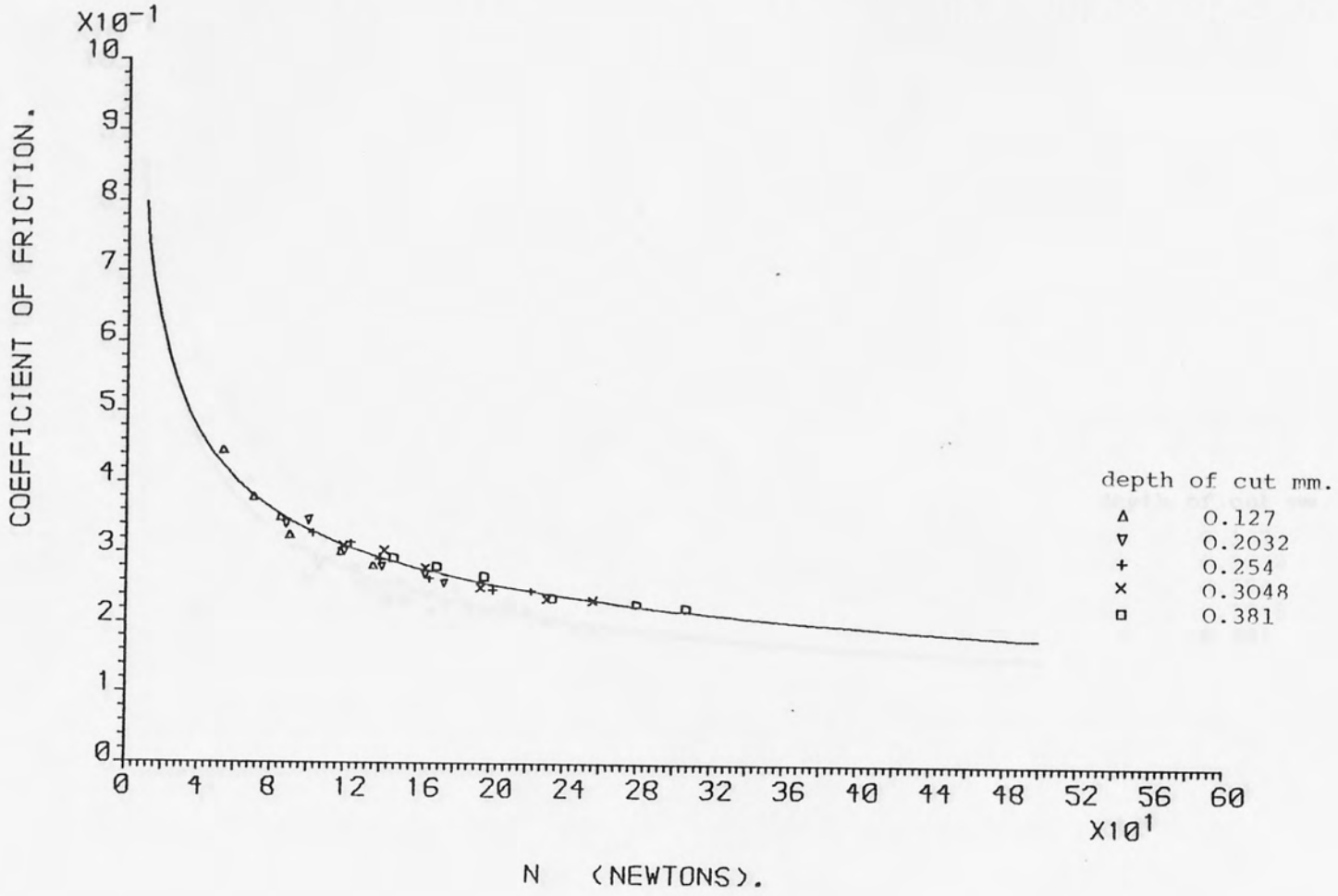

Fig. (7.148)

FIG. (7.148) μ and N relationship for rolled Nylon, cutting speed 15.24 m/min.

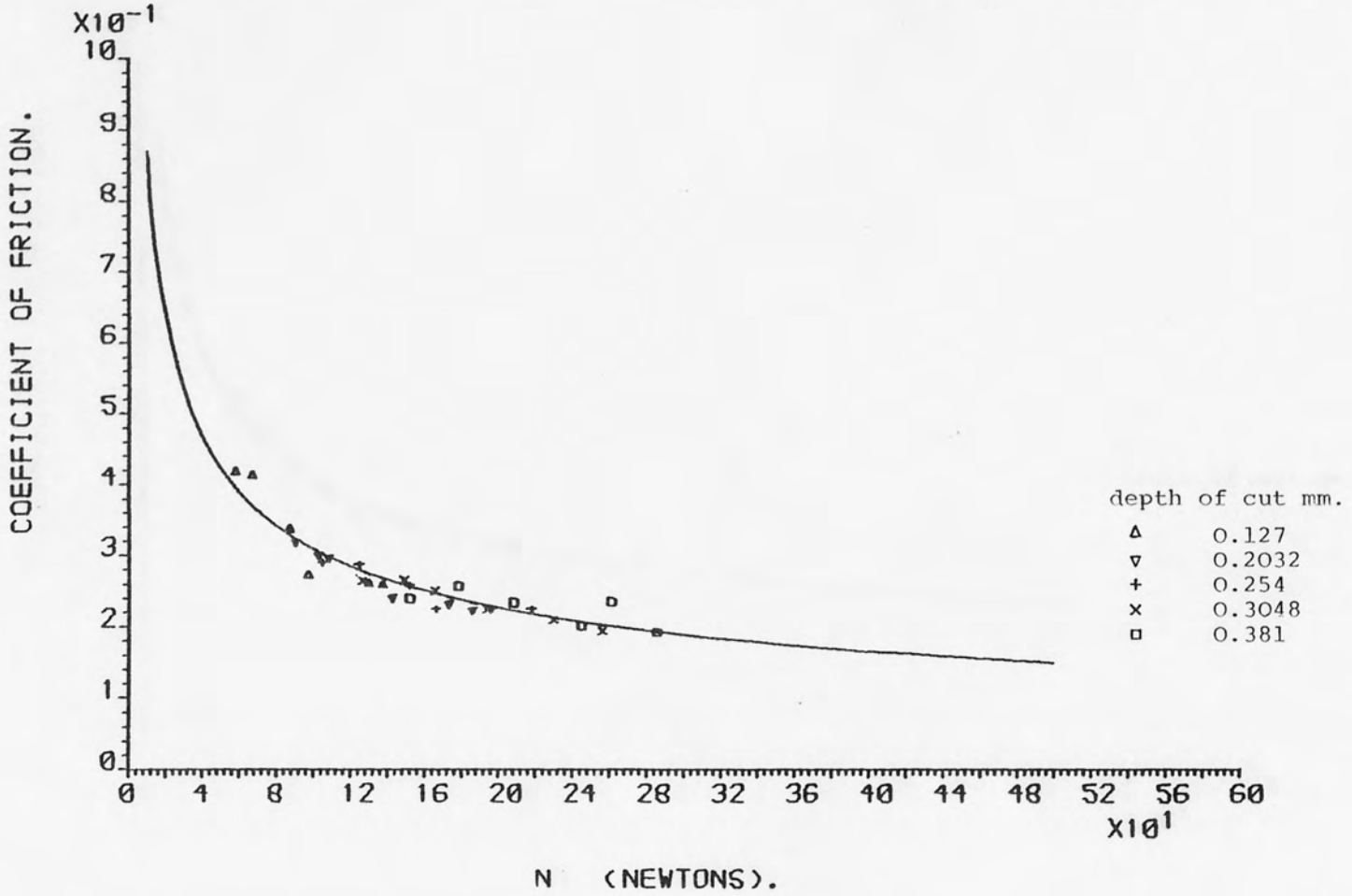

Fig. (7.149)

FIG. (7.149) μ and N relationship for rolled Nylon, cutting speed 30.48 m/min.

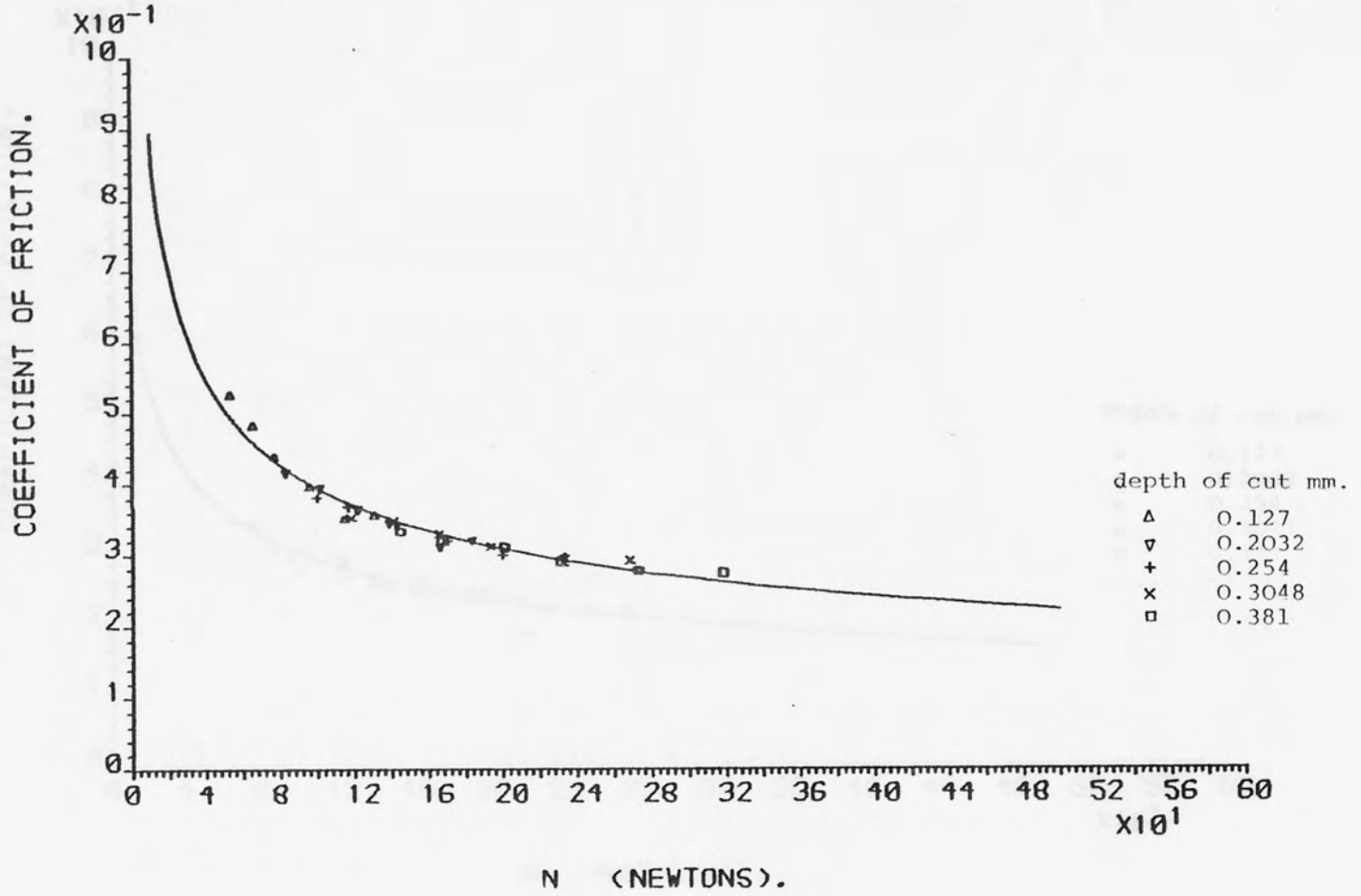

Fig. (7.150)

FIG. (7.150) μ and N relationship for rolled Nylon, cutting speed 9.14 m/min

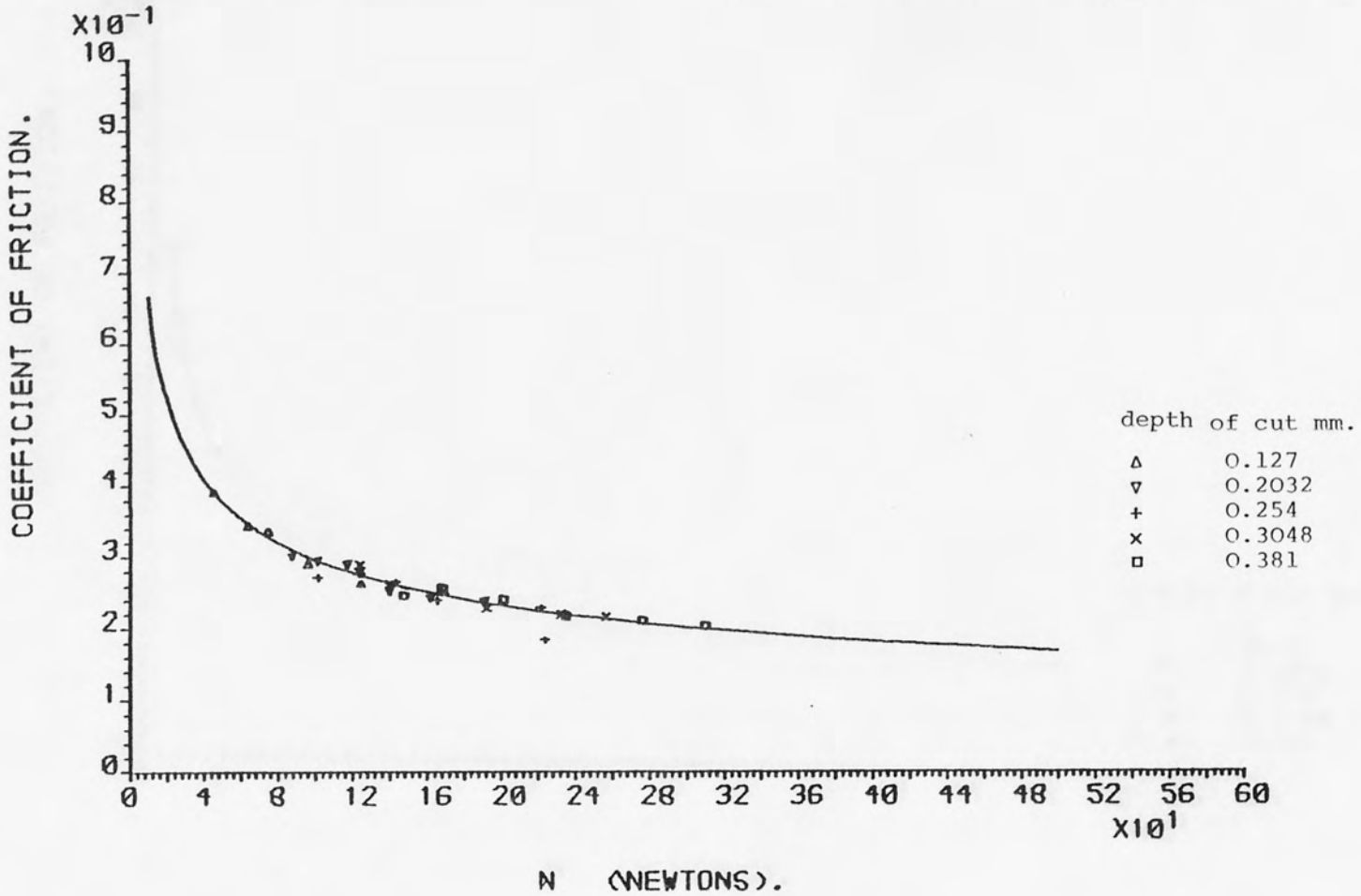

Fig. (7.151)

FIG. (7.151) μ and N relationship for rolled Nylon, cutting speed 22.86 m/min.

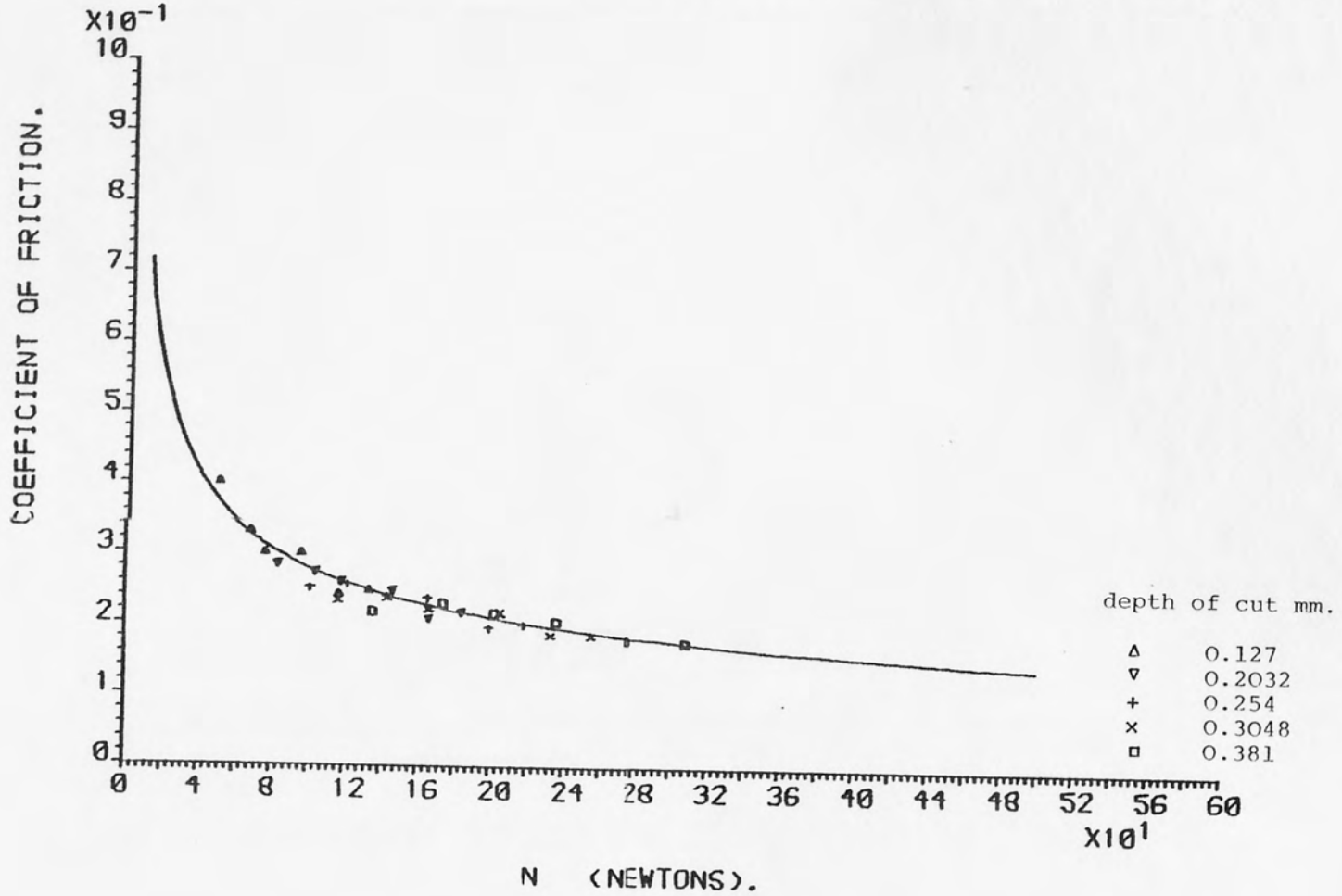

Fig. (7.152)

FIG. (7.152) μ and N relationship for rolled Nylon, cutting speed 36.58 m/min.